HYDRODYNAMIC CHARACTERISTICS OF ANNULAR CENTRIFUGAL EXTRACTOR AND HELICAL COIL BASED FLUIDIC DIODE PUMP

By

M. BALAMURUGAN

(Enrollment Number: ENGG02201204014)

Indira Gandhi Centre for Atomic Research, Kalpakkam
A thesis submitted to the Board of Studies in Engineering Sciences
In partial fulfillment of requirements for the Degree of

DOCTOR OF PHILOSOPHY
of
HOMI BHABHA NATIONAL INSTITUTE

August, 2019

Homi Bhabha National Institute

Recommendations of the Viva Voce Committee

As members of the Viva Voce Committee, we certify that we have read the dissertation prepared by **Mr. M. Balamurugan** entitled **"Hydrodynamic characteristics of ACE & Helical coil based fluidic diode pump"** and recommend that it may be accepted as fulfilling the thesis requirement for the award of Degree of Doctor of Philosophy.

Chairman –**Dr. K. Velusamy**	04/6/2021
Guide / Convener – **Prof. J. B. Joshi**	KBJoshi
Examiner–**Prof. Rajneesh Bhardwaj**	RBhardwaj
Member 1- **Dr. S. Rangarajan**	S. Rang
Member 2- **Dr. S. Murugan**	S. Murugan
Member 3- **Dr. B. P. Reddy**	Reddy
Technology Adviser - **Shri Shekhar Kumar**	Shekhar

Final approval and acceptance of this thesis is contingent upon the candidate's submission of the final copies of the thesis to HBNI.

I hereby certify that I have read this thesis prepared under my direction and recommend that it may be accepted as fulfilling the thesis requirement.

KBJoshi

Date: 4/06/2021

Place: Indira Gandhi Centre for Atomic Research

Kalpakkam

Prof. J. B. Joshi

(Guide)

STATEMENT BY AUTHOR

This dissertation has been submitted in partial fulfillment of requirements for an advanced degree at Homi Bhabha National Institute (HBNI) and is deposited in the Library to be made available to borrowers under rules of the HBNI.

Brief quotations from this dissertation are allowable without special permission, provided that accurate acknowledgement of source is made. Requests for permission for extended quotation from or reproduction of this manuscript in whole or in part may be granted by the Competent Authority of HBNI when in his or her judgment the proposed use of the material is in the interests of scholarship. In all other instances, however, permission must be obtained from the author.

M. Balamurugan

DECLARATION

I, hereby declare that the investigation presented in the thesis has been carried out by me. The work is original and has not been submitted earlier as a whole or in part for a degree / diploma at this or any other Institution / University.

M. Balamurugan

List of Publications Arising from the Thesis

Journal

1. "Development of Helical Coil Based Fluidic Diode Pump for Liquid Pumping", Balamurugan Manavalan, Niranjan K. Pandey, Shekhar Kumar, Kamachi U. Mudali and Jyeshtharaj B. Joshi, *Cand. J. Chem. Eng.*, **2018,** *96*, 62-67, (DOI: 10.1002/cjce.22899)
2. "Separation Characteristics of Liquid- Liquid Dispersions: Gravity and Centrifugal Settlers", Balamurugan Manavalan, Tushar V. Tamhane, Jaysree Patra, Aniruddha J. Joshi, Jyeshtharaj B. Joshi, Niranjan K. Pandey, Shekhar Kumar, Kamachi U. Mudali, Natarajan Rajamani, Vivek S. Vitankar and Raosaheb N. Patil, *Ind. Eng. Chem. Res.,* **2017,** *56(27)*, pp 7814–7823. (DOI: 10.1021/acs.jer.7b00119)
3. "Design Modification in the Stationary Bowl of Annular Centrifugal Extractor to Handle Adverse Conditions" Balamurugan Manavalan, Jyeshtharaj B. Joshi, Niranjan K. Pandey, *Ind. Eng. Chem. Res.*, **2020,** *59(25)*, pp 11757-11766. (DOI: 10.1021/acs.iecr.0c00181)

Conferences

1. "Effect of annular gap in hydrodynamic performance of centrifugal extractor", M. Balamurugan, J.B. Joshi, N.K. Pandey, *Proc. CHEMCON-2018 (on CD),***2018**, *CHO 083,* 27-30 Dec, NIT Jalandhar.
2. "Operating characteristics of CE 30 mm bowl", M. Balamurugan, Shreya Singh, J.B. Joshi, N.K. Pandey, *Proc. CHEMCON-2018 (on CD),***2018**, *CHO 084,* 27-30 Dec, NIT Jalandhar.
3. "Measurement of Dispersion number by Batch and Continuous settling mode", M. Balamurugan, J.B. Joshi, N.K. Pandey, *Proc. CHEMCON-2018 (on CD),***2018**, *CHO 094,* 27-30 Dec, NIT Jalandhar.
4. "Design and validation of a Centrifugal Extractor Stationary Block with stage-overflow provision", M. Balamurugan, SVN Ayyappa, U. Kamachi Mudali, J.B. Joshi, N.K. Pandey, *Proc. CHEMCON-2017 (on CD),* **2017,** *AS-0090,* 27-30 Dec, HIT, Haldia.

5. “Measurement of drop size in CE 30 mm bowl at various operating conditions”, M. Balamurugan, SVN Ayyappa, U. Kamachi Mudali, J.B. Joshi, N.K. Pandey, *Proc. CHEMCON-2017 (on CD),* **2017,** *AS-0089*, 27-30 Dec, HIT, Haldia.
6. “Mass transfer performance of 30 mm Centrifugal Extractor in Tri-iso amyl phosphate system”, M. Balamurugan, Jammu Ravi, U. Kamachi Mudali, J.B. Joshi, N.K. Pandey, *Proc. CHEMCON-2017 (on CD),* **2017,** *AS-00136*, 27-30 Dec, HIT, Haldia.
7. “Comparative Performance Evaluation of a Helical Coil-Based Fluidic Pump with a Conventional Air-Lift Pump”, M. Balamurugan, U. Kamachi Mudali, J.B. Joshi, N.K. Pandey, *Proc. CHEMCON-2017 (on CD)*, **2017,** *TP-0065*, 27-30 Dec, HIT, Haldia.
8. “CFD simulation on helical coil to understand the effects of different design parameters by pressure drop measurement”, M. Balamurugan, Shekhar Kumar, U. Kamachi Mudali, J.B. Joshi, *Proc. CHEMCON-2015 (on CD),* **2015,** 27-30 Dec, IIT Guwahati.
9. “Characterization of 40 mm Dia Centrifugal Extractor by Hydrodynamic and Mass Transfer Experiments”, M. Balamurugan, Shekhar Kumar, U. Kamachi Mudali, R. Natarajan, *Proc. CHEMENT-2014,* **2014,** *ED-03,* 06-07 March, IGCAR Kalpakkam.

M. Balamurugan

Dedicated to my beloved

Parents,

Wife and Kids

ACKNOWLEDGEMENTS

The scientific research is a collective effort of motivated individuals and research organizations towards an improved understanding, enhancing the safety and the progress of society. Without constant guidance and involvement of supervisors, colleagues and the support of family, significant progress in any field of research is difficult. Therefore, with humbleness and gratitude, I am extremely grateful to my research guide **Prof. J. B. Joshi & Dr. U. Kamachi Mudali** for their valuable guidance, constant support, encouragement, motivation and sincere interest throughout my Ph.D. I am highly obliged to them for their constructive criticism, valuable suggestions and sharing their abundance of knowledge with me. Their foresight and keen scientific intuition was absolutely vital for the progress of this work and led to the timely completion of thesis.

I wish to thank the honourable chairman and members of my doctoral advisory committee **Dr. K. Velusamy**, **Dr. M. Saibaba**, **Dr. S. Rangarajan, Dr. S. Murugan, Dr. B.P. Reddy and Shri Shekhar Kumar** for their scientific discussions and helpful suggestions at different time through out to my research, which helps me in redirecting my thinking and keeps me motivated and focused.

The work here has been collaborative throughout and there is a huge array of people to acknowledge. I like to thank my immediate superior **Dr. N. K. Pandey** for his suggestions, continuous support for my doctoral program. My heartiest thanks to **Dr. Ravishankar**, Former Director RpG and PD, FRFCF for their continuous encouragement and constant support in pursuing my research work. His probing questions encouraged to work further on the subject. I thank **Dr. R. Natarajan** for giving me an opportunity to work in this field and pursue my Doctoral programme.

I would also like to thank my colleagues especially **Mr. M. Sampath, Mr. S. V. N. Ayyappa, Mr. Alok Mishra, Mr. Sijo, Mr. Barathi, Dr. Jammu Ravi, Mr. Ramakrishna Reddy, Mr. D. Sivakumar, Mr. Balasubramonian, Dr. Desigan and Dr. Sathyabratha Mishra,** and all other colleagues of RR&DD for the discussions and suggestions during my research work for fruitful scientific discussions and for creating scientific atmosphere. I wish to thank all other members of RR&DD, RpG. I have been benefited one way or the other from their association and timely help.

I would also like to thank **Dr. Ekambara,** Technoforce for his friendly support, suggestions and guidance. I would like to mention special thanks to **G. Sunnel,** BARCF and **R. Rajandran,** IGCAR for their support and guidance.

I am thankful to my wife **Mrs. S. Gajashree** for the support and care she had taken during this work. I thank my daughter **Ms. B. Kanishkaa** for providing cheerful atmosphere at home.

I would like to express my sincere gratitude to my parents **Mr. D. Manavalan** and **Mrs. M. Baby** and to my uncle **Mr. Sripathy** and aunty **Mrs. S. Mallika** and all my family members and relatives for their encouragements and never-ending love, and affection to me.

There are many people that I wish to thank who have helped me to complete this thesis. Although I do not mention you all by name, you are not forgotten - thank you all! Last but not the least, I thank the almighty for protecting all of us from harm and blessing with health and happiness, and for allowing me to reach this far.

M. Balamurugan

TABLE OF CONTENTS

ACKNOWLEDGEMENTS viii

SUMMARY xviii

LIST OF FIGURES xxii

LIST OF TABLES xxviii

NOMENCLATURE xxx

1 A BRIEF OVERVIEW OF NUCLEAR ENERGY AND REPROCESSING OF SPENT NUCLEAR FUELS 1

1.1 Man and Energy 1

1.2 Nuclear Energy 3

1.3 Nuclear Fuel Cycle 5

1.4 Why Reprocessing? 7

1.5 History of Reprocessing 10

1.5.1 Non-Aqueous Reprocessing 10

1.5.2 Aqueous Reprocessing 13

1.6 Three stages of Indian Nuclear Power Program 19

1.7 PUREX process and detailed process steps 20

1.7.1 Head end treatment 21

1.7.2 Solvent extraction 22

1.7.3 Reconversion 23

1.7.4 Auxiliary steps 24

1.7.5 Vitrification 24

1.7.6 Additional steps 24

1.8 Scope of studies 24

1.9 Objective 26

1.10 Summary 27

1.11 References 27

2 BASICS OF SOLVENT EXTRACTION AND CENTRIFUGAL EXTRACTOR 31

2.1.1 Solvent extraction 31

2.1.2 Liquid-liquid extraction-principle 32

2.1.3 Solvent selection 34

2.1.4 Operating conditions 35

2.1.5 Mode of operation 36

2.1.6 Factors affecting extraction efficiency 36

2.1.7 Objective of liquid extraction theory 36

2.2 Design criteria for nuclear reprocessing equipment 37

2.3 Extraction equipment for nuclear reprocessing application 37

2.3.1 Mixer settler 38

2.3.2 Pulse column 38

2.3.3 Centrifugal extractor 38

2.4 Types of commercial centrifugal extractors 39

2.4.1 Podbielniak contactor 39

2.4.2 Robatel multistage centrifugal extractor 41

2.5 Annular centrifugal extractor 42

2.5.1 Initial design of short residence contactors 42

2.5.2 Development of annular centrifugal extractor 47

2.5.3 Working principle of ACE 48

2.5.4 Advantage and disadvantage of ACE 52

2.5.5 Parameters decides the pumping capacity of ACE 53

2.5.6 Parameters decides the mass transfer performance of ACE 53

2.6 Design principles of ACE 54

2.6.1 Liquid entry 54

2.6.2 Mixing inside ACE 54

2.6.3 Separation capacity 60

2.7 Design modification in ACE 65

2.7.1 Dismountable ACE for pharmaceutical application 65

2.7.2 Constant mixing volume ACE 66

2.7.3 Low mixing sleeve 67

2.7.4 Clean-in-place 67

2.7.5 Design modification for nuclear fuel reprocessing application 68

2.8 Summary 69

2.9 References 69

3 DEVELOPMENT OF UNIFIED CORRELATION FOR DISPERSION NUMBER 76

3.1 Introduction 76

3.2 Literature review 76

3.3 Objective 83

3.4 Experiments 83

3.4.1 Physcial properties measurement 83

3.4.2 Batch experiments: Dynamic disengagement method 85

3.4.3 Continuous experiments in annular centrifugal extractors 88

3.5 Results and Discussion 90

3.5.1 Batch experiments 90

3.5.2 Centrifugal separators 91

3.5.3 Solvent characterization by dispersion number 95

3.5.4 Unified Correlation for dispersion number and their applications 96

3.5.5 Correlation based on data driven modeling 100

3.6 Conclusion 105

3.7 References 106

4 DEVELOPMENT AND DEMONSTRATION OF INCLINED OVERFLOW LINE 108

4.1 Introduction 108

4.2 Literature review 109

4.3 Objective 113

4.4 Experimental 114

4.4.1 Chemicals used 114

4.4.2 Experimental setup 1 114

4.4.3 Working principle of experimental setup 1 117

4.4.4 Experimental setup 2 120

4.4.5 Experimental setup 3 123

4.4.6 Flooding experiment 127

4.4.7 Mass transfer experiment 127

4.4.8 Holdup experiment in single stage ACE 30 mm bowl 128

4.4.9 Procedure for new liquid discharge volume method 129

4.5 Results and Discussion 130

4.5.1 Flooding throughput results and discussion 130

4.5.2 Mass transfer results and discussion 134

4.5.3 Holdup and residence time in single stage ACE 30 mm bowl 136

4.6 Conclusions 141

4.7 References 144

5 COMPUTATIONAL FLUID DYNAMIC (CFD) STUDY INSIDE ANNULAR CENTRIFUGAL EXTRACTOR ROTATING BOWL 147

5.1 Introduction 147

5.2 Literature survey 149

5.2.1 CFD simulation details in ACE at annular region 149

5.2.2 CFD simulation details in ACE at rotor region 150

5.2.3 Flow visualization in inside rotor region of ACE 151

5.3 Objective 151

5.4 CFD Simulation Work 152

5.4.1 Governing equation 152

5.4.2 Single phase three dimensional simulation in ACE 155

5.4.3 Two phase 2D CFD simulation 157

5.5 Experimental work 158

5.5.1 Description of the setup 158

5.5.2 Zero point flow experiment 159

5.6 Results and Discussion 160

5.6.1 Single phase three dimensional simulation in ACE 160

5.6.2 Two phase 2D CFD simulation 163

5.6.3 Zero point flow experiment 169

5.6.4 Comparison of experimental result with CFD simulation 169

5.7 Conclusions 170

5.8 References 170

6 DESIGN AND DEVELOPMENT OF HELICAL COIL BASED FLUIDIC DIODE PUMP 173

6.1 Introduction 173

6.2 Literature survey 174

6.3 Objective 178

6.4 Design basics 178

6.4.1 Description of helical coil based fluidic diode pump 179

6.4.2 Details of helical coil 181

6.4.3 Details of helical coil fluidic pump....................................181

6.5 Experimental procedure 181

6.5.1 Pressure drop experiment....................................181

6.5.2 Pumping experiments....................................183

6.6 Results and Discussion....................................184

6.6.1 Pressure drop....................................184

6.6.2 Helical coil pumping capacity 185

6.7 CFD simulation in helical coil 189

6.7.1 Previous work 191

6.7.2 Governing equation....................................192

6.7.3 Numerical framework, mesh details and boundary conditions....................................193

6.8 Results and Discussion....................................195

6.8.1 Mesh independent result 195

6.8.2 Model validation 196

6.8.3 Effect of design parameter on pressure drop inside helical coil 199

6.9 Conclusions 209

6.10 References 210

7 CONCLUSIONS AND FUTURE DIRECTIONS....................................213

7.1 Conclusions 213

7.2 Future directions....214

APPENDIX....216

SYNOPSIS....241

LIST OF FIGURES

Figure 1.1: CO_2 Emissions by energy source [5] ... 3

Figure 1.2: Once through or open fuel cycle [7] ... 6

Figure 1.3: Closed fuel cycle [7] ... 7

Figure 1.4: Time evolution of radiotoxic inventory of spent nuclear fuel [8] ... 8

Figure 1.5: EBR-II fuel cycle activities [17] ... 11

Figure 1.6: Sequence of operations for pyro-electrochemical reprocessing (DDP process) of spent UO_2 and PuO_2 fuels [21] ... 13

Figure 1.7: History of nuclear fuel reprocessing processes [23] ... 14

Figure 1.8: Process flow sheet for first cycle acid Redox process [24] ... 16

Figure 1.9: Schematic process flow sheet for Butex process [24] ... 18

Figure 1.10: Simplified PUREX process flow sheet [24] ... 19

Figure 1.11: Three-Stage Nuclear Power Programme ... 20

Figure 1.12: PUREX process flow sheet [31] ... 21

Figure 1.13: Effect of HNO_3 concentration on the distribution coefficient in 30% TBP [24] ... 23

Figure 2.1: Basics of the solvent extraction ... 33

Figure 2.2: Podbielniak Contactor ... 40

Figure 2.3: Four stage Robetal SGN centrifugal extractor [13] ... 41

Figure 2.4: Short residence time centrifugal extractor with paddle mixer [15] ... 44

Figure 2.5: Air controlled aqueous weir [17] ... 45

Figure 2.6: Single stage mixer settler centrifugal contactor [21] ... 46

Figure 2.7: Assembled 16 stages mixer settler centrifugal contactor [21] ... 46

Figure 2.8: Annular centrifugal extractor with air controlled aqueous weir ... 48

Figure 2.9: Schematic diagram of the annular centrifugal extractor (ACE) ... 50

Figure 2.10: Cut view of rotating bowl ... 51

Figure 2.11: Variation of dispersion band in ACE. 52

Figure 2.12: Different flow pattern in annular gap 55

Figure 2.13: Vane geometry (a) 4 vanes, (b) 8 vanes and (c) curved vanes 58

Figure 2.14: Solvent characterization based on dispersion number 62

Figure 2.15: Fixed weir centrifugal weir 63

Figure 2.16: Schematic view of ECRAN [59] 66

Figure 2.17: Schematic view of low mix sleeve and bottom plate assembly [61] 67

Figure 2.18: Schematic view of clean in place (CIP) design [68] 68

Figure 3.1: Schematic representation of sedimentation and dense packed zones in steady state settler 77

Figure 3.2: Centrifugal separation of immiscible liquids 79

Figure 3.3: Schematic view of good and bad separation 89

Figure 3.4: Parity plot for the comparison of N_D measured experimentally against those estimated by Equation. 3.12 91

Figure 3.5: Variation of N_D with rotor diameter in ACE 92

Figure 3.6: Variation of dispersion number for kerosene-water system under different acceleration field. (*o*) Present study (♦) Kadam et al. [12]. 93

Figure 3.7: Parity plot for the comparison of N_D measured experimentally against those estimated by Equation. 3.16 94

Figure 3.8: Parity plot for the comparison of N_D measured experimentally against those estimated by Equation. 3.17 95

Figure 3.9: Parity plot for the comparison of N_D measured experimentally against those estimated by Equation. 3.18 97

Figure 3.10: Parity plot for the comparison of N_D measured experimentally against random forest based correlation (462 data sets from ACE) 103

Figure 3.11: Parity plot for the comparison of N_D measured experimentally against random forest based correlation 104

Figure 4.1: PEEK coated (a) Rotor and (b) Stator 109

Figure 4.2: Schematic view of Two Modular Structure (a) Rotor Module and (b) Housing Module 110

Figure 4.3: Schematic view of Three Modular Structure 111

Figure 4.4: Schematic view of inter-stage horizontal over flow line 112

Figure 4.5: Schematic view of two separate overflow lines 113

Figure 4.6: 4 stages 30 mm ACE stationary bowl with inter-stage inclined overflow line 115

Figure 4.7: Schematic drawing of 4 stages 30 mm ACE setup with inter-stage inclined overflow line 116

Figure 4.8: Schematic view of aqueous and organic flow in experimental setup 1 at normal operating condition 118

Figure 4.9: Schematic view of aqueous and organic flow in experimental setup 1 at 3rd stage motor failed condition 119

Figure 4.10: Schematic view of aqueous and organic flow in experimental setup 2 at normal operating condition 121

Figure 4.11: Schematic view of aqueous and organic flow in experimental setup 2 at 3rd stage motor failed condition 122

Figure 4.12: Schematic drawing of 4 stages 30 mm ACE setup with inter-stage horizontal overflow line (8) 124

Figure 4.13: Schematic view of aqueous and organic flow in experimental setup 3 at normal operating condition 125

Figure 4.14: Schematic view of aqueous and organic flow in experimental setup 3 at 3rd stage motor failed condition 126

Figure 4.15: Flooding curve for single stage ACE 30 mm bowl at different O/A ratio at 3000 rpm 131

Figure 4.16: Flooding throughput results for all three setups 134

Figure 4.17: Number of theoretical stages calculated by McCabe-Thiele plot 135

Figure 4.18: Holdup and residence time in single stage ACE 30 mm bowl w.r.t different throughput at constant O/A ratio 1 and 3000 rpm 138

Figure 4.19: Liquid height at annular region in single stage ACE 30 mm bowl w.r.t different throughput at constant O/A ratio 1 and 3000 rpm 139

Figure 4.20: Schematic view of height adjustment suggested for inclined overflow line at organic outlet end stage 143

Figure 5.1: ACE 30 mm bowl drawing with dimensions 155

Figure 5.2: ACE 30 mm bowl geometry up to aqueous weir without organic hardware 156

Figure 5.3: 2D geometry with aqueous and organic outlet 157

Figure 5.4: Schematic view of zero point flow experimental setup 159

Figure 5.5: Schematic view of ACE 30 mm rotating bowl with vertical baffle plates and horizontal deflection plate 160

Figure 5.6: Schematic view of ACE 30 mm rotating bowl without vertical baffle plates and horizontal deflection plate 160

Figure 5.7: Velocity magnitude contour plot at radial coordinate of 9 mm and y coordinate of 2 mm 161

Figure 5.8: Total pressure contour plot at radial coordinate of 9 mm and y coordinate of 2 mm162

Figure 5.9: Water volume fraction contour plot from 2D, 2 phase CFD simulation for different mesh size 164

Figure 5.10: Water volume fraction contour plot from 2D, 2 phase CFD simulation for different turbulent model at velocity inlet of 0.014 m/s 168

Figure 6.1: Basic geometry of helical coil 174

Figure 6.2: Schematic diagram of the helical coil based fluidic diode pump. 180

Figure 6.3: Photographic view of helical coil. 181

Figure 6.4: Photographic view of pressure drop experimental setup. 182

Figure 6.5: Friction factor fc vs Reynolds number for given helical coil 185

Figure 6.6: Pumping capacity of given helical coil pump at different on and off pulsing frequency (inlet pressure 49 kPa during pulsing on time and inlet pressure to ejector is 0 kPa (open to atmosphere) during pulsing off time)................................ 186

Figure 6.7: Pumping capacity of given helical coil pump at different on and off pulsing frequency (inlet pressure 49 kPa during pulsing on time and inlet pressure to ejector is 49 kPa during pulsing off time)... 187

Figure 6.8: Pumping capacity of given helical coil pump at different on and off pulsing frequency (inlet pressure 49 kPa during pulsing on time and inlet pressure to ejector is 98 kPa during pulsing off time)... 187

Figure 6.9: Pumping capacity of given helical coil pump at different on and off pulsing frequency (inlet pressure 98 kPa during pulsing on time and inlet pressure to ejector is 0 kPa (open to atmosphere) during pulsing off time)................................ 188

Figure 6.10: Pumping capacity of given helical coil pump at different on and off pulsing frequency (inlet pressure 98 kPa during pulsing on time and inlet pressure to ejector is 49 kPa during pulsing off time)... 188

Figure 6.11: Pumping capacity of given helical coil pump at different on and off pulsing frequency (inlet pressure 98 kPa during pulsing on time and inlet pressure to ejector is 98 kPa during pulsing off time)... 189

Figure 6.12: Parity plot for pressure drop (laminar region) between experimental measurements and correlation by Srinivasan et al. [10] 190

Figure 6.13: Parity plot for pressure drop (turbulent region) between experimental measurements and correlation by Mishra et al. [11], Ito et al. [7] and White et al. [17] 191

Figure 6.14: (a) Schematic drawing of helical coil with dimensions (No of turns = 5), (b) Geometry created in the ANSYS software and (c) actual experimental setup......... 194

Figure 6.15: Contour plot from STD k-epsilon model for mesh size of 403990 at inlet velocity of 2.52 m/s (a) Pressure contour plot (b) Velocity contour plot.............................. 196

Figure 6.16: Contour plot from SST k-omega model for mesh size of 379500 at inlet velocity of 2.52 m/s (a) Pressure contour plot (b) Velocity contour plot.............................. 196

Figure 6.17: Pressure drop parity plot between the experiment and CFD simulation (STD k-epsilon model) 198

Figure 6.18: Pressure drop parity plot between the experiment and CFD simulation (SST k-omega model) 198

Figure 6.19: Pressure drop calculated by CFD simulation (SST k-omega model) across given helical coil up to 100000 Reynolds number 199

Figure 6.20: Pressure drop w.r.t to different coil diameter 200

Figure 6.21: Contour plot for 16 mm helical coil diameter (a) Pressure contour plot (b) Velocity Contour plot 201

Figure 6.22: Contour plot for 40 mm helical coil diameter (a) Pressure contour plot (b) Velocity Contour plot 201

Figure 6.23: Pressure drop w.r.t to different helical coil pitch 203

Figure 6.24: Contour plot for 10 mm helical coil pitch (a) Pressure contour plot (b) Velocity Contour plot 203

Figure 6.25: Contour plot for 20 mm helical coil pitch (a) Pressure contour plot (b) Velocity Contour plot 204

Figure 6.26: Pressure drop w.r.t to different helical coil turns 205

Figure 6.27: Contour plot for helical coil with two turns (a) Pressure contour plot (b) Velocity Contour plot 206

Figure 6.28: Contour plot for helical coil with eight turns (a) Pressure contour plot (b) Velocity Contour plot 206

Figure 6.29: Pressure drop w.r.t to different helical coil pipe diameter 208

Figure 6.30: Contour plot for 4 mm pipe diameter helical coil (a) Pressure contour plot (b) Velocity Contour plot 208

Figure 6.31: Contour plot for 8 mm pipe diameter helical coil (a) Pressure contour plot (b) Velocity Contour plot 209

LIST OF TABLES

Table 1.1: Nuclear reactors operating in India 5

Table 1.2: Nuclear reactors under construction in India 5

Table 1.3: Disposition of various constituents of spent fuel 9

Table 1.4: World commercial reprocessing capacity [9, 10] 9

Table 2.1: Classification of centrifugal extractors 39

Table 3.1: Solvent pairs selected for dispersion number measurement 86

Table 3.2: Dispersion number for phosphoric acid system 96

Table 3.3: Different forms of dimensionless dispersion number correlations 98

Table 4.1: Physical properties of chemicals used in this work 114

Table 4.2: Equilibrium data of 30% TBP/n-Dodecane–HNO_3–Water system at room temperature 128

Table 4.3: Flooding capacity of single stage ACE 30 mm bowl at 3000 rpm 131

Table 4.4: Flooding results of different experimental setup 133

Table 4.5: Mass transfer experiment results 136

Table 4.6: Liquid holdup inside single stage ACE 30 mm bowl 137

Table 4.7: Residence time in second stage at experimental setup 1 140

Table 4.8: Residence time in second stage at experimental setup 3 140

Table 5.1: Model equations for turbulence 153

Table 5.2: ACE 30mm bowl dimension 155

Table 5.3: Pumping capacity with respect to different mesh size 160

Table 5.4: Average mass flow rate of water for 0.1 sec with respect to different mesh size 163

Table 5.5: Zero point flow CFD simulation results for k-ε model 165

Table 5.6: Zero point flow CFD simulation results for k-ε RNG model 166

Table 5.7: Zero point flow CFD simulation results for SST K-ω model 166

Table 5.8: Zero point flow CFD simulation results for Reynolds Stress model 167

Table 5.9: Zero point flow in ACE 30 mm bowl 169

Table 5.10: Zero point flow with respect to different turbulent models 170

Table 6.1: Correlation for critical Reynolds number calculation for helical pipe 176

Table 6.2: Correlation for friction factor calculation for helical coil in laminar region 177

Table 6.3: Correlation for friction factor calculation for helical coil in turbulent region 178

Table 6.4: Friction factor and Reynolds number from pressure drop experiment 184

Table 6.5: Grid independent results 195

Table 6.6: Comparison between experiment and simulation results at different inlet velocity condition 197

Table 6.7: Pressure drop with respect to different coil diameter 200

Table 6.8: Pressure drop with respect to different helical coil pitch.. 202

Table 6.9: Pressure drop with respect to different number of helical coil turns 205

Table 6.10: Pressure drop with respect to different helical coil pipe diameter........................... 207

Table A.1: Batch experiment dispersion number data with its variables................................... 216

Table A.2: Centrifugal extractor dispersion number data with its variables 220

Table A.3: The pumping capacity of a given helical coil based fluidic pump at different operating condition 236

CHAPTER 7

CONCLUSIONS AND FUTURE DIRECTIONS

7 CONCLUSIONS AND FUTURE DIRECTIONS

7.1 Conclusions

In present investigation concerned with:

1. Development of unified correlation for dispersion number.
2. Design modification in ACE to handle the adverse condition in multistage operation.
3. CFD simulation in ACE to select a suitable model for further studies.
4. Development of helical coil based fluidic pump for reprocessing application.

The major conclusions arrived in the thesis are discussed below:

- A novel data-driven based dimensionless dispersion number correlation was developed by using the Random Forest technique in artificial intelligence. The developed correlation could be used for the design of gravity as well as centrifugal separators. Such a correlation is especially useful for the high radioactive or hazardous systems where the measurement of dispersion number is not possible.
- A simple and innovative modification of inclined overflow line has been proposed for smoother operation of multistage ACE in the event of motor/bearing failed condition. From the experimental results of flooding, it is concluded that hydrodynamic performance of ACE with above modification is much better than the other designs reported in the literature.
- Incorporation of liquid-liquid centrifuge as an end stages improved the hydrodynamic performance of CE cascade during normal as well as motor/bearing failed conditions.
- As regards to the prediction of zero-point flow rate, it is concluded that the SST k-omega model is suitable for the separator region of ACE.

- Helical coil based pulsating pump has been developed and demonstrated for reprocessing application by pumping experiments. This new design is expected to be useful for reprocessing applications.
- The experimental pressure drop data was found to be closer to those estimated by the correlation of Srinivasan et al. in the laminar region. However, for turbulent flow the correlation of Mishra et al. was found to give superior estimates.
- As regards to CFD simulation, SST k-omega model was found to perform superior as compared with the standard k-epsilon model. Since in the published literature, SST k-omega based CFD simulations have been performed over a limited range of Reynolds number (< 48000) and helical coil geometries, a wider range has been covered in the present work.

7.2 Future directions

- Inclusion of inclined overflow line in ACE ensured the smooth operation of multistage cascade during the motor/bearing failed condition. The optimization of the length and diameter of the above-inclined overflow line has to be completed.
- 2D two-phase CFD simulation was completed in the ACE rotor zone to validate the turbulent model. 3D with three-phase CFD simulation will give in situ view of flow behavior inside the rotating bowl. Design of ACE is based on thumb rules, 3D CFD simulation will be useful to optimize the various design parameters such as underflow width, no of baffles, the distance between deflection plate, aqueous weir diameter, organic weir diameter, etc.
- Drop size distribution decides the mass transfer performance and settling behavior of any solvent extraction equipment. CFD simulation with the population model in the ACE annular region will be helpful for the prediction of mass transfer performance for any given operating condition.

- The Helical coil-based pump was developed and demonstrated, and its performance depends upon the various design and operating parameters. The development of the design equation with its design and operating parameters may help to design helical coil pumps for any given process condition.

SUMMARY

Nuclear energy comes under non-renewable energy and does not create any global warming. The major disadvantage is radiotoxicity (generation of radioactive elements). Nuclear reprocessing helps to separate radiotoxic materials from spent nuclear fuel and it enhances nuclear energy utilization by recycling the separated fissile and fertile materials. The main objective of nuclear reprocessing is to separate uranium (un-burnt), plutonium (converted from uranium by n,γ reaction inside the nuclear reactor) from spent nuclear fuel. PUREX (Plutonium Uranium Reduction Extraction) process was a well-established solvent extraction process to separate uranium and plutonium from spent nuclear fuel. However, the radioactivity level in fast breeder fuel reprocessing is 10 to 15 fold higher than in the thermal reactor fuel reprocessing plant.

Increased radiation level increases the solvent degradation products (MBP and DBP), forming a stable complex with Pu and leading to Pu loss in the organic phase. To reduce solvent degradation, extraction should be completed in seconds and an annular centrifugal extractor (ACE) is a candid candidate for the above nuclear reprocessing application. ACE is robust solvent extraction equipment widely used in different process industries. Although it is designed based on various thumb rules, the reliable design and scale-up of ACE are yet to be developed, especially for nuclear reprocessing applications. Flow inside the ACE is highly turbulent, unsteady due to liquid level fluctuation in the annular region, air ingression and three-phase (air, heavy and light phase) operation during solvent extraction operation. In addition, the details of flow and mass transfer are not yet precise.

The dispersion number (N_D) is the primary design input for ACE, which decides the size and operating speed for any given process throughput. N_D value depends upon the system's physical properties, such as density, viscosity, and interfacial tension. The measurement of N_D is impossible for hazards (radioactive, corrosive, etc.) systems. The N_D is measured by batch and continuous experiments, similarly data's from various literatures are collected for different aqueous and organic systems to cover a wide range of physical properties $100 < \Delta\rho < 625$ kg/m^3, $3 < \sigma < 58.3$ mN/m, $0.3 < \mu_C$ & $\mu_D < 12.2$ mPa.s. N_D correlation has been developed using 542 data points and its fitting was poor for the batch experimental data and it yielded two separate correlations. Finally, a novel data-driven based unified dimensionless dispersion number correlation was developed by using the Random Forest technique in artificial intelligence. The developed data-driven correlation could be used for the design of gravity as well as centrifugal separators. In addition, such a correlation is beneficial to calculate the dispersion number for the high radioactive or hazardous liquid-liquid systems, where the measurements are not possible.

The ACE comes under a stage-wise contactor and requires a counter currently operated multiple stages to achieve the required separation factor. Failure of motor or bearing in any single stage in multistage operation leads to the stoppage of an entire cascade. In nuclear reprocessing applications, the stoppage of cascade leads to solvent degradation and defeats the advantage of ACE. Therefore, an innovative and simple design modification of inclined overflow line has been proposed for the smoother operation of multistage ACE in motor/bearing failed conditions. The four-stage, 30 mm rotating bowl diameter of ACE setup with an inter-stage inclined overflow line is developed to demonstrate the smooth operation of multistage ACE in any single-stage motor/bearing failed condition.

Furthermore, the flooding and mass transfer experiments are conducted in above experimental setup to evaluate the inter-stage line performance with motor failed conditions. Results show that the inter-stage inclined overflow line ensured the smooth operation of cascade during the motor failed condition. Similarly, the addition of a liquid-liquid centrifuge

at the end-stages was increased the flooding capacity of multistage ACE for both the regular and motor failed conditions. From the experimental results, it is concluded that the hydrodynamic performance of ACE with the above modifications is much better than the other designs reported in the literature.

Flow inside the rotating bowl is one of the grey areas in the ACE design. CFD may be a key tool to address or solve the above problem and also it can be used to evaluate the existing ACE to optimize the operating parameters. It also helps to design a robust ACE. Several authors reported the CFD simulations inside the rotor region to understand the flow behavior. Two-phase and three-phase CFD simulations have been reported in the literature. However, mesh independence has not been performed. Also, the validity of the chosen turbulence model has not been presented. In the present work, single-phase (water) 2D simulations have been carried out in the ACE rotating bowl region. Mesh size was selected based on mesh independent studies.

At relatively low flow rates of water, it flows through an aqueous outlet. However, it also starts taking the path of an organic outlet at a critical water flow rate. This critical flow rate is called the zero-point flow rate. The CFD simulations have been performed for the prediction of zero-point flow rate. For this purpose, four different turbulent models have been employed. They are: (i) k-epsilon STD model, (ii) k-epsilon RNG model, (iii) SST K-omega model and (iv) Reynolds Stress model. The predictions of the SST k-omega model are closer to the experimental measurements. Regarding the prediction of zero-point flow rate, it is concluded that the SST k-omega model is suitable for the separator region of ACE.

Airlift pumps are widely used for metering applications in reprocessing plants. The main advantages of airlift pumps are a simple design, high reliability and free from mechanical maintenance. However, airlift and fluidic pumps are not suitable for low

throughput metering operations. A suitable alternate pumping system of a helical coil-based pulsating pump has been developed and demonstrated. The pumping experiments are conducted with different operating conditions to understand the performance of a given helical coil-based pulsating pump. The experimental pressure drop data on a given helical coil was found to be closer to those estimated by the correlation of Srinivasan et al. in the laminar region. However, for turbulent flow, the correlation of Mishra et al. was found to give superior estimates. The CFD simulations have been performed for the prediction of the pressure drop across the given helical coil. The predictions of the SST k-omega model are closer to the experimental measurements. Since in the published literature, SST k-omega based CFD simulations have been performed over a limited range of Reynolds number (< 48000) and helical coil geometries, a wider range has been covered in the present work. A helical coil based pulsating pump has been developed and demonstrated for reprocessing application by pumping experiments. This new design is expected to be useful for reprocessing applications.

CHAPTER 1

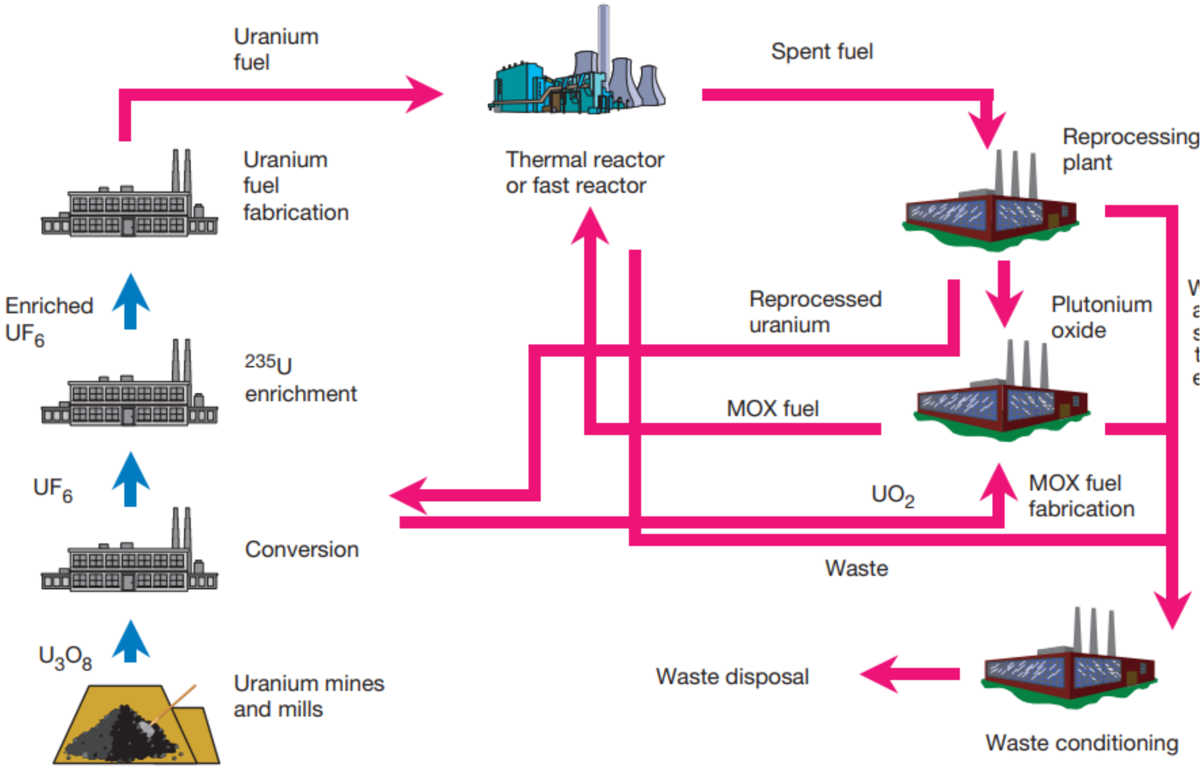

Closed nuclear fuel cycle

A BRIEF OVERVIEW OF NUCLEAR ENERGY AND REPROCESSING OF SPENT NUCLEAR FUELS

1 A BRIEF OVERVIEW OF NUCLEAR ENERGY AND REPROCESSING OF SPENT NUCLEAR FUELS

1.1 Man and Energy

Food, shelter and clothing are the basic requirements for human life. Energy, the basic building block or inseparable partner in human life, ensures the availability of all the above necessities with quality of life such as education, health, life expectancy, etc. There are different forms of energy available and widely it is categorized into (i) Chemical Energy is energy stored in the form of chemical bonds and it is released during chemical reaction (ex:- coal, oil, wood, etc.), (ii) Electrical Energy is nothing but moving of electron in an electrical conductor. It is most useful form of energy and it is easily transferable and readily convertible into the light, mechanical, chemical etc., (iii) Mechanical Energy, (iv) Thermal Energy related to temperature or vibration of molecules, (v) Nuclear Energy is a form of energy trapped inside the atom which could be produced either by splitting of an atom (fission) or combining atoms (fusion) and (vi) Gravitational Energy (potential energy) ex: water flowing from a mountain.

Before industrial revolution [1], humans generated the mechanical energy by the power of themselves, animal, wind and water. Heat and light are generated by burning wood, biomass, oil etc. After industrialization, energy consumption per person increased drastically and different forms of energy is explored and it is readily available in market such as petrol, diesel, battery, electric current, etc. Per capita energy is generally measured in terms of tons of oil-equivalent (toe). Between 1850 and 2015, overall energy production and use grew more than 50-fold from a global total of approximately 0.2 billion toe to 13.6 billion toe [2, 3]. On a per capita basis, people in modern societies now use more than 100 times the quantity of energy that was used by their ancestors before humans learned to exploit the energy potential of fire [4].

Energy resources are categorized into two types and they are (i) renewable and (ii) non-renewable. Renewable energy resources are inexhaustible and they are solar, wind, tidal, geothermal, biomass, hydraulic etc. Its major disadvantages are (i) commercially non-viable, (ii) location specific, (iii) energy storage, (iv) seasonal etc. Non-renewable energy resources are exhaustible and they are coal, petroleum products, natural gas, nuclear energy, etc. Its major disadvantages are (i) it cannot be replaced immediately once their energy source is used up, (ii) environmental concern (pollution, green house effect), etc.

Global warming is a very big challenge and it should be addressed as early as possible to stabilize the ecosystem. CO_2 and other greenhouse gases are generated mainly from non-renewable energy sources. Renewable energy resources also contribute considerable level of CO_2 generation during equipment manufacturing, plant construction phase, during maintenance, etc. Nuclear energy is one of the cleanest technologies for electricity power production and it is shown in below Fig. 1.1 [5]

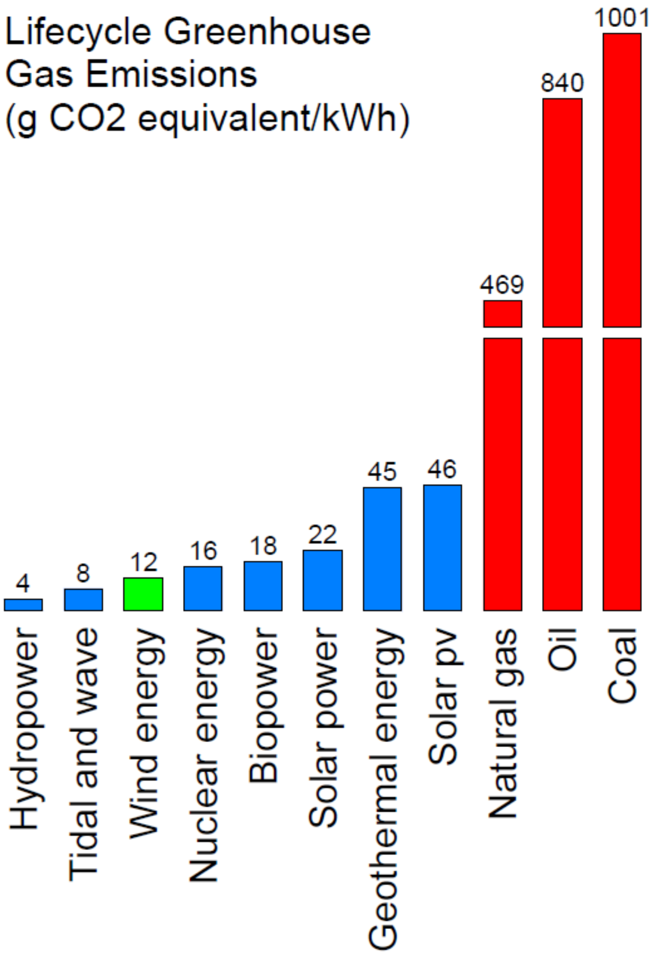

Figure 1.1: CO_2 Emissions by energy source [5]

1.2 Nuclear Energy

The rise of electricity demand and depletion of oil and gas sources and commitment towards reduction of greenhouse gas emissions are the important driving factors for the development of nuclear energy to fulfill the present and future requirements. As on date around 11% electricity throughout world is produced by around 450 nuclear power reactors. It is second largest power source with low carbon foot print. In addition to that around 225 research reactors are under operation to produce various isotopes for medical and industrial applications and also for training. During nuclear reactor operation, ^{235}U (fissile material) is fissioned by bombardment with neutrons and generates highly radioactive fission products (FPs), fission neutrons and about 194 MeV energy [6].

$$ {}^{235}_{92}\mathrm{U} + {}^{1}_{0}\mathrm{n} \rightarrow \text{Fission products} + 2.5\,{}^{1}_{0}\mathrm{n} + 194\ \mathrm{MeV} \qquad (1.1)$$

During nuclear reaction around 2.5 neutrons are generated in each fission reaction to sustain the nuclear fission reaction and simultaneously converts fertile ^{238}U into ^{239}Pu fissile material.

$$ {}^{238}_{92}\mathrm{U} + {}^{1}_{0}\mathrm{n} \rightarrow {}^{239}_{92}\mathrm{U} \xrightarrow[23.5\ \text{min}]{\beta^-} {}^{239}_{93}\mathrm{Np} \xrightarrow[2.356\ \text{days}]{\beta^-} {}^{239}_{94}\mathrm{Pu} \qquad (1.2)$$

Heat released during nuclear fission reaction is utilized to heat the water to generate the steam. Above steam is used to spin the turbine coupled with generator to produce electricity. Fission products generated during nuclear reaction absorbs the neutron required for nuclear fission and increases the radiation intensity inside the nuclear reactor. Burnup (expressed as MWD/tonne) of the fuel indicates the availability of fissile material and radiation intensity inside nuclear fuel pin. To ensure uninterrupted operation of the reactor, the spent fuel has to be replaced with fresh fuel. The spent fuel discharged from reactors contains fissile nuclides (unutilized ^{235}U and newly formed ^{239}Pu) which can be re-used either in existing and future nuclear power plants depending on the type. The process of separating the fissile and fertile materials (Pu and U) from the FPs, activation products and minor actinides present in the spent fuel after allowing for the decay of short-lived fission products is termed as spent fuel reprocessing.

In India, around 2.6% (6200 MWe) electricity is produced from nuclear reactor. Total 22 nuclear reactors are under operation and its list is shown in below Table 1.1 and also list of nuclear reactor under construction is shown in Table 1.2.

Table 1.1: Nuclear reactors operating in India

S. No	**Reactor**	**Type**	**MWe net (each)**	**Commercial operation**
1.	Tarapur 1&2	GE BWR	150	1969
2.	Kaiga 1&2	PHWR	202	1999, 2000
3.	Kaiga 3&4	PHWR	202	2007, 2012
4.	Kakrapar 1&2	PHWR	202	1993, 1995
5.	Madras 1&2 (MAPS)	PHWR	202	1984, 1986
6.	Narora 1&2	PHWR	202	1991, 1992
7.	Rajasthan 1&2	Candu PHWR	90, 187	1973, 1981
8.	Rajasthan 3&4	PHWR	202	1999, 2000
9.	Rajasthan 5&6	PHWR	202	2010 (both)
10.	Tarapur 3&4	PHWR	490	2006, 2005
11.	Kudankulam 1&2	PWR (VVER)	917	2014, 2017

Table 1.2: Nuclear reactors under construction in India

S. No	**Reactor**	**Type**	**MWe net (each)**	**Commercial operation due**
1.	Kalpakkam PFBR	FBR	470	2022
2.	Kakrapar 3&4	PHWR	630	2022
3.	Rajasthan 7&8	PHWR	630	2022
4.	Kudankulam 3&4	PWR	917	2025, 2026

1.3 Nuclear Fuel Cycle

Various activities/industrial process associated with electricity generation from nuclear reactor is called nuclear fuel cycle. It starts from uranium mining and ends at final disposal of nuclear waste.

Two types of nuclear fuel cycle are adopted based on the policies of countries.

a) Open or once through fuel cycle involves direct disposal of spent fuel in deep geological formations (Fig. 1.2 [7]). In this cycle, the spent fuel coming out from the reactor is treated as waste. The main advantage of the open fuel cycle is proliferation resistance.

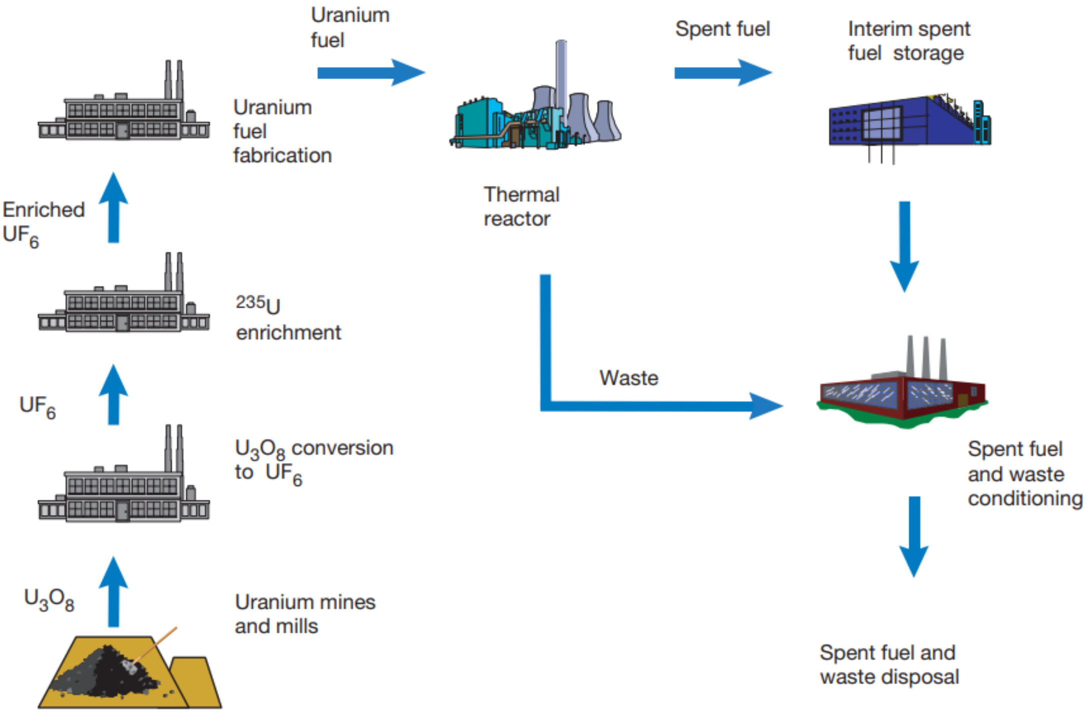

Figure 1.2: Once through or open fuel cycle [7]

b) Closed fuel cycle (Fig. 1.3 [7]) that involves reprocessing the spent fuel using PUREX (Plutonium Uranium Recovery by Extraction), UREX and TRUEX process to extract fissile material generated by nuclear reaction like ^{239}Pu, ^{233}U and unused ^{238}U, ^{232}Th for reuse in new fuel and conditioning of residual wastes that contain FPs and minor actinides in highly durable glass matrix followed by interim storage and then disposal. France, India, Russia, Japan, UK are adopting closed fuel cycle. The depleting reserves of uranium and the increased demand to nuclear fuel for power generation has forced many countries like India to follow a closed fuel cycle. Inclusion of breeder reactor in a closed fuel cycle produces the fissile material at the rate that exceeds its consumption.

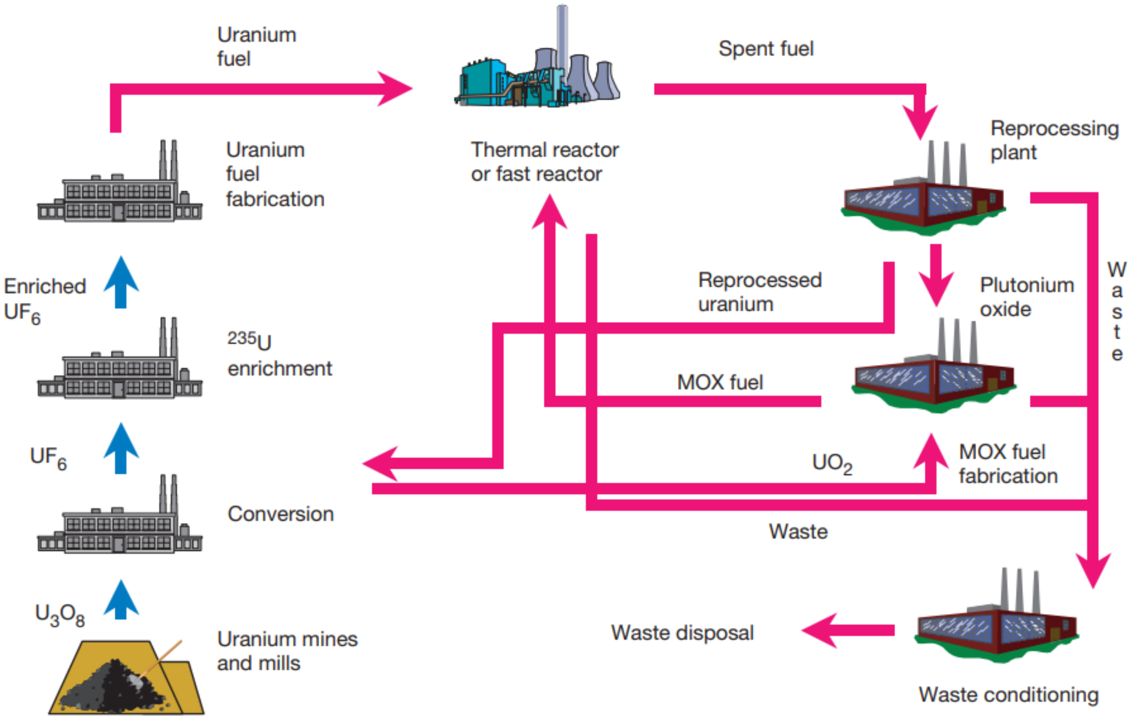

Figure 1.3: Closed fuel cycle [7]

1.4 Why Reprocessing?

The principle reason for reprocessing used fuel is to recover unused uranium and plutonium in the used fuel elements to gain more energy from the original uranium in the process and thus contribute towards energy security. A secondary and equally important reason is to reduce the volume of material to be disposed of as high-level waste to about one-fifth. In addition, the level of radioactivity in the nuclear waste from reprocessing is much smaller and after recycling all actinide into a fast nuclear reactor the radioactive level falls more rapidly and it reaches equivalent to natural uranium ore in 400 years (Fig. 1.4 [8]).

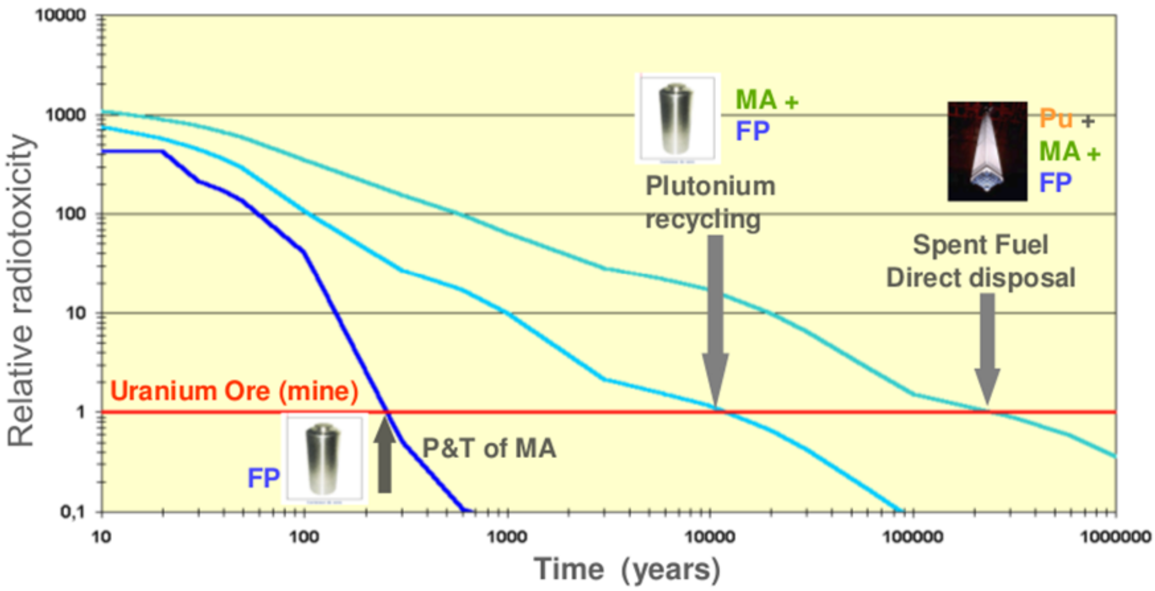

Figure 1.4: Time evolution of radiotoxic inventory of spent nuclear fuel [8]

Spent fuel contains an almost the entire quantity of radioactivity encountered in the nuclear fuel cycle. The composition of the spent fuel from a typical PWR and how these constituents are disposed in the fuel cycle are given in Table 1.3.

The spent fuel reprocessing aims at the segregation of the constituents into various fractions depending upon their disposition strategy. The list of commercially operating reprocessing plants and their capacity are shown in Table 1.4.

Table 1.3: Disposition of various constituents of spent fuel

Percentage	**Component**	**Disposition**
95.6	Uranium	Recycled back to the reactor or disposed of as waste
3	Stable or short lived fission products	Decays in a short time resulting in no significant disposal problem
0.3	Major fission products	Cause of heat generation in near long term storage; ^{137}Cs, ^{90}Sr; decays in a few centuries
0.1	Long-lived fission products (LLFP)	Constitutes transmutable nuclides; primarily iodine and technetium: stored presently along with major fission products. Strategy exists for their removal and transmutation
0.9	Plutonium	Separated and burned as fuel
0.1	Long-lived minor actinides	Primarily Np, Am, and Cm; Presently stored along with fission products. Strategy exists for separation and fissioning using fast neutrons

Table 1.4: World commercial reprocessing capacity [9, 10]

	Reprocessing Plant	**Capacity (tonnes per year)**
LWR fuel	France, La Hague	1700
	UK, Sellafield (THORP)	600
	Russia, Ozersk (Mayak)	400
	Japan (Rokkasho)	800
	Total LWR (approx)	**3500**
Other nuclear fuels	UK, Sellafield (Magnox)	1500
	India (PHWR, 4 plants)	330
	Japan, Tokai MOX	40
	Total other (approx)	**1870**
Total civil capacity		**5370**

1.5 History of Reprocessing

Initially, nuclear reprocessing technology was developed to extract plutonium from spent nuclear fuel to make nuclear weapons by a chemical separation process. Due to the commercialization of nuclear power, reprocessed uranium and plutonium are recycled back into nuclear reactors for electricity generation. Recycling of uranium is economical when the supply of uranium is low or prices are high. Reprocessing may leads to nuclear proliferation, vulnerability to nuclear terrorism, the political challenges of repository siting, etc. The spent fuel reprocessing can be categorized into two main classes: “Non-Aqueous” and “Aqueous Reprocessing".

1.5.1 Non-Aqueous Reprocessing

The non-aqueous methods exploit the differences in the physical and chemical properties of the fuel and fission products to separate them. They can be classified into;

- Volatility based methods
- Pyrometallurgical methods and
- Pyrochemical methods

1.5.1.1 Volatility based methods

The fluoride volatility [11] and the nitrofluor [12] processes come under this category. Both the processes utilize the high volatility of UF_6 and PuF_6 over their fission product counterparts. As large scale experience with this compound is available with the operation of enrichment plants, the adaptation of this process for spent fuel reprocessing was considered feasible. The fluoride volatility process has been developed for uranium recovery from spent fuels as UF_6 due to its high volatility compared to other species present in the fuel. It was used extensively at Oak Ridge National Laboratory (ORNL) for recovering uranium from the spent fuel discharged from nuclear driver submarine and research reactors.

General Electric developed the aqua fluor process [13] and it is used in Moris Plant, Illinois after plutonium and uranium separation from fission products by solvent extraction and ion exchange, the final purification of uranium was carried out by the conversion of uranyl nitrate to its fluoride. Subsequently, purification from plutonium, neptunium and other volatile fluorides is done by adsorption in NaF and MgF_2 beds and later by fractional distillation. This plant was not operated with irradiated fuel due to operational problems [14, 15].

Fluoride volatility based processes could not succeed in plant operation of spent fuels due to the difficulties in containing the volatile fission products.

1.5.1.2 Pyrometallurgical methods

In Pyrometallurigcal methods, spent fuel materials are maintained in the metallic state throughout the process. During the 1960s, EBR-II (experimental breeder reactor II) fuel was reprocessed by using melt refining process [16] and its fuel cycle [17] is shown in Fig. 1.5 [17].

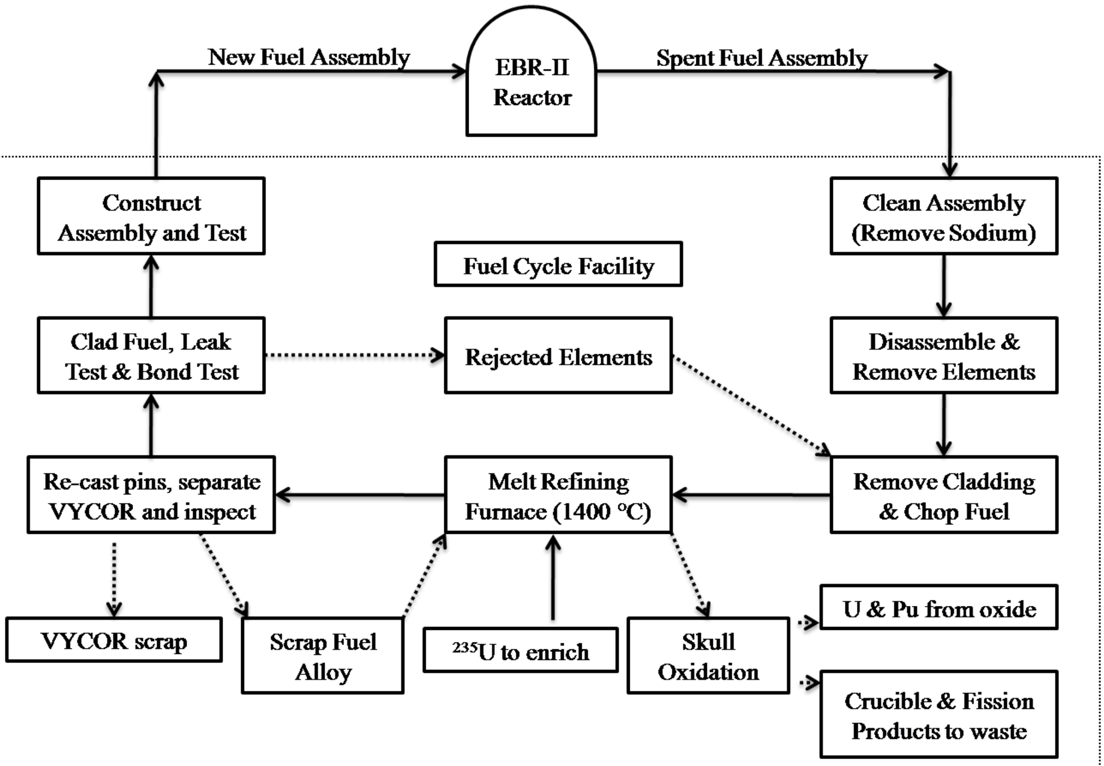

Figure 1.5: EBR-II fuel cycle activities [17]

In this process, spent fuel is melted in a lime stabilized zirconia crucible and heated at 1400°C for 3 h under inert atmosphere. The volatile FPs escape, leaving stable FP elements such as yttrium, strontium, barium, lanthanum and lanthanide elements in their oxide form, which follow uranium in the melt and are cast into an ingot. The layer of oxide formed by this FP over the ingot is called as "skull". The distribution of rare earths is very poor and only about 99% would be removed during the process. Recoveries of U and Pu will be only to the extent of 90-95%; hence a “skull reclamation process” [18] has been used wherein the skull is oxidized under Ar-O_2 atmosphere at 700^{o}C and reduced using molten Zn and Zn-Mg alloys in the presence of molten halide salts. But owing to the nature of Pu to follow the Zn-Mg alloy waste stream, the process is not compatible for processing alloy fuels with Pu. Cesium, strontium, barium and lanthanides must be removed periodically from the crucible to ensure the salt's purity. The waste is required to be treated to enable recycling of the salt and any residual actinides. In the above processes, the recovery of adhering Pu from crucible lining, crucible, spent electrodes and related equipment waste is a difficult task.

1.5.1.3 Pyrochemical methods

In the early fifties of the twentieth century, molten salt technology (higher than room temperature) is employed for nuclear materials purification. The salt cycle [19] and salt transport [20] process are examples of this method and it was developed for low Pu bearing fuels.

It involves the use of either molten salts or volatilization to metal fluorides. Processes based on molten salts involve, dissolution of the fuel in molten alkali chlorides at 450-700 ^{o}C and decontamination by electrolysis. This approach has been applied to oxide fuel (RIAR, Russia), metal fuel (ANL, US) and nitride fuel (JAERI, Japan) with suitable modifications.

The experience in Russia is very satisfactory. Few tens of kilograms of irradiated fuel containing Pu have been successfully reprocessed in RIAR, Dimitrovgrad by a process called

Dimitrovgrad Dry Process (DDP). A schematic view of DDP process flow sheet for MOX fuel is shown in Fig. 1.6 [21]. The pyrochemical processes involve high temperature and corrosive chloride environment; hence the material of construction is a major issue.

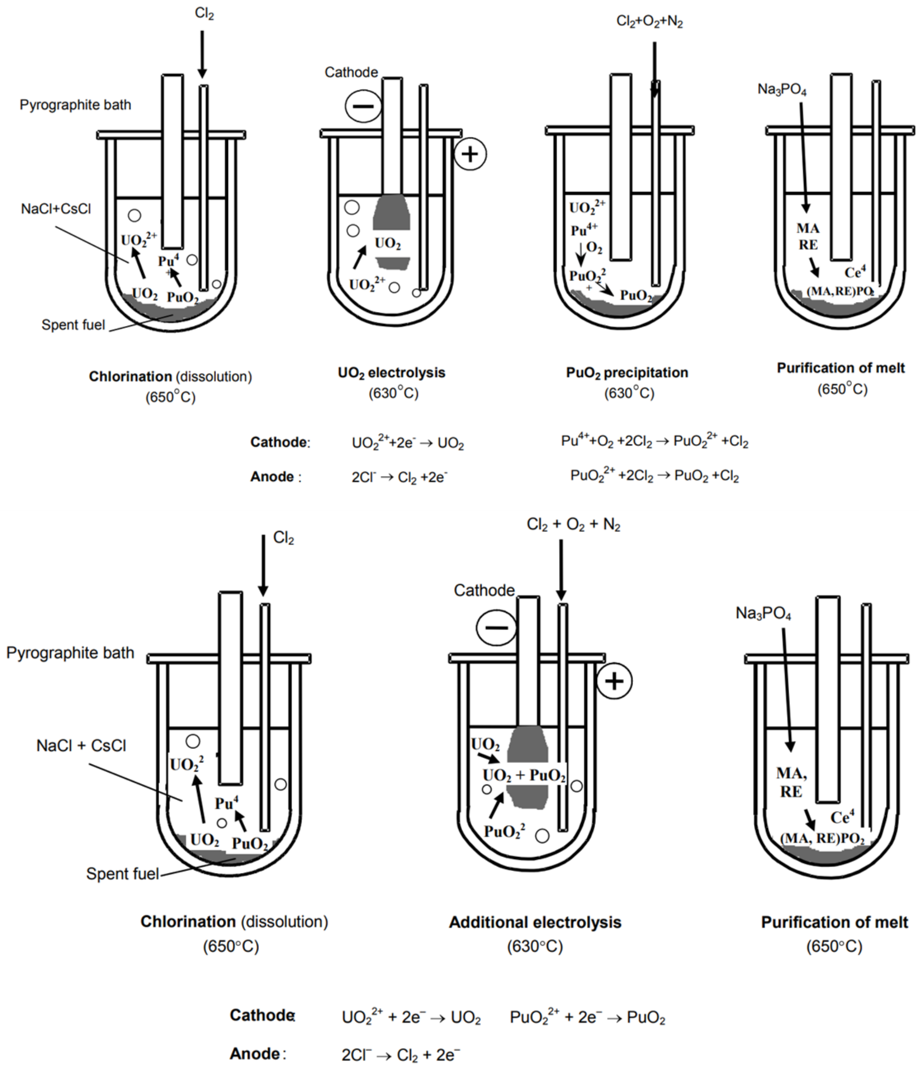

Figure 1.6: Sequence of operations for pyro-electrochemical reprocessing (DDP process) of spent UO_2 and PuO_2 fuels [21]

1.5.2 Aqueous Reprocessing

Aqueous processes for spent nuclear fuel reprocessing were deployed around 1940s to extract the plutonium from the spent fuel to meet the requirements of World War II. In 1943, several aqueous processing methods were proposed for separating the relatively small quantity of plutonium from the uranium and fission products. ORNL produced the first macroscopic quantities (grams) of separated plutonium with these processes.

The history of the development of various processes for nuclear fuel reprocessing [22] namely, Bismuth Phosphate, REDOX, PUREX and Trigly processes. The time-line of deployment of these processes is shown in Fig. 1.7 [23].

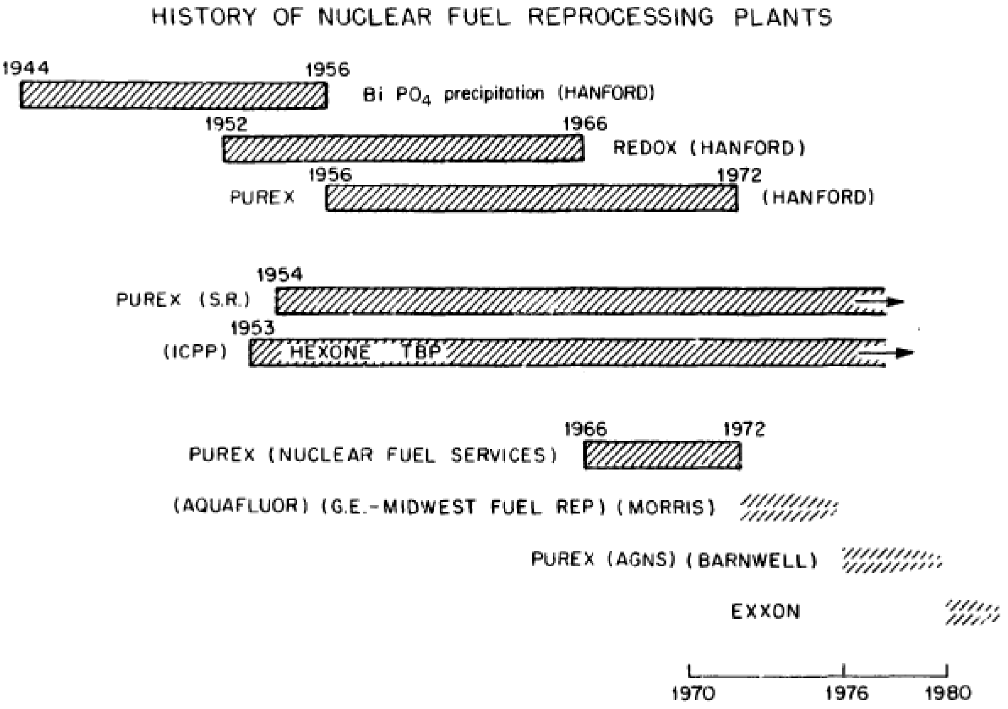

Figure 1.7: History of nuclear fuel reprocessing processes [23]

1.5.2.1 Bismuth phosphate process

Manhattan Project, in Hanford, USA is the first reprocessing plant, which produced Pu with significant quantities by adopting Bismuth Phosphate precipitation process. The method was developed and tested at the ORNL to produce plutonium for weapons programs. Bismuth phosphate is a co-precipitation process and its principles are shown in below equations.

$$Pu(s) + X(s) \xrightarrow{HNO_3, H_2SO_4} Pu^{4+}(aq) + X^{y+}(aq) \quad (1.3)$$

$$Pu(s) + X(s) \xrightarrow{HNO_3, H_2SO_4} Pu^{4+}(aq) + X^{y+}(aq) \quad (1.4)$$

$$Pu^{4+}(aq) + X^{y+}(aq) + Bi^{3+}(aq) \xrightarrow{H_3PO_4} Pu_3(PO)_4(s) + X^{y+}(aq) + BiPO_4(s) \quad (1.5)$$

$$Pu_3(PO)_4(s) + BiPO_4(s) \xrightarrow{HNO_3,\text{Oxid.agent}} Pu^{6+}(aq) + Bi^{3+}(aq) \quad (1.6)$$

$$Pu^{6+}(aq) + Bi^{3+}(aq) \xrightarrow{H_3PO_4} Pu^{6+}(aq) + BiPO_4(s) \quad (1.7)$$

$$Pu^{6+}(aq) \xrightarrow{H_2O_2} PuO_2{}^{2+}(aq) \xrightarrow{\text{Red.agent}} Pu(s) \quad (1.8)$$

X(s) = fission products or Uranium; $^{y+}$ = oxidation state

It is a batch process with frequent manual intervention resulting in a considerable level of radiation exposures and it does not facilitate the U recovery.

1.5.2.2 Redox process

The redox process is also called as Hexone process. It is the first solvent extraction process used on a plant scale. It was developed by ANL and tested in ORNL in pilot scale during 1948 and 1949. Hanford plant of the U.S. Atomic Energy Commission was operated using this process from 1952 to 1967. Replacement of complex bismuth phosphate process by redox solvent-extraction process resulted in huge cost saving.

Hexone (Methyl Isobutyl Ketone, MIBK) is used as a solvent that was already being used for uranium purification from its ore. In the redox process, hexone extract selectively uranyl and plutony nitrates from fission product nitrates in presence of adequate nitrate concentration in the aqueous phase. Hexone undergoes decomposition by concentrated nitric acid. To overcome the acid degradation, aluminum nitrate is used as a salting out agent to maintain low nitric acid concentration.

A simplified schematic flow sheet [24] for the first cycle of a Redox process is shown in Fig. 1.8 to illustrate how the basic separations of uranium, plutonium, and fission products were made. This process was much better than the bismuth phosphate process with respect to plutonium recovery and its operability/adaptability in continuous mode. Major disadvantages in the above process are (i) high solubility of solvent, (ii) low flash point, (iii) high toxicity of hexone, (iv) large waste volumes due to the salting out agent (aluminum nitrate).

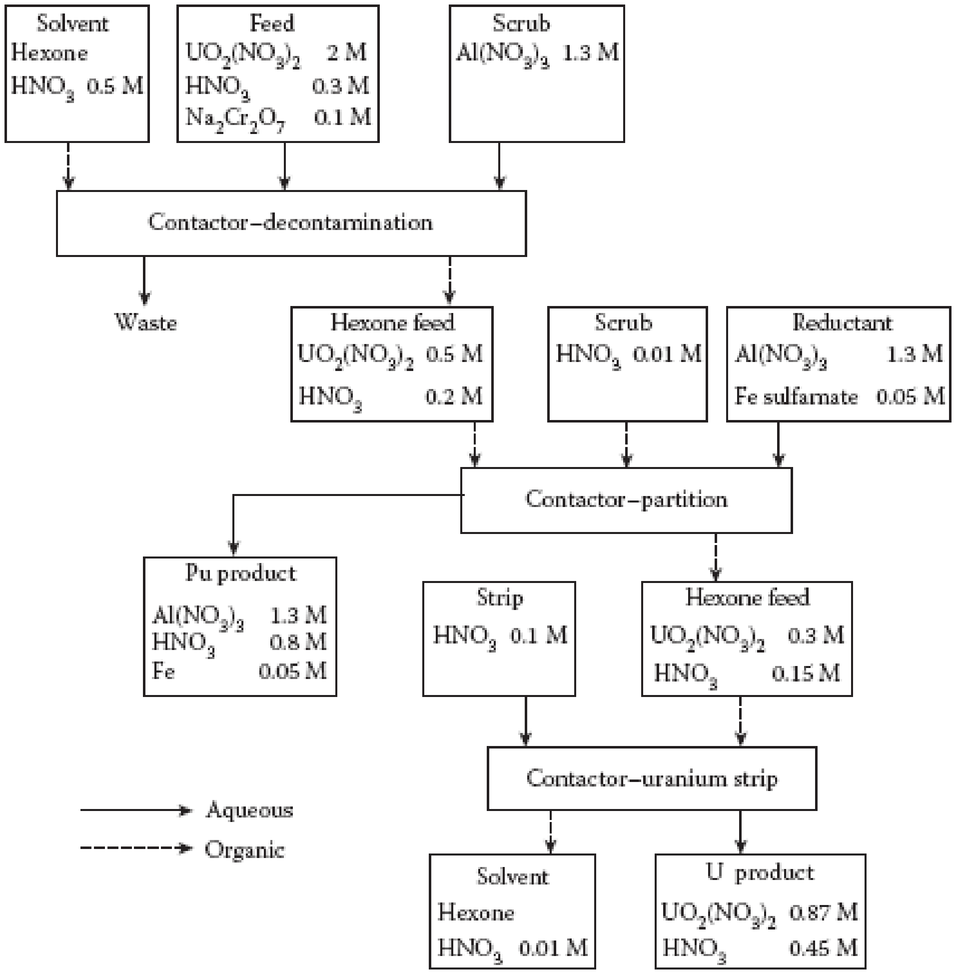

Figure 1.8: Process flow sheet for first cycle acid Redox process [24]

1.5.2.3 Trigly process

The "Trigly" process was developed at Chalk River, Ontario and it is probably the first solvent extraction process applied on a plant scale [25]. The solvent is triglycol dichloride and it is used in the first extraction cycle and hexone and thenoyltrifluoroacetone (HTTA) are used in plutonium purification cycles in the above process. It has several advantages over the redox process such as (i) better extractability of plutonium over uranium and fission products, (ii) trigly is relatively stable to concentrated nitric acid and (iii) a higher flash point of 121^{o}C.

The plutonium separation plant using this process was started in late 1948. The process involves (i) dissolving the aluminium sheathing from the spent uranium metal of NRX fuel rods by caustic soda, (ii) dissolving the uranium by nitric acid, (iii) conditioning the dissolver solution with ammonium nitrate, (iv) extraction of plutonium with trigly, (v) scrubbing the trigly extract with ammonium nitrate and nitric acid and (vi) precipitating the plutonium as a phosphate. The precipitation had never worked properly and it is replaced with hexone process. Ammonium nitrate used for conditioning was undesirable and it posed a serious explosion hazard. Hence the above process was modified with uranyl nitrate and tri-n-butyl phosphate (TBP) in place of aluminium nitrate and hexone respectively. Usage of multiple extractants and two separate precipitation-dissolution cycles suffered from excessive complexity and it failed to recover uranium. The plant was shut down in 1954 when development work on an alternative process using anion exchange showed more promise.

1.5.2.4 Butex process

The process was developed by British scientists at Chalk River, Canada for uranium and plutonium separation from the fission products and its decontamination factor (DF) was in the order of 10^8. Two solvents were used in this process and they are (i) undiluted dibutyl carbitol (Butex) for primary separation and uranium purification and (ii) 20% TBP in kerosene for plutonium purification. The main advantages of this process compare to REDOX process is (i) no addition of salting agent so that the nitric acid can be recovered and waste volume with fission product can be reduced by evaporation. Spence et al. [26] and Howells et al. [27] have given a complete account of the developments of the chemical aspects and chemistry of butex process, respectively.

Butex process flow sheet is shown in Fig. 1.9 [24]. In this process, 3M nitric acid used as a scrubbing agent in the initial solvent extraction cycle which enables to concentrate the highly radioactive raffinate stream considerably. As butex is not stable in highly concentrated nitric acid, ammonium nitrate is used as salting agent were high nitrate concentrations are needed. Main disadvantages of Butex process are (i) high viscosity, (ii) high density (iii) tendency to form crystalline uranium complexes of the type $UO_2(NO_3)_2.3H_2O.C_{12}H_{26}O_3$, (iv) complication in the process operation due to employment of two solvents, and (v) usage of explosive ammonium nitrate in the process.

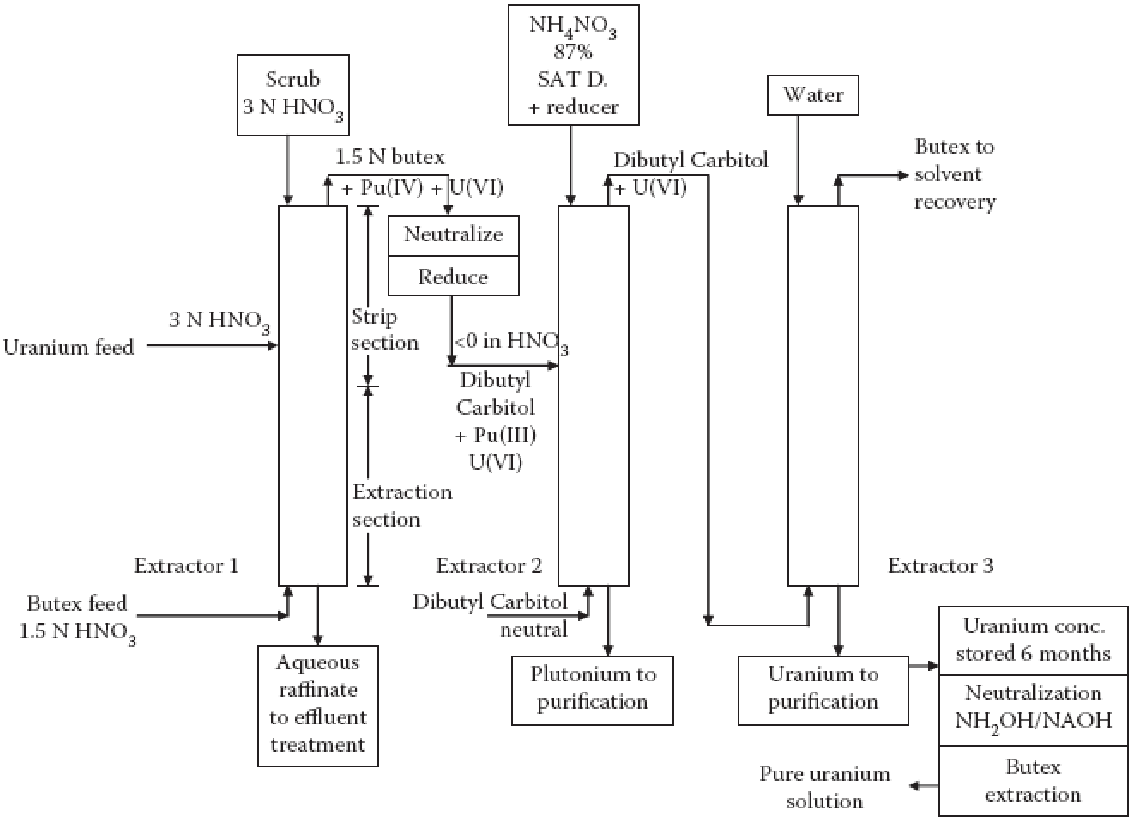

Figure 1.9: Schematic process flow sheet for Butex process [24]

1.5.2.5 PUREX process

PUREX (Plutonium Uranium Reduction Extraction [28]) process is a TBP based process and it was developed at the Knolls Atomic Power Laboratory and demonstrated at Oak Ridge pilot plant in 1952. It is very similar to Hexone process, with following advantages (i) low solvent volatility, (ii) low flammability, (iii) low solvent solubility in nitric acid and (iv) TBP has good radiation and chemical stabilities compared to the other competing solvents of the candidate processes. It was put into initial production at the Savannah River Site in 1954.

It is the most widely used reprocessing technology in the world. The PUREX process replaced the redox process at Hanford in 1956 and has since been used in countries such as the Russia, India, Germany, France, and Japan.

TBP diluted with a kerosene-type hydrocarbon is used as a solvent in PUREX process. Fig. 1.10 [24] shows the general schematic of the process flow sheet. Several variations of this process have been adopted not only to recover plutonium and uranium but also neptunium. This process was originally developed for low plutonium bearing thermal reactor fuels, but now it is adopted for plutonium rich fast reactor and Mixed Oxide (MOX) fuels of thermal reactors also.

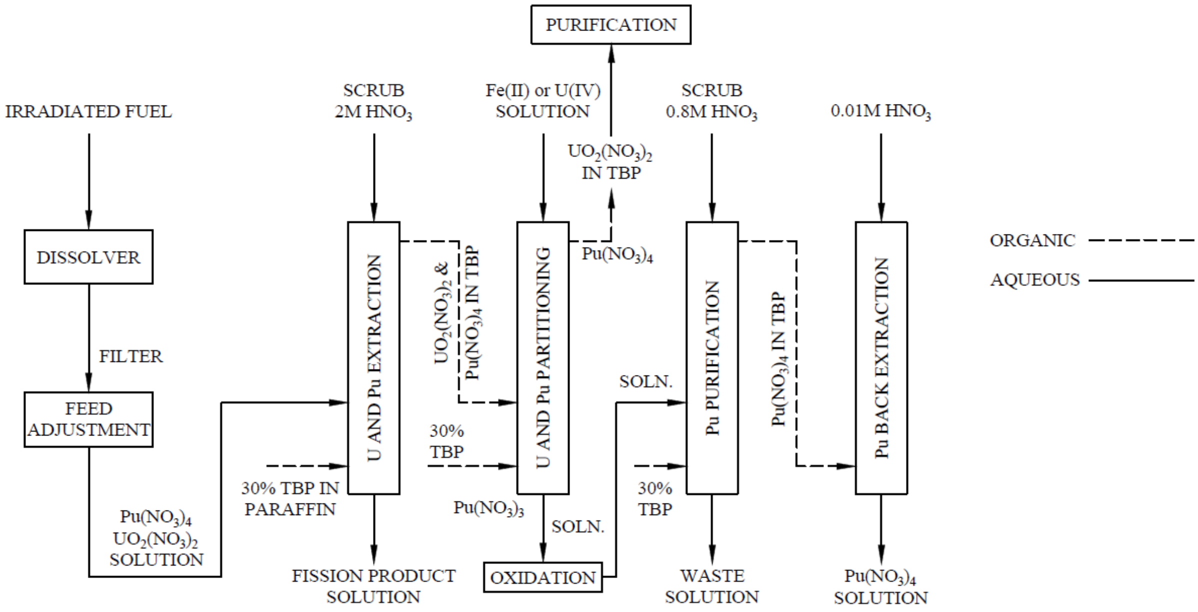

Figure 1.10: Simplified PUREX process flow sheet [24]

1.6 Three stages of Indian Nuclear Power Program

The Indian Nuclear Power Programme (INPP) was formulated by Dr. Homi Jehangir Bhabha for meeting the increasing energy demands of independent India. Self-reliance and energy security are the key objectives of this programme. The adoption of this unique three-stage programme is based on the optimum utilization of the indigenous resource profile of modest uranium resources and abundant thorium in our country. The three stages of Indian Nuclear

Power Programme are shown in Fig. 1.11. The first stage consists of the natural uranium fuelled Pressurized Heavy Water Reactors (PHWRs) which are already in the commercial domain in our country. The second stage consists of Fast Breeder Reactors (FBRs) which are in the technology demonstration stage. The third stage is comprised of the thorium based reactors fuelled with U-233 which is in the technology development stage.

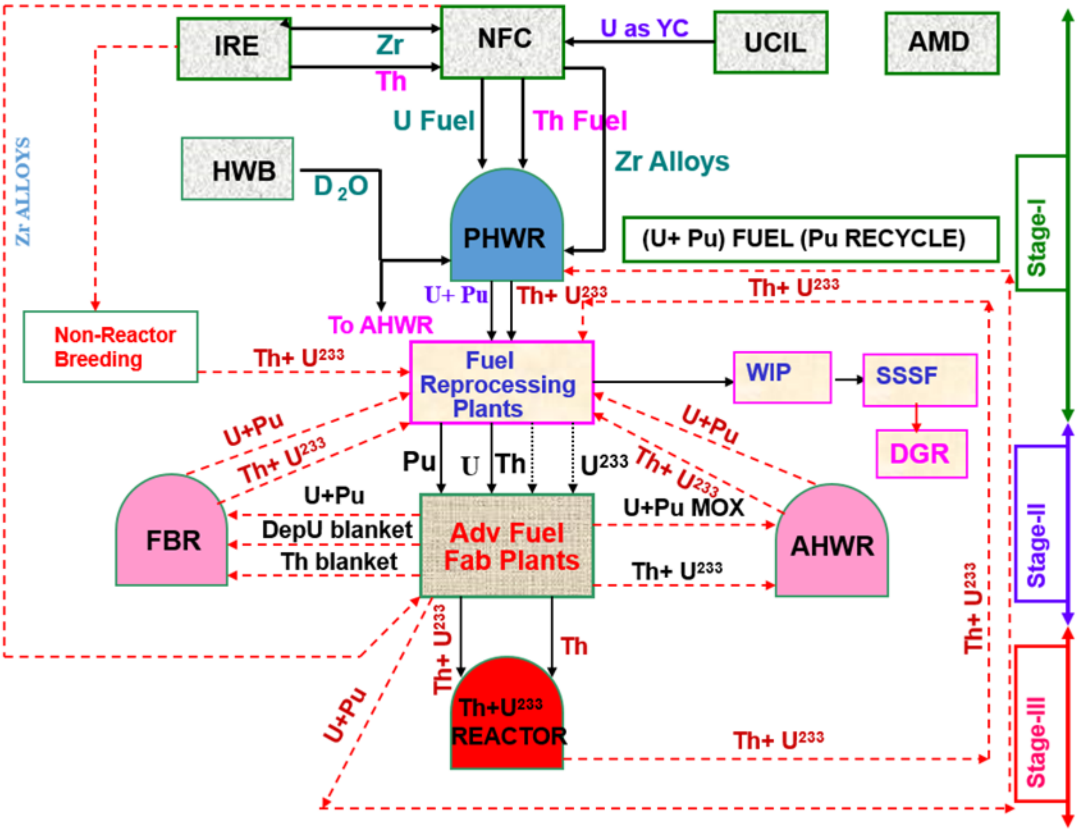

Figure 1.11: Three-Stage Nuclear Power Programme

PUREX process is work horse for 1st and 2nd stage nuclear programme to close the fuel cycle by separating and recycling the uranium and plutonium from spent nuclear fuel coming from thermal and fast breeder reactor.

1.7 PUREX process and detailed process steps

The TBP based solvent extraction process was first suggested by Warf [29] for the recovery of Ce(IV) from rare earth nitrates. It is the most widely used aqueous reprocessing technology in the world. CRC press has published a three volume monograph entitled “The Science and

Technology of Tributyl Phosphate” owing to the large scale application in the nuclear industry. The 3rd volume is dedicated to nuclear fuel reprocessing [30].The major process steps are explained in details and its general flow sheet is given in Fig. 1.12 [31].

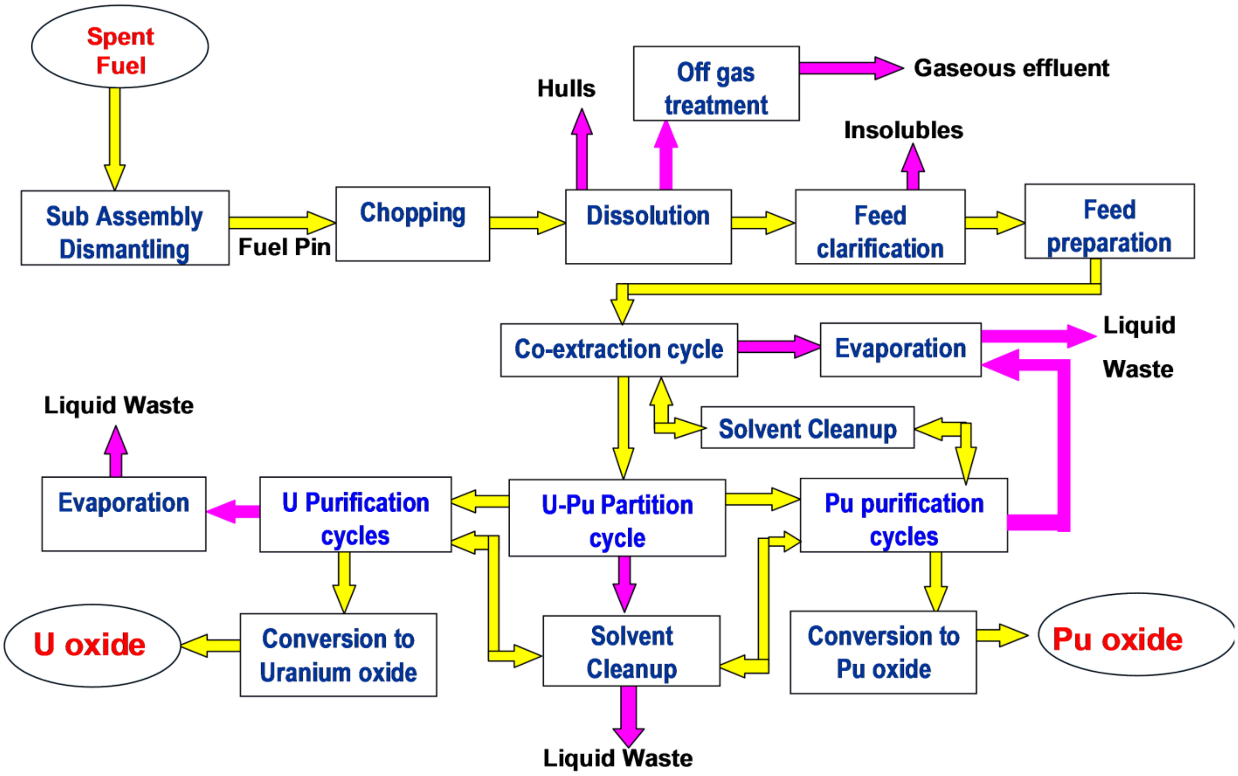

Figure 1.12: PUREX process flow sheet [31]

1.7.1 Head end treatment

Following steps are involved in head end treatment and they are (i) dismantling of sub assembly, (ii) chopping to enable dissolution of fuel for which the fuel has to be exposed to nitric acid medium, (iii) dissolution of chopped fuel in nitric acid, (iv) feed clarification to remove undissolved particles and (v) conditioning of the resulting solution suitable for the subsequent solvent extraction. To enable co-decontamination which is the first step in the solvent extraction, the valencies of U and Pu are adjusted to U(VI) and Pu(IV) in the nitric acid medium. Under these conditions both U and Pu are highly extractable.

1.7.2 Solvent extraction

In co-decontamination cycle, uranium and plutonium are co-extracted in to 30% TBP leaving fission product in the aqueous phase. The extraction mechanism of U and Pu is by the formation of covalent bonds by UO_2^{2+} & Pu^{4+} with the solvent TBP to form organic soluble complexes. The following equations show the stoichiometry equation for U and Pu with TBP solvent:

$$UO_2^{2+} + 2NO_3^- + 2TBP \rightarrow UO_2(NO_3)_2.2TBP \qquad (1.9)$$

$$Pu^{4+} + 4NO_3^- + 2TBP \rightarrow Pu(NO_3)_4.2TBP \qquad (1.10)$$

U and Pu are separated from each other in partitioning cycle by reducing selectively Pu_4^+ to Pu_3^+ while retaining U as UO_2^{2+}. The lesser extractability of Pu_3^+ is exploited for this purpose. Uranium in the solvent stream is back extracted in to aqueous phase in stripping stage using dilute nitric acid. Both uranium and plutonium product streams are purified further in separate solvent extraction cycles using the above principle. The distribution co-efficient is defined as ratio of concentration of component in organic phase to concentration of component in aqueous phase. Distribution co-efficient [24] of various species in 30% TBP with nitric acid concentration is shown in below Fig. 1.13.

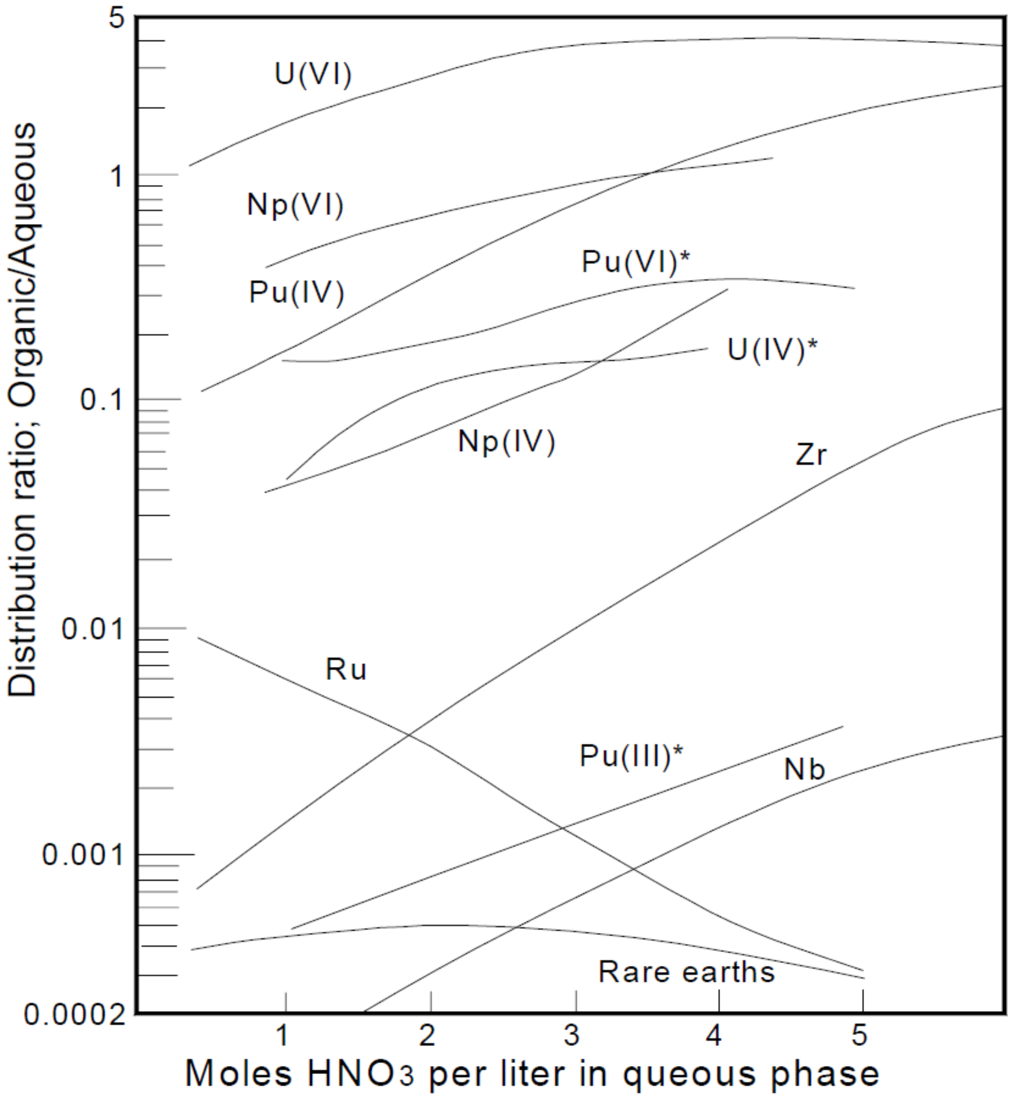

Figure 1.13: Effect of HNO_3 concentration on the distribution coefficient in 30% TBP [24]

1.7.3 Reconversion

In this step, uranyl nitrate and plutonium nitrate salt solution is precipitated and converted into their respective oxides. Plutonium is precipitated as its oxalate using oxalic acid. During calcination, above precipitate is converted into its oxide. Similarly, U from the uranyl nitrate solution is either directly denitrated or precipitated as ammonium diuranate with ammonium hydroxide which is then calcined, for getting uranium oxide. These oxides are sent for refabrication and conversion to fuels for reuse in the reactor.

1.7.4 Auxiliary steps

To reduce waste volumes, (i) solvent washing step is included to recycle the solvent by removing the degradation products and (ii) Evaporation step is included in the aqueous route to reduce the aqueous radioactive waste volume for long term storage before final disposal.

1.7.5 Vitrification

This is a major step in waste conditioning where more than 99% of the fission products are converted to vitrified solid for final disposal.

1.7.6 Additional steps

There are always efforts to modify the flow sheet from the point of view of improving the recoveries and purities of uranium and plutonium, reduce the waste volumes and simplify and reduce the process steps for economy of operation. Recently directions are towards removing the long lived actinides and fission products from the high active raffinate wastes to reduce the volume of wastes that are required to be monitored for a very long time. Efforts have been also made to modify the process steps such that plutonium as a pure stream is avoided as a measure of proliferation resistance.

1.8 Scope of studies

Boudry and Miquel [32] explored the possibility of adapting the PUREX process for the reprocessing of Fast Reactor spent fuels. Though the well-established PUREX process was deployed for both Thermal Reactor Fuel Reprocessing and Fast Reactor Fuel Reprocessing, modifications in the process flow sheet and development in the design of the equipment have been made in Fast Reactor Fuel Reprocessing. This was primarily due to the high Pu inventories (up to 70% in fast reactor spent fuel as compared to 0.03% in thermal reactor spent fuel) and high specific activities (5.6×10^{13} Bq/kg as compared to 6.5×10^{12} Bq/kg) in the irradiated fuel from fast reactors. No country than India is pursuing developmental work in the area of Fast Reactor Fuel Reprocessing at present. Designing of fast reactor reprocessing equipment [33] is highly challenging as these equipment should satisfy the following criteria: (i) minimum operating life should be about 40 years, (ii) they should either be maintenance free or remotely maintainable, (iii) they should not lose their mechanical and chemical properties due to high radiation background and (iv) shape and size should meet the criticality safe condition.

Centrifugal extractor is a candid candidate for fast breeder reprocessing solvent extraction operation and it comes under stage wise equipment. It requires minimum eight stages for separation of U and Pu from fission products. Several design modification were incorporated in centrifugal extractor as per process condition and its application. Still it needs rational and reliable design procedures for nuclear reprocessing application. One of its main disadvantage is it requires frequent maintenance due to high rotation speed.

(i) Design of annular centrifugal extractor is based on dispersion number [34] measured by batch experiments and its internal sizings are based on thumb rules [35]. Kadam et al. [36] developed dispersion number correlation for gravity (batch) and centrifugal extractor (continuous system) separately. Still, there was no unified correlation for dispersion number.

(ii) During multistage operation, failure of any stage motor/bearing in the centrifugal cascade leads to stoppage of entire cascade and it takes hours to change the ACE motor/bearing by remote operation. During maintenance, solvent present inside the cascade undergoes radioactive degradation and leads to plutonium loss and reduces the decontamination factor. To ensure ACE cascade smooth operation during motor/bearing failed condition, two types of overflow line was suggested in literature and they are (i) horizontal overflow line [37, 38] and (ii) two overflow line [39] (separate overflow lines for aqueous and organic phase) which leads to recirculation during normal operation. Internal recirculation leads to radiation degradation of the solvent and above methods cannot be implemented in the nuclear reprocessing application.

(iii) Flow inside the rotating bowl is one of the grey areas in annular centrifugal extractor design. CFD (Computational Fluid Dynamic) simulation helps to understand the flow behaviour inside any complex geometry. Patra et al. [40] simulated single phase CFD simulation in the rotor region and calculated the pumping capacity of CE with different bowl diameters. Two-phase and three-phase CFD simulations [41, 42] also reported in the literature but there were no systematic study such as mesh independent test, model selection, etc.

(iv) Annular centrifugal extractor is widely used in solvent extraction operation, especially in fast reactor reprocessing application. Flow fluctuation in annular centrifugal extractor system drastically affects the steady state operation and reduces its mass transfer performance [43]. In fast reactor reprocessing flow sheet, throughputs for aqueous and organic phases varies from few mL/min to L/min. Air lift pumping system is not suitable for low throughput metering operation. Other fluidic pumps are also not suitable for low throughput as well as metering operation. To address this issue, an alternate pump suitable for reprocessing operation should be developed.

1.9 Objective

The main objectives of the present work are,

- Development of unified correlation for dispersion number for the design and scale-up of settling zone in liquid-liquid settler for both batch and continuous operations (annular centrifugal extractor rotating bowl). It would help one to couple the simplicity of gravity settling experiments with the ability of predicting the settling capacity of centrifugal separators (as these represent the two extreme of acceleration fields). The developed correlation could be used for the design of gravity or centrifugal separators especially for high radioactive or hazardous system where measurement of dispersion number is impossible.

- Development of novel annular centrifugal extractor stationary bowl to handle adverse condition, especially for motor/bearing failed conditions. Inter-stage inclined overflow design ensures smooth flow of aqueous and organic phases in multistage annular centrifugal extractor from motor failed bowl to corresponding adjacent bowls without shutting the entire stages.
- Design procedure for annular centrifugal extractor is purely empirical. In literature, there is no detailed systematic analysis of flow dynamics inside the rotor region. Flow dynamics inside the rotor region was studied using 2D CFD simulation with different turbulent models. Simulation results with different turbulent models were compared with an experimental result to select the suitable turbulent model for 3D multiphase ACE simulation.
- Helical coil based fluidic pump has been developed and demonstrated to replace the existing pumps to ensure smooth operation of annular centrifugal extractor especially at low throughput flow sheet condition. CFD simulation also done to understand the effect of design parameter in helical coil based fluidic pump performance.

1.10 Summary

In this chapter, a brief background of the problems considered in the present study has been given. Broad outlines of the thesis and salient features of the respective chapters have also been highlighted.

1.11 References

1. P. N. Stearns, “The Industrial Revolution in World History”, *Taylor & Francis Inc*, **2013,** *4th Edition*.
2. “Renewable in Global Energy Supply - Fact Sheet”, *International Energy Agency, IEA publications*, **2007**.
3. “Key World Energy Statistics”, *International Energy Agency, IEA publications*, **2017**.

4. H. H. Rogner, A. Popescu, “Chapter 1. World Energy Assessment”, *UNDP (2000),* **2000**.
5. “Comparison of Lifecycle Greenhouse Gas Emissions of Various Electricity Generation Sources”, *World Nuclear Association, WNA Report,* **2011**.
6. S. Glasstone, A. Sesonske, “Nuclear Reactor Engineering”, *Springer Science,* **1994,** *4th Edition, Vol. II.*
7. “Country nuclear fuel cycle profiles”, *Technical report series No. 425, IAEA*, **2005,** 2nd Edition, ISBN 9201148038.
8. J. Bouchard, “The Gen IV roadmap: The way towards sustainable development of nuclear energy”, *IAEA workshop on Energy Technology, Energy Technology Roadmaps, May 15-16,* **2008,** IEA, Paris, France.
9. K. D. Kok, “Nuclear Engineering Handbook”, *CRC Press,* **2016,** *2nd Edition*.
10. “Nuclear Energy Data 2007”, *OECD Nuclear Energy Agency*, ISBN 9789264034532.
11. M. J. Steindler, L. J. Anastasia, L. E. Trerorrow, A. A. Chilenskas, “Laboratory-Development Of The Fluoride Volatility Process For Oxidic Nuclear Fuels”, *Nucl. Met., Met. Soc. AIME,* **1969,** *15,* 177-210
12. G. Strickland, F. L. Horn, “Nitrofluor process - a non-aqueous fluoride-volatility method for recovering uranium and plutonium from various reactor fuels”, *Progress in Nuclear Energy, Series III, Process Chemistry,* **1970,** *4*, 399-425.
13. General Electric Company, “Design and Analysis of Midwest Fuel Recovery Plant”, **1967,** Report Docket 50-268.
14. General Electric Company, “Midwest Fuel Recovery Plant Technical Report”, **July 5, 1974**.
15. W. A. Rodger, “Reprocessing of Spent Nuclear Fuel”, *Presentation to California Energy Resources Conservation and Development Commission,* **Mar. 7, 1977**.
16. C. E. Stevenson, “EBR-II Fuel cycle story”, *Amer. Nucl. Soc.,* **1987**
17. M. Goff, “Treatment of Spent Nuclear Fuel with Molten Salts”, *Idaho National Laboratory (2008) Joint Symposium on Molten Salts, October 20,* **2008,** Kobe, Japan
18. L. Burris, Jr., I. G. Dillon, R. K. Steunenberg, “The EBR-II Skull Reclamation Process, Part I. General Process Description and Performance, **1964,** ANL-6818.

19. K. M. Harmon, G. Janse, Jr., “The Salt Cycle Process”, *Prog. in Nucl. Ener. Series III, Process Chemistry,* **1970,** *4,* 429
20. J. B. Knighton, R. K. Steunenberg, “Preparation of metals by Magnesium-Zinc Reduction. Part III. Reduction of Plutonium Dioxide”, **1965,** ANL-7059.
21. Pierre Joly, Eva Boo, “ROADMAP, Actinide separation process 2015”, *SACSESS,* **2015**
22. F. Baumgartner, *Fortschr. chem. Forschg.,* **1969,** *12(712).*
23. E. D. North, “Nuclear fuel reprocessing”, CONF-830788-1, **1983 Jan 01**
24. M. Benedict, T. H. Pigford, H. W. Levi, “Nuclear Chemical Engineering”, *Mc Graw Hill Book Co., N.Y.,* **1981,** *2nd Edition.*
25. W.M. Campbell, “Canadian Fuel Reprocessing”, *Nucleonics,* **1956,** *14(92).*
26. R. Spence, “Chemical Process Development for the Windscale Plutonium Plant”, *J. Roy. Inst. Chem.,* **1957,** *81,* 357.
27. G. R. Howells, T. G. Hughes, D. R. Mackey, K. Saddington, “The chemical processing of irradiated fuels from thermal reactors”, *Proc. The Second United Nations International Conference on the Peaceful Uses of Atomic Energy, Geneva,* **1958,** *17,* 3-21.
28. W. B. Lanham, T. C. Runion, “Purex Process for Plutonium and Uranium Recovery”, *USAEC,* **1949,** ORNL-479.
29. J. C. Warf, “Extraction of cerium(IV) nitrate by butyl phosphate”. *J. Am. Chem. Soc.,* **1949,** *71,* 3257–3258.
30. W. W. Schulz, L.L. Burger, J. D. Navratil, K.P. Bender (Eds), “Science and Technology of Tributyl Phosphate”, *CRC Press Inc., Boca Raton,* **1984,** *Vol. III.*
31. R. Natarajan, “Reprocessing of spent nuclear fuel in India: Present challenges and future programme”, *Prog. Nucl. Energy,* **2017,** *(101A),* 118-132.
32. P. Miquel, J. C. Boudry, “Adaptation of The Purex Process to the Reprocessing Of Fast Reactor Fuels”, *International solvent extraction conference, Lyon (France),* **1974**.
33. R. Natarajan, B. Raj, “Fast Reactor Fuel Reprocessing Technology in India", *J. Nucl. Sci. Technol.,* **2007,** *44(3),* 393-397.

34. R. A. Leonard, G. J. Bernstein, R. H. Pelto and A. A. Ziegler, "Liquid-liquid Dispersion in Turbulent Couette Flow", *AIChE J.,* **1981,** *27(3),* 495-503.

35. R. A. Leonard, "Design principles and applications of centrifugal contactors for solvent extraction", *In Ion Exchange and Solvent Extraction edited by B. A. Moyer CRC Press, New York, USA,* **2010,** *Chapter 10,* 563-616.

36. B. D. Kadam, J. B. Joshi, S. B. Kogani, R. N. Patil, "Hydrodynamic and mass transfer characteristics of annular centrifugal extractors", *Chem. Eng. Res. Des.,* **2008,** *86,* 233-244.

37. R. T. Jubin, "Centrifugal contactor modified for end stage operation in a multistage system", *US Patent 4925441,* **May 15, 1990.**

38. T. Washiya, M. Takeuchii, H. Ogino, S. Aose, "Development of centrifugal contactor system in JNC", *Proceedings of the GLOBAL 2005, Tsukuba, Japan, October 9–13,* **2005**.

39. Duan W., Song C., Wu Q., Zhou X., Zhou J., "Development and Performance of a New Annular Centrifugal Contactor for Semi-Industrial Scale", *Sep. Sci. Tech.,* **2005,** *40,* 1871–1883.

40. J. Patra, N. K. Pandey, U. K. Mudali, R. Natarajan, J. B. Joshi, "Hydrodynamic Study of Flow in the Rotor Region of Annular Centrifugal Contactors Using CFD Simulation", *Chem. Eng. Comm.,* **2013,** *200,* 471-493.

41. K. E. Wardle, T. R. Allen, R. Swaney, "CFD Simulation of the Separation Zone of an Annular Centrifugal Contactor", *Sep. Sci. Technol.,* **2009,** *44,* 517-542.

42. S. Li, W. Duan, J. Chen, J. Wang, "CFD Simulation of Gas−Liquid−Liquid Three-Phase Flow in anAnnular Centrifugal Contactor", *Ind. Eng. Chem. Res.,* **2012,** *51,* 11245-11253.

43. R. A. Leonard, D B. Chamberlain, C. Coneer, "Centrifugal Contactors for Laboratory-Scale Solvent Extraction Tests", *Sep. Sci. Technol.,* **1997,** *32(1),* 193-210.

CHAPTER 2

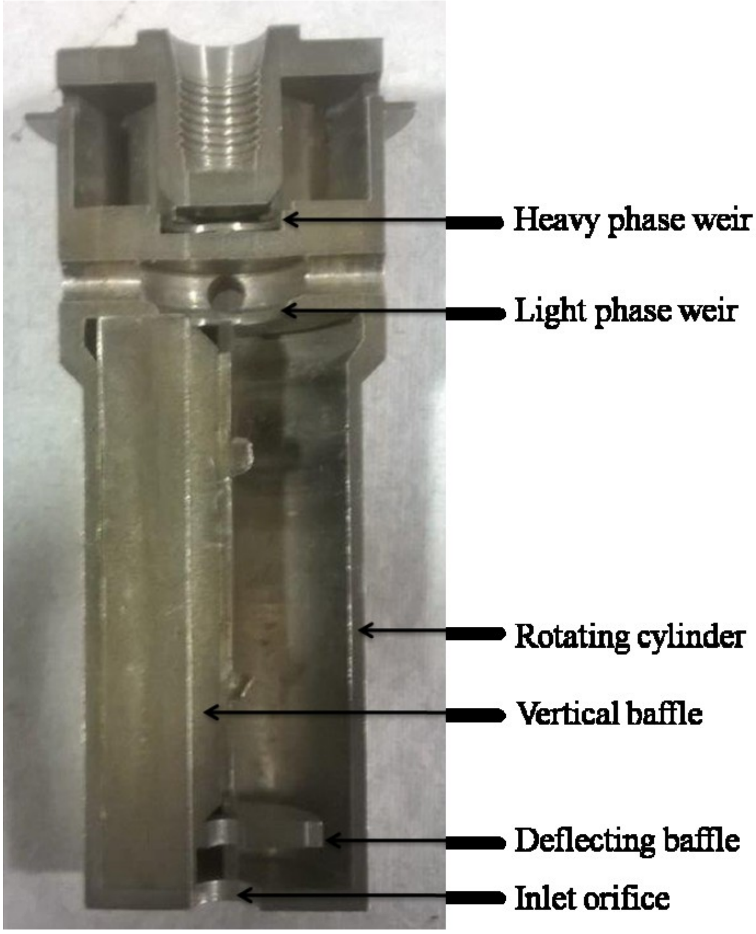

Cut view of Annular Centrifugal Extractor rotating bowl

BASICS OF SOLVENT EXTRACTION AND CENTRIFUGAL EXTRACTOR

2 BASICS OF SOLVENT EXTRACTION AND CENTRIFUGAL EXTRACTOR

2.1.1 Solvent extraction

Liquid-liquid extraction commonly known as solvent extraction is a technique for separating the components of a solution by distributing between two phases. Liquid extraction employs an added solvent as the separating agent. The solvent is immiscible (or partially miscible) with the feed solution. The separation is achieved by taking into account the difference in relative solubilities of the desired component in the liquid feed at solvent phase. Two streams result from this contact, the extract is the solvent rich solution containing the desired extracted solute and the raffinate is a residual feed solution containing little solute. The simplest form of extraction is a single stage extraction. A higher degree of separation is achieved in a multistage extraction.

Liquid-liquid extraction has an important role in chemical, petroleum, petrochemical, pharmaceutical and in nuclear chemical engineering applications. Liquid–liquid extraction is the most sought unit operation after distillation. It is utilized for separation of components using liquid solvents. It is a unique process and efficiently used for heat sensitive, close boiling components and for separation of components not possible by other unit operations. Extraction process main advantage is it operates at ambient temperature, which makes it more attractive compared to distillation, evaporation and other processes of separation in terms of energy conservation. The application of liquid extraction falls in various categories, those where extraction is directly compared with other unit operations like distillation, evaporation, centrifuging and crystallization etc and those where it is uniquely qualified.

The mixing in the liquid extraction provides a large interfacial area so that efficient mass transfer can occur. The liquid-liquid dispersion created during the mixing is then separated by gravity or by centrifugal force depending upon the type of extractor selected. The mixing and separation steps constitute one stage of extraction. The solvent is generally chosen to selectively extract certain components from the feed solution.

2.1.2 Liquid-liquid extraction-principle

Principle is based on an unequal distribution of substances to be separated between two insoluble phases. When an aqueous solution (nitric acid with uranium) of an extractable component (uranium) is brought in to equilibrium with an immiscible solvent (30% TBP in nDD) for the component and the two phases are then separated, the component (uranium) will be found distributed between the two phases. The distribution is characterized by the distribution coefficient, D, defined as

$$\mathrm{D} = \frac{\text{Concentration of componenet in organic phase}}{\text{Concentration of component in aqueous phase}} = \frac{\mathrm{y}}{\mathrm{x}} \qquad (2.1)$$

for the two phases leaving the equilibrium contactor.

A high value of the distribution coefficient is desirable because the volume of the solvent required is small. The distribution coefficient is a function of the nature of the solvent, the temperature and the equilibrium composition of the aqueous and organic phases, but it is independent of the amount of either phase.

In fractional extraction, when a separation is to be made between two extractable components, the ratio of their distribution coefficients should differ from unity as much as possible.

The concentrations of component A in organic phase y_A and aqueous phase x_A leaving a stage are related by

$$y_A = D_A\, x_A \qquad (2.2)$$

The concentrations of component B in organic phase y_B and aqueous phase x_B leaving a stage are related by

$$y_B = D_B\, x_B \qquad (2.3)$$

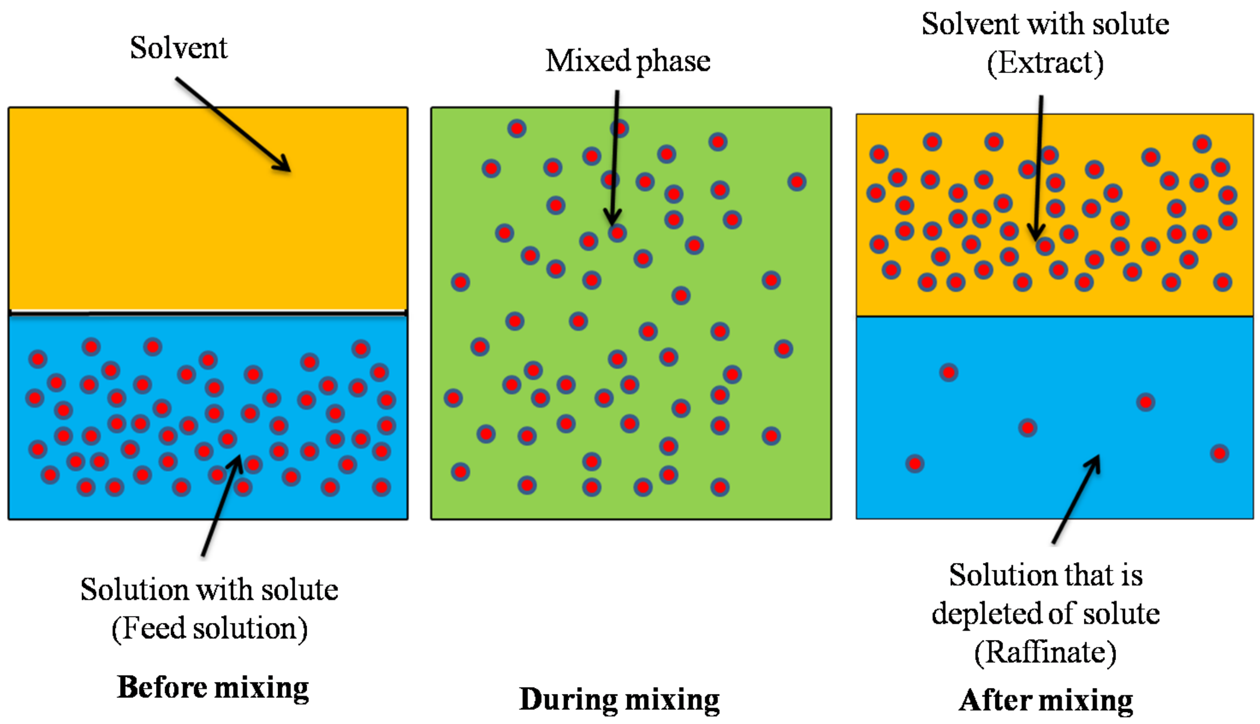

Figure 2.1: Basics of the solvent extraction

The ratio of concentrations in the organic phase is related to the ratio of concentrations in the aqueous by

$$\frac{y_A}{y_B} = \frac{D_A x_A}{D_B x_B} \tag{2.4}$$

The separation is possible when $D_A/D_B \neq 1$.

The ratio of distribution coefficients is a measure of the difficulty of a separation by fractional extraction and is known as the separation factor α_{AB}, which is analog of relative volatility in distillation:

$$\alpha_{AB} = \frac{y_A / x_A}{y_B / x_B} = \frac{D_A}{D_B} \tag{2.5}$$

The following has to be evaluated for the operation of extraction processes.

- Solvent selection
- Operating conditions

- Mode of operation
- Factor affecting extraction efficiency

2.1.3 Solvent selection

The key to an effective extraction process is the discovery of a suitable solvent. A good solvent should meet the following requirements:

(i) **Selectivity:** The solvent should be selective for the desired solute over impurities, i.e., the ratio of distribution coefficients should be high.

(ii) **Capacity:** A high value of the distribution coefficient is desirable because the volume of solvent required is small, i.e., it should have ability to load high concentration of solute.

(iii) **Physical properties:** Its density should be different from the feed solution, and it should have low viscosity and fairly high interfacial tension. These physical properties are important in promoting separation of phases.

(iv) **Reversibility:** it should be readily stripped, i.e., distribution coefficients in stripping section should be less than unity.

(v) **Safety:** For safety reasons it should be relatively nonvolatile, nonflammable, and non toxic.

(vi) **Chemical and radiation stability:** It should be stable in the presence of chemical reagents used in the process. Solvents used for radioactive applications should also have good radiation stability.

Tri-butyl phosphate (TBP) meets most of the requirements except those of low viscosity and a density different from water. These deficiencies are corrected by diluting TBP with a light saturated hydrocarbon such as n-dodecane, kerosene, NPH. This solvent is one of the most commonly used at present in the reprocessing of spent nuclear fuels.

2.1.4 Operating conditions

Depending on the nature of the extraction process, the temperature, pH and residence time could have an effect on the yield and selectivity.

(i) **Operating pressure**: It has a negligible effect on extraction performance and therefore most extraction operation takes place at atmospheric pressure unless governed by vapour pressure considerations.

(ii) **Temperature:** It also used as a variable to alter the selectivity of the solvent. Elevated temperatures are sometimes used in order to keep viscosity low and thereby minimizing mass transfer resistance.

(iii) **pH:** It is significant in metal and bio extractions. In bio extractions (e.g. penicillin) and some agro chemicals (e.g. orthene), pH is maintained to improve distribution coefficient and minimize degradation of product. In metal extractions, kinetic considerations govern the pH. In dissociation based extractions of organic molecules, pH can play a significant role (e.g. cresols separation). Sometimes, the solvent itself may participate in undesirable reactions under pH conditions.

(iv) **Residence time:** Residence time is an important parameter in reactive extraction processes (e.g., metal separations, formaldehyde extraction from aqueous streams) and in processes involving short-life components (e.g.: antibiotics and vitamins).

(v) **Choice of continuous and dispersed phase:** The dispersed phase normally has the smaller holdup in column. For reason of inventory cost and fire hazard, it is more desirable to disperse the more costly or more flammable liquid. Mass transfer rate also greatly influenced by the direction of mass transfer. Mass transfer rate is higher in the case of continuous phase → dispersed phase whereas in dispersed → continuous phase coalescence rate is faster.

2.1.5 Mode of operation

Extractors can be operated in cross current or counter current mode.

(i) **Cross current mode:** It is mostly used in batch operation. Batch extractors have traditionally been used in low capacity multi-product plants such as pharmaceutical and agrochemical industries. For washing and neutralization operations that require very few stages.

(ii) **Counter current mode:** Cross current operation is particularly practical, economical and offers a great deal of flexibility. Though operation in cross current mode offers more flexibility, it is not very desirable due to the high solvent requirements and low extraction yields. For larger volume operation and more efficient use of solvent, counter current mixer-settlers or columns are employed. Counter current operation conserves the mass transfer driving force and hence gives optimal performance.

2.1.6 Factors affecting extraction efficiency

The design of the equipment is concerned with rate at which such process occurs. The rate of mass transfer between the liquid phases is described by

$$N_a = K\, a_i\, \Delta C \qquad (2.6)$$

By maintaining each of the last three items large, the rate of mass transfer is kept high.

The overall mass transfer includes

(i) Diffusional resistance residing within the disperse and continuous phases

(ii) Any resistance that may be found at the interface

2.1.7 Objective of liquid extraction theory

Liquid extraction theory has the objective of establishing quantitative relationship between system properties, equipment characteristics and relevant physical properties to enable extractor performance to be predicted over a wide range of operating conditions.

The theoretical treatment concerns two separate aspects of contactor behavior.

(i) Permissible throughput: It is expressed as the sum of the superficial velocities of aqueous and organic phase. The throughput of a mixer-settler stage is controlled by the coalescence and settling rate in the settler and this, in turn, determines the stage volume and hence the solvent inventory. For column extractors, limit on the throughput is determined by the flooding rate.

(ii) Mass transfer performance: Mass-transfer performance of contactor is determined by the number of stages or length of the column required to produce a given degree of separation.

2.2 Design criteria for nuclear reprocessing equipment

Designing of nuclear reprocessing equipment [1] are very challenging and it should satisfy the following criteria: (i) minimum operating life should be 40 to 50 years, (ii) either they should be maintenance free or remotely maintainable, (iii) they should not lose their mechanical and chemical properties due to high radiation background and (iv) shape and size should meet the criticality safe condition.

The type of equipment chosen for solvent extraction operation in nuclear reprocessing [2] are based on several factors and they are (i) process foot print and building size/height, (ii) operational flexibility such as continuous operation or frequent start and shutdown condition, (iii) low inventory which makes the process safer, (iv) processing time should be low to address solvent degradation, (v) it should reach steady state as early as possible, (vi) entrainment of other phase should be low, (vii) tolerance to process upsets, (viii) tolerance to solid handling, (ix) remote maintenance capability and (x) criticality constraints.

2.3 Extraction equipment for nuclear reprocessing application

Three distinctive equipment are generally used for solvent extraction operation. These include: (i) mixer-settler [3], (ii) columns (plate, pulsed extraction, etc.) [4] and (iii) centrifugal contactors [5].

2.3.1 Mixer settler

Mixer-settler comes under the category of stage wise contacting. It contains mixer followed by gravity settler combined to form single stage extraction units. In nuclear extraction processes, two phase contacting (mixing) takes few minutes and the settling takes several minutes because of gravity settling. As a consequence, the mixer sizes are relatively small as compared to settlers. Advantage of mixer-settler is operation flexibility, tolerance to process upset, easy scale up, tolerance to solid handling, etc. Its disadvantage is high solvent inventory, high time required to reach steady state, maintenance requirement for mixer, high process foot print, etc. The number of stages are decided based on equilibrium consideration (separation factor) and size is fixed by the efficiency of mass transfer and the throughput.

2.3.2 Pulse column

Two types of columns are generally used in reprocessing industry and they are packed and liquid pulse columns [6]. Pulsed columns comes under the category of differential contacting devices, unlike mixer settler and annular centrifugal extractor, the number of stages is determined by its height equivalent to theoretical stages. To reduce the columns height and the efficiency of contacting as well as separation is improved by providing perforated plates or dispersion is pulsed to decrease the droplet size and improve the mass transfer performance. Sieve plate pulse column are widely used in reprocessing industries because of maintenance free operation.

2.3.3 Centrifugal extractor

Centrifugal extractor comes under stage wise contacting where mixing and settling are accomplished inside a single unit. Mixing is due to spinning of rotor and settling occurs inside the rotor where the centrifugal force of the order of 100 to 600 g. Its stage efficiency is very high (greater than 95%) due to intense mixing and residence time is of the order of seconds.

Radioactivity level in fast breeder fuel reprocessing is 10 to 15 fold higher than the thermal reactor fuel reprocessing plant. Because of high radiation, solvent degradation is very high and degradation products (MBP and DBP) form complex with Pu and back extraction of Pu is difficult and it leads to Pu loss in the organic phase. Diluent degradation products alter physical properties of solvent and its affects the equipment performance and reduces the decontamination factor. To avoid degradation, extraction needs to be completed in the order of seconds. Centrifugal extractor is a candid candidate for fast breeder reprocessing applications.

2.4 Types of commercial centrifugal extractors

There are different types of centrifugal extractors are available for industrial applications and it may be classified under three categories: (i) differential, (ii) multistage and (iii) single stage as shown in Table 2.1.

Table 2.1: Classification of centrifugal extractors

Sr. No.	Orientation	Type	Name
1.	Horizontal	Differential	Podbielniak [7, 8] Quadronic [9] Coil Planet Centrifuge [10] Two-Fluid Taylor-Couette [11, 12]
		Multistage	Centrifugal Mixer Settler
2.	Vertical	Differential	α – Laval [9] Unpressurized Vertical Extractor (UPV) Coil Planet Centrifuge [10]
		Multistage	Luwesta Robatel SGN [13] Robatel BXP [14]
		Single-stage	Westfalia TA SRL [15], ANL

2.4.1 Podbielniak contactor

Podbielniak Contactor [7, 8] is popularly known as "Pod" and its schematic drawing is shown in Fig. 2.2. It is very compact and comes under differential countercurrent extractor with airtight rotor. It is successfully used for more than fifty years in solvent extraction unit operation in different chemical process industries. Up to 5 theoretical stages can be achieved in single unit and it can handle as low as 0.01 specific gravity difference process liquids. It can handle emulsified systems due to internal clarification zones and free of entrainment in most of the cases. The unique design reduces the solvent usage and operating cost while producing better product at higher yields in a safer environment. Unique feature of Pod contactor is it reduces the possibility of product contamination, prevents oxidation or degradation of product by avoiding contact with air and also it minimizes the solvent and product losses.

Pod cannot to be used in nuclear reprocessing plant due to its frequent maintenance.

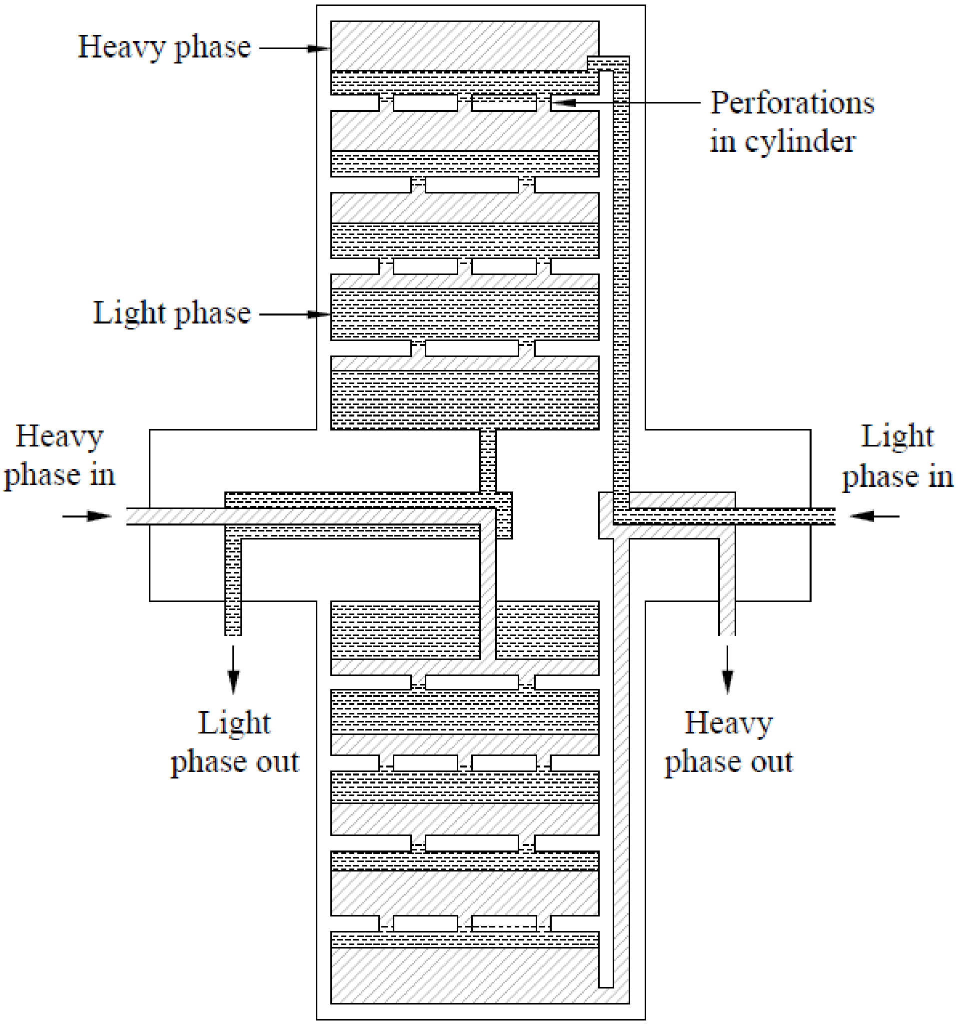

Figure 2.2: Podbielniak Contactor

2.4.2 Robatel multistage centrifugal extractor

Robatel SGN [13] comes under multistage centrifugal extractors or stage-wise contactors and it is very compact and high efficient. Schematic view of Robatel SGN extractor is shown in Fig. 2.3. Working principle: feed solution enters from the top (heavy phase inlet, containing solute) and solvent enters from top and feed at bottom, opposite end of the multistage contactor (light phase inlet). Each stage consists mixer and settler with inter-stage connection similar to pump mixer settler.

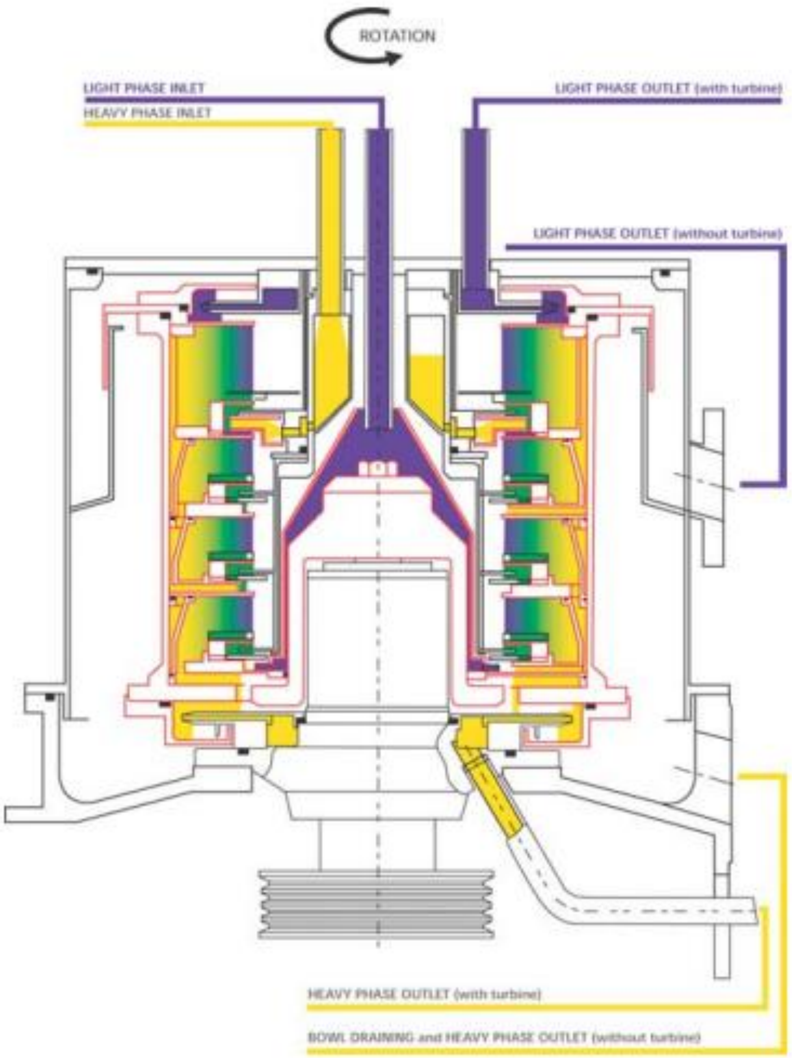

Figure 2.3: Four stage Robetal SGN centrifugal extractor [13]

Both aqueous and organic phases are mixed by stationary agitation disc mounted on the central drum inside the mixing chamber. The agitation disc and the mixing chamber's inlet and outlet channels form a pump which draws the two phases from the adjacent stages and also transfers the dispersion to the settling chamber. Due to centrifugal force, dispersed phase get separated inside the settling chamber. Position of liquid/liquid interphase is regulated by weir diameter of lighter phase and heavy phase. Each mechanical stage is nearly equivalent to a theoretical stage. Due to the presence of intermediate inlets, it can be used for fractional extraction and the extraction and scrubbing operation can be completed in a single unit.

2.5 Annular centrifugal extractor

2.5.1 Initial design of short residence contactors

In 1960s, solvent degradation was one of the major problems in spent fuel reprocessing. Conventional equipment: mixer settler, pulse column and other extractors has residence time in the order of one to ten minutes per stage, and it leads to solvent degradation and necessitates purification of the solvent after every pass in the process. To address the above problem the short residence contactor was developed.

Initial design of short residence time, paddle mixer type centrifugal contactor was developed by Savannah River Laboratory (SRL) and it is shown in Fig. 2.4 [15], which consists both the mixing and separating sections in a single stage. Several such units are connected in series to form a multi stage mixer-settler. Mixer region consists the paddle mixer, which mixes the phases and also pumps the phases from adjacent stages through the mixing chamber into the settler (centrifuge bowl). Dispersed phase entered inside the centrifuge bowl get separated due to high centrifugal acceleration. Separated heavy phase flows under a baffle at the periphery, then inward and over a weir, while the light phase flows inward and over a weir of smaller radius. Each phase is thrown out from the rotating bowl to a surrounding collector ring in the casing. The size of the extractor casing (for vessels that are not made of materials containing nuclear poisons) was limited to a diameter of about 7 inches due to criticality requirements. Actual phase separation takes place in about a 6-inch length of the 5-inch-diameter bowl.

The separating capacity of the above short residence extractor was estimated by the following equation 2.7.

$$Q_s = 4.39 * 10^{-8} \frac{N^2 D_b^3 H}{N_m D_m} \tag{2.7}$$

Critical speed of the shaft and rotor assembly decides operating speed and it limits the rotor length. Any vibration due to imbalance at the critical speed leads to excessive deflection, high stresses, and possible failure of the equipment. Because the Argonne National Laboratory (ANL) contactor has a long rotor, its critical speed is of much greater significance to its design than the critical speed of the rotor for the Savannah River (SR) contactor. An indication of the relative significance can be found by the use of a general equation for determining the critical speed of a steel shaft of uniform diameter [16].

$$N_{cs} = \frac{11{,}290{,}407 d_s^2}{\left(W {L_s}^3\right)^{1/2}} \tag{2.8}$$

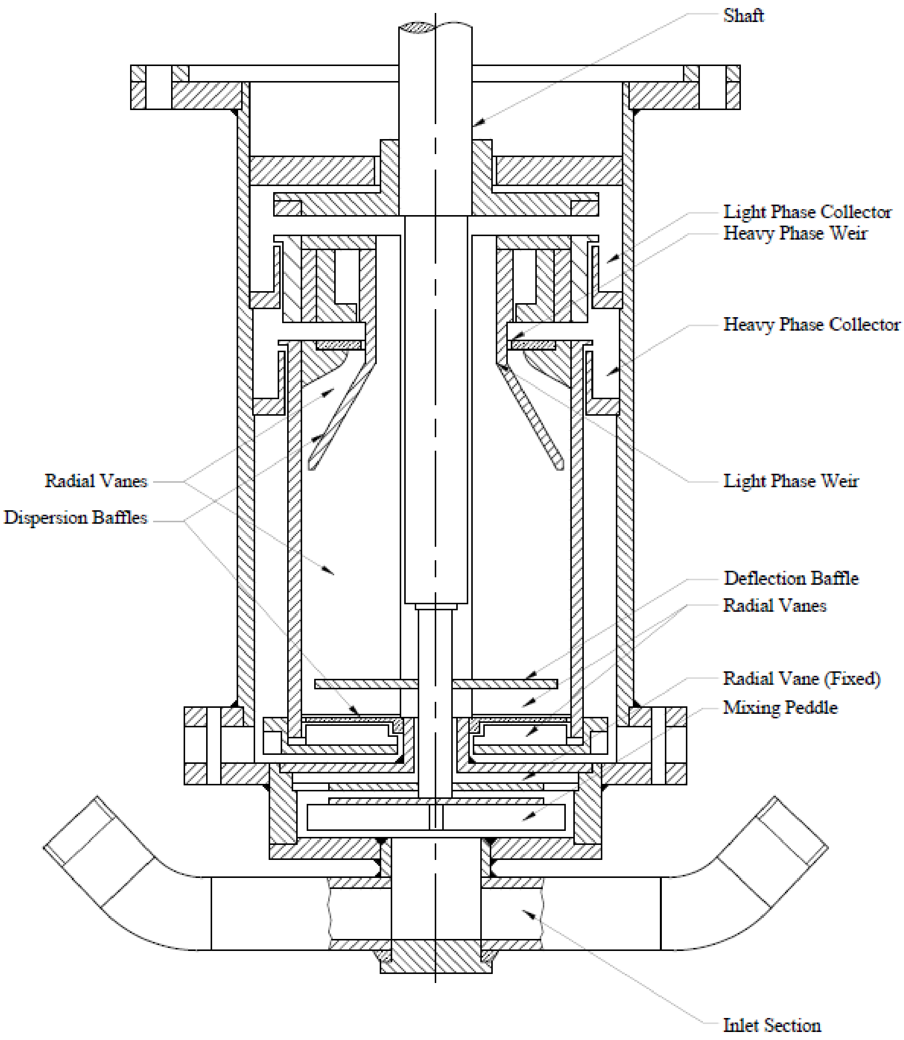

Figure 2.4: Short residence time centrifugal extractor with paddle mixer [15]

Main drawback of above contactor is the entrainment of air in both the aqueous and organic phases and it reduces the separating capacity of centrifugal bowl. Another drawback is that it requires weir change according to the liquid pair. To overcome the above said problems, a new centrifugal contactor was designed in which back pressure exerted by the aqueous weir is controlled by air pressure as shown in Fig. 2.5 [17].

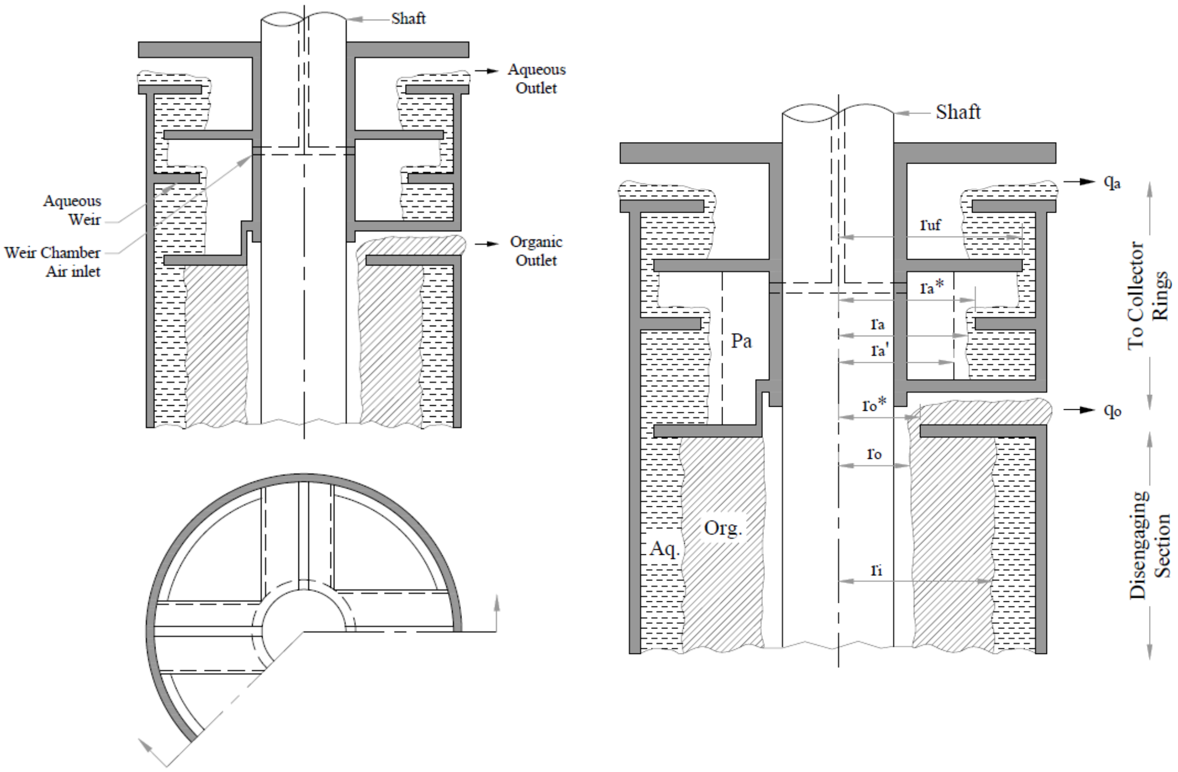

Figure 2.5: Air controlled aqueous weir [17]

Centrifugal extractor with an air-controlled aqueous phase weir to vary the position of the emulsion band (or interface) that is formed in the separating section between the heavy aqueous phase and the light organic phase. Mathematical expressions were derived [18, 19] and it is shown in equation 2.9 for calculating the air pressure as a function of rotor speed, aqueous and organic flow rates, and aqueous and organic phase densities.

$$P_a = 2 * 10^{-10} \frac{\omega^2 \rho_a}{(60)^2 (12)^4} \left[r_a^2 - \frac{\rho_o}{\rho_a} r_o^2 - \left(1 - \frac{\rho_o}{\rho_a}\right) r_i^2 \right] \qquad (2.9)$$

During the same period ANL developed miniature [20] centrifugal contactor with different sizes, which has a holdup less than 10ml per stage and it is operable with residence time of the organic solvent as low as two seconds per stage. Photographic view of single stage with mixer and settler and assembled 16-stage contactor is shown in Fig. 2.6 & 2.7 respectively [21]. The organic and aqueous phase flow into the mixer along the shaft and are discharged radially from the mixer at bottom periphery to the bottom of the settler. The dispersed phase flows from bottom of the settler to top and phases get separated due to high centrifugal acceleration (350 times of gravity (g)). The separated phases then flow over circular discharge weirs within the settler into collector rings in the stationary housing. The ducts out of the collector rings are tangential to the collector rings, so the solutions ejected from the settler are pumped to the next mixer by centrifugal force.

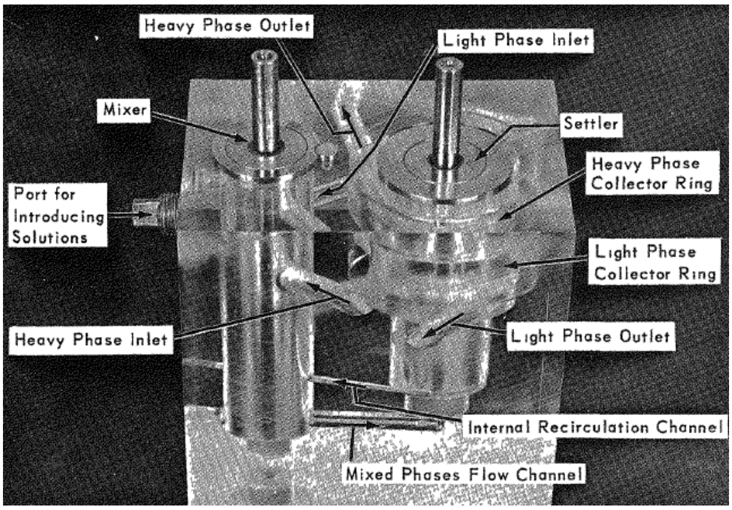

Figure 2.6: Single stage mixer settler centrifugal contactor [21]

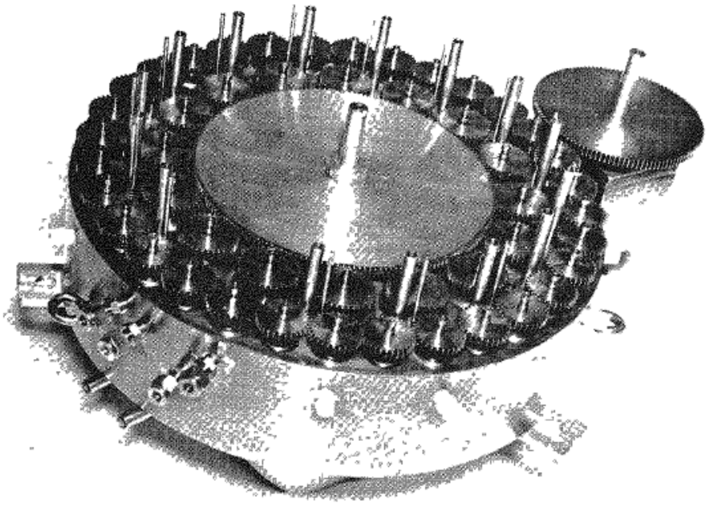

Figure 2.7: Assembled 16 stages mixer settler centrifugal contactor [21]

The short-residence contactors can be used only if the chemical reactions for the extraction process completes within order of seconds and PUREX process results showed that performance were equivalent to the conventional mixer-settlers.

2.5.2 Development of annular centrifugal extractor

Paddle type mixer attached with centrifugal extractor (Fig. 2.4) is designed such a way that the drive motor, the bearing assembly and the rotary air seal through which air pressure is applied to the weir are remotely maintainable. However, the mixing paddle is held captive in the mixing chamber and it is necessary to use concentric shaft so the inner shaft remains behind with the bowl while the external shaft is removed with the motor and the bearing assembly. This requires special fabrication since such assemblies are not commercially available.

To overcome the above problem a new centrifugal extractor design was conceived, especially for mixing the liquids, which completely eliminated the mixing paddle, mixing chamber and injection nozzle [22]. New contactor is called the Annular Centrifugal Extractor (ACE) and it is shown in Fig. 2.8. The aqueous and organic streams are enters into the sides of the casing and mixed by skin friction. Dispersed phase generated in annular region due to skin friction flow downward and enters inside the rotating bowl through orifice. The main objective for development of annular centrifugal extractor is to simplify the construction and improve the remote maintenance.

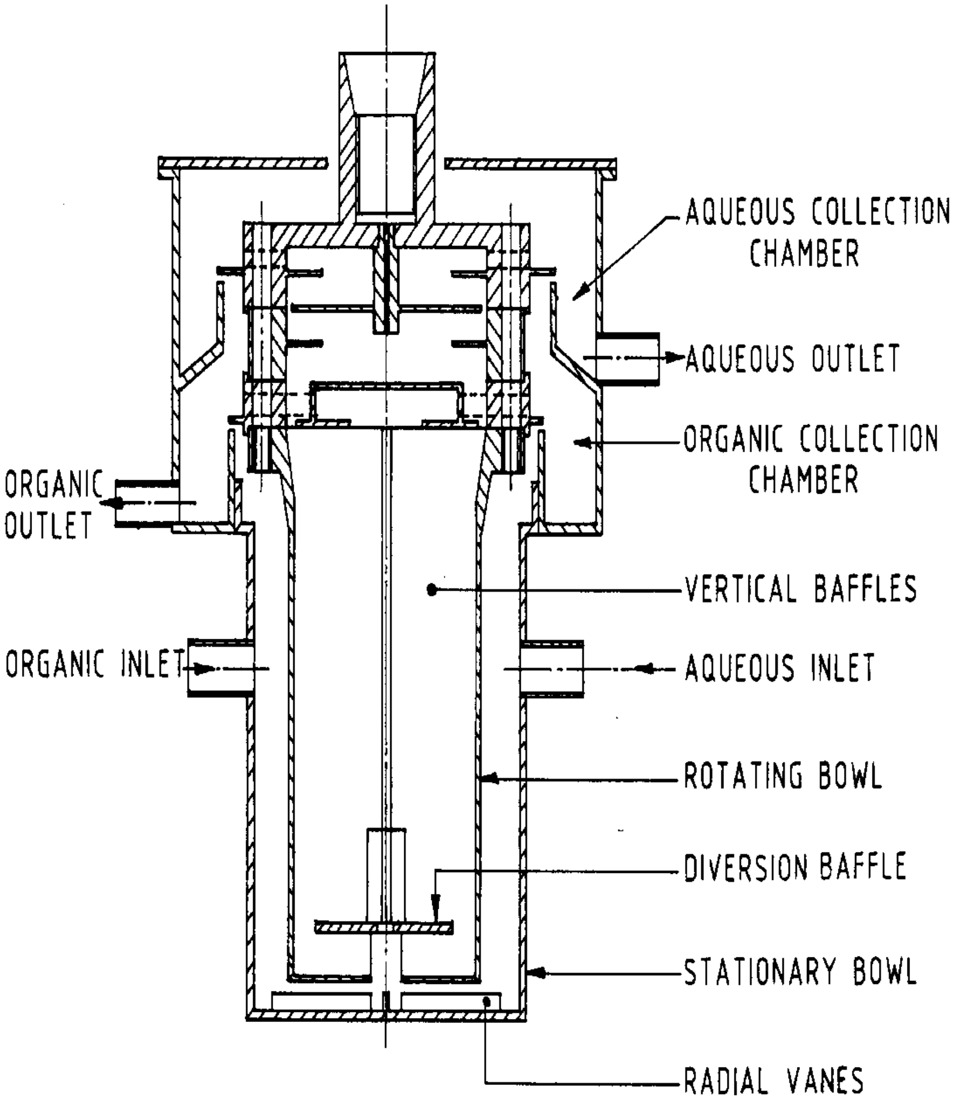

Figure 2.8: Annular centrifugal extractor with air controlled aqueous weir

2.5.3 Working principle of ACE

The schematic diagram of ACE is shown in Fig. 2.9 and cut view of rotating bowl in ACE is shown in Fig. 2.10. During normal operation heavy phase (blue) and light phase (yellow) enters through ACE via aqueous feed pipe (1B) and organic feed pipe (1A) in-between stationary bowl (2) and rotating bowl (3). Both phases mixed vigorously in annular region by shear force/ skin friction due to high speed rotation of inner bowl and turbulent liquid-liquid dispersion promotes the mass transfer between two phases. Mixed phase (dispersion) flows down by gravity in annular region and enters inside rotating bowl through orifice (5) via bottom baffle (4) (mixing vane).

Main function of bottom baffle is to break the vortex formation and provided in the bottom region which are either attached to the base of the outer cylinder or to the bottom of the rotating cylinder in the case of paddle type contactors. Dispersion entering inside the rotating bowl is deflected towards the wall of the rotating cylinder by deflecting baffle (6) to enhance the centrifugal separation of heavy and light phases. Dispersion phase gets separated and also flows from bottom to top inside the rotating bowl and it is confined inside the chambers (four to eight numbers) by vertical baffles (7). The rotating cylinder imparts a rigid body rotation to the liquid and creates vertically cylindrical free surface of liquid and it is coaxial with the axis of rotation because of high ‘g’. The central portion is occupied by air. The dispersion entering at the bottom gets separated as it moves upwards. The separation rate of dispersed phase depends upon density difference between continuous and dispersed phase, viscosity of continuous phase, drop size distribution, settling velocity of dispersed phase under centrifugal acceleration ($r\omega^2$) and coalescing behavior of the two phases. For complete separation (which is considered to be a flagship advantage of ACEs) of dispersion, adequate height of rotating bowl needs to be provided for a given level of centrifugal acceleration. Separated lighter phase (yellow) flow over light phase weir (8) and it is thrown out in to lighter phase collection chamber (11) located at stationary bowl. Similarly, heavy phase (blue) flows over heave phase weir (10) via under flow (9) and it is thrown out in to heavy phase collection chamber (12) located above lighter phase collection chamber at stationary bowl. Finally both heavy phase and light phase comes out or flows in to adjacent stages through light phase outlet (13A) and heavy phase outlet (13B).

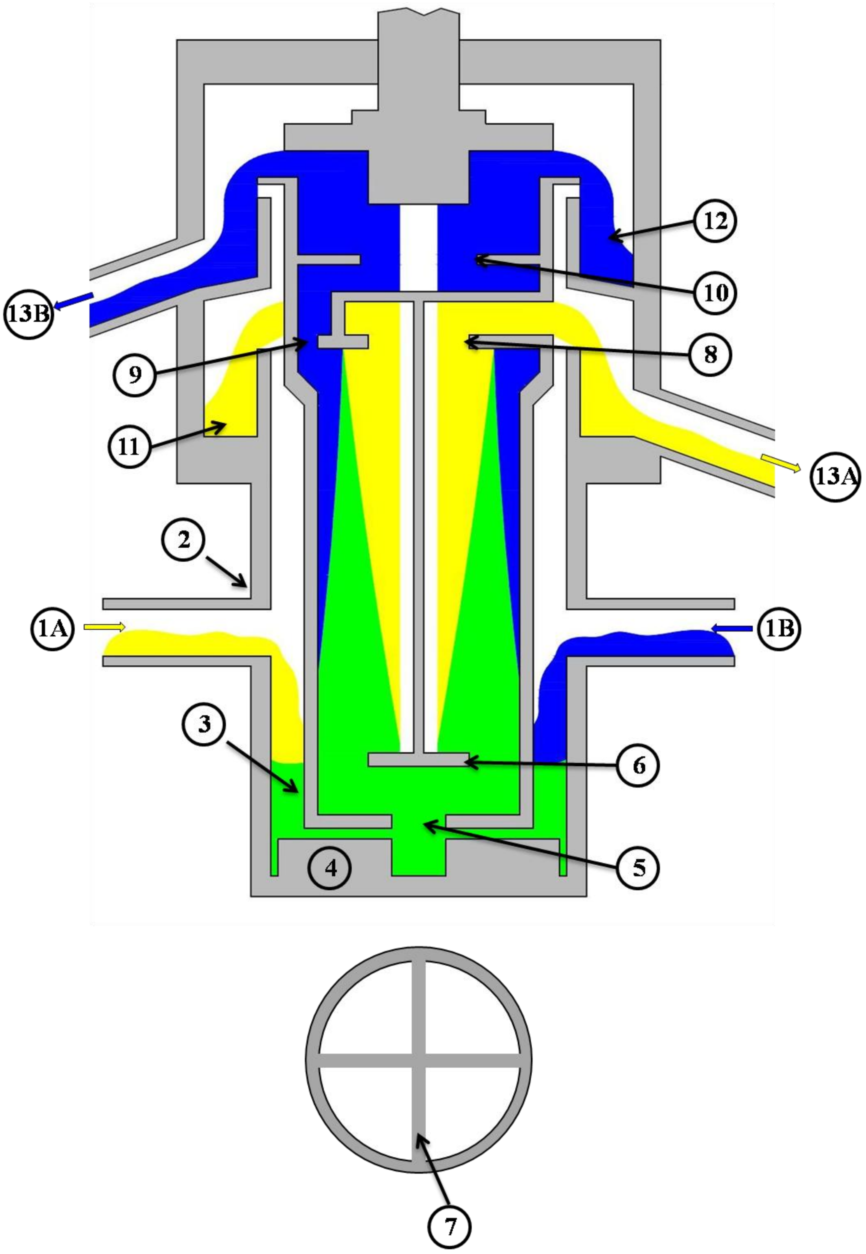

Figure 2.9: Schematic diagram of the annular centrifugal extractor (ACE)

(1A) Light phase inlet, (1B) heavy phase inlet, (2) Stationary cylinder, (3) rotating cylinder, (4) radial baffles on the stationary bottom plate, (5) central opening for rotating cylinder, (6) deflecting baffle in the rotor, (7) vertical baffles in the rotor, (8) light phase weir, (9) under flow region for heavy phase, (10) heavy phase weir, (11) light phase collection chamber, (12) heavy phase collection chamber and (13A and B) outlets for light and heavy phases, respectively.

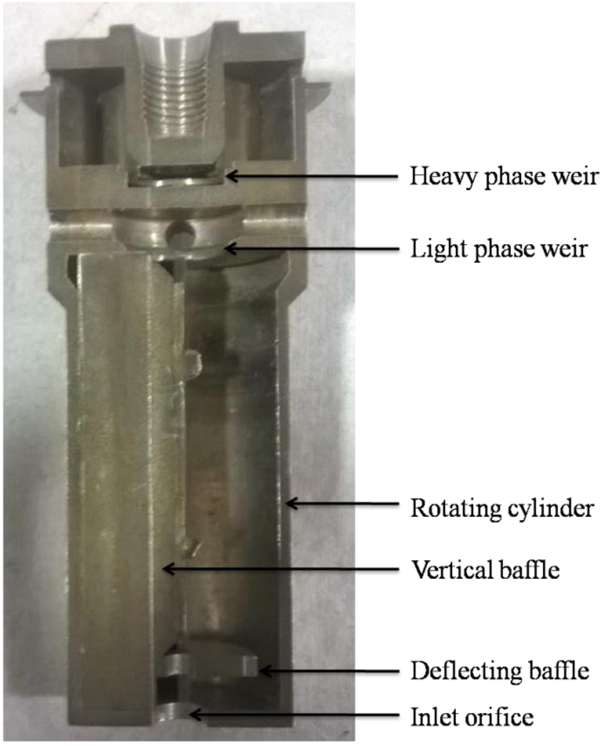

Figure 2.10: Cut view of rotating bowl

Idealized behavior of ACE is shown in Fig. 2.11, in that the variation of volume fraction of dispersed phase against the vertical distance (inside rotating bowl) for various throughput condition is shown. The mixed phase enters at bottom orifice of rotating bowl and it is deflected towards wall by horizontal deflecting plate and at level 1 rotating bowl was completely filled with mixed phase. Further liquid moves up in vertical direction, aqueous phase (heavy phase) moves towards the rotating wall due to high centrifugal acceleration and organic phase (light phase) moves towards the centre due to buoyancy as shown in level 2 and level 3. Liquid moves further in vertical direction both organic and aqueous phase get separated as shown in level 4 and completely separated organic and aqueous phase flow over through organic weir and underflow respectively.

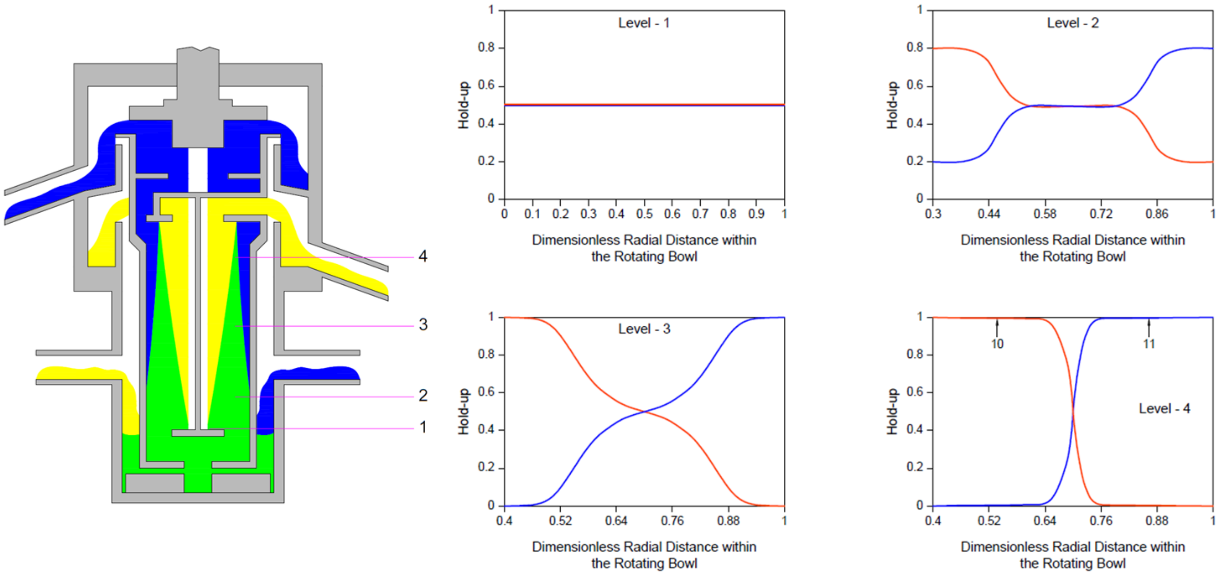

Figure 2.11: Variation of dispersion band in ACE.

(11) Aqueous phase width, (10) Organic phase width.

2.5.4 Advantage and disadvantage of ACE

Advantages of ACE over conventional contactors are

i. Centrifugally accelerated settling

ii. Short residence times

iii. Low hold-up volumes

iv. Excellent phase separation

v. High mass transfer efficiency

vi. Compact and short pieces of equipment

vii. Easy start up and shut down

viii. Reduced exposure of solvent to radiation

ix. Critically safe geometry

Major disadvantage of ACE are

i. Expensive due to precision manufacturing

ii. Easy appearance of emulsifying layer

iii. Sensitive to solid particle

iv. Frequent maintenance

2.5.5 Parameters decides the pumping capacity of ACE

2.5.5.1 Design parameters

i. Rotating bowl diameter

ii. Rotating bowl height

iii. Rotor inlet diameter

iv. Organic and aqueous weir diameter

v. Underflow width

vi. Distance between diverter disk and rotor inlet

vii. Diverter disk diameter

viii. Bottom baffle design and its height

ix. Gap between bottom baffle and rotary bowl bottom

x. Annular gap

2.5.5.2 Operating parameters

i. Rotor speed

ii. Aqueous and organic flow rate

iii. Ratio between aqueous and organic flow rate

2.5.6 Parameters decides the mass transfer performance of ACE

2.5.6.1 Design parameters

i. Rotor inlet diameter

ii. Bottom baffle design and its height

iii. Gap between bottom baffle and rotary bowl bottom

iv. Annular gap

2.5.6.2 Operating parameters

i. Rotor speed

ii. Aqueous and organic flow rate

iii. Ratio between aqueous and organic flow rate

2.6 Design principles of ACE

2.6.1 Liquid entry

Entry point for aqueous and organic phase decides both mass transfer and hydrodynamic performance of ACE in multistage operation. Aqueous and organic entry point in annular region is about 180^{o} from each other and its orientation is either perpendicular or tangential to rotating cylinder. Orientation of liquid inlet doesn't have any impact in ACE operation when dispersed phase is below the entry point. When dispersed phase level in annular region above the entry point the tangential inlet to rotating cylinder is prepared, where spinning liquid assist to pull the liquid from feed pipe line. If it is perpendicular to rotating cylinder then liquid builds up in inlet port and drastically reduces the hydrodynamic performance.

Entry point for both the phases are too high than liquids splash up and reaches the lower collector ring and drastically reduces both mass transfer (by pass) and hydrodynamic performance (carryover of heavy phase in lighter phase). In multistage ACE operation, flow between one stage to another stage is gravity driven and it requires static head. During low throughput multistage operation, slug flow was observed [23] in aqueous and organic inter-stage line. Above flow fluctuation reduces both the mass transfer performance. To reduce flow fluctuation, insertion of wire rope inside the inter-stage line is suggested in the literature [23].

2.6.2 Mixing inside ACE

Mixing inside the annular region is due to velocity difference between inner rotating cylinder and outer stationary cylinder and it induces the hydro-dynamically instability, which is called Taylor-vortex flow [24, 25]. At low Taylor number ($Ta < 1708$), flow inside the annular gap is purely circumferential. Further increase in throughput or rotating velocity the Ta number reaches the Taylor critical number (Ta_{Cr}), a centrifugal instability gives rise to Taylor vortex flow (TVF). In TVF, the velocity field consist a sequence of counter rotating vortex pairs stacked along the cylinder. The velocity field varies periodically with the distance from the system axis and it is constant in the azimuthal direction [24]. The first time-dependent regime, wavy vortex flow (WVF) in which an azimuthal travelling wave is superimposed on TVF, occurs for slightly greater Taylor number in a large radius ratio system. Upon further increasing Ta, the flow first becomes quasi-periodic and then weakly turbulent. The flow eventually (when $Ta \geq 1000\ Ta_{Cr}$) reaches a turbulent Taylor vortex flow (TTVF), in which the vortex boundaries become difficult to discern. Several other unstable flow regimes have also been reported in the literature with a variation in the Ta number. Annular centrifugal extractors are operated in TTVF region. The liquid flow pattern in the annular region for the inner cylinder rotating and outer stationary cylinder, such as circular couette flow, annular poiseuille flow and Taylor vortex flow is shown in Fig. 2.12.

Taylor number is defined as the ratio of centrifugal force to the viscous force and is given by

$$Ta = \frac{4\Omega_i^2 d^4 (\vartheta - \eta^2)}{\upsilon^2(\eta^2 - 1)} \tag{2.10}$$

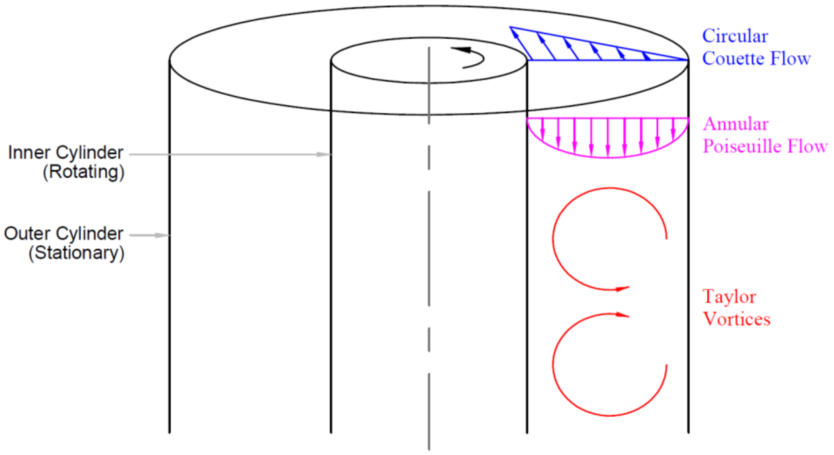

Figure 2.12: Different flow pattern in annular gap

Chandrasekhar et. al. [25] used the Galerkin method to determine the variation of $\mathrm{Ta_{Cr}}$, for $\mathrm{Re_z}$ up to 100. In the analytical solution, he modified the governing equations with approximations and found $\mathrm{Ta_{Cr}}$ to be

$$\mathrm{Ta_{Cr}} = \frac{1708}{0.5\,(1+\vartheta)} \tag{2.11}$$

Chandrasekhar et. al. [25] reconsidered the narrow gap problem in the presence of an axial flow based on perturbation theory and he arrived at an expression for $\mathrm{Ta_{Cr}}$, as

$$\mathrm{Ta_{Cr}} = 1708 + 27.15\,\mathrm{Re_Z^2} \tag{2.12}$$

2.6.2.1 Annular gap

Annular gap plays major role in the mixing inside ACE and it is one of the determinative factor for degree of turbulence of TVF [26]. Both Taylor and Reynolds number increases with increase in the annular gap and it increases the turbulence of TVF in ACE and enhances the mixing/ mass transfer performance. Increase in annular gap increases the liquid holdup and decreases the liquid height.

Throntan et. al. [27] investigated the rotary annular column with various sizes of rotor with different annular gap and correlated overall mass transfer coefficient with the equipment geometry and it is shown below (eq. 2.13)

$$\mathrm{K_C}\underline{\mathrm{a}} = \frac{\mathrm{v_d}}{\mathrm{C_1 r_{oi}}}\left(\frac{\mathrm{R_{oi}}\omega^2}{\mathrm{g}}\right)^{0.74}\left(\frac{\mathrm{R_{io}}}{\mathrm{R_{oi}}}\right)^{-2.31} \tag{2.13}$$

Davis et. al. [28] measured the holdup in rotary annular column with different diameter and annular gap and related with geometry parameter (shown in equation 2.14) and similarly they measured mass transfer coefficient and proposed the correlation as shown in equation 2.15.

$$\varepsilon_\mathrm{D} = \mathrm{C_2}\left(\frac{\omega \mathrm{R_m^{0.5} d^{1.5}} \rho_\mathrm{C} \mathrm{r_{io}}}{\mathrm{R_{io}}\mu_\mathrm{C}}\right)^2 \frac{\mathrm{v_d^{0.5}}}{\mathrm{d^3}} \tag{2.14}$$

$$K_C\underline{a} = C_3 \frac{d^{3.65} v_d}{\left(\omega R_m^{0.5} d^{1.5} \rho_c \, {}^{R_{io}}\!/_{R_{oi}} \, \mu_c\right)^{2.2}} \frac{\left(m\left({}^{v_d}\!/_{v_c}\right) - 1\right)}{\ln\left(m\left(v_d / v_c\right)\right)} \tag{2.15}$$

From the above equations 2.13 to 2.15, it is understood that the annular gap is one of the influential parameters for holdup and mass transfer performance in the Taylor vortex flow.

Cao et. al. [29] reported the mass transfer and hydrodynamic performance of ACE with respect to different annular gap and concluded that increase in annular gap increases the mass transfer efficiency and flooding throughput. Deshmukh et. al. [30] reported the effect of annular gap in mixing process by measuring Residence Time Distribution (RTD).

Increase in annular gap reduces the liquid height in the mixing zone and reduces the mixing performance. Decrease in annular gap increases the shear rate and leads to formation of stable or persistent emulation and reduces the hydrodynamic performance of ACE. Leonard [31] suggested, typical width of annular gap may be around 9% of the rotor diameter to balance the competing needs. Recently, Kadam et. al. [32] reported the mass transfer coefficient for ACE with respect to geometry parameters including annular gap and it is shown in below equation 2.16.

$$\frac{K_C\underline{a}}{N} = 10.2 \left(\frac{2R_{io} N \mu_C}{g}\right)^{0.81} \left(\frac{b}{2R_{io}}\right)^{-0.2} \left(\frac{d}{2R_{io}}\right)^{-0.19} \left(\frac{g}{2R_{io} N^2}\right)^{0.61} \left(\frac{\mu_C}{\rho_C D_C}\right)^{-0.53} \tag{2.16}$$

2.6.2.2 Bottom vanes

Radial vanes are attached either at base of the contactor housing (stationary vanes) or to the bottom of the rotating cylinder. Main function of radial vane is to dissipate the rotational velocity of dispersion created in the annular region and guide the dispersion to reach the rotor inlet orifice. Without stationary vanes the dispersion would back up in the annular region due to vortex formation at bottom of the rotating cylinder and it leads to build up of dispersion in the annular mixing zone and flows out through light phase collector ring. The gap [23, 33-35] between radial vanes and bottom of rotating cylinder play major role in the liquid height at annular gap. Increase in gap increases the liquid height in the annular mixing zone. Number and shape of radial vanes [36-39] also plays major role in the liquid height at annular mixing zone. Wardle et. al. [38] reported increase in the number of straight vane decreases the liquid hold up in annular region. Leonard [31] suggested, typical height of bottom vane should be around 0.3 cm plus 6% of the rotor diameter and gap between the top of the bottom vanes to the bottom of the rotor should be around 0.15 cm plus 2% of the rotor diameter. Schematic view of straight and curved vane are shown in Fig. 2.13.

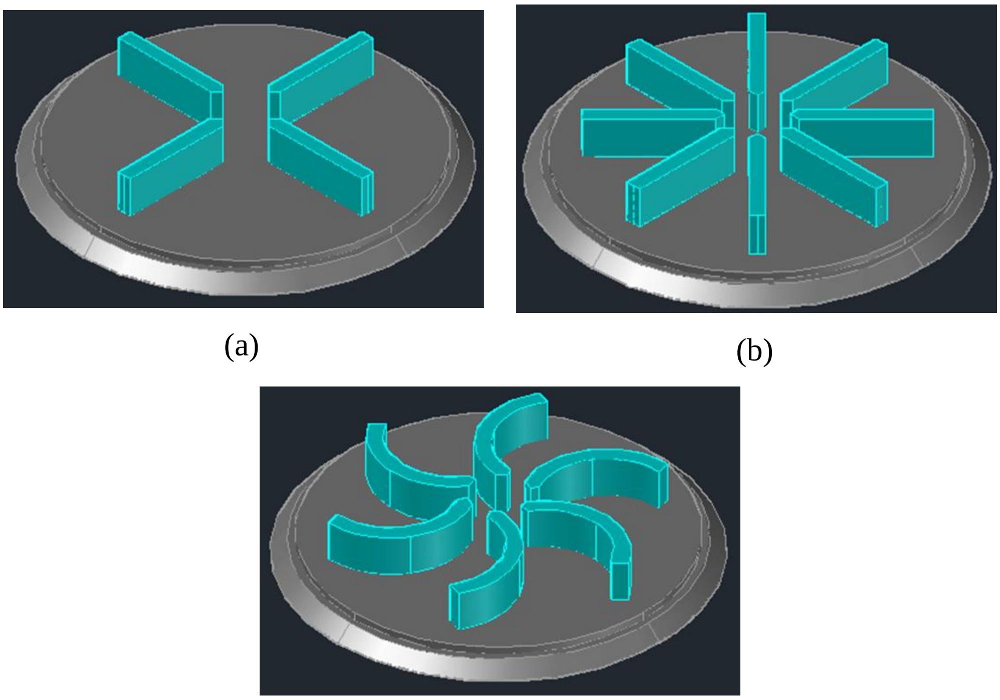
(a) (b)

(c)

Figure 2.13: Vane geometry (a) 4 vanes, (b) 8 vanes and (c) curved vanes

2.6.2.3 Radius of rotor inlet orifice

Radius of rotor inlet orifice decides the pumping capacity and liquid hold up in annular region inside ACE. Relation between rotor inlet radius with light phase weir radius is shown below equation 2.17.

$$r_{rinlet\ max} = \sqrt{((r_o{}^*)^2 - \frac{2 * g * H}{\omega^2})} \tag{2.17}$$

Rotor inlet radius should be small enough that any liquid entering inside the rotor should be pumped up to light phase weir. Eq. 2.17 shows maximum rotor inlet radius for complete pumping. If radius is greater then $r_{\text{rinlet max}}$ than rotor is said to be partially pumping and liquid may be pumped is less than H. To compensate the liquid level in the annular region must rise so liquid can flow through the rotor. Patra et al. [40] studied the effect of inlet orifice radius in pumping capacity of rotor by CFD simulation in simplified rotating geometry.

2.6.2.4 Rotor speed

Critical speed decides the operating speed of ACE. In general, rotor speed will decrease with increase in rotor diameter and it should be operated below 20-30% [31] of its first critical speed. It is one of the operating parameter, which decides the liquid height/mixing intensity in annular region inside any given ACE.

Liquid height inside the annular region increases with increase in the rotor speed and increases the degree of emulsification in the rotor zone and increases the mass transfer performance [32, 41]. Interface radius inside the rotor zone increases with rotor speed, thus makes the emulsion layer thinner and increases the separation capacity [29, 34, 42-44]. Combined effect [45] of degree of emulsification in rotor zone and emulsion layer thinner inside rotor decides the operating capacity of ACE for any give system. In large contactors [46], increase in rotor speed leads to over mixing and reduces the performance. During multistage operation, end stages should be operated in low mixing region to reduce entrainment, especially in nuclear reprocessing application or the process requires high decontamination factors.

Arafat et al. [47] theoretically derived equation for power consumption in a rotary annular column (Taylor-Couette flow) and it is shown in below Eq. 2.18 to 2.20.

$$P = 0.0261\, h_c\, R_{io}^{3.75}\, (j\omega)^{2.75}\, \rho_c^{0.75} \left(\frac{\mu_c}{d}\right)^{0.25} \tag{2.18}$$

$$j = 0.0554(\log Re) + 1.368 \quad (3\times10^{3} < Re < 1\times10^{6}) \tag{2.19}$$

$$\mathrm{Re} = \frac{2j\rho_c \omega R_{io} d}{\mu_c} \tag{2.20}$$

The above equation does not include the effect of bottom clearance and baffle height on the power consumption. Based on Energy dissipation per unit mass, mixing intensity is classified as (i) 435 W/Kg (High), (ii) 114W/Kg (medium) and (iii) 27W/Kg (low). From above Eq. 2.18 understood that mixing intensity is directly proportional to the rotor speed with power 2.75.

Later, Kadam et al. [48] proposed a new correlation for the power number in an annular centrifugal extractor and it is shown below in Eq. 2.21.

$$\frac{P}{N^3 (2R)_{io}^5 \rho} = 40.85 \left(\frac{N(2R)_{io}^2 \rho}{\mu}\right)^{-0.5} \left(\frac{d}{2R_{io}}\right)^{-0.068} \left(\frac{h_C}{2R_{io}}\right)^{0.83} \left(\frac{c}{2R_{io}}\right)^{0.026} \left(\frac{b}{2R_{io}}\right)^{-0.036} \tag{2.21}$$

The above correlation was proposed for single phase, it is also applicable for dispersions, when the single phase properties are replaced by the properties of the dispersion. Generally, bowl rotating speed is fixed based on the dispersion number to meet the design capacity and also it should satisfy both centrifugal acceleration and natural frequency. Leonard [31] suggested that the ACE rotating bowl should be operated between 100g and 600g of centrifugal acceleration to break the dispersion using a high centrifugal force.

2.6.3 Separation capacity

Bernstein et al. [49] studied the separating capacity of 31.8 mm size rotor ACE. The rotor speed was varied in the range of 33.33 to 58.33 r/s, total (organic plus aqueous) throughput ranged from 3.33×10^{-4} m^3/sec to 1.133×10^{-3} m^3/sec with a flow ratio ranging from 0.25 to 4 of organic to aqueous phase. They used 0.5M HNO_3 as aqueous phase and 30% tri-n-butyl phosphate (TBP) as the organic phase. They also studied the effect of solids by using an aqueous feed solution containing MnO_2 up to 1600 ppm. At steady state conditions, no MnO_2 appeared in the effluent streams. The solids were found to get accumulated inside the rotor, and no significant effect on the performance of the unit was observed up to an accumulation of 50 gm. Leonard et al. [50] used ACE having rotor diameter in the range of 30 to 250 mm, rotor speed in the range of 10 to 100 r/s and the annular gap varied from 3.3 to 23.6 mm and the separation capacity of the rotor was investigated. They also investigated the separation of dispersion under gravity conditions. The effectiveness of separation for gravity system was expressed in terms of the following dimensionless number called dispersion number (N_D).

$$N_D = \frac{1}{t}\sqrt{\frac{\Delta Z}{g}} \tag{2.22}$$

Where t is the time required for complete separation in batch settler. ΔZ is the initial height and g is acceleration due to gravity.

For continuous system equation 2.22 becomes

$$N_D = \frac{Q}{V}\sqrt{\frac{\Delta Z}{a}} \tag{2.23}$$

Where a is either g or $\bar{r}\omega^2$ depending upon the condition of separation. Where $\bar{r}$ is the average radius and it is shown in Eq. 2.24.

$$\bar{r} = \frac{2(r_u^3 - (r_o^*)^3)}{3(r_u^2 - (r_o^*)^2)} \tag{2.24}$$

The value of N_D was found to depend upon the physical properties of the liquid-liquid systems (ρ_c, ρ_d, μ_c, μ_D, σ, etc.) and independent of the method of separation (i.e. gravity or centrifugal). The authors also analyzed the literature data along with their own and found the value of N_D to be in the range of 0.0001 to 0.02 depending upon the liquid-liquid system.

Leonard. et. al [51] has discussed the details of standard tests to find out N_D and its application in characterization of solvents used in the solvent extraction operation. Solvent characterization based on dispersion number is shown in Fig. 2.14. He measured dispersion number for different combination of solvents and they are (1) plasticizer leaching, (2) PUREX and TRUEX solvents in nuclear industry and (3) TRUEX-SREX solvents in nuclear industry etc.

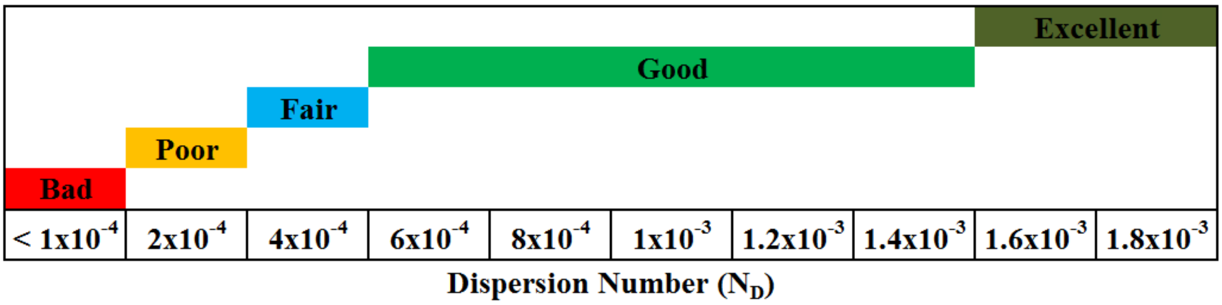

Figure 2.14: Solvent characterization based on dispersion number

Kadam et al. [32] has investigated separating capacity of centrifugal extractor over a wide range of design and operating variables and proposed a new non dimensional dispersion correlation (Eq. 2.25) with a correlation coefficient of 0.93.

$$N_D = 0.037\left(\frac{Q_C}{N(2R)_{ii}^3}\right)^{0.24}\left(\frac{Q_D}{N(2R)_{ii}^3}\right)^{0.38}\left(\frac{c}{2R_{ii}}\right)^{-0.26}\left(\frac{d}{2R_{ii}}\right)^{0.06}\left(\frac{g}{2R_{ii}N^2}\right)^{0.17} \qquad (2.25)$$

2.6.3.1 Organic weir radius

Fig. 2.15 shows the schematic of the centrifugal separation of two immiscible liquids. Volume of separator depends upon the light/organic phase weir radius [35, 52]. ΔZ shown in Eq. 2.23 is distance between the outer radius of dispersion (under flow radius) to inner radius of dispersion (organic weir radius). Increase in organic weir radius will reduce the settling volume and reduces the residence time inside the settler. Decrease in the organic weir radius leads to partial pumping and increases the liquid height in the annular region and reaches the lower collection ring. Leonard [31] suggested the ratio between light phase weir to under flow radius should be minimum 0.46 and further decrease in above ratio will not result in further increases in total throughput. Similarly, Leonard [31] suggested the ratio between under flow diameter to rotating bowl inner diameter is typically about 0.91.

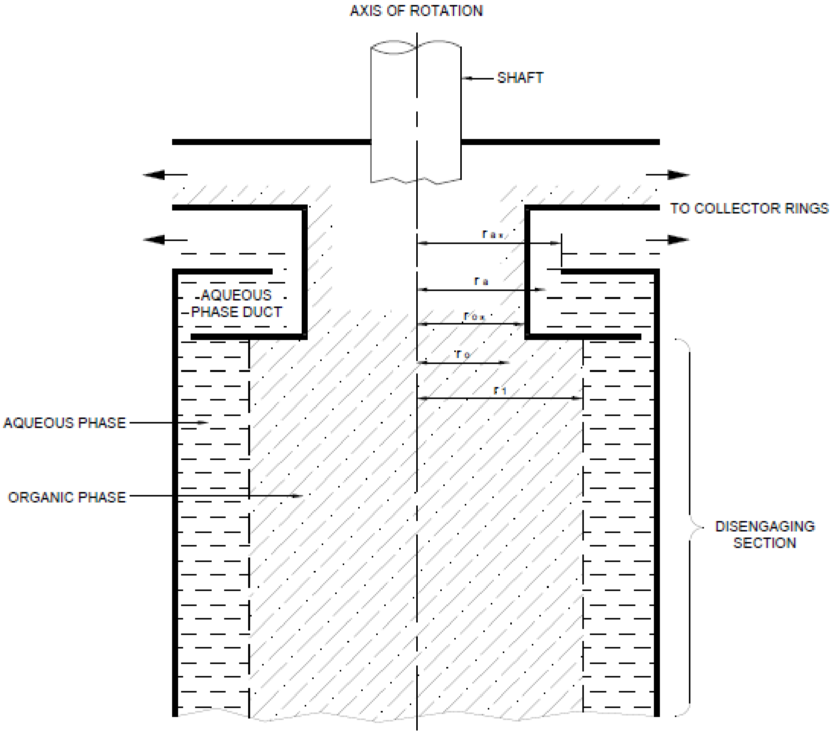

Figure 2.15: Fixed weir centrifugal weir

2.6.3.2 Aqueous weir radius

Aqueous weir radius depends upon the organic and inter-phase radius inside the rotating bowl for any given aqueous and organic system. Relation between aqueous and organic weir is shown in below equation 2.26.

$$(r_i^2 - r_a^2)\,\rho_a = (r_i^2 - r_o^2)\,\rho_o \qquad (2.26)$$

Above equation 2.26 is valid for no flow condition in ACE. During operating condition, flow above weir should be considered and it is shown in equation 2.27 [53] and unknown in the above equation is rise over weir (Δr).

$$\frac{1}{2}\rho_a\omega^2(r_i^2 - (r_a + \Delta r_a)^2) = \frac{1}{2}\rho_o\omega^2(r_i^2 - (r_o + \Delta r_o)^2) \qquad (2.27)$$

Rise over weir can be calculated using below equation 2.28 [18].

$$q = kf\pi\omega[2\Delta r\left(r - \frac{\Delta r}{2}\right)]^{3/2} \qquad (2.28)$$

Webster et al. [18] evaluated the circular weir coefficients by using volume displacement methods, as well as from visual observations. In the experiments on plastic unit, they observed the maximum rise behind the radial vanes located in the aqueous phase duct at the weir, which they attributed to coriolis influence and presented a correlation which takes this influence of coriolis force on the rise over the weir into account.

$$k = k_{*} \exp\left[-\left(\frac{4}{bn}\right)(k_{*}\pi f)^{\frac{2}{3}}\left(\frac{q}{\omega}\right)^{1/3}\right] \tag{2.29}$$

Mizushna et al. [54] conducted experimental study on discharge coefficients for the case of water issuing from a small hole. The hole drilled through a rotating inner cylinder wall into kerosene in the annular space between concentric inner and outer cylinders rotating at the same angular velocity. They have studied the effect of hole diameter, wall thickness, cylinder diameter, rotational speed, interfacial tension on the discharge coefficients and correlated through Froude number, Weber number and Reynolds number. Later Leonard et al. [55] conducted study on weir coefficients on an ANL type contactor with air-controlled aqueous weir. They have used a bowl of 90 mm in diameter, with aqueous weir and organic weir radius of 3.33 cm and 2.22 cm respectively. The unit was run at 1765 rpm. They have shortened the radial vanes of the aqueous channel such that they match with the weir, unlike that of SRL type where vanes were extending to the axis. The vanes at organic weir were extending to the axis as that of SRL type. They reported less rise over the weir compared to those reported earlier, for nearly same conditions of operation. By using a correction factor in the correlation developed by earlier authors [18], they have matched their aqueous weir however, while the organic weir data did not need any correction in the correlation.

Hiromichi et al.[53] et al investigated the stability of interface of two liquid phases in a centrifugal mixer settler type extractor of dimension, rotor outer diameter 7 cm, length of the settler 18.1 cm, the inner weir radius 1.9cm and outer weir radius was 2.1 cm. In order to observe the correct diameter of the interface, the experimental equipment was made of transparent plastic and the diameter was determined by taking photos, lighting a flash. The effect of flow rate and rotation speed (500 to 4500 rpm) on the interface radius has been calculated. They have found out the average value of discharge coefficient was found to be 0.103, and they have observed that the higher rotational speed is required to hold the interface within settling region. They have used equation (2.28) in order to add the effect of flow on the weirs.

Slocum et al.[56] have studied flow profiles experimentally for Newtonian fluids having viscosity from 2×10^3 to 5×10^5cP (centipoise), flowing over knife edged weirs with heights varying from 0.1' to 4.6'.They have defined four dimensionless groups correspond to generalised fluid height, distance upstream, flow rate, and viscosity. They have observed that the head on the weir is the primary factor causing the flow.

Bernstein et al. [57] performed preliminary tests with plastic contactors, in these tests throughput capacity of a 4'. OD rotor operating at various speeds with a variety of orifice sizes, annular gaps and depths of water in the annulus was measured. They observed throughput was being limited by the flow through the orifice dependent on the height of the liquid in annulus. Aqueous weir is back calculated using equation 2.26 to 2.29 by fixing interfacial radius r_i by equal volume method.

2.7 Design modification in ACE

2.7.1 Dismountable ACE for pharmaceutical application

Complete disassembly and inspection is required to meet good manufacturing practice (GMP) compliance. Meikrantz et. al. [58] developed a new rapid disassemble ACE for inspection and cleaning of all wetted parts to meet the GMP for pharmaceutical industry. Standard industrial ACE is welded version and its internals are inaccessible for cleaning and inspection. Slight contamination from previous batch may leads to product contamination especially in pharmaceutical application. A 5" CINC ACE rapidly dismountable is demonstrated [58] without losing its mass transfer and hydrodynamic performance.

2.7.2 Constant mixing volume ACE

Main draw back in ACE is its holdup present inside the mixing region (annular region) is depends upon the flow rate, rotor speed, material of construction (wettability) etc. and also it cannot handle the sheer sensitive process liquids. To overcome above problem, CEA France developed a new ACE (ECRAN) [59] and its schematic is shown in below Fig. 2.16. ECRAN consist two rotors driven by same shaft. Upper portion accomplishes the separation of the phases and lower one is for mixing. During normal operation, aqueous and organic phases are feed into bottom and it passes through Couette mixing zone before entering inside the settler zone. It offers advantage of constant mixing time and low mixing can be done by selecting suitable thin mixing rotor for Couette mixing with standard separation rotor. They demonstrated above ECRAN for solvent cleanup application in nuclear reprocessing industry.

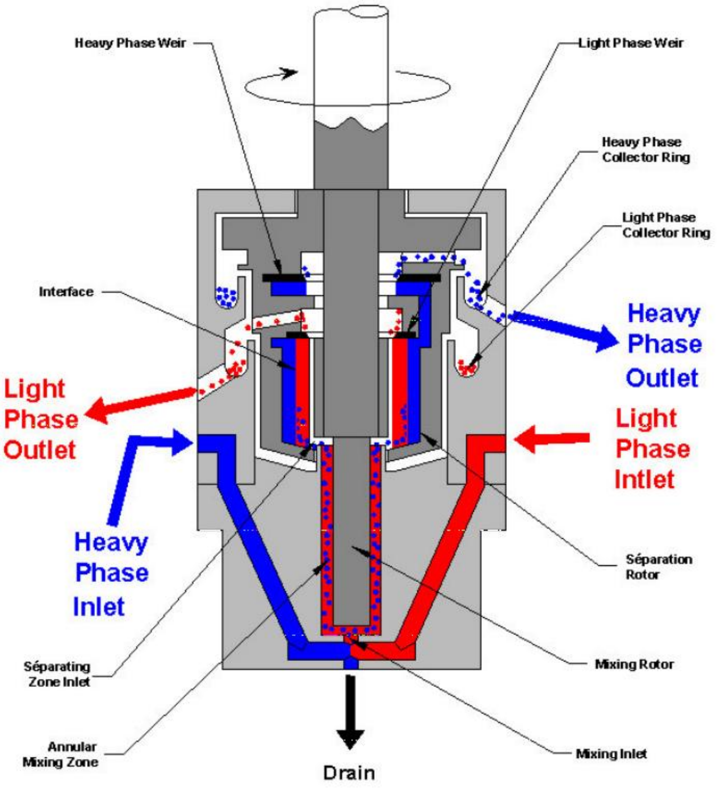

Figure 2.16: Schematic view of ECRAN [59]

2.7.3 Low mixing sleeve

In biopharmaceutical industry liquids are shear sensitive especially in the production of therapeutic antibodies and vaccines. Conventional solvent extraction equipment can damage cells or lead to product loss or lower yields. Mixing inside ACE is based on skin friction and it cannot be used in biopharmaceutical industry. Macluso et. al. [60] developed rotor sleeve for centrifugal extractor to handle shear sensitive liquids. A cylinder slightly higher than the rotor was fixed inside the annular region. During normal operation, liquids flow in-between outside diameter of inner sleeve and inner diameter of stationary bowl and radial vanes direct the feed liquids into the centre of the rotor bottom and into the rotor inlet orifice. Schematic view of low mix sleeve and bottom plate assembly is shown in below Fig. 2.17.

Figure 2.17: Schematic view of low mix sleeve and bottom plate assembly [61]

2.7.4 Clean-in-place

Solid particles exist in two-immiscible phases which add more complication in rotating bowl operation. In nuclear reprocessing solvent extraction operation two types of solid particles are encountered and are categorized into two types. Primary sludge [62, 63] which is mainly due to fine particles and insoluble residue generated during dissolution and it can be removed by clarification process. Secondary sludge that is formed mainly due to chemical reaction between degraded solvent and fission products (molybdenum zirconium hydrate, crud etc). Secondary sludge [64-66] is generated after the clarification step and it reaches the solvent extraction operation which drastically affects the centrifugal extractor operation. To address above problem Clean-In-Place (CIP) [67 - 69] was developed in Idaho National Laboratory (INL). Schematic view of CIP design is shown in Fig. 2.18.

ACE with CIP design contains a hollow shaft with high pressure spray nozzles in each quadrant. Spray nozzles covers complete area inside the rotor including aqueous underflow region and upper rotor assembly. A permanent rotary union is attached to the tail shaft to provide inlet to the cleaning solution to wash solid particles settled inside in the rotor. During washing, liquid with high pressure pumped inside the hollow shaft through rotor union until unit is clean. Liquid with sludge collected through bottom drain line connected at bottom of the stationary bowl. After sufficient cleaning, ACE is put back in solvent extraction operation.

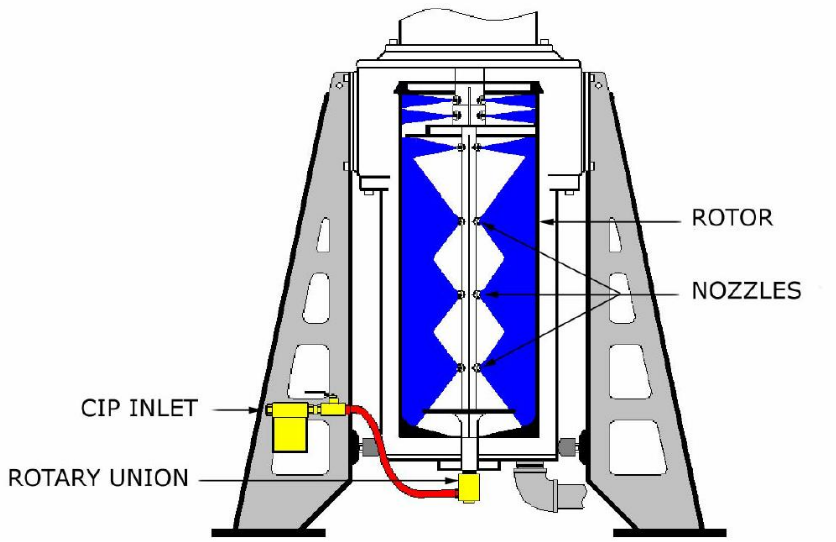

Figure 2.18: Schematic view of clean in place (CIP) design [68]

2.7.5 Design modification for nuclear fuel reprocessing application

ACE requires frequent maintenance and it leads to solvent degradation and radiation exposure to maintenance crew in nuclear fuel reprocessing application. To reduce frequent maintenance in ACE following modifications are reported in the literature and they are (i) Two modular structure

[70-72], (ii) Three modular structure [73, 74], (iii) Inter-stage horizontal over flow line for mixed phase flow [75, 76], (iv) Two separate overflow lines [77] for aqueous and organic phases. Details of above modification and working principle are explained in detail at chapter 4 in this thesis.

2.8 Summary

Solvent extraction and its basic are discussed in details. Equipment related to reprocessing application is discussed and selection basis of Annular Centrifugal Extractor for Fast Breeder Reprocessing with working and design principle also explained. Design modifications specific to process requirement in ACE is explained with details in this Chapter.

2.9 References

1. R. Natarajan, B. RAJ, "Fast Reactor Fuel Reprocessing Technology in India", *J. Nuc. Sci. & Tech.,* **2007,** *44(3),* 393-397.
2. M. Benedict, T. H. Pigford, H. W. Levi, "Nuclear Chemical Engineering", *McGraw-Hill Book Company,* **1981,** *2nd edition.*
3. J. A. Williams, L. Lowes, M. C. Tanner, "The Design of a Simple Mixer Settler", *Trans. Instn. Chem. Engrs.,* **1958,** *35(6),* 465-475
4. W. J. D. Van Dijk, "Process and Apparatus for Intimately Contacting Fluids" *U.S. Patent No. 2,011.186,* **1935**.
5. G. J. Bernstein, D. E. Grosvenor, F. F. Lenc, N. M. Levitz, "A High capacity annular centrifugal extractor", *Nucl. Technol.,* **1973,** *20(3),* 200-202.
6. G. Sege, F. W. Woodfield, "Pulse column variables: solvent extraction of uranyl nitrate with tri-butyl phosphate in a 3-inch diameter pulse column", *Chem. Eng. Progr.,* 1954, *50.*
7. N. Barson, G. H. Beyer, "Characteristics of a Podbielniak centrifugal extractor", *Chem. Eng. Prog.,* **1953,** *49(5),* 243-252
8. F. M. Jacobsen, G. H. Beyer, "Operating Characteristics of a Centrifugal Extractor", *AIChE J.,* **1956,** *2(3),* 283-289.
9. S. A. Zhukovskaya, V. N. Rusin, V. I. Medvedeva, "Contemporary technique in centrifugal extraction (a review of the literature)", *Pharm. Chem. J.,* **1972,** *6(11),* 714-723.

10. Y. Ito, M. A. Weinstein, I. Aoki, R. Harada, E. Kimura, K. Nunogaki, K., "The coil planet centrifuge", *Nature,* **1966,** *212,* 985–987.
11. G. I. Taylor, "Stability of a viscous liquid contained between two rotating cylinders," *Proceedings of The Royal Society A: Mathematical, Physical and Engineering Sciences,* **1923,** *102(718),* 541-542.
12. G. Baier, M. D. Graham, "Two-fluid Taylor–Couette flow: Experiments and linear theory for immiscible liquids between corotating cylinders", *Physics of Fluids,* **1998,** *12(10),* 3045-3055.
13. SGN-Robatel, "Multi-stage centrifugal contactor for liquid-liquid extraction (brochure)", *Saint-Gobain Techniques Nouvelles, Gcnas, France,* **1972**.
14. Rousselet Robatel Company Presentation 2017, "Monostage Liquid/Liquid Centrifugal Contactors (Model BXP)", Available online: *http://www.rousselet-robatel.com/brochures/Monostage_centrifugal_contactors_ BXP_Eng.pdf.*
15. D. S. Webster, C. L. Williamson, J. F. Ward, "Hydraulic performance of a 5-inch centrifugal contactor", *USAEC Report,* **1962,** DP-370.
16. R. T. Kent, "Mechanical Engineers' Handbook, Design Shop Practice", *John Wiley and Sons, Inc., New York,* **1938,** *11th Edition,* 11-09.
17. G. J. Bernstein, D. E. Grosvenor, J. F. Lenc, N. M. Levitz, "Development and performance of a high-speed, long rotor centrifugal contactor for application to reprocessing LMFBR fuels", **1973,** ANL-7968.
18. D. S. Webster, C. L. Williamson, and J. F. Ward, "Flow Characteristics of a Circular Weir in a Centrifugal Field", *USAEC report,* **June 1961,** DP-371.
19. A. A. Kishbaugh, "Performance of a Multi-stage Centrifugal Contactor", *USAEC report,* **1963,** DP-841.
20. A. S. Jennings, "A Miniature Centrifugal Contactor", *Savannah River Laboratory, Aiken, S. C. USAEC Report,* **1962,** DP-680.
21. C. S. Schlea, H. E. Henry, M. R. Caverly, W. J. Jenkins, "PUREX process performance with short-residence contactors", *USAEC Report,* **1963,** DP-809.

22. G. J. Bernstein, R. A. Leonard, A. A. Ziegler, M, J. Steindler, “An improved annular centrifugal contactor for solvent extraction reprocessing of nuclear reactor fuel”, *84th National Meeting, American Institute of Chemical Engineers, Atlanta, GA,* **1978**.

23. R. A. Leonard, S. B. Aase, H. A. Arafat, “Development of an Improved 2-cm Centrifugal Contactor for Cesium Removal from High-Level Waste”, *Argonne National Laboratory Report,* **2001a,** ANL-01/23, Argonne, IL.

24. E. L. Koschmieder, “Benard Cells and Taylor Vortices”, *Cambridge University Press,* New York, USA, **1993**.

25. S. Chandresekhar, “The hydrodynamic stability of visid flow between coaxial cylinders”, *Proc. Natl. Acad. Sci. USA,* **1960,** *46,* 141-146.

26. S. Vedantam, J. B. Joshi, “Annular Centrifugal Contactors- a review”, *Chem. Eng. Res. Des.,* **2006,** *84,* 522-542.

27. J. D. Thronton, H. R. C. Pratt, “Liquid–liquid extraction: Part VII. Flooding rates and mass transfer data for rotary annular columns”, *Trans. Inst. Chem. Engrs. (London),* **1953,** *31(4),* 289-305.

28. M. W. Davis, E. J. Weber, “Liquid–liquid extraction between rotating concentric cylinders”, *Ind. Eng. Chem. Res.,* **1960,** *52(11),* 929–934.

29. S. Cao, W. Duan, C. Wang, “Effects of Structure parameters on the hydraulic performance of the dia. 20 annular centrifugal contactor”, *Energy procedia,* **2013,** *39,* 461-466.

30. S. S. Deshmuh, M. J. Sathe, J. B. Joshi, “Residencet Time Distribution and Flow Patterns in the Single –Phase Annular Region of Annular Centrifugal Extractor”, *Ind. Eng. Chem. Res.,* **2009,** *48,* 37-46.

31. R. A. Leonard, “Design Principles and Applications of Centrifugal Contactors for Solvent Extraction”, *Ion Exchange and Solvent Extraction, A Series of Advances, Chapter 10,* **2009,** *Volume - 19.*

32. B. D. Kadam, J. B. Joshi, S. B. Koganti, R. N. Patil, “Hydrodynamic and mass transfer characteristics of annular centrifugal extractors”, *Chem. Eng. Res. Des.,* **2008,** *86,* 233-244.

33. M. Zhao, S Cao, W. Duan, “Effect of some parameters on mass-transfer efficient of a dia 20 mm annular centrifugal contactor for nuclear solvent extraction”, *Prog. Nucl. Energy,* **2014,** *75,* 154-159.

34. K. Mandal, S. Kumar, V. Vijayakumar, U. K. Mudali, A. Ravisankar, R. Natarajan, “Hydrodynamic and mass transfer studies of 125 mm centrifugal extractor with 30% TBP/nitric acid system”, *Prog. Nucl. Energy,* **2015,** *85,* 1-10.

35. H. L. Chen, J. C. Wang, W. H. Duan, J. Chen, “Hydrodynamic characteristics of 30% TBP/kerosene-HNO3 solution system in an annular centrifugal contactor”, *Nucl. Sci. Tech.,* **2019,** *30:89.*

36. K.E. Wardle, T.R. Allen, R. Swaney, “Computational fluid dynamics (CFD) study of the flow in an annular centrifugal contactor”, *Sep. Sci and Tech.,* **2006,** *41,* 2225-2244.

37. K.E. Wardle, T.R. Allen, M. H. Anderson, R. E. Swaney, “Analysis of the Effect of Mixing Vane Geometry on the Flow in an Annular Centrifugal Contactor”, *AIChE J.,* **2009,** *55(9),* 2244-2259.

38. K.E. Wardle, T.R. Allen, M. H. Anderson, R. E. Swaney, “Experimental Study of the Hydraulic Operation of an Annular Centrifugal Contactor with Various Mixing Vane geomentries”, *AIChE J.,* **2010,** *56(8),* 1960-1974.

39. K. E. Wardle, “ Liquid-Liquid Mixing Studies in Annular Centrifugal Contactors comparing Stationary Mixing Vane Options”, *Solvent Extr. Ion Exch.,* **2015,** *33,* 671-690.

40. J. Patra, N. K. Pandey, U. K. Mudali, R. Natarajan, J. B. Joshi, “ Hydrodynamic Study of Flow in the Rotor Region of Annular Centrifugal Contactors using CFD simulation”, *Chem. Eng. Comm.,* **2013,** *200,* 471-493.

41. W. Duan, X. Zhou, J. Zhou, “Extraction of Caffeine with Annular Centrifugal Contactors”, *Solvent Extr. Ion Exch.,* **2006,** *24,* 251-259.

42. J. Q. Xu, W. H. Duan, X. Z. Zhou, J. Z. Zhou, “Extraction of phenol in wastewater with annular centrifugal contactors”, *J. Hazard. Mater.,* **2006,** *131(1-3),* 98-102.

43. H Chen, Q. Zheng, W. Duan, “Hydraulic characteristics of n-octanol/aqueous solution systems in a 25-mm annular centrifugal extractor”, *Sep. Sci. Technol.,* **2009,** *DOI:10.1080/01496395.2019.1597887.*

44. T. Sun, W. Duan, J. Wang, J. Wang, J. Chen, “Hydraulic and Mass-Transfer performance of a 20-mm-diameter Annular Centrifugal Contactor for the Solvent Extraction of Cesium by Bis(2-Propyloxy)Calix[4]-Crown-6 in N-Octanol”, *Solvent Extr. Ion Exch.,* **2015,** *33,* 75-90.
45. B. Schuur, W. J. Jansma, J. G. M. Winkelman, H. J. Heeres, “Determination of the interfacial area of a continuous integrated mixer/separator (CINC) using a chemical reaction method”, *Che. Eng. Process., Process Intensification,* **2008,** *47(9-10),* 1484-1491.
46. D. Meikrantz, T. Garn, N. Mann, J. Law, T. Todd, “Hydraulic performance and Mass Transfer Efficiency of Engineering Scale Centrifugal Contactors”, **2007,** INL/CON-07-121967.
47. H. A. Arafat, M. C. Hash, A. S. Hebden, R. A. Leonard, “Characterization and Recovery of Solvent Entrained During the use of Centrifugal Contactors”, **2001,** ANL-02/08.
48. B. D. Kadam, J. B. Joshi, S. B. Koganti, R. N. Patil, “Dispersed phase hold-up, effective interfacial area and Sauter mean drop diameter in annular centrifugal extractors”, *Chem. Eng. Res. Des.,* **2009,** *87,* 1379-1389.
49. G. J. Bernstein, D. E. Grosvenor, J. F. Lenc, N. M. Levitz, “Development and performance of a high-speed, centrifugal contactor for application to reprocessing to LMFBR fuels”, **1973,** ANL-7698.
50. R. A. Leonard, G. J. Bernstein, R. H. Pelto, A. A. Ziegler, “Liquid-liquid dispersion in turbulent Couette flow”, *AIChE J.,* **1981,** *27,* 495-503.
51. R. A. Leonard, “Solvent Characterization Using the Dispersion Numeber”, *Sep. Sci. Technol.,* **1995,** *30(7-9),* 1103-1122.
52. Q. Lu, K. Li, M. Zhang, Y. Shi, “Study of a Centrifugal Extractor for Protein Extraction Using Reversed Micellar Solutions”, *Sep. Sci. Technol.,* **1998,** *33(15),* 2397-2409.
53. H. Fumoto, R. Kiyose, “Interface Characteristics in Settler of Centrifugal Extractor”, *J. Nucl. Sci. Technol.,* **1980,** *17(9),* 694-699.
54. T. Mizushna, T. Takamatsu, T. Takashashi, K. Tanaka, “Discharge Coefficients in the centrifugal Field for the water Kerosene system”, *Japanese Report,* **1966**.
55. R. A. Leonard, H. Pelto, A. A. Ziegler, G. J. Bernstein, “Flow over Circular Weirs in a centrifugal field”, *Can. J. Chem. Eng.,* **1980,** *58(4),* 531-534.

56. E. W. Slocum “Flow of viscous fluid over weirs”, *Can. J. Chem. Eng.,* **1964,** *42(5),* 196-200.
57. G. J. Bernstein, D. E. Grosvenor, J. F. Lenc, N. M. Levitz, “A High Capacity Annular Centrifugal Contactor”, *Nucl. Technol.,* **1973,** *20(3),* 200-203.
58. D. H. Meikrantz, L. L. Macaluso, W. D. Flim, C. J. Heald, G. Mendoza, S. B. Meikrantz, “A New Annular Centrifugal Contactor for Pharmaceutical processes”, *Chem. Eng. Commun.,* **2002,** *189(12),* 1629-1639.
59. P. Rivalier, F. Gandi, J. Duhamet, “Development of a new annular centrifugal solvent extraction contactor”, *Atlante 2004, Nimes, France,* June 21-25, **2004,** PI-48.
60. D. H. Meikrants, A. G. Federici, L. L. Macaluso, H. W. Sams, “Rotor Sleeve for a Centrifugal Separator”, *U.S. Patent 5,571,070,* **1996**.
61. D. H. Meikrantz, J. D. Law, T. A. Todd, “Design Attributes and Scale Up Testing of Annular Centrifugal Contractors”, *Presented at the Chemical Engineering Division of the AIChE Spring National Meeting,* **April 10-14, 2005,** Atlanta, GA (INL/CON-05-00088)
62. H. Kleykamp, “The chemical state of fission products in oxide fuels at different stages of the nuclear fuel cycle”, *Nucl. Tech.,* **1988,** *80,* 412-422.
63. J. Lausch, R. Berg, L. Koch, M. Coquerelle, P. J. Glatz, T. C. Walker, K. Mayer, “Dissolution residues of highly burnt nuclear fuels”, *J. Nucl. Mater.,* **1994,** *208,* 73-80.
64. A. Magnaldo, H. M. Noire, E. Esbelin, P. J. Dancausse, S. Picart, “Zirconium molybdate hydrate precipitates in spent nuclear fuel reprocessing”, *Atlante 2004, Nimes, France,* June 21-25, **2004,** P1-25bis.
65. J. F. Doucet, T. D. Goddard, M. C. Taylor, S. I. Denniss, M. S. Hutchson, D. N. Bryan, “The formation of hydrated zirconium molybdate in simulated spent nuclear fuel reprocessing solutions”, *Phys. Chem. Chem. Phys.,* **2002,** *4,* 3491-3499.
66. T. Usami, T. Tsukada, T. Inoue, N. Moriya, T. Hamada, D. Purroy, R. Malmbeck, P. J. Glatz, “Formation of zirconium molybdate sludge from an irradiated fuel and its dissolution into mixture of nitric acid and hydrogen peroxide”, *J. Nucl. Mater.,* **2010,** *402,* 130-135.
67. L. L. Macaluso, D. H. Meikrants, “Self Cleaning Rotor for a Centrifugal Separator”, *U. S. Patent 5,908,376,* **1999**.

68. N. R. Mann, T. G. Garn, D. H. Meikrantz, J. D. Law, T. A. Todd, “Clean-in-place and reliability testing of a commercial 12.5 cm annular centrifugal contactor at the INL”, *Proceedings of the GLOBAL 2007, Boise, Idaho, USA, September 9–13,* **2007**.

69. T. G. Garn, D. H. Meikrantz, N. R. Mann, J. D. Law, T. A. Todd, “Hydraulic and clean-in-place evaluations for 12.5 cm annular centrifugal contactor at the INL”. *Proceedings of the ISEC 2011, Santiago, Chile, October 3–7,* **2011**.

70. W. Duan, Q. Cheng, X. Zhou, J. Zhou, “Development of a ϕ20 mm annular centrifugal contactor for the hot test of the total TRPO process”, *Prog. Nucl. Energy,* **2009,** *51,* 313.

71. Leonard, R. A.; Chamberlain, D. B.; Conner, C. Centrifugal Contactors for Laboratory-Scale Solvent Extraction Tests. *Sep. Sci. Technol.* **1997,** *32*, 193.

72. H. Xiang-Ming, Y. Yu-Shun, Z. Quan-Rong, L. Bin-Ken, “Recent advances of annular centrifugal extract or for hot test of nuclear waste partitioning process”, *Nucl. Sci. Tech.,* **1998,** *9*,157.

73. P. Rivalier, J. Y. Lanoe, “Development of a new miniature short-residence-time annular centrifugal solvent extraction contactor for tests of process flow sheets in hot cells” *Proceedings of the ATALANTE 2000, Palais des Papes, Avignon, France, October 24-26,* **2000,** 28.

74. J. D. Law, D. H. Meikrantz, T. G. Garn, L. L. Macaluso, “Advanced Remote Maintenance Design for Pilot-Scale Centrifugal Contactors”, *Nucl. Technol.,***2011,** *173*, 191.

75. R. T. Jubin, “Centrifugal contactor modified for end stage operation in a multistage system”, *US Patent 4925441,* **May 15, 1990**.

76. T. Washiya, M. Takeuchii, H. Ogino, S. Aose, “Development of centrifugal contactor system in JNC”. *Proceedings of the GLOBAL 2005, Tsukuba, Japan, October 9–13,* **2005.**

77. W. Duan, C. Song, Q. Wu, X. Zhou, J. Zhou, “Development and Performance of a New Annular Centrifugal Contactor for Semi-Industrial Scale”, *Sep. Sci. Technol.* **2005,** *40,* 1871-1883.

CHAPTER 3

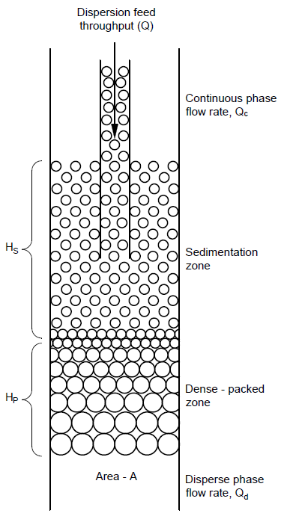

sedimentation and dense packed zones in steady state settler

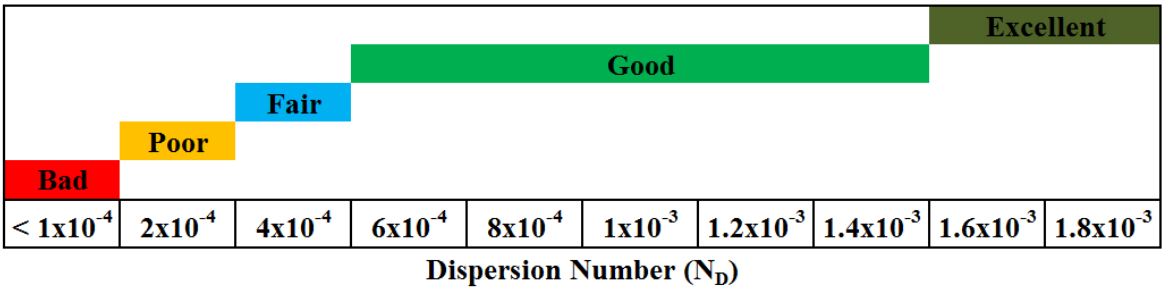

Solvent characterization based on dispersion number

DEVELOPMENT OF UNIFIED CORRELATION FOR DISPERSION NUMBER

3 DEVELOPMENT OF UNIFIED CORRELATION FOR DISPERSION NUMBER

3.1 Introduction

Many industrial processes require efficient liquid-liquid separator such as separation of water from crude oil, separation of dispersion in the solvent extraction settlers, separation of dispersion at the end of the differential columns [1], etc. Settling (sedimentation) and drops coalescence are two distinct processes that happen inside the gravity settler. Two types of coalescence are observed, (i) coalescence of drops with each other (binary coalescence) and (ii) coalescence with an interface. Both settling and coalescence need to be understood for the sound design of gravity settler. The determining factor for designing a settler is the coalescence rate of the dispersed phase, which can be obtained experimentally. Coalescence refers to the merging two or more drops with each other, requiring puncturing the film surrounding the drops. Interfacial tension is the driving force, and it decides the coalescence rate.

3.2 Literature review

During steady-state operation, dispersion band exits in-between separated phases of the light phase (upper layer) and heavy phase (lower layer) inside liquid-liquid settler. Barnea and Mizrahi [2-5] studied holdup inside the dispersion band within the dispersed phase in deep layer gravity settler. They observed two main sub-layers inside the dispersion band and shown in Fig. 3.1. They are (i) dense-packed sub-layer and (ii) sedimentation or settling zone.

The “dense-packed sub-layer” (also called as a dense-packed zone), in which holdup is much higher than in the feed and increases sharply towards active interface (also called as coalescence front or interface), where it reaches unity. The dense sub-layer occupies a 10-20% volume of the dispersion band.

The “even concentration sub-layer” (also called as sedimentation or settling zone), where the holdup level is almost constant and lower than the feed. The actual holdup decreases linearly towards the passive-interface (sedimenting or settling interface), where the droplets are more or less to zero.

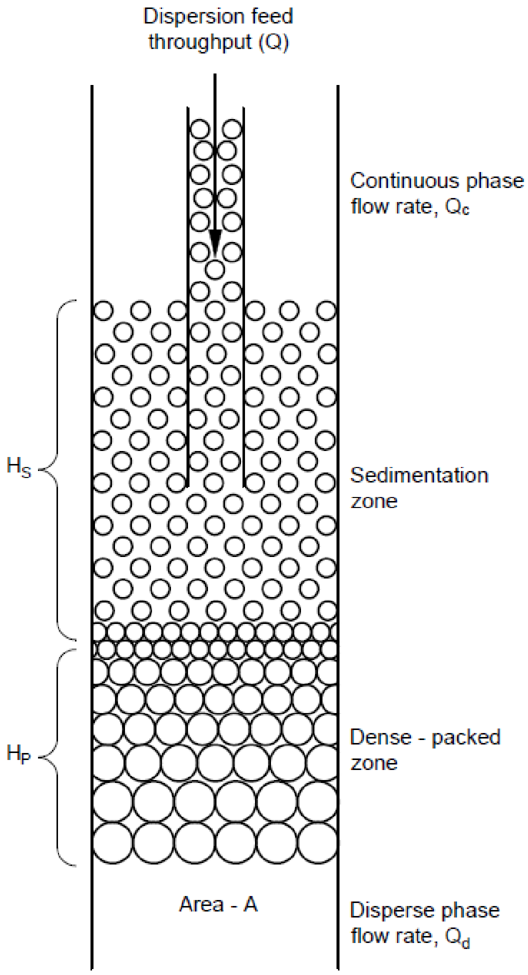

Figure 3.1: Schematic representation of sedimentation and dense packed zones in steady state settler

Steady state dispersion height (H)

In gravity settler, during unsteady-state operation, the liquid-liquid dispersion band thickness (H) increases in-between lighter (top layer) and heavy (bottom layer) phase with time until it reaches the steady-state condition. During steady-state operation, dispersion height (H) increases with the volume metric flow rate of the dispersed phase per unit area (Q_d/A) until the flooding point is reached. Steady-state dispersion height (H) decides the settler size, such as length and cross-sectional area for a given dispersed and continuous phase flow rates.

Stonner and Wholer [6] proposed the analogy for steady state height (H) with dispersion flux (Q/A) and it is shown in Eq. 3.1.

$$\frac{1}{Q/A} = \frac{1}{k_1 H} + \frac{1}{k_2} \tag{3.1}$$

Where k_1 and k_2 are constants, which are to be determined from experimental data. The variation in steady state dispersion height H and volumetric flow rate of dispersion per unit area Q/A may also be represented by power law:

$$H = K\left(\frac{Q}{A}\right)^{w} \tag{3.2}$$

in which K and w are constants, which was first implicitly proposed and verified experimentally by Ryon et al. [7]

During continuous operation, dispersion phase from mixer is fed to the settler continuously. The droplets entering the dispersions first sediment, grow in size through inter-drop coalescence (binary coalescence) before entering the dense-packed zone and finally coalesce with their bulk phase at the coalescing interface (interfacial coalescence). The dense-packed zone forms when the rate of sedimentation is faster than the rate of interfacial coalescence during the growth period. At steady-state, the volume rates of droplet sedimentation and interfacial coalescence must be equal to the volume throughput of the dispersed phase.

Both steady state continuous and unsteady state batch dispersions usually contain sedimentation and dense-packed zone. Rate of sedimentation and interfacial coalescence decide the heights of dispersed phase zone and in turn influenced by binary coalescence. Sedimentation and dense-packed zones heights decide the dispersion height in both batch and continuous operation.

Annular centrifugal extractor:

The schematic view of separation of two immiscible liquids inside the annular centrifugal extractor rotating bowl is shown in Fig. 3.2. A cylindrical interface of radius r_i separates the layers of heavy and light phases, denoted by A and B, respectively. Compare to centrifugal force, the force due to gravity is negligible, and the interface is almost vertical. If there is negligible frictional resistance to the flow of the liquids, the position of the liquid-liquid interface is established by hydrostatic balance and the relative “heights” (radial distances from the axis) of the overflow ports (1) and (2).

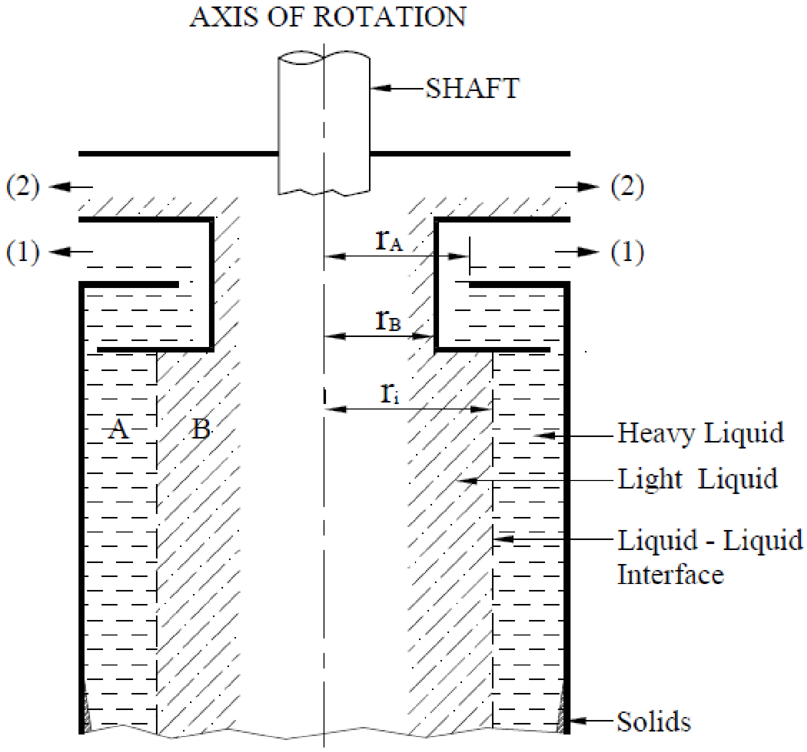

Figure 3.2: Centrifugal separation of immiscible liquids
(1) heavy phase (2) light phase

Assume (i) heavy phase (density ρ_A) overflows at radius r_A,, (ii) light phase (density ρ_B) leaves through the port at radius r_B. If both liquids rotate with the bowl and friction is negligible, the pressure difference in the light phase between r_B and r_i must be equal to that in the heavy phase between r_A and r_i.

Thus

$$p_i - p_B = p_i - p_A \tag{3.3}$$

Where p_i = pressure at the liquid-liquid interface

p_B = pressure at the free surface of light phase at r_B

p_A = pressure at the free surface of light phase at r_A

Balancing centrifugal force with pressure force leads to Eq. 3.4 and 3.5.

$$p_i - p_B = \frac{\omega^2 \rho_B (r_i^2 - r_B^2)}{2} \text{ and } p_i - p_A = \frac{\omega^2 \rho_A (r_i^2 - r_A^2)}{2} \tag{3.4}$$

Solving for r_i gives

$$r_i = \sqrt{\frac{r_A^2 - (\rho_B / \rho_A) r_B^2}{1 - \rho_B / \rho_A}} \tag{3.5}$$

Eq. 3.5 shows that r_i the radius of interface, is sensitive to the density ratio, especially when the ratio is nearly unity.

Dispersion band:

Flooding limit (carryover of other phase should be lesser than 1%) decides the operating capacity of any solvent extraction equipment. In view of this, several investigations have been carried out to study the separation mechanism of liquid-liquid dispersion in a gravity settler as well as Annular Centrifugal Extractors (ACE). The structure of dispersion band and the drop distribution [8, 9] in ACE was studied experimentally for a wide range of parameters. In chapter 2.5.3, Fig. 2.11 shows idealized behavior for the variation of volume fraction of dispersed phase against the vertical distance from the coalescence front for various throughputs in ACE. In an actual gravity separation also, a similar phenomenon is observed. Thus, the dispersion band thickness increases with an increase in throughput.

Settling time and Dispersion number:

Leonard et al. [10] have presented a systematic analysis and identified two characteristic times: (a) residence time of dispersion in a continuous separator or batch time provided for the dispersion to break in batch systems (t_B) and (b) time for a droplet to travel through the thickness of the separating zone (settling time, t_S).

It has been reported [2-4] that the settling time is proportional to the square root of the ratio of dispersion band height to the acceleration (either gravity or centrifugal):

$$t_s \propto \sqrt{\frac{\Delta Z}{a}} \tag{3.6}$$

Using the equation (3.6), the dispersion number defined [11] here is a characteristic of dispersions and settling as follows:

For a batch separator, the definition of N_D is

$$N_D = \frac{1}{t_B}\sqrt{\frac{\Delta Z}{a}} \tag{3.7}$$

For a continuous separator, the definition of N_D takes the following form:

$$N_D = \frac{Q}{V}\sqrt{\frac{\Delta Z}{a}} \tag{3.8}$$

where, V/Q is the residence time (t_R).

From equation (3.8), it can be seen that, for a given equipment size and a given acceleration field, the throughput varies directly as the dispersion number. In the latter section, the application of dispersion number analysis in predicting the separation capacity has been elaborated. In a gravity settler, acceleration is simply the acceleration due to gravity (g) and in a centrifugal settler, acceleration is given by,

$$a = \bar{r}\,\omega^2 \tag{3.9}$$

where,

$$\bar{r} = \frac{\int_{ro}^{ru} 2\pi r^2 dr}{\int_{ro}^{ru} 2\pi r\, dr} = \frac{2}{3}\left(\frac{r_u^3 - r_o^3}{r_u^2 - r_o^2}\right) \tag{3.10}$$

It includes both the dispersion band thickness and time required for dispersion to settle.

The value of N_D was found to depend upon the physical properties of the liquid-liquid systems (ρ_C, ρ_D, μ_C, μ_D, σ etc) and independent of the method of separation (i.e. gravity or centrifugal). The authors also analyzed the literature data along with their own and found the value of N_D to be in the range of 0.0001 to 0.02 depending upon the liquid-liquid system.

Leonard et al. [11] have discussed the details of standard tests to determine N_D and its application in characterization of extraction solvents. He covered many applications, i.e.: (1) centrifugal extractor stage-wise operation (2) plasticizer leaching (3) solvent development (4) Purex and TRUEX solvents in nuclear industry (5) TRUEX-SREX solvents in nuclear industry. Thus, the dispersion number is considered to be a measure of efficiency of separation in liquid -liquid extraction equipment [11].

Kadam et al. [12] have proposed a correlation for dispersion number in a annular centrifugal separator based on operating and geometric parameters and it is shown below in Eq. 3.11.

$$N_D = 0.037\left(\frac{Q_C}{ND_i^3}\right)^{0.26}\left(\frac{Q_D}{ND_i^3}\right)^{0.41}\left(\frac{c}{D_i}\right)^{-0.26}\left(\frac{d}{D_i}\right)^{0.062}\left(\frac{g}{D_i N^2}\right)^{0.17} \tag{3.11}$$

It relates different dimensions such as annular gap, bottom clearance and bottom vanes height along with the individual flow rates and rotor speed. It is a very useful correlation as it predicts the behavior of a particular system in a given annular centrifugal separator. As an extension to this work, it was thought desirable to propose a unified correlation for dispersion number that will combine the physical properties inherent to a particular system and be independent of the operating (except flow ratio) and geometric parameters. The motivation behind this was that as equations (3.6), (3.7) and (3.8) indicate, either for a batch system or a continuous system, dispersion number, by its very definition takes into account the capacity, the settling height and settling time.

3.3 Objective

Dispersion number remains almost constant over a wide range of operating parameters and is also independent of the type of settler. Dispersion number depends upon the physical properties of the continuous and dispersed phase. An attempt has been made to develop a unified correlation using available literature and experimental data of dispersion number based on continuous and dispersed phase physical properties respective to the type of settlers.

3.4 Experiments

3.4.1 Physcial properties measurement

Density measurement

Density is defined as its mass per unit volume (SI unit for density is kg/m^3). There are different methods available for density measurement and determination of density is a well established tool for product monitoring and quality control. High precision density meter, DMA 5000 was used to measure the density in this work.

The density measurement is based on measuring the period of oscillation of a Utube sample tube which is filled with sample liquid or through which the sample liquid flows continuously. The following relationship exists between the period P and density ρ.

$$\rho \;= \mathrm{A} * \mathrm{P}^2 - \mathrm{B} \qquad (3.12)$$

Where A and B are instrument constants which are determined by calibrating with fluids of known density.

A U-shaped glass tube of known volume and mass is filled with the liquid sample and exited electronically with a piezo element. The U-Tube is kept oscillating continuously at the characteristic frequency f. Optical pick-ups record the oscillation period P as P=1/f. After less than one minute, an acoustic signal informs that the measurement is finished. There is a reference oscillator which speeds up the measurement at various measuring temperatures. Once the instrument has been adjusted with air and water, density of the sample can be determined.

Viscosity measurement

Dynamic viscosity is defined as ratio between shear stress and rate of shear of a liquid (SI unit for dynamic viscosity is Pa.s). Dynamic viscosity or viscosity measures the resistance to flow or deformation of a liquid. There are different methods available for viscosity measurement. Cannon Fenske routine viscometer, size of 75 was used to measure the dynamic viscosity of the solution used in this work.

Dynamic viscosity measurement is based on time taken to flow constant volume through the capillary by gravity. The time is measured for a fixed volume of liquid to flow under gravity through the capillary of a calibrated viscometer under a reproducible driving head and at a closely controlled and known temperature. The following relationship exists between the flow time for given sample t_s, density of given sample ρ_s, flow time for standard sample (usually Grade-1 DM water) t_w, density of standard sample ρ_w, viscosity of standard sample μ_w and viscosity of given sample μ_s.

$$\mu_s = \frac{\mu_w * \rho_s * t_s}{\rho_w * t_w} \tag{3.13}$$

Interfacial tension measurement

Interfacial tension (IFT) is the force of attraction between the molecules at the interface of two fluids. At the air-liquid interface, this force is often referred to as surface tension (SI unit for surface/interfacial tension is mN/m). There are different methods available for interfacial tension measurement. The drop weight method was used to measure the interfacial tension of the liquid-liquid pair in this work.

In all measurements, 5 mL of each of the equilibrated organic and aqueous phases were taken for IFT measurements. The diameter of the capillary tip used was 0.5 mm. An ‘‘Agla(R)’’ micrometric syringe with a micrometer capable of delivering volumes as low as 0.2 mL was used. A glass vial containing the organic/light phase was kept in a double walled thermostatic vessel through which water from a constant temperature water bath was circulated. The capillary end was immersed in the light phase to a constant depth for all the measurements and the heavy phase was dropped slowly by turning the micrometer head. The volume of the drop was calculated from the weight difference between the weight of the glass vial before and after the aqueous/heavy phase addition and the density of the aqueous/heavy phase. The average time required for a drop to form was approximately 3 min which is sufficient for the equilibration of the drop formed as described by Harkins and Brown [13]. From the measured drop weight and the radius of the capillary, the IFT value was arrived at by using the equation 3.14.

$$\sigma = \frac{V(\rho_{aq} - \rho_{org})g}{2\pi r f_s} \qquad (3.14)$$

3.4.2 Batch experiments: Dynamic disengagement method

Over a wide range of solvent pairs were selected to cover wide physical properties: $120 < \Delta\rho < 625$ kg/m^3, $3 < \sigma < 58.3$ mN/m, $0.3 < \mu_C < 12.2$ and $0.3 < \mu_D < 12.2$ mPa.s for batch experimental study. Details of solvent pair and its physical properties are shown in Table 3.1.

Table 3.1: Solvent pairs selected for dispersion number measurement

Sr. No.	Sample composition	Density (kg/m^3) (Equilibrated Aqueous)	Density (kg/m^3) (Equilibrated Organic)	Interfacial tension, σ (mN/m) at 30°C by Drop weight method
1	Treated weak Phosphoric acid (27 % P_2O_5) -1.2 M D_2EHPA + 0.182 M TBP in HNP	1302	845	17.9
2	Treated weak Phosphoric acid (27 % P_2O_5) - 1.25 M D_2EHPA + 0.25 M TOPO in HNP	1313	861	8.3
3	Treated mixed acid (40 % P_2O_5) - 1.2 M D_2EHPA + 0.182 M TBP in HNP	1417	848	18.2
4	Treated mixed acid (40 % P_2O_5) - 1.25 M D_2EHPA + 0.25 M TOPO in HNP	1416	861	9.4
5	Treated Merchant Grade Phosphoric Acid (54 % P_2O_5 (as such without filtering) - 1.2 M D_2EHPA + 0.182 M TBP in HNP	1479	848	17.2
6	Treated Merchant Grade Phosphoric Acid (54 % P_2O_5) (as such without filtering) - 1.25 M D_2EHPA + 0.25 M TOPO in HNP	1476	863	10.7
7	Treated Merchant Grade Phosphoric Acid (54 % P_2O_5) (after filtering using Whatman 1001 125 filter paper) - 1.2 M D_2EHPA + 0.182 M TBP in HNP	1471	847	16.7

8	Treated Merchant Grade Phosphoric Acid (54 % P_2O_5) (after filtering using Whatman 1001 125 filter paper) - 1.25 M D_2EHPA + 0.25 M TOPO in HNP	1470	862	9.9
9	Hexane-water	998	660	58.3
10	(Hexane+10% CCl_4)-water	998	750	56.5
11	(Hexane+20% CCl_4)-water	998	850	55
12	(Hexane+58% CCl_4)-water	998	800	45
13	(Hexane+69% CCl_4)-water	998	700	42
14	Butanol-water	998	810	3
15	Toluene-water	998	780	35.5
16	Butyl acetate-water	998	880	16.2
17	Butyl acetate-25% DEG	1050	880	15
18	Butyl acetate-50% DEG	1025	880	14
19	Kerosene-water	998	780	48.5
20	Carbon tetrachloride-water	998	400	45

Graduated glass cylinder with 200 mm height and 25 mm diameter is selected for dispersion number measurement and following experimental procedure was adopted:

(a) Organic and aqueous phases were equilibrated to ensure no mass transfer or volume change during settling experiments.

(b) The measuring cylinder was filled with the aqueous and organic phases and then sealed with a ground glass stopper. The position of the interface between the two phases was noted by using the volume marks on the cylinder. After that, it was shaken vigorously in such a way that the dispersion of a two-phase mixture covered the entire volume of the cylinder (i.e., ΔZ is close to 200mm). For the solvents with higher viscosities, the cylinder was shaken horizontally so that the two liquids could extend the entire length of the cylinder.

(c) After the completion of shaking, the cylinder was placed on the top of the table and the movement of interface with respect to time was observed carefully until the final interface reached the initial position. The time taken for the dispersion to settle was denoted as 't_B'. Such settling measurements were made at least three times with the same solution mixture and the average value was selected which was within 5% deviation.

(d) Additional care was taken to observe of continuous phase and dispersed phase when A/O ratio was close to 1, because at this ratio, either of the phases could be continuous phase. If the viscosity of the two phases differed significantly, then the dispersion number varied depending on the viscosity of continuous phase. The variation was found to be as much as a factor of two. Hence, the value of dispersion number was noted for the particular continuous phase.

(e) Experiments were performed with different volume ratio (A/O) covering the range of 0.1 to 10.

In order to identify the continuous phase (aqueous or organic) in the dispersion band, a standard test was conducted in two beakers. One beaker was filled completely with the aqueous phase and the other was filled with the organic phase. A small amount of dispersion was injected at the bottom of the beaker containing heavy phase and at the top of the beaker containing light phase. If the heavy phase was the dispersed phase, then the droplets start moving towards bottom of the beaker containing light phase whereas, the droplets moved upward in the beaker filled with heavy phase indicating that the light phase is dispersed.

3.4.3 Continuous experiments in annular centrifugal extractors

Similarly, various solvent pairs were used in ACE experiments to measure the dispersion number to cover wider range of physical properties, such as density difference of $120 < \Delta\rho < 600$ kg/m^3, viscosity in the range of $0.6 < \mu_C < 12.2$ mPa.s and $0.6 < \mu_D < 12.2$ mPa.s and interfacial tension is $3 < \sigma < 58.3$ mN/m. Experiments were performed with aqueous phase as a dispersed as well as continuous phase. Initially, the organic and the aqueous phases were saturated with respect to each other so that no mass transfer occurred during experiment runs. In order to determine the dispersion number, the extractor was filled with aqueous phase and the rotor speed and the aqueous phase flow rates were adjusted to the predetermined values. The dispersed phase flow rate was increased in small steps and sufficient time (>10 times the residence time) was provided for attaining the steady state. The organic phase from organic outlet and aqueous phase from aqueous outlet were collected in test tubes. The clear separation is usually obvious as non-hazy liquid collection in aqueous and/or organic phase test tubes (as indicated by single colours in Fig. 3.3 (A) and (B)). In all the experiments, the collected liquids in both the test tubes were allowed to settle. Any small light phase carryover appears as a small layer at the top (Fig. 3.4 (C)) and heavy phase carryover appears in the bottom (Fig. 3.4 (D)) and the flooding limit was designated when carryover of one phase exceeded more than ~0.5% into the other phase. The analysis is based on visual observations and quantitative measurement of entrained amount of one phase into the other.

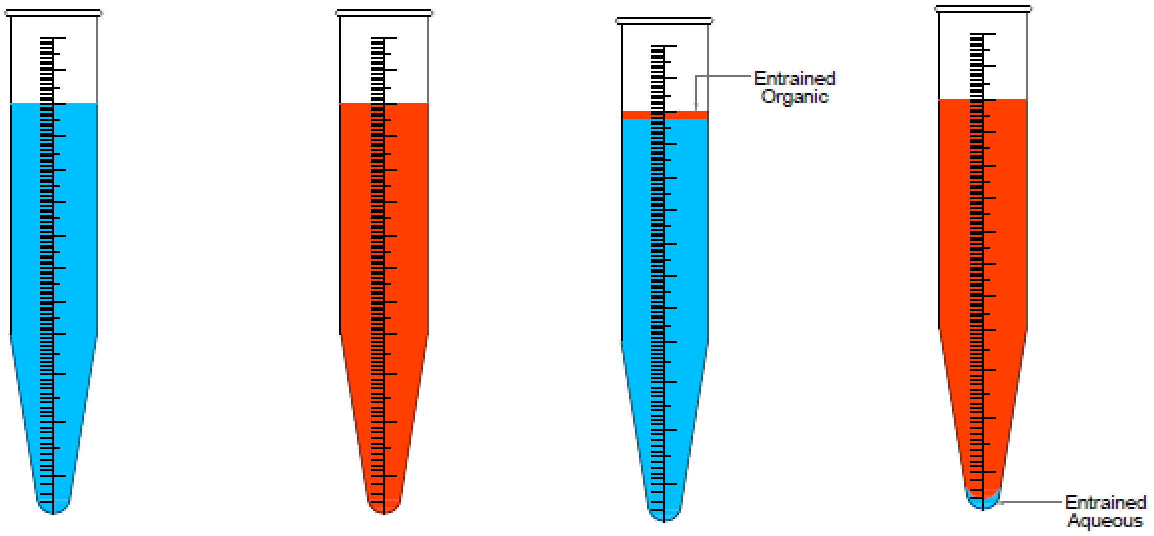

(A) Clear aqueous phase

(B) Clear organic phase

(C)

(D)

Good Separation

Bad Separation

Figure 3.3: Schematic view of good and bad separation

3.5 Results and Discussion

3.5.1 Batch experiments

To facilitate solvent characterization, Leonard [11] proposed a simple test based on the dimensionless dispersion number (N_D). It allows one to characterize the ability of the solvent to separate from a two-phase dispersion and to estimate process throughput for equipment of a given size. Dispersion number (N_D) is an important tool in the design of separating zones for liquid-liquid dispersions. In particular, N_D allows one to calculate the separating-zone volume required for a given throughput of a specific system at a given operating condition. Typically, this volume determines the maximum throughput for solvent extraction equipment. The significance of the values of dispersion number is its applicability to the other types of separation equipment also as it mostly depends upon the physical properties of the system.

A number of investigators [2-6, 14] have suggested the possibility of using experimental data obtained from batch experiments to the design of continuous gravity settlers. In view of this fact, the batch experiments were performed on various pairs of solvents, using different phase ratios. The values of dispersion number for the different solvent pair were calculated using Eq. 3.7 and it is shown in Appendix (Table A.1).

Based on batch data following correlation was developed:

$$N_D = 2.5 \times 10^{-4} \left(\frac{\sigma^3 \Delta\rho}{\mu_C^4 g} \right)^{0.04} \left(\frac{C}{D} \right)^{0.06} \left(\frac{\Delta\rho}{\rho_D} \right)^{-0.34} \left(\frac{\mu_C}{\mu_D} \right)^{0.09} \qquad (3.15)$$

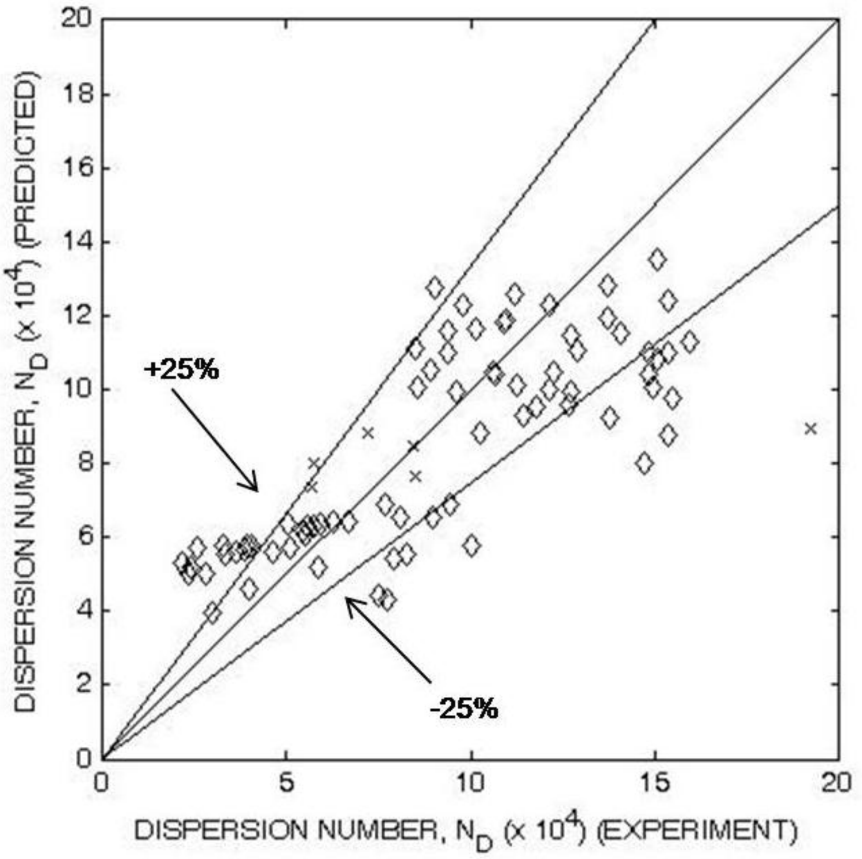

Figure 3.4: Parity plot for the comparison of N_D measured experimentally against those estimated by Equation. 3.12

(◊) (Present study, gravity settling) (×)Leonard [10]

Fig. 3.4 shows the parity plot of dispersion number. It is noticed from this figure that the developed correlation (Eq. (3.15)) gives poor representation of experimental data, which is reflected in the R^2 value of 0.53.

3.5.2 Centrifugal separators

Experiments were carried out on in centrifugal extractors with different rotor sizes and also at different speeds. Complete set of dispersion number data calculated using equation 3.8 and it is shown in Appendix Table A.2.

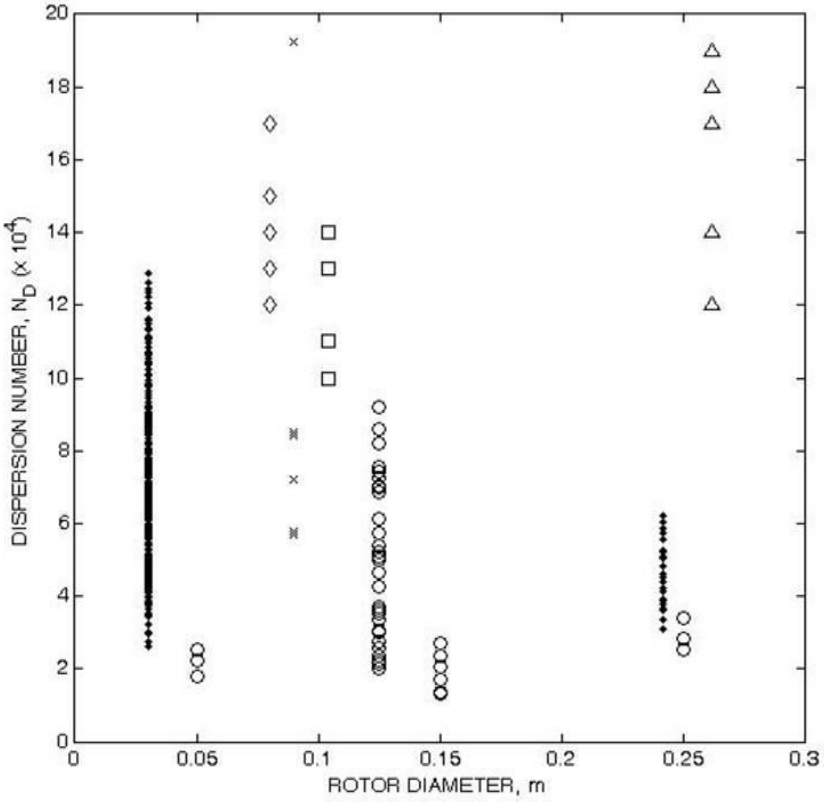

Figure 3.5: Variation of N_D with rotor diameter in ACE

(Δ) Webster et al. [15] (□) Bernstein et al. [16] (o) Present study (×) Leonard [10] (◊) Roth et al. [17] (♦) Kadam et al. [12].

It was considered to be a logical step to check the applicability of dispersion number for the scale-up of other designs of settlers such as centrifugal separators.

Fig. 3.5 shows the range of dispersion number as reported by various authors using centrifugal extractor of various rotor sizes for the systems with a wide range of physical properties. From this figure, it can be observed that the dispersion number depends upon the rotor size and physical properties of the system. Fig. 3.6 shows the variation of dispersion number for kerosene-water system. It can be seen that the dispersion number, for a given system, remains practically constant over a wide range of acceleration fields right from 1 to 510 ‘g’. This observation signifies that, for the measurement of dispersion number for a given liquid-liquid system, any size ACE (say, 50 mm rotor) is a suitable tool for the design and scale-up.

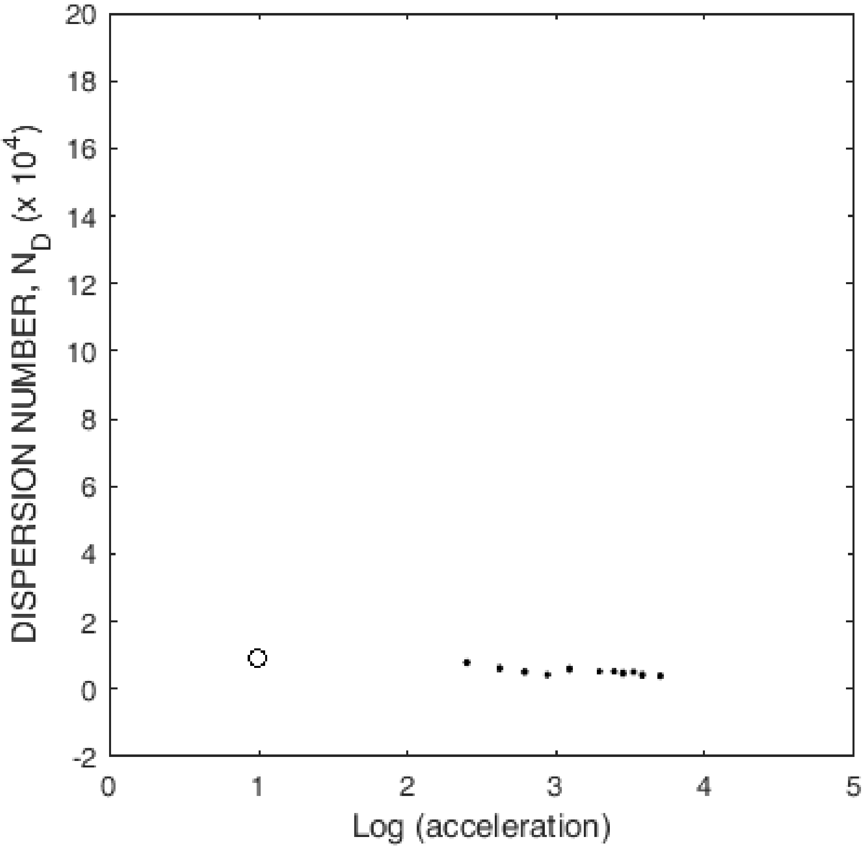

Figure 3.6: Variation of dispersion number for kerosene-water system under different acceleration field. (o) Present study (♦) Kadam et al. [12].

A dimensionless correlation was developed for continuous liquid-liquid separator by selecting dimensionless quantities involving only geometrical parameters. The following is the resulting correlation, which is very similar to Eq. 3.11:

$$N_D = 0.0462\left(\frac{Q_C}{ND_i^3}\right)^{0.58}\left(\frac{Q_D}{ND_i^3}\right)^{0.22}\left(\frac{c}{D_i}\right)^{-0.29}\left(\frac{d}{D_i}\right)^{0.04}\left(\frac{g}{D_iN^2}\right)^{0.08} \qquad (3.16)$$

The parity plot is shown in Fig. 3.7. It is noted that Eq. 3.16 fits the experimental data having R^2 value of 0.94.

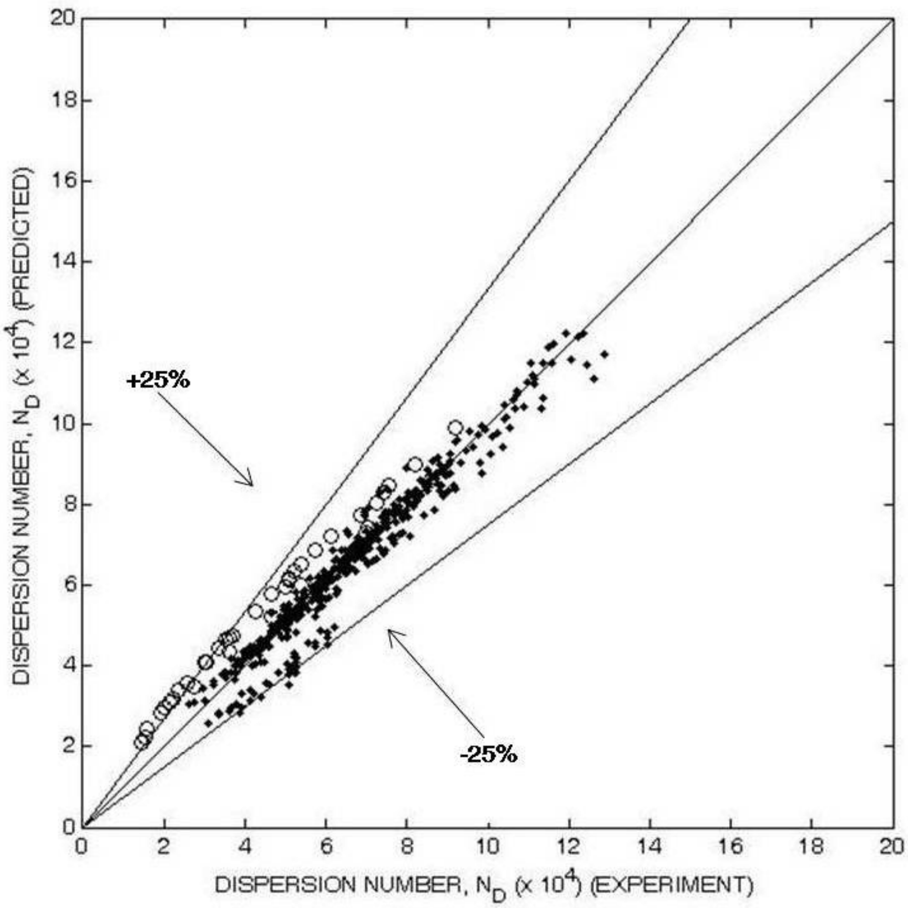

Figure 3.7: Parity plot for the comparison of N_D measured experimentally against those estimated by Equation. 3.16

(Annular centrifugal extractor) (o) Present study (♦) Kadam et al. [12]

Eq. 3.16 does not contain any physical properties data. Therefore, an attempt was made to combine the dimensionless numbers of Eqs. 3.15 & 3.16, which resulted in the following correlation:

$$N_D = 0.0156\left(\frac{\sigma^3\Delta\rho}{\mu_C^4 g}\right)^{0.03}\left(\frac{C}{D}\right)^{-0.93}\left(\frac{\Delta\rho}{\rho_C}\right)^{-0.04}\left(\frac{\mu_C}{\mu_D}\right)^{0.06}\left(1+\frac{a}{g}\right)^{2.68} \left(\frac{Q_C}{ND_i^3}\right)^{1.52}\left(\frac{Q_D}{ND_i^3}\right)^{-0.72}\left(\frac{c}{D_i}\right)^{-0.5}\left(\frac{d}{D_i}\right)^{0.05}\left(\frac{g}{D_i N^2}\right)^{-0.01} \quad (3.17)$$

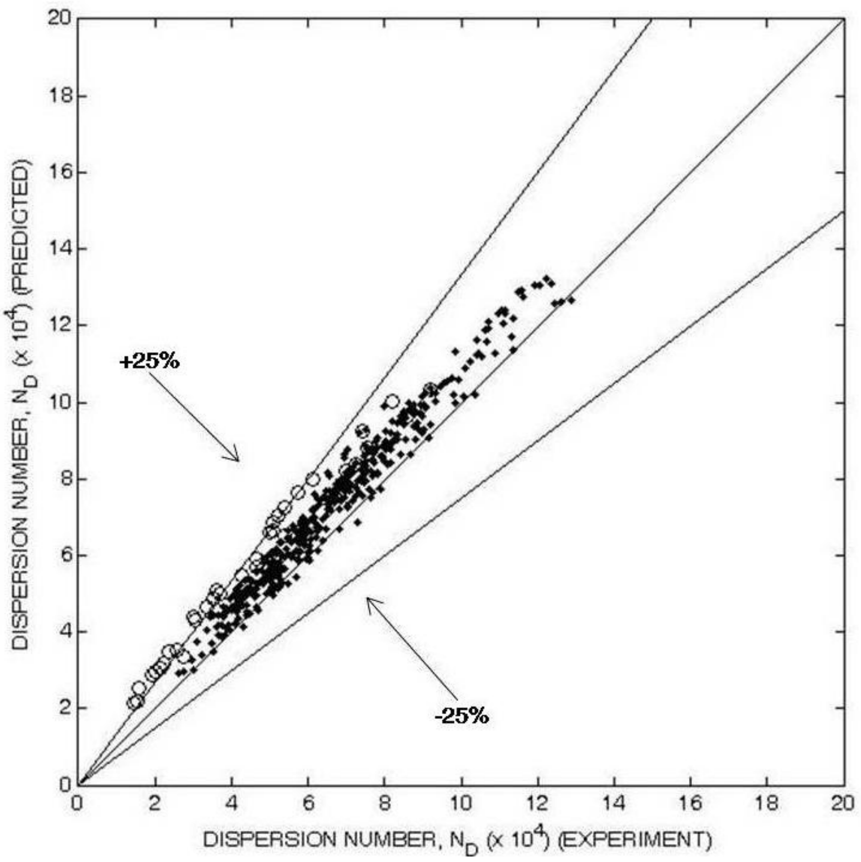

Figure 3.8: Parity plot for the comparison of N_D measured experimentally against those estimated by Equation. 3.17

(o) (Present study) (♦)Kadam et al. [12]

The parity plot of dispersion number for Equation 3.17 is shown in Fig. 3.8. The values of R^2 (0.96) improved to as compared with 0.94 of Fig. 3.7.

3.5.3 Solvent characterization by dispersion number

Leonard et al. [11] found that N_D values are typically in the range of 0.0001 to 0.020. The authors have stated that the value of N_D of 0.0001 indicates the solvent to be poor and very difficult to separate. Further, the N_D values of 0.0004, 0.0008 and 0.0016 to be fair, good and excellent, respectively. From our experimental data (shown in Table 3.2), it is observed that the lowest value of dispersion number is 0.000159 for 27% weak H_3PO_4 and the highest value is 0.003483 for 0.5 N HNO_3-NPH systems.

Table 3.2: Dispersion number for phosphoric acid system

Sr. No.	Solvent - Pair	Dispersion number (Aq. Dispersion)
1	27% Weak Phosphoric acid and 1.2 M D2EPHA + 0.182 M TBP	0.000587
2	40% Mixed Phosphoric acid and 1.2 M D2EPHA + 0.182 M TBP	0.000395
3	54% Phosphoric acid and 1.2 M D2EPHA + 0.182 M TBP	0.000770
4	27% Weak Phosphoric acid and 1.25 M D2EHPA+0.25 M TOPO in HNP	0.000159
5	40% Mixed Phosphoric acid and 1.25 M D2EHPA+0.25 M TOPO in HNP	0.000169
6	54% Phosphoric acid and 1.25 M D2EHPA+0.25 M TOPO in HNP	0.000298
7	0.5 N HNO3 - NPH	0.003483
8	30% TBP n-DD – 0.5 N HNO3	0.001470

3.5.4 Unified Correlation for dispersion number and their applications

Even though separate correlations have been developed for batch (Equation. (3.15)) and continuous (Equation. (3.17)). The quality of fit is not satisfactory, particularly for batch data. Further, two separate correlations are needed for batch and continuous liquid-liquid settlers. Hence, it was thought desirable to develop a unified correlation for gravity and centrifugal settling over the range of variables. (Tables 3.1, A.1 and A.2). For this purpose, the important parameters affecting the value of dispersion number were identified. The various combination of dimensionless groups was considered and using the dimensional analysis, five different correlations (shown in Table 3.3) were attempted to arrive at a unified correlation for gravity as well as centrifugal liquid-liquid separator. The corresponding R^2 value of each correlation has are also given in Table 3.3. The parity plot of dispersion number estimated using Eq. 3.18 is shown in Fig. 3.9.

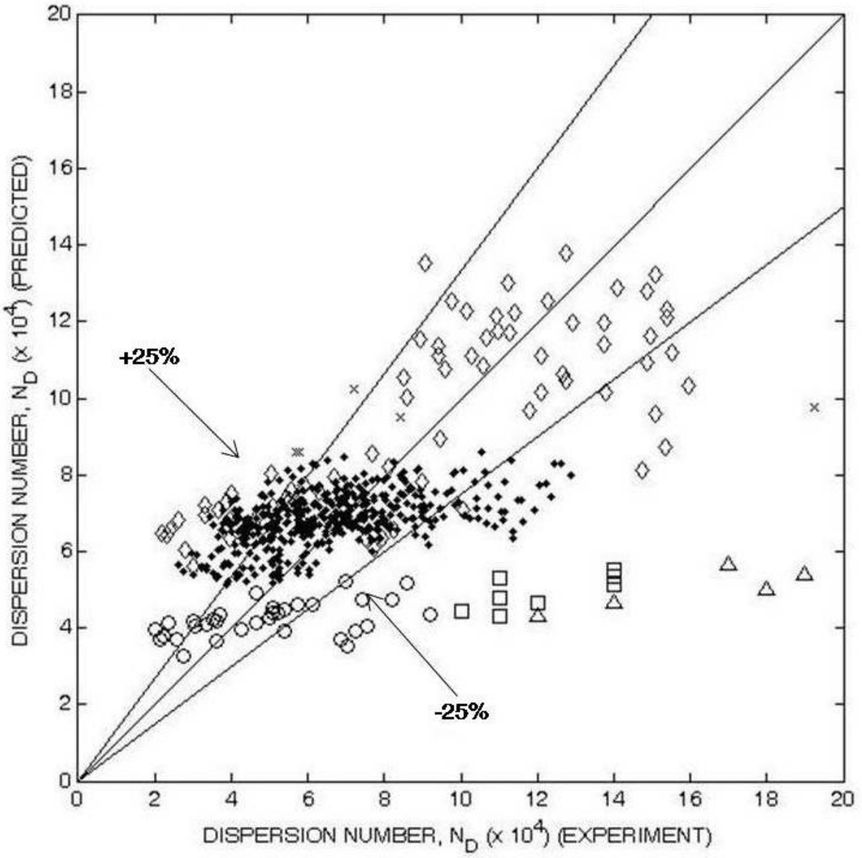

Figure 3.9: Parity plot for the comparison of N_D measured experimentally against those estimated by Equation. 3.18

(o) (Present study, annular centrifugal extractor) (◊) (Present study, gravity settling) (Δ) Webster et al. [15] (□) Bernstein et al. [16] (×) Leonard [10] (♦) Kadam et al. [12]

Table 3.3: Different forms of dimensionless dispersion number correlations

Dispersion number correlation	**R^2 value**	
$N_D = 5.08\times 10^{-4}\left(\frac{\sigma^3\Delta\rho}{\mu_C^4 g}\right)^{0.03}\left(\frac{C}{D}\right)^{0.08}\left(\frac{\Delta\rho}{\rho_C}\right)^{-0.09}\left(\frac{\mu_C}{\mu_D}\right)^{0.07}\left(1+\frac{a}{g}\right)^{-0.14}$	0.31	(3.18)
$N_D = 6.4\times 10^{-4}\left(\frac{\sigma^3\Delta\rho}{\mu_C^4 g}\right)^{0.03}\left(\frac{C}{D}\right)^{0.05}\left(\frac{\rho_C}{\rho_D}\right)^{-0.22}\left(\frac{\mu_C}{\mu_D}\right)^{0.10}\left(1+\frac{a}{g}\right)^{-0.14}$	0.30	(3.19)
$N_D = 6.17\times 10^{-4}\left(\frac{\sigma^3\Delta\rho}{\mu_C^4 g}\right)^{0.03}\left(\frac{A}{O}\right)^{-0.01}\left(\frac{\rho_{aq}}{\rho_{org}}\right)^{0.06}\left(\frac{\mu_{aq}}{\mu_{org}}\right)^{-0.06}\left(1+\frac{a}{g}\right)^{-0.15}$	0.27	(3.20)
$N_D = 9.89\times 10^{-4}\left(\frac{\sigma}{\sigma_w}\right)^{0.15}\left(\frac{C}{D}\right)^{0.09}\left(\frac{\Delta\rho}{\rho_C}\right)^{-0.10}\left(\frac{\mu_C}{\mu_D}\right)^{0.02}\left(1+\frac{a}{g}\right)^{-0.13}$	0.25	(3.21)
$N_D = 3.05\times 10^{-4}\left(\frac{\sigma^3\Delta\rho}{\mu_C^4 a}\right)^{0.03}\left(\frac{C}{D}\right)^{0.14}\left(\frac{\Delta\rho}{\rho_C}\right)^{-0.09}\left(\frac{\mu_C}{\mu_D}\right)^{0.1}$	0.17	(3.22)

It may be noted that the value of dispersion number is used for the evaluation of the general ability of a two-phase dispersion to separate quickly and yield a good solvent extraction process. In this context, Eq. 3.7 was used where t_B is the settling time. Thus, the solvent selection can be made by performing simple batch experiments. However, it may be pointed out that the continuous separation depends on centrifugal acceleration (a), the thickness of dispersion band (ΔZ) and the drop diameter in the liquid-liquid dispersion (which is a function of annular gap (d)). The values of acceleration (a), ΔZ and drop diameter depend upon geometry and power consumption (in addition to physical properties). Therefore, the correlations are given by equations 3.16 and 3.17 consist of geometrical parameters. In fact, we find the value of N_D using batch operation. When an acceptable value of N_D is obtained (by selecting proper solvent), the same value of N_D needs to be obtained in the ACE. In this context the development of equations 3.15 to 3.22 becomes useful. The foregoing discussion brings out the limitations of empirical correlations. In all these cases the quality of correlation can be seen to be poor. This is because of the limitations of practically all the forms of empirical correlations such as equations 3.18 to 3.22. This is true even though the real liquid-liquid systems (sometimes having surface active impurities) have been used for batch as well as continuous extractors of different sizes. The origin of limitations of empiricism is the methodology by which the empirical correlations are built. For instance, Eq. 3.18 suggests that N_D is directly proportional to, for instance, $\mu_C^{0.07}$ or practically independent of μ_C. In fact, the exponent on μ_C depends upon, actual values of interfacial tension, density difference, rotor diameter, etc. It may be emphasized that, any objective (such as N_D or mass transfer coefficient) depends upon the combined and simultaneous effect of all the design and operating parameters and any type of dimensionless correlation is unable to result into a desirable level of accuracy. In view of these observations it was thought desirable to implement the techniques of artificial intelligence (AI) for developing a predictive platform which can accommodate both batch and continuous operations. It may be emphasized that, any objective (such as N_D or mass transfer coefficient) depends upon the combined and simultaneous effect of all the design and operating parameters and any type of dimensionless correlation is unable to result into a desirable level of accuracy. In view of these observations it was thought desirable to implement the techniques of artificial intelligence (AI) for developing a predictive platform which can accommodate both batch and continuous operations.

3.5.5 Correlation based on data driven modeling

Data-driven modeling techniques have been finding increasing relevance and usage in the development of correlations for design parameters for equipment in Chemical Process Industry. The goal of data-driven modeling is to build a prototype that can adapt and learn from the practical data. Three techniques based on data driven modeling that are gaining popularity are artificial neural networks (ANN), support vector regression (SVR) and random forest (RF). ANN is based on artificial intelligence whereas support vector and random forest are machine learning methods. Among them, ANN is the most commonly and widely used data-driven modeling technique. Recently, SVR and RF are gaining popularity as they are rigorously based on statistical learning theory data. SVR uses structural risk minimization; hence it accounts for model complexity as well as minimizes training data error, while ANN makes use of empirical risk minimization which minimizes training data error only. The present paper uses random forest which is briefly described below:

3.5.5.1 Random Forest (RF)

Recently there has been a lot of interest in “ensemble learning”- methods that generate many classifiers and aggregate their results. Two well-known methods are boosting and bagging of classification trees. In boosting, successive trees give extra weight to points incorrectly predicted by earlier predictors. In the end, a weighted vote is taken for prediction. In bagging, successive trees doesn't depend on earlier trees, by using bootstrap method each one is independently constructed from the data set. Finally, a simple majority vote is taken for prediction.

Breiman [18] proposed an additional layer of randomness to bagging, which is nothing but random forest. In addition to constructing each tree using a different bootstrap sample of the data, random forests change how the regression trees are constructed. In standard trees, each node is split using the best split among all variables. In a random forest, each node is split using the best among a subset of predictors randomly chosen at that node. This somewhat counterintuitive strategy turns out to perform very well compared to many other classifiers, including discriminant analysis, support vector machines and neural networks, and is robust against over fitting. In addition, it is very user-friendly in the sense that it has only two parameters (the number of variables in the random subset at each node and the number of trees in the forest), and is usually not very sensitive to their values.

The random forests algorithm for regression has the following steps:

(a) Draw n_{tree} bootstrap samples from the original data.

(b) For each of the bootstrap samples, grow an un-pruned classification or regression tree, with the following modification: at each node, rather than choosing the best split among all predictors, randomly sample m_{try} of the predictors and choose the best split from among those variables. (Bagging can be thought of as the special case of random forests obtained when $m_{try}=p$, the number of predictors.)

(c) Predict new data by aggregating the predictions of the n_{tree} trees (i.e., average for regression). The randomForest package optionally produces two additional pieces of information: a measure of the importance of the predictor variables, and a measure of the internal structure of the data (the proximity of different data points to one another).

Variable importance: This is a difficult concept to define in general, because the importance of a variable may be due to its (possibly complex) interaction with other variables. The random forest algorithm estimates the importance of a variable by looking at how much prediction error increases when (OOB) data for that variable is permuted while all others are left unchanged. The necessary calculations are carried out tree by tree as the random forest is constructed. (There are actually four different measures of variable importance implemented in the classification code)

Proximity measure: The (i, j) element of the proximity matrix produced by randomForest is the fraction of trees in which elements i and j fall in the same terminal node. The intuition is that “similar” observations should be in the same terminal nodes more often than dissimilar ones. The proximity matrix can be used to identify structure in the data or for unsupervised learning with random forests.

Random forests are an effective tool in prediction. Because of the law of large numbers they do not overfit. Injecting the right kind of randomness makes them accurate classifiers and regressors. Furthermore, the framework in terms of strength of the individual predictors and their correlations gives insight into the ability of the random forest to predict. Using out-of-bag estimation makes concrete the otherwise theoretical values of strength and correlation.

Random inputs and random features produce good results in regression. The only type of randomness used in this study is bagging and random features. It may well be that other types of injected randomness give better results. For instance, one of the referees has suggested use of random boolean combinations of features.

The forests consist of randomly selected inputs or combinations of inputs at each node to grow each tree. The resulting forests give accuracy. This class of procedures has the following desirable characteristics:

1. Its accuracy is as good as adaboost and sometimes better.

2. It is relatively robust to outliers and noise.
3. It is faster than bagging or boosting.
4. It gives useful internal estimates of error, strength, correlation and variable importance.
5. It is simple and easily parallelized.

3.5.5.2 Performance of random forest based correlation

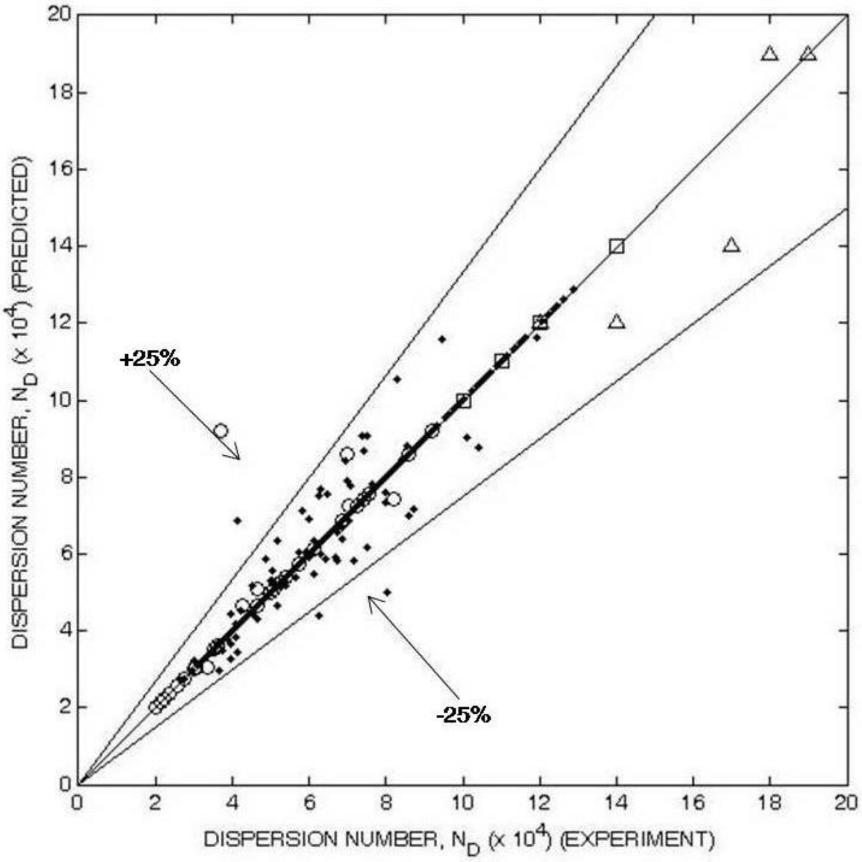

Figure 3.10: Parity plot for the comparison of N_D measured experimentally against random forest based correlation (462 data sets from ACE)

(o) (Present study, annular centrifugal extractor) (Δ) Webster et al. [15] (□) Bernstein et al. [16] (♦) Kadam et al. [8]

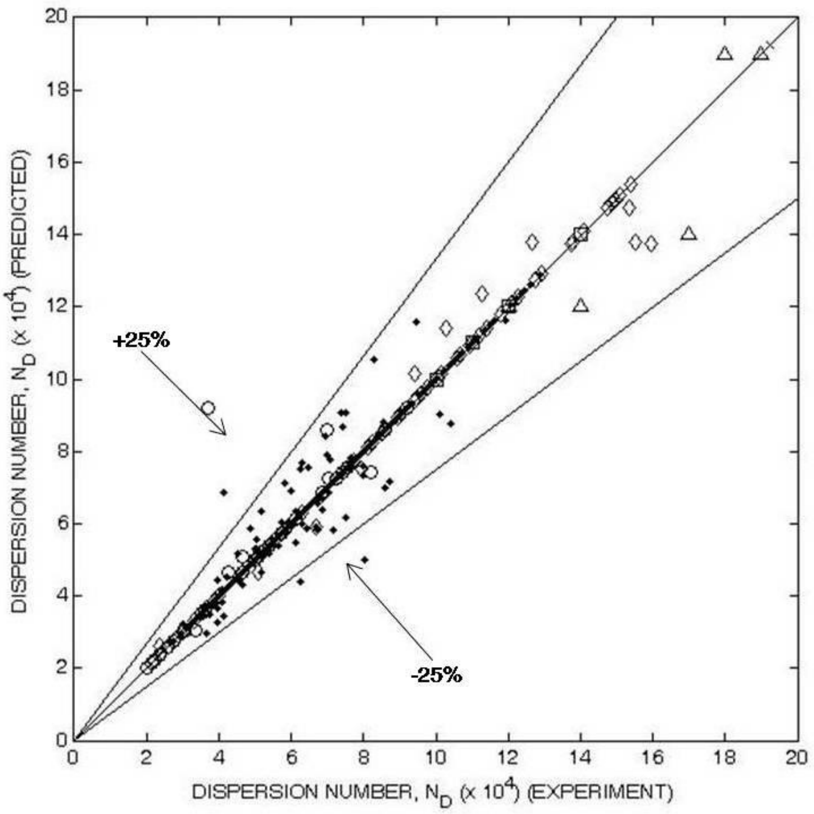

Figure 3.11: Parity plot for the comparison of N_D measured experimentally against random forest based correlation

(o) (Present study, annular centrifugal extractor) (◊) (Present study, gravity settling) (Δ) Webster et al. [15] (□) Bernstein et al. [16] (×) Leonard [10] (♦) Kadam et al. [8]

To establish data driven based correlations 542 data sets were collected out of which 80 were from batch. For training the estimated models 66% data was used and 34% data was used to test the models. Parity plots were generated after testing the data set. These parity plots are shown for 462 data sets from ACE and all the data sets in Fig. 3.10 and 3.11, respectively. In order to give a quantitative idea of performance of random forest based data driven correlation, a statistical term, coefficient of determination (COD) was introduced. The values of COD for ACE data and all the data were found to be 0.95 and 0.97, respectively. These values can be seen to be substantially superior to those correlations given by equations 3.15 to 3.22, and represented in Fig. 3.4 & 3.7 to 3.9.

Parametric sensitivity analyses of the proposed model were carried out by checking the effects of the input parameters.

3.6 Conclusion

The dimensionless dispersion number concept is used for determining the performance of solvent in solvent extraction equipment and prediction of maximum throughput in a stage wise contactor.

In this work, dispersion number correlation was developed for batch and continuous operation and fitting was poor especially for batch operation and it yielded two separate correlation. In order to improve the quality of fitting to experimental data, a novel data driven based dimensionless dispersion number correlation was developed by using Random Forest technique in artificial intelligence. Coefficient of determination was found to be much superior compare to all other dispersion number correlations. The dispersion number was found to be dependent on the physical properties of the phases used.

Thus, the dispersion number analysis serves the following purposes:

(1) It would help one couple the simplicity of gravity settling experiments with the ability of predicting the settling capacity of centrifugal separators (as these represent the two extremes of acceleration fields).

(2) A unification exercise carried out would enable the prediction of dispersion number based only upon the physical properties that are inherent to the pair of liquids and independent of the geometric and operating variables. This is important as the basic definition of dispersion number includes these variables and hence it is imperative to be able to predict its value when the values of these variables are not available.

(3) It has to be noted that, the exact prediction of the physical properties is neither always feasible nor possible. Even if properly measured, the actual system properties may vary. A

slight variation in, say, interfacial tension would make a big difference in the dispersion characteristics.

(4) In spite of these factors, a unified correlation would prove useful as it is based on the collection of data from various sources. It will save time of experiments as well as minimize the possibility of experimental error.

3.7 References

1. C. Nadiv, R. Semiat, "Batch Settling of Liquid-Liquid Dispersion", *Ind. Eng. Chem. Res.,* **1995,** *34(7),* 2427-2435.
2. E. Barnea, J. Mizrahi, "Separation and mechanism of liquid-liquid dispersion in deep layer gravity settler. I: Structure of the dispersion band", *Trans. Inst. Chem. Engrs.,* **1975a,** *53,* 61-69.
3. E. Barnea, J. Mizrahi, "Separation and mechanism of liquid-liquid dispersion in deep layer gravity settler. II: Flow patterns of dispersed and continuous phases within the dispersion band", *Trans. Inst. Chem. Engrs.,* **1975b,** *53,* 70-74.
4. E. Barnea, J. Mizrahi, "Separation and mechanism of liquid-liquid dispersion in deep layer gravity settler. III: Hindered settling and drop to drop coalescence in the dispersion", *Trans. Inst. Chem. Engrs.,* **1975c,** *53,* 75-82.
5. E. Barnea, J. Mizrahi, "Separation and mechanism of liquid –liquid dispersion in deep layer gravity settler. IV: Continuous settler characteristics", *Trans. Inst. Chem. Engrs.,* **1975d,** 53, 83-92.
6. H. M. Stonner, F. Wohler, "An engineers approach to a solvent extraction problem", *Inst. Chem. Engrs. Symp. Ser.,* **1975,** *42,* 14.1.
7. A. D. Ryon, F. L. Daley, R. S. Lowrie, "Design and scale-up of mixer-settler for a Dapex solvent extraction process", *Report No. ORNL-2951,* **1960**.
8. B. D. Kadam, J. B. Joshi, S. B. Koganti, R. N. Patil, "Dispersed phase hold-up, effective interfacial area and Sauter mean drop diameter in annular centrifugal extractors", *Chem. Eng. Res. Des.,* **2009,** *87(10),* 1379-1389.

9. T. V. Tamhane, J. B. Joshi, U. K. Mudali; R. Natarajan, R. N. Patil, “Measurement of drop size characteristics in Annular Centrifugal extractors using phase Doppler particle analyzer (PDPA)”, *Chem. Eng. Res. Des.,* **2012,** *90(8),* 985-997.
10. R. A. Leonard, G. J. Bernstein, R. H. Pelto, A. A. Ziegler, “Liquid-Liquid dispersion in turbulent couette flow”, *AIChE J.,* **1981,** *27(3),* 495-503.
11. R. A. Leonard, “Solvent characterization using the dispersion number”, *Sep. Sci. Technol.,* **1995,** *30(7-9),* 1103-1121.
12. B. D. Kadam, J. B. Joshi, S. B. Koganti, R. N. Patil, “Hydrodynamic and mass transfer characteristics of annular centrifugal extractors”, *Chem. Eng. Res. Des.,* **2008,** *86(3),* 233-244.
13. W. D. Harkins, F. E. Brown, “The determination of surface tension (free surface energy) and the weight of falling drops: the surface tension of water and benzene by the capillary weight method”, *J. Am. Chem. Soc.,* **1919,** *41(4),* 499-524.
14. S. A. K. Jeelani, S. Hartland, “Prediction of steady state dispersion height from batch settling data”, *AIChE J.,* **1985,** *31(5),* 711-720.
15. D. S. Webster, A. S. Jennings, A. A. Kishbaugh, H. K. Bethmann, “Performance of centrifugal mixer-settler in the reprocessing of nuclear fuel”, *Chem. Eng. Prog. 65: Symp. Ser. No. 94,* **1969,** 70-7.
16. G. J. Bernstein, D. E. Grosvenor, J. F. Lenc, N. M. Levitz, “Development and performance of a high-speed, centrifugal contactor for application to reprocessing to LMFBR fuels”, **1973,** ANL-7698.
17. B. F. Roth, “Centrifugal extractors for the reprocessing of nuclear fuels with high burn up and plutonium content”, **1969,** KFK-862.
18. L. Breiman, “Random forests”, *Machine learning,* **2001,** *45,* 5-32.

CHAPTER 4

4 stages 30 mm ACE stationary bowl with inter-stage inclined overflow line

(1) Aqueous feed pipe, (2) Organic feed pipe, (3) Aqueous outlet, (4) Organic outlet, (5) Aqueous inter-stage line and (6) Inclined over flow line

DEVELOPMENT AND DEMONSTRATION OF INCLINED OVERFLOW LINE

(TO HANDLE MOTOR/BEARING FAILURE OF ANY SINGLE STAGE IN MULTISTAGE CENTRIFUGAL EXTRACTOR SYSTEM)

4 DEVELOPMENT AND DEMONSTRATION OF INCLINED OVERFLOW LINE

4.1 Introduction

In this chapter, modification suggested in the literature for the smooth operation of multistage annular centrifugal extractor (ACE) system is explained. A new inclined overflow line is developed and incorporated in a multistage annular centrifugal extractor (ACE) stationary bowl for nuclear reprocessing application or handling hazardous process liquid during motor/bearing failure of any single-stage in multistage ACE. The performance of an inclined overflow line is explained and validated by hydrodynamic and mass transfer experiments.

The solvent extraction/liquid-liquid extraction (LLE) is an essential unit operation for the hydrometallurgical process to separate or recover metallic elements [1-3]. It has used in several applications such as chiral compound purification [4], removal of a dissolved organic compound from water [5], and in the nuclear industry [6-11]. ACE comes under a stage-wise contactor. Mass transfer and hydrodynamic performance of ACE is superior to conventional stage-wise contactors. Savannah River Laboratory (SRL) [12] developed paddle-type centrifugal extractor (CE) with air controlled aqueous weir to control the interface position inside the separating zone, which facilitates the handling of a wide range of aqueous and organic densities at different organic and aqueous phase flow ratios (O/A ratios). Later, Argonne National Laboratory (ANL) modified the paddle type into an annular type centrifugal extractor [13]. ACE has several advantages: compact design, less holdup, high throughput, high mass transfer performance, low residence time, small footprint, low height, etc.

Employing ACE in nuclear fuel reprocessing is a challenging task due to frequent maintenance, which leads to solvent degradation and man rem exposure to the plant operators and maintenance crew. It also requires a specialized tool for remote maintenance. Frequent motor/bearing failure due to overheating, corrosive, and radioactive environment during multistage operation and requires a more extended period to bring back the multistage ACE system to operating condition. During the maintenance, stagnant organic present inside the multistage ACE gets exposed to high radiation dose and leads to the formation of degraded products. Degraded solvent drastically affects the stripping performance, and it reduces the decontamination factor and increases the plutonium and uranium losses.

4.2 Literature review

Three methods are available to address frequent motor/bearing failures in multistage ACE operation. They are

1. Life enhancement of moving parts,
2. Mechanical design modification for easy and rapid remote maintenance, and
3. Process fluid flow pipe modification to ensure the fluid flow from the failed stage to the adjacent stages by providing a suitable bypass or overflow line.

(i) Life enhancement of moving parts

Replacement of conventional bearing with ceramic bearing and coating the stampings of the electrical motors with a chemical and radiation-resistant material reduces the failure frequency of bearing and motors [14]. The photographic view of the PEEK coated rotor and stator is shown in Fig. 4.1. Still, motor and bearing failure in the multistage system is inevitable and leads to the stoppage of the entire cascade for remote maintenance.

(a) (b)

Figure 4.1: PEEK coated (a) Rotor and (b) Stator

(ii) Mechanical design modification for easy and rapid remote maintenance

(a) Two modular structure [15-17] (rotating bowl with motor as one modular and another one is stationary bowl with interconnection line) for easy remote operation. Schematic view of two modular structure is shown in Fig. 4.2. Major disadvantage is that it requires high lifting capacity manipulator to lift the motor with rotating bowl. During remote maintenance, the liquid inside the rotating bowl may drip, further contaminate inside the lead cells. Separation of the centrifugal rotor from the failed motor may lead to a high radiation dose to the maintenance crew.

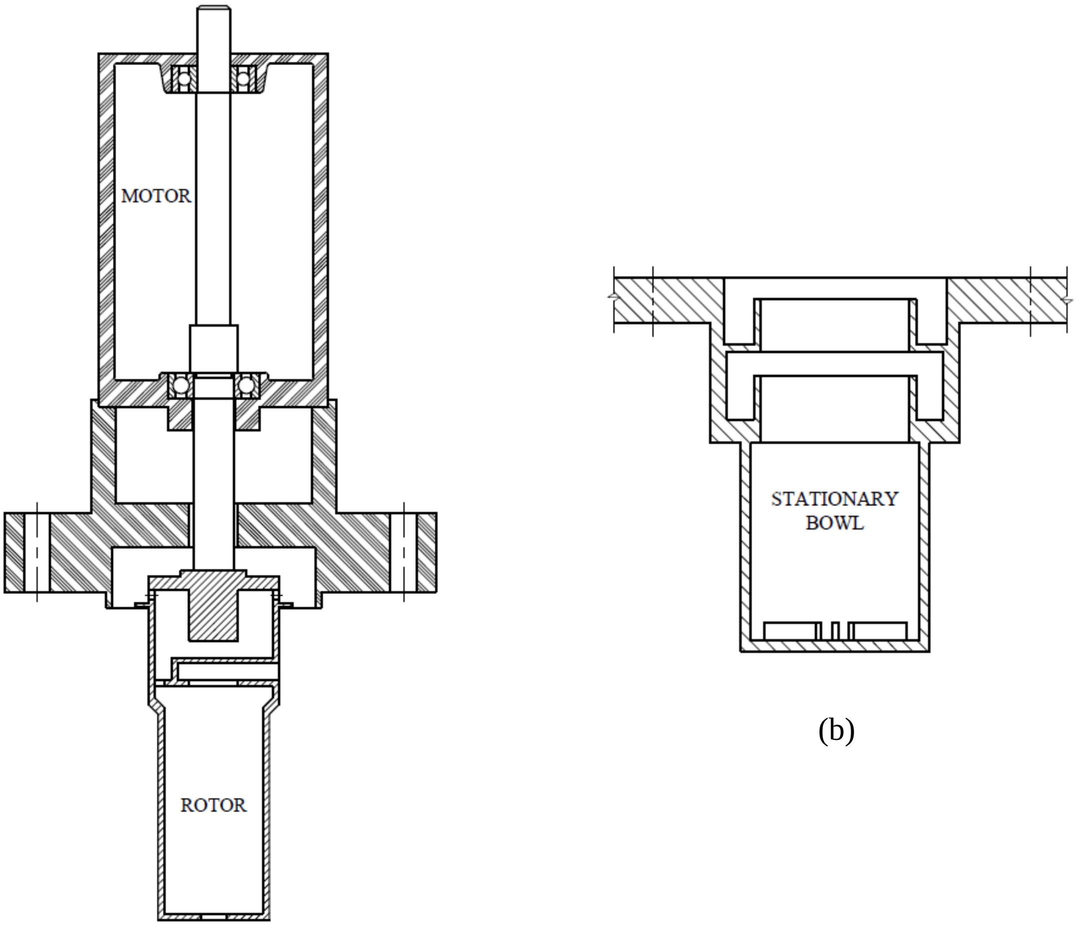

(b)

(a)

Figure 4.2: Schematic view of Two Modular Structure (a) Rotor Module and (b) Housing Module

(b) Three modular structure [18, 19] (motor as one modular, rotating bowl with coupling as second modular and third modular is a stationary bowl with interconnection line) design drastically reduces the maintenance time when compared to the two modular structure since the rotating bowl is always inside the stationary bowl which avoids the contamination inside the lead cells. The schematic view of three modular structures shown in Fig. 4.3. Still, solvent degradation occurs inside the multistage centrifugal extractor system during maintenance. Another disadvantage is that it requires more time for maintenance compared to the two modular structures in the event of bearing failure coupled with the rotating bowl.

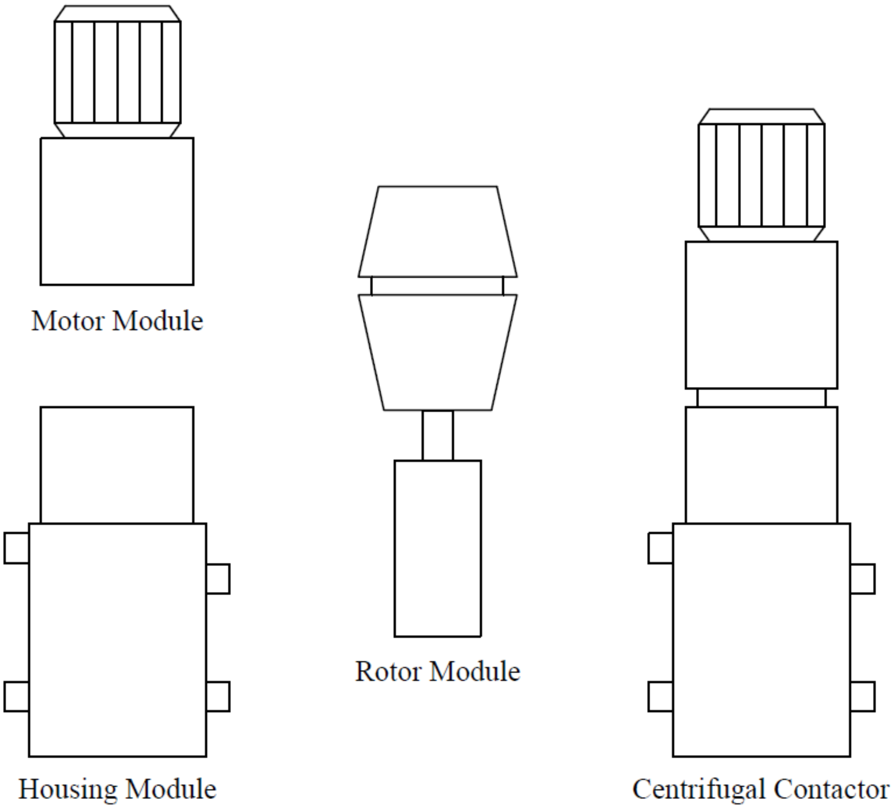

Figure 4.3: Schematic view of Three Modular Structure

(iii)Process fluid flow pipe modification

(a) Inter-stage horizontal overflow line for mixed-phase flow [20, 21] between the motor/bearing failed bowl to adjacent bowls was demonstrated to ensure the smooth operation of the multistage ACE without stopping the entire cascade. The schematic view of the inter-stage horizontal overflow line shown in Fig. 4.4. Both aqueous and organic phase flows into adjacent stages, and it leads to the internal recirculation in-between the failed stage and adjacent stages. Internal recirculation increases back mixing and radiation degradation of the solvent due to prolonged exposure. Another major disadvantage is it will not work during the end-stage failure, which leads to the stoppage of the entire cascade or a gravity settler [20] should be attached at the end stages.

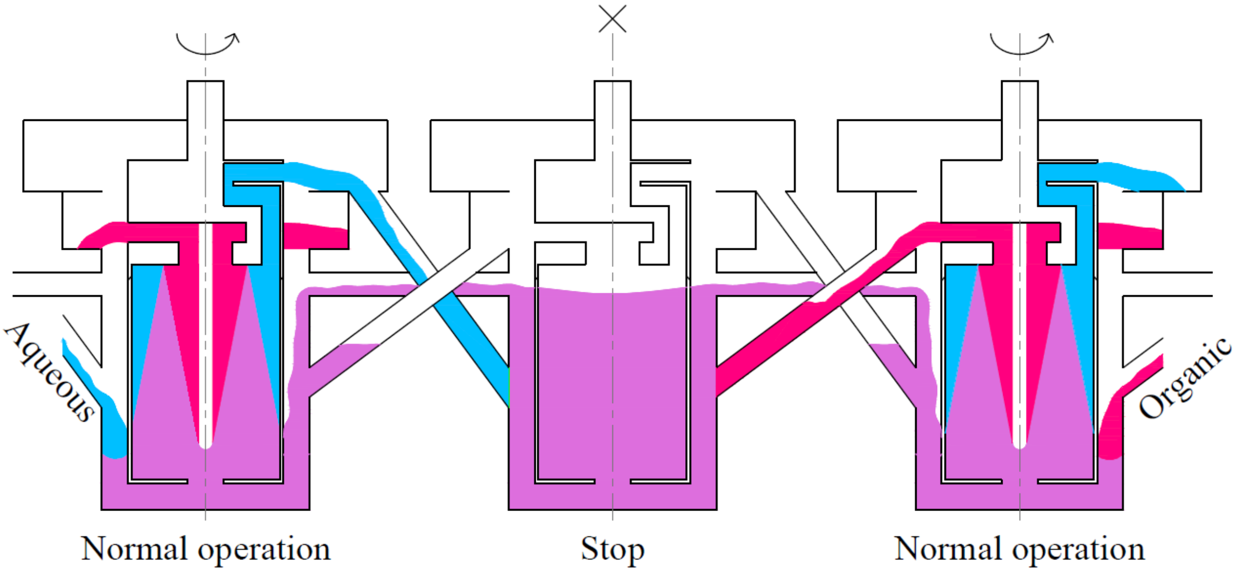

Figure 4.4: Schematic view of inter-stage horizontal over flow line

(b) Two separate overflow lines [22] for aqueous and organic phases were demonstrated, and it does not require any gravity settler in the event of end-stage failure. The schematic view of two separate overflow lines shown in Fig. 4.5. In the above design, the aqueous overflow line is situated above the aqueous and organic inlet in the stationary bowl, and the organic phase may flow through aqueous overflow line in the event of motor/bearing failed condition. It leads to back mixing and increases the load in the adjacent stages. Holdup inside the annular region depends on the total throughput and increases with an increase in throughput. During the regular operation with higher throughput, the dispersed phase may flow from one stage to another stage by above overflow line and affects the mass transfer performance of the ACE in the multistage cascade.

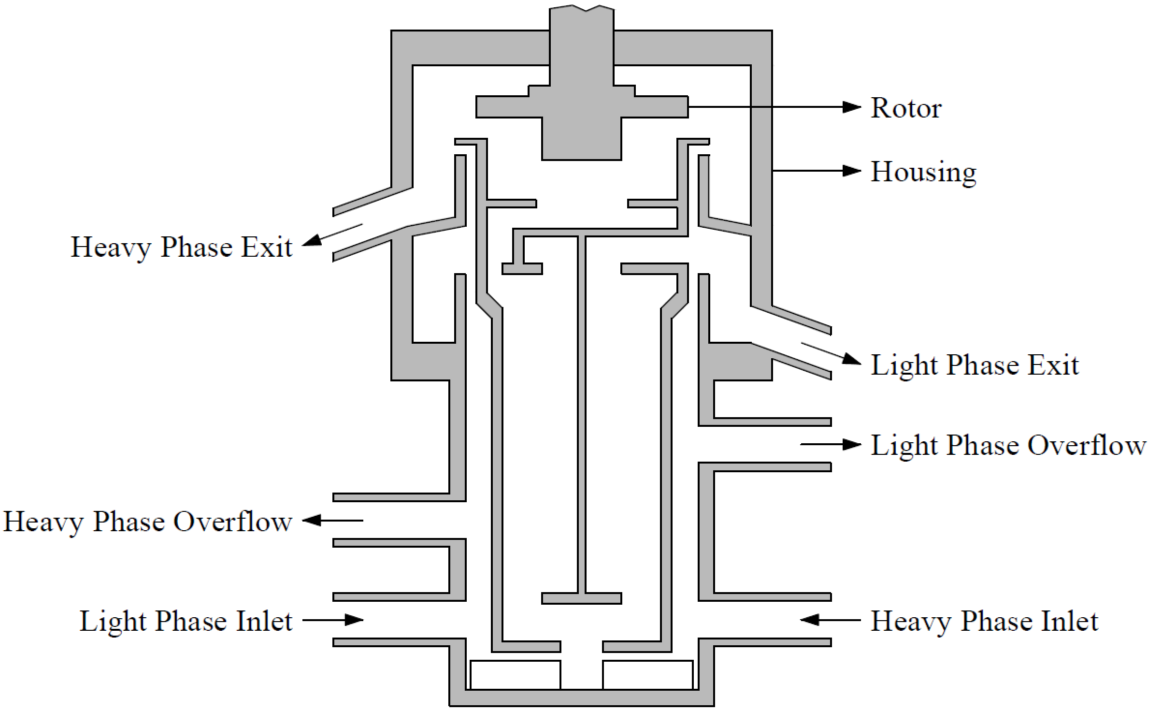

Figure 4.5: Schematic view of two separate overflow lines

After detailed literature analysis and considering the above flow conditions, a centrifugal extractor stationary bowl with an inter-stage inclined overflow line developed to ensure the smooth operation of the multistage centrifugal extractor system during motor/bearing failed condition.

4.3 Objective

Development and demonstration of inter-stage inclined overflow line to ensure the smooth operation and reduce the solvent degradation due to radiation in motor/bearing failed condition in the multistage centrifugal extractor system.

4.4 Experimental

4.4.1 Chemicals used

Tri-n-butyl phosphate (30% (v/v), TBP) solution is prepared by using TBP (HWP, Talcher, India, > 99%) by diluting with commercial n-Dodecane (98% n-dodecane, Orion Chemicals, Mumbai). 0.3 N and 4 N nitric acid solutions were prepared by using nitric acid (69–72% AR, Chemspure) and Millipore water. Sodium hydroxide solution is used for the acid-base titration. The physical properties of the above chemicals are shown in Table 4.1.

Table 4.1: Physical properties of chemicals used in this work

Compound	Formula	M.W.	B.P (^{o}C)	Density (g/mL)	Viscosity (cP)
Nitric Acid	HNO_3	63.01	83	1.4086	-
Water	H_2O	18.015	100	0.9970	0.90
TBP	$(C_2H_9O_3)PO$	266.32	289	0.9728	3.32
n-Dodecane	$C_{12}H_{26}$	170.34	216	0.7452	1.37

4.4.2 Experimental setup 1

Four stage CE 30 mm centrifugal extractor stationary bowl with inter-stage inclined overflow line (6) was designed and developed, and its photograph and schematic drawing are shown in Figures 4.6 and 4.7, respectively. Top-end of the inclined overflow line connected below the organic collection chamber in the annular region at the adjacent stationary bowl, and the bottom end is connected below the aqueous and organic inlet in its annular region. It ensures the aqueous flow from bottom to top from one inclined overflow line and organic flow from top to bottom from another inclined overflow line connected in between the failed stage to the next stages. The orientation of inclined overflow line ensures the aqueous and organic flow follows its path in a multistage ACE system.

Figure 4.6: 4 stages 30 mm ACE stationary bowl with inter-stage inclined overflow line (1) Aqueous feed pipe, (2) Organic feed pipe, (3) Aqueous outlet, (4) Organic outlet, (5) Aqueous inter-stage line and (6) Inclined over flow line

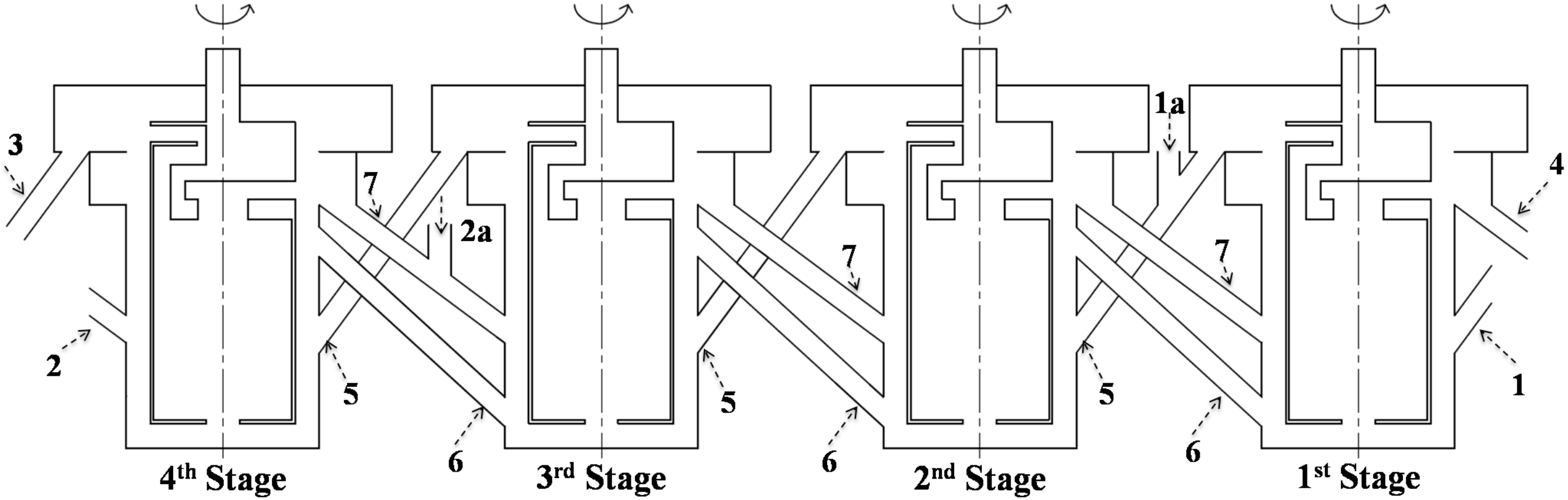

Figure 4.7: Schematic drawing of 4 stages 30 mm ACE setup with inter-stage inclined overflow line

(1 and 1a) Aqueous feed pipe, (2 and 2a) Organic feed pipe, (3) Aqueous outlet, (4) Organic outlet, (5) Aqueous inter-stage line, (6) Inclined over flow line and (7) Organic inter-stage line

4.4.3 Working principle of experimental setup 1

The aqueous enters into the first stage through the aqueous inlet line (1) (Fig. 4.8.) and mixed with the organic phase (coming from the second stage) in the first stage annular region. The dispersed phase generated in an annular region settles inside the rotating bowl by centrifugal acceleration. Aqueous comes out from the first stage flows into the second stage through aqueous inter-stage (5) line. Similarly, organic enters into the fourth stage through the organic inlet line (2) and mixed with the aqueous phase (coming from the third stage) in the fourth stage annular region. Dispersed phases get separated inside the fourth stage rotating bowl by centrifugal acceleration. Separated organic phase flows into the third stage through an organic inter-stage line (7). Both the aqueous and organic streams flow in a counter-current mode from first to the fourth and fourth stage to the first stage, respectively. Finally, the aqueous phase comes out from the above cascade through aqueous outlet (3) from the fourth stage, and the organic phase comes out from the above cascade through organic outlet (4) from the first stage.

Failure or malfunction of a single stage in the multistage ACE leads to the accumulation of the aqueous and organic phases inside the failed stage, disturbing the counter-current mode operation. An inclined inter-stage overflow line (6) is incorporated in the multistage ACE system to ensure smooth operation during motor/bearing failed conditions. In the motor failed stage, aqueous settles at the bottom and organic accumulate at the top. The aqueous stream flows from the bottom of the motor failed stage to the top of the left running stage via inclined overflow line (6) due to the hydraulic head. The organic stream flows from top to bottom to the right running stage via another inclined overflow line (6) by gravity. Incorporated inclined overflow line (6) ensures the smooth counter-current mode operation without any interference. The schematic view of flow, during standard and third stage motor, failed conditions for experimental setup one is shown in Figures 4.8 and 4.9, respectively.

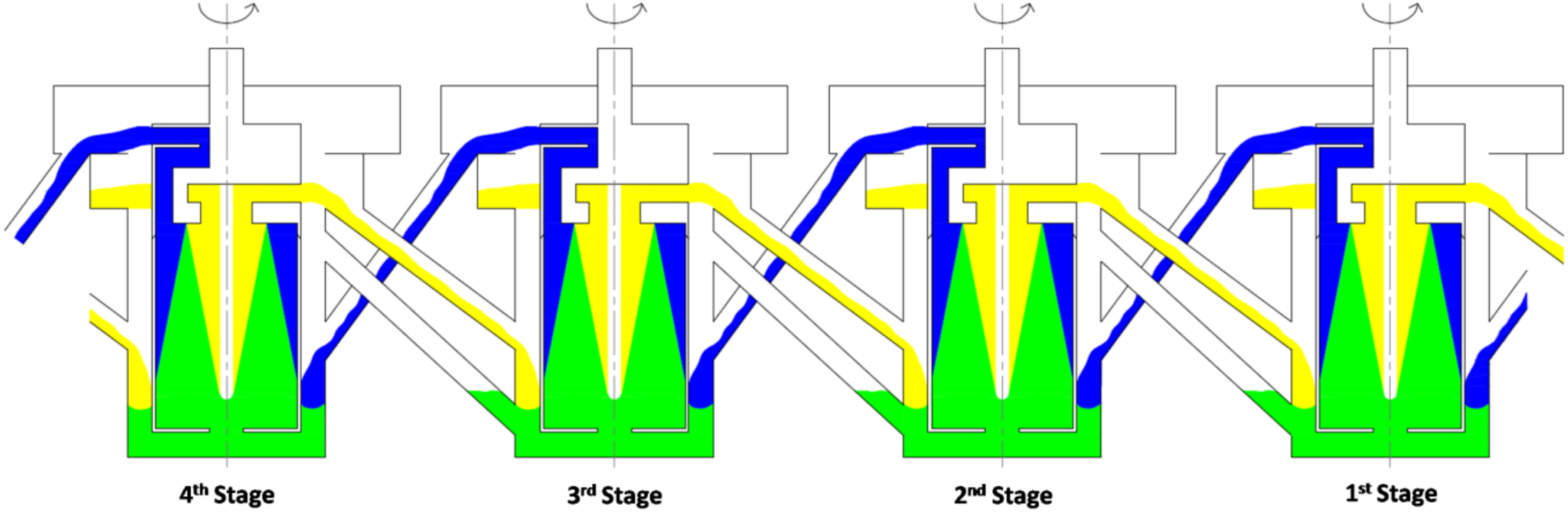

Figure 4.8: Schematic view of aqueous and organic flow in experimental setup 1 at normal operating condition (blue colour - aqueous phase, green colour - mixture, yellow colour - organic phase)

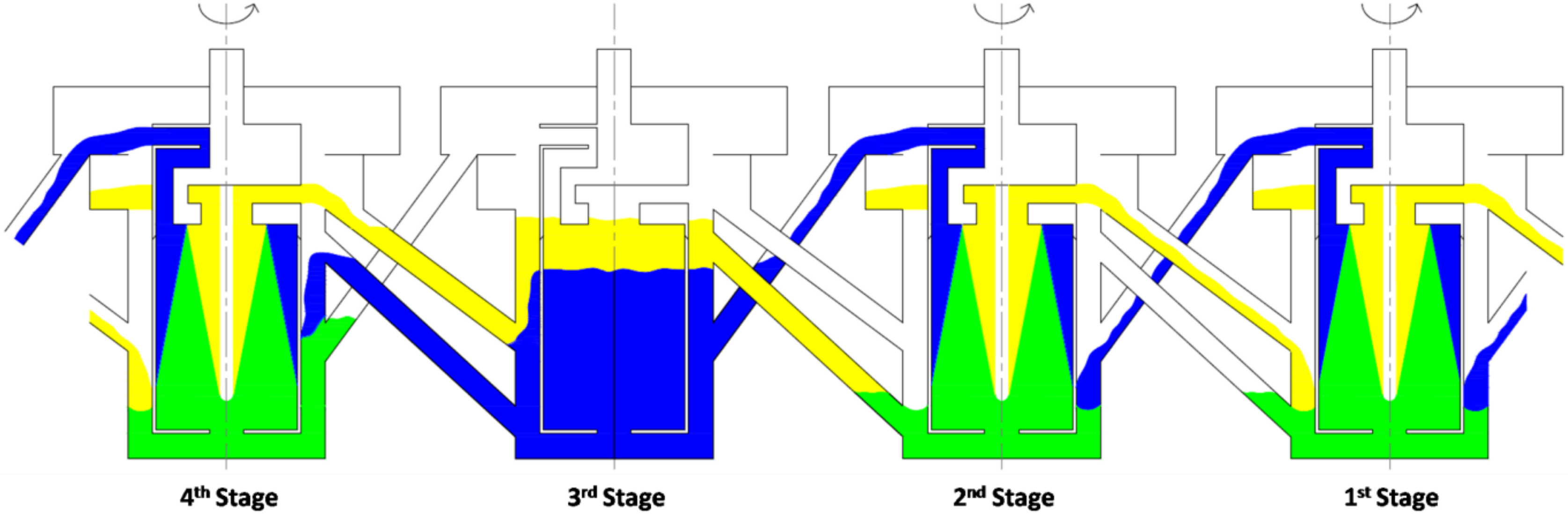

Figure 4.9: Schematic view of aqueous and organic flow in experimental setup 1 at 3rd stage motor failed condition

(blue colour - aqueous phase, green colour - mixture, yellow colour - organic phase)

4.4.4 Experimental setup 2

To reduce carryover of other phases in the aqueous and organic product stream, aqueous feed at the second stage via aqueous inlet (1a) and organic feed at the third stage via organic inlet (2a) as shown in Fig. 4.7. The first and fourth stages in 4 stage CE 30 mm setup acts as an aqueous and organic centrifuge to reduce carryover of other phases in the product outlets. The major drawback is above two ACEs would not be available for mass transfer operation in the multistage ACE system. The working principle of setup two is the same as experimental setup one during normal, and motor failed conditions except end stages. The schematic view of both standard and third stage motor failed conditions for experimental setup two is shown in Figures 4.10 and 4.11, respectively.

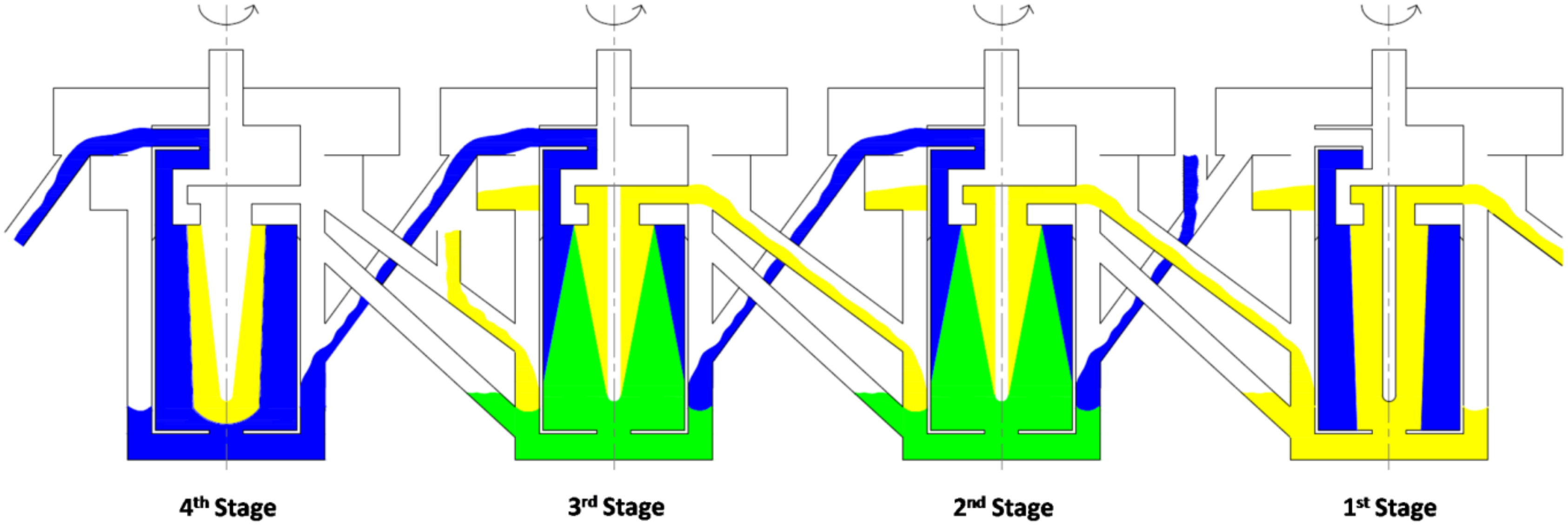

Figure 4.10: Schematic view of aqueous and organic flow in experimental setup 2 at normal operating condition (blue colour - aqueous phase, green colour - mixture, yellow colour - organic phase

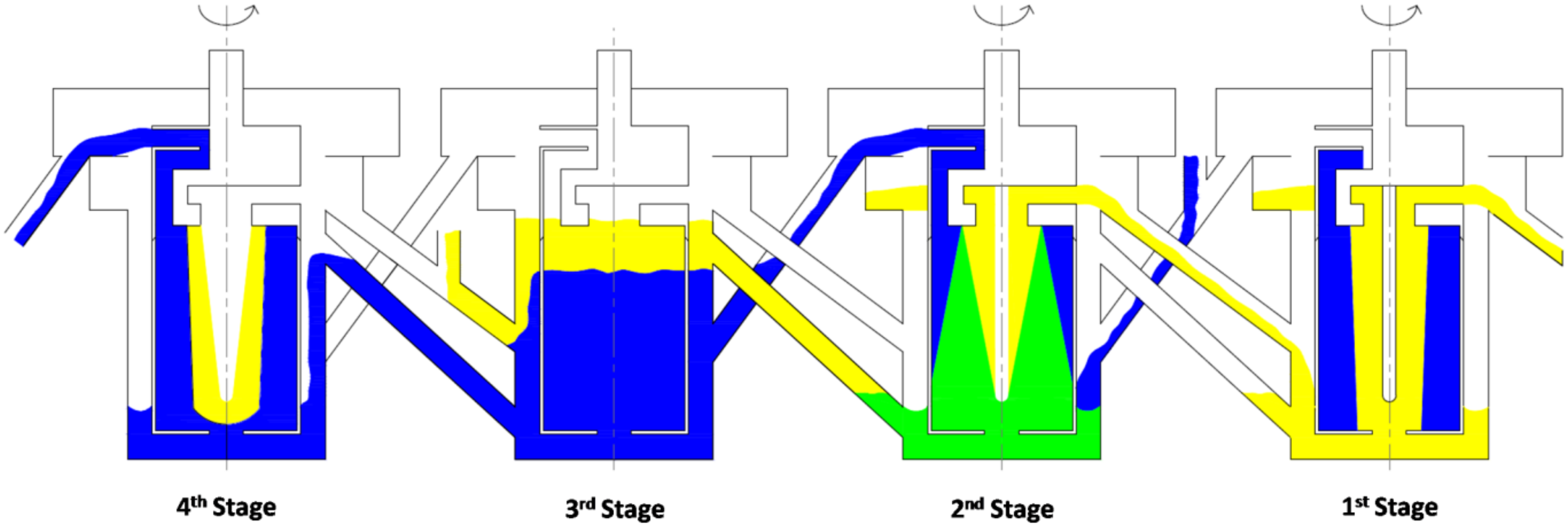

Figure 4.11: Schematic view of aqueous and organic flow in experimental setup 2 at 3rd stage motor failed condition

(blue colour - aqueous phase, green colour - mixture, yellow colour - organic phase)

4.4.5 Experimental setup 3

A horizontal overflow line (8) [23, 24] based experimental setup has been developed to compare its performance with the inclined overflow line. The schematic drawing of experimental setup three is shown in Fig. 4.12. During the normal operation, aqueous and organic flow is similar to experimental setup 1. Failure or malfunction of any single stage in the above multistage ACE leads to the accumulation of aqueous and organic phases inside the motor/bearing failed stage. Accumulated aqueous and organic phase flows into the next stages through a horizontal inter-stage overflow line (8). The major disadvantage is that aqueous or organic phase flows back into its feed stages, leading to back mixing and reducing the mass transfer and hydrodynamic performance. The schematic view of both normal and third stage motor failed conditions for experimental setup three is shown in Figures 4.13 and 4.14, respectively.

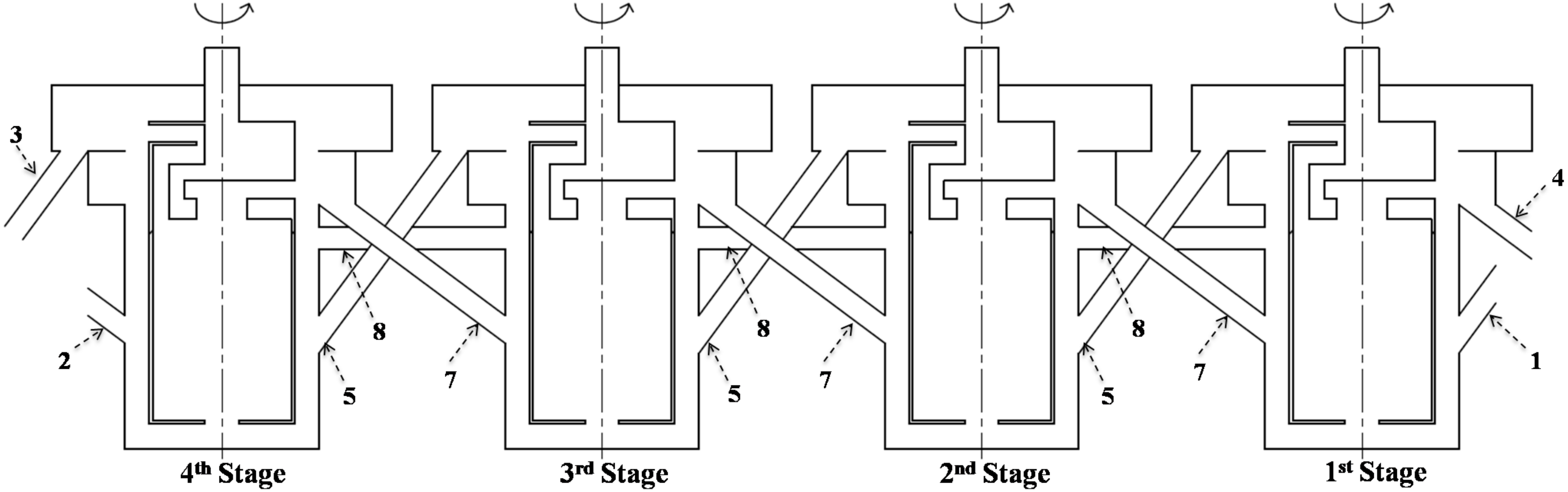

Figure 4.12: Schematic drawing of 4 stages 30 mm ACE setup with inter-stage horizontal overflow line (8)

(1) Aqueous feed pipe, (2) Organic feed pipe, (3) Aqueous outlet, (4) Organic outlet, (5) Aqueous inter-stage line, (7) Organic inter-stage line and (8) Horizontal over flow line

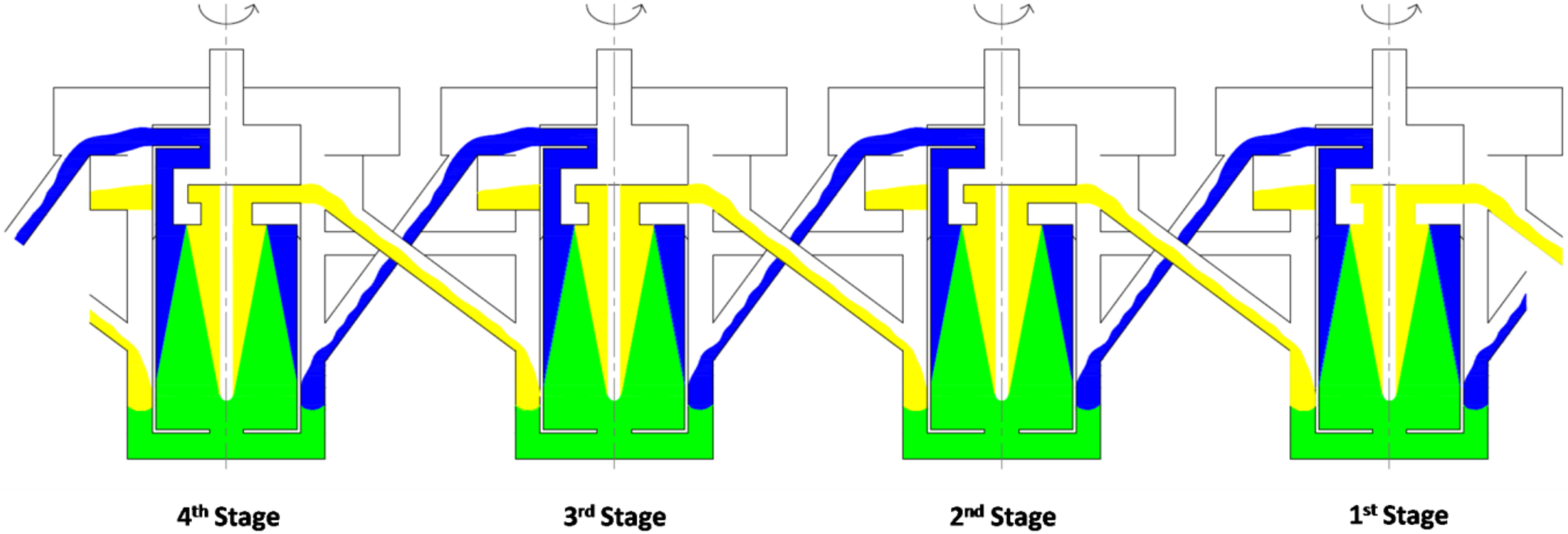

Figure 4.13: Schematic view of aqueous and organic flow in experimental setup 3 at normal operating condition (blue colour - heavy phase, green colour - mixture, yellow colour - light phase)

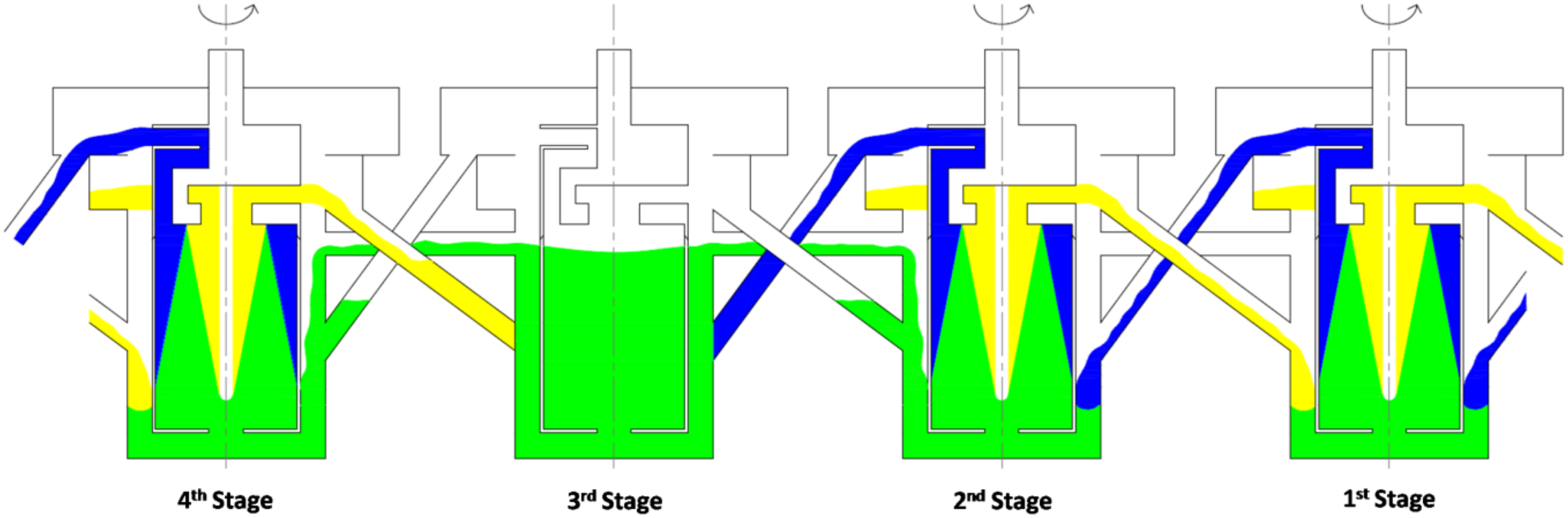

Figure 4.14: Schematic view of aqueous and organic flow in experimental setup 3 at 3rd stage motor failed condition

(blue colour - aqueous phase, green colour - mixture, yellow colour - organic phase)

4.4.6 Flooding experiment

Flooding experiments are conducted in the single-stage ACE and also in the four stages CE 30 mm experimental setups (three experimental setups). In flooding experiments, 0.3 N HNO_3 pre-equilibrated with 30% TBP is used as the aqueous phase, and 30% TBP pre-equilibrated with 0.3 N HNO_3 is used as an organic phase. Aqueous and organic phase comes out from product outlets are collected in a 15mL centrifuge tube (+/- 0.1 mL accuracy), and the carryover of the other phase is measured by centrifuging the above samples. Flooding limit was designated as 1%, such as carry of other phases in aqueous/organic outlets should be less than 1%. During flooding experiments, all ACE bowls in the above experimental setups (Setup one, two, and three) are operated at 3000 rpm, and the O/A ratio is maintained at 1. Motor failed conditions also simulated by switching off either the second or third stage motor in all the three experimental setups.

4.4.7 Mass transfer experiment

Mass transfer experiments are conducted in all the above three experimental setups with 4N HNO_3 as an aqueous phase, and 30% acid-free TBP as an organic phase [25]. ACE bowls in four-stage CE 30 mm setup are operated at 3000 rpm, and O/A ratio was maintained around 4 (aqueous flow rate = 80 mL/min and organic flow rate = 20 mL/min). O/A ratio four is fixed based on a theoretical calculation to avoid plait point in the McCabe-Thiele plot. Samples were collected after 20 minutes from aqueous and organic product outlet to ensure steady stage condition and analyzed for nitric acid concentration by acid-base titration. In order to understand the flow pattern inside the overflow line (in all three experimental setups) in-between stage motor (either the second or third stage) was switched off, and mass transfer experiments are continued. The flow rate in the above experiments is fixed, such that the internal recirculation could be avoided during the normal operating condition.

Balamurugan [26] equilibrium data between nitric acid and 30% TBP were used to generate McCabe-Thiele [27] plot to calculate the overall mass transfer efficiency. Mass transfer efficiency is defined as the ratio of the number of stages calculated by McCabe-Thiele plot by the actual number of centrifugal stages.

Table 4.2: Equilibrium data of 30% TBP/n-Dodecane–HNO_3–Water system at room temperature

Sr. No	Aqueous phase Conc. (mol/L)	Organic phase Conc. (mol/L)
1.	0	0
2.	0.0017	0.0013
3.	0.0049	0.0014
4.	0.0074	0.0018
5.	0.0453	0.0031
6.	0.0970	0.0042
7.	0.4310	0.0578
8.	0.8035	0.1573
9.	0.8845	0.1806
10.	1.5587	0.3267
11.	1.7625	0.3959
12.	2.2987	0.5279
13.	2.8950	0.6304
14.	3.3538	0.6859
15.	3.6171	0.7581
16.	4.5664	0.8789
17.	6.6024	1.0316

4.4.8 Holdup experiment in single stage ACE 30 mm bowl

Three different techniques were reported in the literature to measure the liquid holdup in ACE. The first one is a weighing technique; Schuur et al. [28] measured total liquid hold up in the mixing and separation zone by weighing the feed and product vessels. The disadvantage is it measures the total volume of aqueous and organic inside the ACE (including mixing, separation zone, and liquid inside the inlet and outlet pipe). The second method is a liquid discharge technique, Schuur et al. [28] also used the above technique to measure liquid hold up in both zones (mixing and separation zone). In the liquid discharge method, feed pumps are stopped after reaching the steady-state condition, and the liquid present in the annular region is drained through the bottom drain line. After complete draining, the rotating bowl was stopped, and the liquid present inside the rotating bowl is collected, and volumes are measured. Liquid discharge method having the following errors: (i) while draining liquid from the annular region is pumped into a rotating bowl, (ii) similarly, aqueous and organic phase present inside the rotor is thrown into aqueous and organic phase collector ring during draining operation. To overcome the above disadvantages: Duan et al. [29] reported a liquid fast separation method. In liquid fast separation method, CE motor, feed pumps are switched off simultaneously (after reaching steady-state condition), and CE rotating bowl was lifted within one second, and liquid present inside the rotor is collected separately. Later, the liquid present in the stationary bowl is drained through the bottom drain line. Error in the above measurement technique is low, and it helps to calculate overflow above the aqueous phase and organic phase weirs. The main disadvantage is that lifting the rotating bowl within one second is a big challenge for bigger size ACEs. A new liquid discharge volume method is used in this work to measure total holdup after thorough consideration of the above techniques.

4.4.9 Procedure for new liquid discharge volume method

During steady-state operation of ACE, liquid present in the annular region is drained and discarded. Subsequently, the motor is switched off, and liquid present inside the rotating bowl is drained and measured using 100 mL measuring cylinder (make: Borosil, +/- 1 mL accuracy). Again ACE operation is initiated, after reaching the steady-state condition both rotating bowl, feed pumps are stopped, and rotation of rotating bowl due to inertia is arrested simultaneously by an active break. The total volume of liquid present inside both the mixing and rotating region is collected in a 100 mL measuring cylinder (make: Borosil, +/- 1 mL accuracy). Liquid present in the annular region is back-calculated by measuring the difference between the above two volumes. The new liquid discharge volume technique is much superior compare to other previous techniques [28], and it may be implemented in bigger ACE bowls.

During the holdup experiment, the above single stage CE bowl was operated at 3000 rpm, and O/A ratio was maintained at 1. Based on single-stage ACE experimental results, maximum operating throughput can be fixed in a multistage centrifugal extractor system to ensure that the mixed-phase in the annular region should not reach other stages through the overflow line.

4.5 Results and Discussion

4.5.1 Flooding throughput results and discussion

4.5.1.1 Single stage CE 30mm bowl

Flooding throughput results of a single-stage CE 30 mm bowl for different O/A ratios at operating speed for 3000 rpm is shown in Table 4.3 and Fig. 4.15. The results indicate that the single-stage CE 30 mm bowl can be operated up to total throughput of 720 mL/min (Aq. flow rate = 360 mL/min and Org. flow rate = 360 mL/min) at O/A ratio of 1 and operating speed of 3000 rpm.

Table 4.3: Flooding capacity of single stage ACE 30 mm bowl at 3000 rpm

Sr. No	O/A Ratio	Total flow rate (mL/min)
1.	10	1100
2.	5	770
3.	2	750
4.	1	720
5.	0.5	525
6.	0.2	420
7.	0.1	412

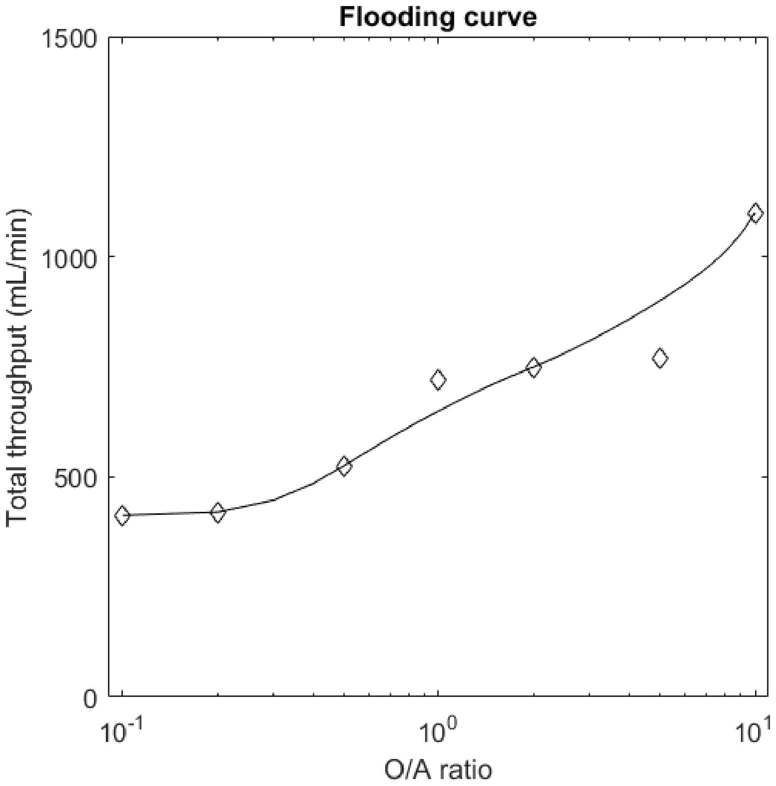

Figure 4.15: Flooding curve for single stage ACE 30 mm bowl at different O/A ratio at 3000 rpm

4.5.1.2 Four stage ACE 30 mm bowl setup without any overflow line

Flooding experiment was conducted in a four-stage ACE 30 mm setup without any overflow lines (6) or (8). The experiment showed that four-stage ACE 30 mm could be operated up to a total throughput of 550 mL/min at O/A ratio of 1 and an operating speed of 3000 rpm.

Compare to single-stage, four-stage CE 30 mm flooding throughput is less. The main reason for the reduction in flooding throughput is a reduction in hydraulic head available for aqueous and organic streams in the inter-stage line because of an increase in liquid holdup (height) in the annular region with an increase in total throughput [30, 31]. For a single-stage ACE, the aqueous and organic outlets are open to atmospheric pressure. Whenever there are multiple stages of ACE downstream of any phase, aqueous or organic flow must overcome the resistance offered by the subsequent downstream stages; hence, its corresponding flow rate also decreases. Besides, some recirculation of aqueous or organic phase occurs in the vicinity of its outlet in every stage outlet. Such a recirculation results in a mixing zone, and hence the organic phase (for instance, the first stage) tends to get carried over to the second stage.

As a consequence, the overall throughput needs to be reduced to avoid flooding. Since this phenomenon occurs at the outlet of every stage, the throughputs of two stages, three stages, and four stages modules progressively get reduced. Therefore, the net effect of these factors is a decrease in flooding throughput with an increase in the number of stages.

4.5.1.3 Four stage CE 30 mm bowl with end stage liquid-liquid centrifuge

Flooding experiment was conducted in a four-stage CE 30 mm setup without any overflow lines (6) or (8) and the end stages acting as an aqueous and organic centrifuge. The experimental result showed that the flooding throughput is 600 mL/min at O/A ratio of 1 and the operating speed of 3000 rpm. Flooding capacity is slightly higher due to end centrifuges. However, it is to be noted that the mass transfer occurs only in the second and third stages, whereas the first and fourth stages act mainly as a liquid-liquid centrifuge. Of course, some mass transfer occurs during phase separation (which is expected to be small).

4.5.1.4 Flooding experiment in all three experimental setup

Flooding experiments were conducted in all three experimental setups with the following conditions. They are:

(i) All four stages are running.

(ii) The second stage motor is switched off (failure condition).

(iii) The third stage motor is switched off (failure condition).

During these experiments, CE bowls were operated at 3000 rpm and O/A ratio of 1. From the flooding experiment results for experimental setup 1, carryover of the other phase in the aqueous and the organic outlets was found to be 0.38% and 0.35%, respectively, at a total throughput of 650 mL/min with O/A = 1. Further, an increase in total throughput to 660 mL/min (again O/A = 1) the carryover in both the aqueous and the organic outlets was found to be greater than 1%. Similar trends were observed in all the other experimental setups, and the corresponding flooding throughputs are shown in Fig. 4.16 (Table 4.4). The flooding limits were found to be 650, 700 and 600 mL/min, respectively for (i) experimental setup 1 (with inclined overflow line), (ii) experimental setup 2 (with inclined overflow line with liquid-liquid end-stage centrifuges) and (iii) experimental setup 3 (horizontal overflow line) during normal operation.

Table 4.4: Flooding results of different experimental setup

S. No	**Stages running condition**	**Flooding throughput (mL/min)**		
		Setup 1	**Setup 2**	**Setup 3**
1.	All four stages are running	650	700	600
2.	2nd stage motor switched off	450	650	350
3.	3rd stage motor switched off	450	650	350

From the Table 4.4 and Fig. 4.16, it can be seen that the hydrodynamic performance of inter-stage inclined overflow line (Expt. setup 1) is much better than the inter-stage horizontal overflow line (Expt. setup 3) and the addition of liquid-liquid centrifuge (Expt. setup 2) at the end of the multistage centrifugal extractor system improves the hydrodynamic performance of the cascade during normal as well as failure mode conditions.

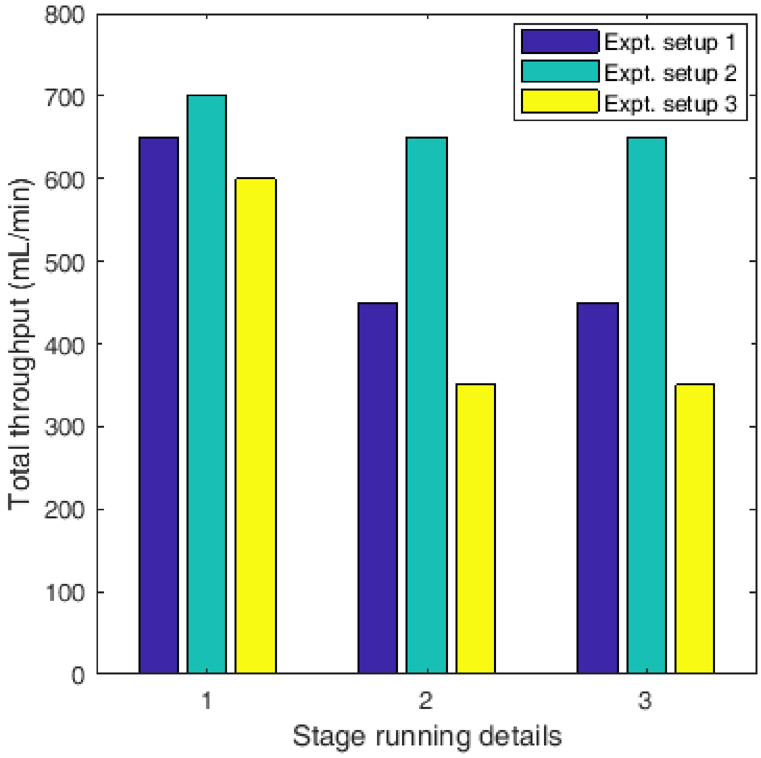

Figure 4.16: Flooding throughput results for all three setups

(Stage running details is shown in x-axis and number one corresponds to all four stages in running condition, number two corresponds to 2nd stage motor switched off condition out of four stages and number three corresponds to 3rd stage motor switched off condition out of four stages)

4.5.2 Mass transfer results and discussion

Extraction experiments were conducted with 4N Nitric acid and 30% TBP in n-DD in all the three experimental setups with and without motor failure conditions. In all the cases, the nitric acid concentration of aqueous and organic of all the net in and outflows were measured. These results enable the estimation of theoretical stages using McCabe-Thiele Plot. McCabe-Thiele plot for the mass transfer experiment in experimental setup one during the normal operation shown in Fig. 4.17.

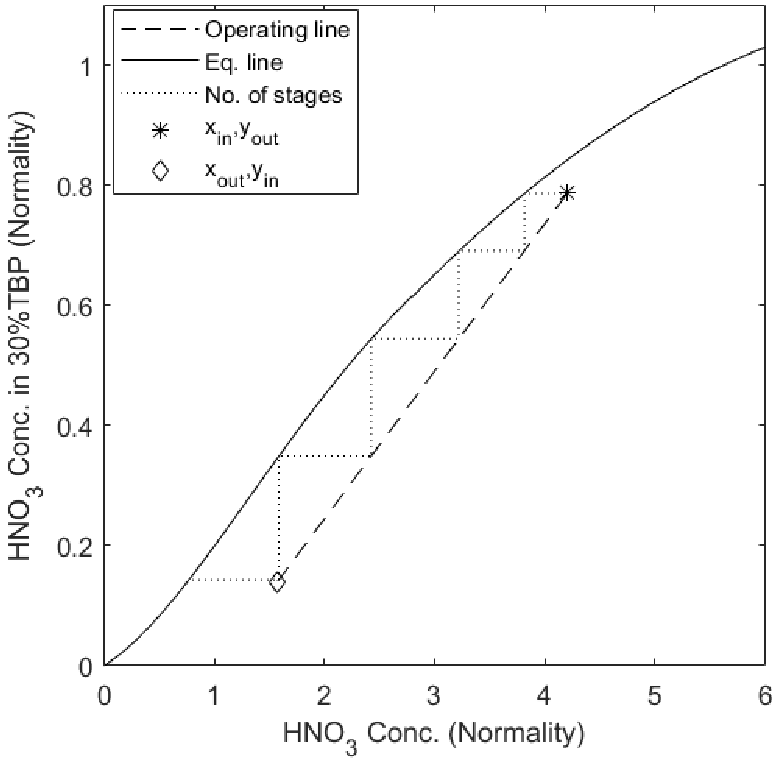

Figure 4.17: Number of theoretical stages calculated by McCabe-Thiele plot

In the McCabe-Thiele Plot (Fig. 4.17), the operating line was constructed by connecting the points between (a) the aqueous inlet and organic outlet concentrations (x_{in} = 4.2 N, y_{out} = 0.79 N) and (b) the organic inlet and aqueous outlet concentrations (x_{out} = 1.6 N, y_{in} = 0.14 N) from the mass transfer experimental results. Equation for the above operating line is $y = 0.25*x - 0.14$. Equilibrium data were fitted using second-order Spline interpolation. The horizontal line is drawn from a feed inlet (aqueous inlet concentration) to the equilibrium curve. A vertical line is then drawn from the above intersection point to the operating line. The above procedure was repeated until the vertical line reaches y_{in}. Each horizontal line corresponds to one theoretical stage.

Experimental results show that the number of theoretical stages (NTS) calculated from the experiment and the actual number of stages is equal to four. Then the overall efficiency of the above setup for the above mass transfer condition is equal to 100%. Extraction experiments were repeated in all the three experimental setups with second or third stage motor in switch off condition. From the above experimental results, the values of NTS were calculated by McCabe-Thiele plot, and the results for all the experimental setups are shown in Table 4.5.

Table 4.5: Mass transfer experiment results

S. No	**Setup details**	**Stage switched off**	**No. of stages calculated by McCabe-Thiele plot**	**Overall efficiency**
1.	Experimental setup 1	Nil	4	100
2.		2	2.5	62.5
3.		3	2.6	65
4.	Experimental setup 2	Nil	1.9	95
5.		2	1	50
6.		3	0.9	45
7.	Experimental setup 3	Nil	4	100
8.		2	2.4	60
9.		3	2.65	66.2

Table 4.5 shows practically no difference in the mass transfer performances in inter-stage inclined (setup-1) and horizontal overflow line (setup 3). The end-stage centrifuges (setup-2) do not improve the mass transfer (as expected).

4.5.3 Holdup and residence time in single stage ACE 30 mm bowl

Holdup experimental result for single stage CE 30 mm bowl at an operating speed of 3000 rpm and O/A ratio of 1 is shown in Table 4.6. and in Fig. 4.18.

Table 4.6: Liquid holdup inside single stage ACE 30 mm bowl

S. No	Aq. flow rate (mL/min)	Org. flow rate (mL/min)	Rotating bowl holdup (mL)	Total holdup (mL)	Total residence time (sec)
1.	50	50	39 40 40	67 66 67	40
2.	100	100	40 39 40	71 71 71	21.3
3.	125	125	39 39 39	76 76 75	18.1
4.	150	150	39 39 39	81 80 82	16.2
5.	200	200	39 39 39	91 90 90	13.5

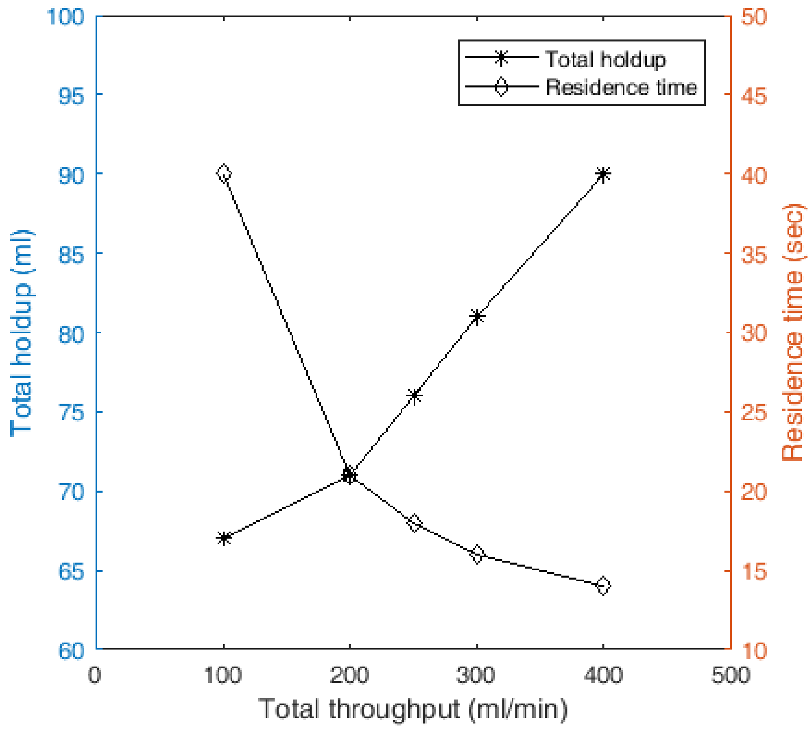

Figure 4.18: Holdup and residence time in single stage ACE 30 mm bowl w.r.t different throughput at constant O/A ratio 1 and 3000 rpm

Results show that the liquid holdup increases with an increase in the total throughput, and residence time decreases with an increase in the total throughput. From above holdup results, liquid height in the annular region is back-calculated from CE 30 mm dimension, assuming that there is no air entrainment and no fluctuation in the liquid height. The resulting values of liquid height are shown in Fig. 4.19.

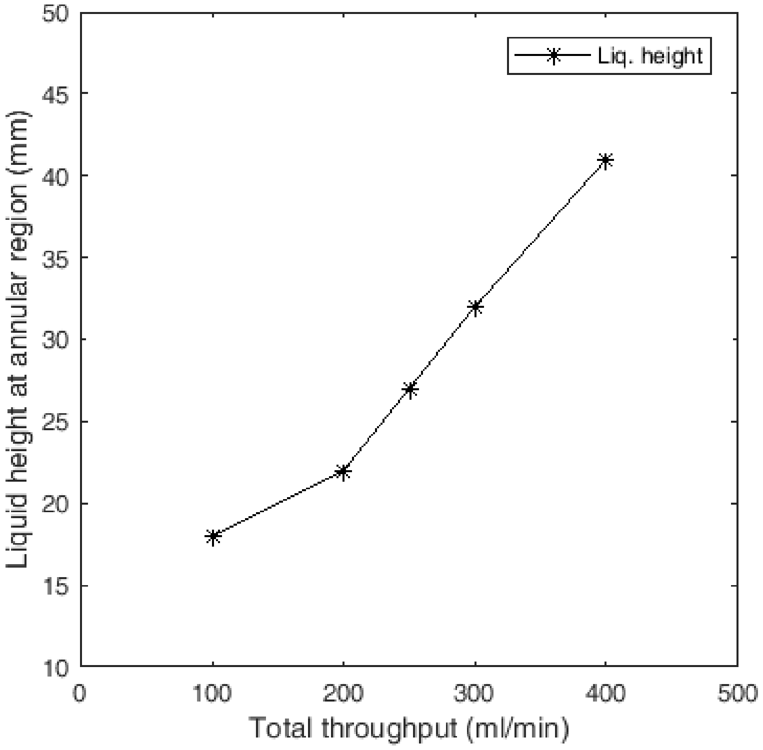

Figure 4.19: Liquid height at annular region in single stage ACE 30 mm bowl w.r.t different throughput at constant O/A ratio 1 and 3000 rpm

Liquid height in the annular zone shows that the multistage cascaded system with an inclined overflow line (experimental setup one or two) should be operated well below the total throughput of 400 mL/min. At a throughput of about 400 mL/min, there would be a carryover of mixed-phase into the adjacent bowl through inclined overflow line at the normal operating condition. Any carryover of the phases into the adjacent stages increases the back mixing, which affects the mass transfer performance of the cascaded system. During motor or bearing failure of any single-stage in cascade, the same throughput (< 400 mL/min) is maintained, and the inclined overflow line ensures smooth operation without a further liquid build-up in the motor or bearing failed stage.

The cascaded setup (experimental setup 3) with horizontal overflow lines should be operated well below the total throughput of 400 mL/min at the normal operating condition. Around total throughput of 400 mL/min, there may be a carryover of the dispersed phase into the adjacent bowl through the horizontal overflow lines. Carryover of the dispersed phase into the adjacent stages increases the back mixing, which affects the mass transfer performance of the cascaded system. During the motor failure, aqueous and organic phases flow back into its feed stages, and the throughput in adjacent running stages increases until it reaches a steady-state condition. Due to the backflow, the horizontal overflow line setup should be operated well below 200 mL/min, where throughput in the adjacent running stages may reach twice the feed throughput**.

Based on the above single-stage holdup experimental results and ACE dimensions, residence time inside the second stage (mixing zone + settling zone) for the experimental setup one and three with normal and motor failed conditions are back calculated and it is shown in Tables 4.7 and 4.8, respectively.

Table 4.7: Residence time in second stage at experimental setup 1

S. No	Setup details	Stage Running status (Yes/No)	Total throughput (mL/min)	Residence time in second stage (sec)
1.	Experimental setup 1	Yes	100	40
2.		No	100	45
3.		Yes	200	21
4.		No	200	22
5.		Yes	300	16
6.		No	300	11.3

Table 4.8: Residence time in second stage at experimental setup 3

S. No	Setup details	Stage Running status (Yes/No)	Total throughput (mL/min)	Residence time in second stage (sec)
1.	Experimental setup 3	Yes	100	40
2.		No	200**	Infinity*
3.		Yes	200	21
4.		No	400**	Infinity*

*Infinity time is mentioned because of internal recirculation of aqueous and organic phase into its feed stages.

**It is to be noted that the flow rate is doubled due to internal recirculation in-between failed stage to adjacent running stages, and it is based on the assumption that 50% of aqueous and 50% organic phase flows in one horizontal flow line and remaining is flowing in another horizontal line. During failure, it reaches the flow rate twice to normal flow rate to attain steady-state conditions.

4.6 Conclusions

a) In this work, a new inter-stage inclined overflow line has been proposed. It has been demonstrated that a smooth operation of multistage ACE continuous even in the event of any single-stage motor or bearing failure. It does not require any additional settler or hardware in the case of end-stage failure. To ensure better performance at organic end stage failure, slight height adjustment is suggested for the inclined overflow line, and its schematic drawing is shown in Fig. 4.20. The operating limit of multistage ACE during normal and motor failure conditions is back-calculated from single-stage experiments and was found to be the same for both cases, unlike the horizontal overflow line (Table 4.7 & 4.8).

b) From the flooding result of experimental setup two, it is concluded that the incorporation of the liquid-liquid centrifuge as end stages increases the hydrodynamic performance [limiting (flooding) capacity increases] of multistage ACE during motor/bearing failed condition (Table 4.4).

c) From the flooding experiments, it is concluded that the flooding capacity of the inclined overflow design (experimental setup-1) is higher (up to 8%) than the horizontal overflow design (Table 4.4). Further, the advantage is that the operating throughput during motor failure condition is even much higher (up to 25%) than that of horizontal overflow design (Table 4.4).

d) The main advantages of inclined overflow line design are (i) reduction in solvent degradation, and (ii) spillage of radioactive liquid inside the cell is negligible. Since it ensures flushing of radioactive liquid from the failed rotating bowl.

e) The new liquid volume discharge method is suggested to measure total holdup for bigger centrifugal extractors with accuracy within +/- 1 mL.

f) It is proposed that one or two extra stages be incorporated in the cascade. This will ensure a high level of mass transfer efficiency even in the event of failure of any stage. As far as smoothness of interstage flows is concerned, the inclined overflow lines provide that facility.

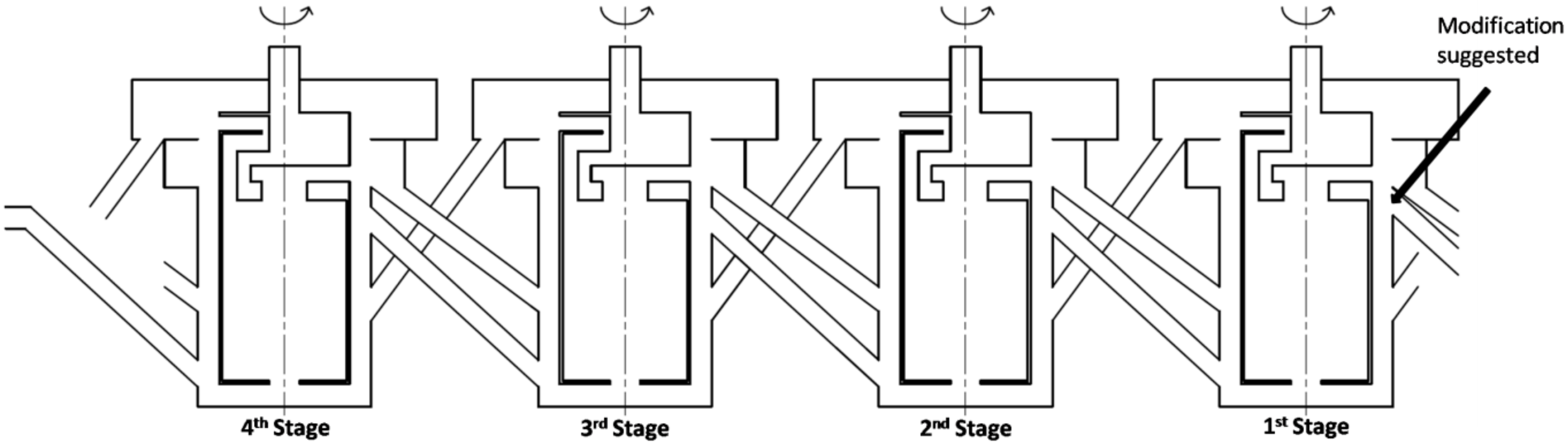

Figure 4.20: Schematic view of height adjustment suggested for inclined overflow line at organic outlet end stage

4.7 References

1. J. Zhou, W. Duan, X. Zhou, C. Zhang, “Application of annular centrifugal contactors in the extraction flowsheet for producing high purity yttrium”, *Hydrometallurgy,* **2007,** *85(2),* 154-162.

2. X. Jing, P. Ning, P., H. Cao, Z. Sun, Z., J. Wang, “Separation of V(V) and Cr(VI) in leaching solution using annular centrifugal contactors”, *Chem. Eng. J.,* **2017,** *315,* 373–381.

3. X. Jing, J. Wang, H. Cao, P. Ning, Z. Sun, “Rapid selective extraction of V(V) from leaching solution using annular centrifugal contactors and stripping for NH_4VO_3”, *Sep. Purif. Technol.,* **2017,** *187,* 407-414.

4. K. Tang, H. Zhang, Y. Liu, “Experimental and simulation on enantioselective extraction in centrifugal contactor separators”, *AICHE J.,* **2013,** *59(7),* 2594-2602.

5. J. Zhou, W. Duan, J. Xu, Y. Yang, “Experimental and simulation study on the extraction of p-cresol using centrifugal extractors”, *Chin. J. Chem. Eng.,* **2007,** *15(2),* 209-214.

6. S. L. Yarbro, S. B. Schreiber, “Using process intensification in the actinide processing industry, *J. Chem. Technol. Biotechnol.,* **2003,** *78(2-3),* 254-259.

7. W. Duan, J. Wang, J. Chen, J. Zhou, X. Zhou, “Development of annular centrifugal contactors for TRPO process tests”, *J. Radioanal. Nucl. Chem.,* **2007,** *273(1),* 103-107.

8. X. He, “Development of compact miniature annular centrifugal contactor for hot cell placement”, *Chem. Eng. Commun.,* **2008,** *195(10),* 1227-1239.

9. W. Duan, Q. Cheng, X. Zhou, J. Zhou, “Development of a ϕ20mm annular centrifugal contactor for the hot test of the total TRPO process”, *Prog. Nucl. Energy,* **2009,** *51(2),* 313-318.

10. W. Duan, J. Chen, J. Wang, S. Wang, X. Feng, X. Wang, S. Li, C. Xu, “Application of annular centrifugal contactors in the hot test of the improved total partitioning process for high level liquid waste”, *J. Hazard. Mater.,* **2014,** *278C,* 566-571.

11. T. Sun, W. Duan, J. Wang, J. Wang, J. Chen, “Hydraulic and mass-transfer performance of a 20-mm-diameter annular centrifugal contactor for the solvent extraction of cesium

by bis(2-propyloxy)calix[4]-crown-6 in n-octanol", *Solvent Extr. Ion Exch.,* **2015,** *33(1),* 75-90.

12. D. S. Webster, A. S. Jennings, A. A. Kishbaugh, H. K. Bethmann, "Performance of centrifugal mixer-settler in the reprocessing of nuclear fuel", *Chem. Eng. Progr. 65: Symp. Ser. No. 94,* **1969,** *70-7.*
13. G. J. Bernstein, D. E. Grosvenor, J. F. Lenc, N. M. Levitz, "A High-Capacity Annular Centrifugal Contactor", *Nucl. Technol.,* 1973, *20(3),* 200-202.
14. Falix Lawrence, "Development of PEEK composites and PEEK coating for radiation environment", *PhD Thesis,* **2013,** IIT Madras.
15. W. Duan, Q. Cheng, X. Zhou, J. Zhou, "Development of a ϕ20 mm annular centrifugal contactor for the hot test of the total TRPO process". *Prog. Nucl. Energy,* **2009,** *51(2),* 313-318.
16. R. A. Leonard, D. B. Chamberlain, C. Conner, "Centrifugal Contactors for Laboratory-Scale Solvent Extraction Tests", *Sep. Sci. Technol.,* **1997,** *32(1),* 193-210.
17. H. Xiang-Ming, Y. Yu-Shun, Z. Quan-Rong, L. Bin-Ken, "Recent advances of annular centrifugal extract or for hot test of nuclear waste partitioning process", *Nucl. Sci. Tech,* **1998,** *9(3),*157-162.
18. P. Rivalier, J. Y. Lanoe, "Development of a new miniature short-residence-time annular centrifugal solvent extraction contactor for tests of process flow sheets in hot cells", *Proceedings of the ATALANTE 2000, Palais des Papes, Avignon, France, October 24-26,* **2000,** 28.
19. J. D. Law,D. H. Meikrantz, T. G. Garn, L. L. Macaluso, "Advanced Remote Maintenance Design for Pilot-Scale Centrifugal Contactors", *Nucl. Technol.,* **2011,** *173(2),* 191-199.
20. R. T. Jubin, "Centrifugal contactor modified for end stage operation in a multistage system", *US Patent 4925441,* **May 15, 1990**.
21. T. Washiya, M. Takeuchii, H. Ogino, S. Aose, "Development of centrifugal contactor system in JNC", *Proceedings of the GLOBAL 2005, Tsukuba, Japan, October 9–13,* **2005.**

22. Duan, W.; Song, C.; Wu, Q.; Zhou, X.; Zhou, J. Development and Performance of a New Annular Centrifugal Contactor for Semi-Industrial Scale. *Sep. Sci. Technol.* **2005,** *40,* 1871.

23. Jubin, R.T. Centrifugal contactor modified for end stage operation in a multistage system. *US Patent 4925441*, **May 15, 1990**.

24. Washiya, T.; Takeuchii, M.; Ogino, H.; Aose, S. Development of centrifugal contactor system in JNC. *Proceedings of the GLOBAL 2005, Tsukuba, Japan, October 9–13,* **2005.**

25. K. Mandal, S. Kumar, V. Vijaykumar, U. K. Mudali, A. Ravisankar, R. Natarajan, "Hydrodynamic and mass transfer studies of 125 mm centrifugal extractor with 30% TBP/nitric acid system", *Prog. Nucl. Energy,* **2015,** *85,* 1-10.

26. M. Balamurugan, "Mass transfer and Hydrodynamic studies with CFD simulation in a single stage Inline Static Mixer", *M. Tech Report,* **2010**, HBNI.

27. W. L. McCabe, J. C. Smith, "Unit Operation of Chemical Engineering", *McGraw-Hill, Inc.,* **1993,** *5th Edition*.

28. B. Schuur, G. N. Kraai, J. G. M. Winkelman, H. J. Heeres, "Hydrodynamic features of centrifugal contactor separators: Experimental studies on liquid hold-up, residence time distribution, phase behavior and drop size distributions", *Chem. Eng. Process.,* **2012,** *55,* 8-19.

29. W. Duan, S. Cao, "Determination of the Liquid Hold-Up Volume and the Interface Radius of an Annular Centrifugal Contactor Using the Liquid-Fast-separation Method", *Chem. Eng. Commun.,* **2016,** *203(4),* 548-556.

30. K. E. Wardle, "Liquid-liquid mixing studies in annular centrifugal contactors comparing stationary mixing vane option", *Solvent Extr. Ion Exch,.* **2015,** *33(7),* 671-690.

31. H. L. Chen, J. C. Wang, W. H. Duan, J. Chen, "Hydrodynamic characteristics of 30% TBP/Kerosene-HNO_3 solution system in an annular centrifugal contactor", *Nucl. Sci. Tech.,* **2019,** *30(6),* 89.

CHAPTER 5

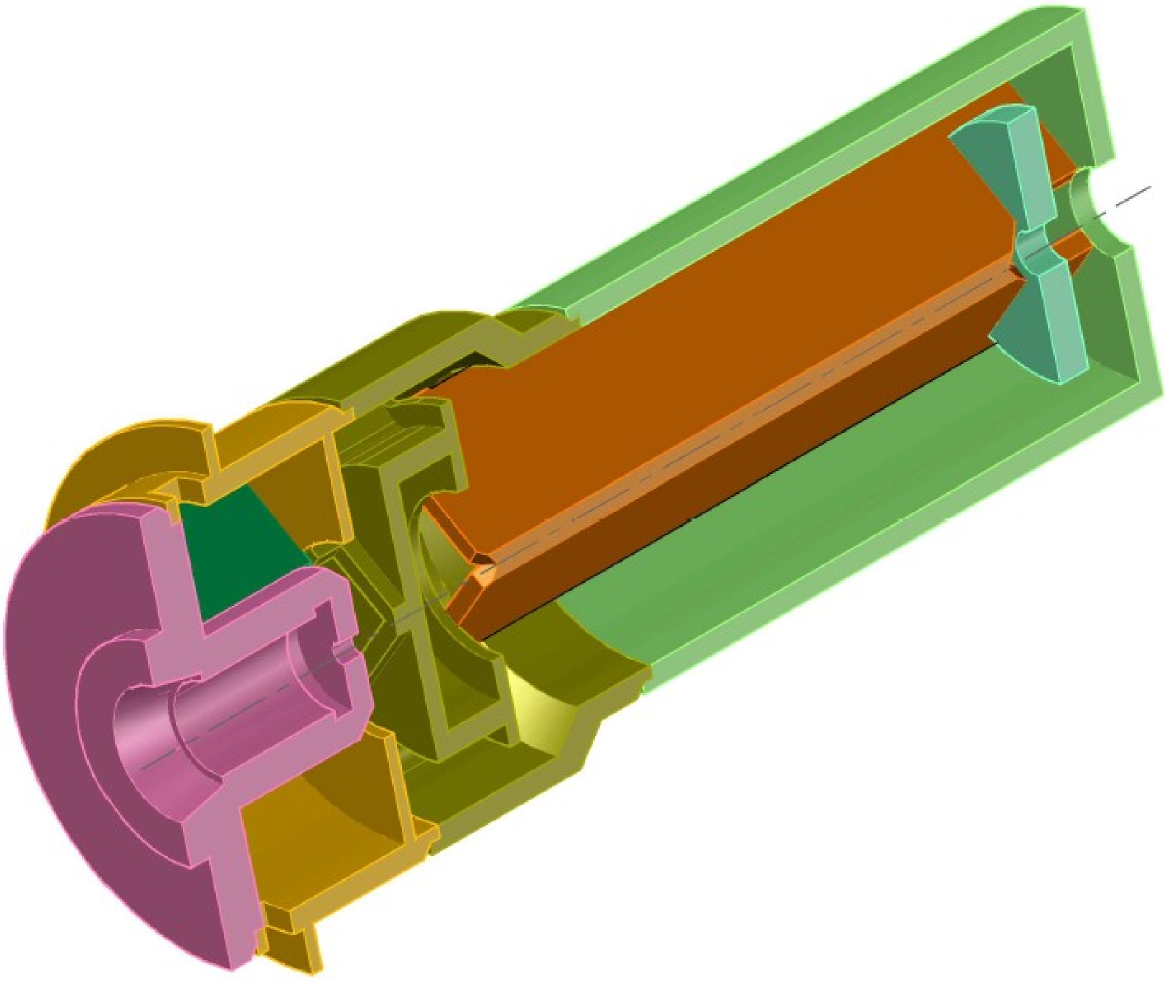

3D cut view of Annular Centrifugal Extractor rotating bowl

COMPUTATIONAL FLUID DYNAMIC STUDY INSIDE ANNULAR CENTRIFUGAL EXTRACTOR ROTATING BOWL

5 COMPUTATIONAL FLUID DYNAMIC (CFD) STUDY INSIDE ANNULAR CENTRIFUGAL EXTRACTOR ROTATING BOWL

5.1 Introduction

Several reports on experiments and analytical research of Annular Centrifugal Extractor (ACE) are available in the literature. Still, reliable design and scale-up of ACE are yet to be developed and the details of flow and mass transfer are still unclear. Flow inside the ACE is highly turbulent, unsteady, air ingression in mixing zone and three-phase (air, aqueous and organic phase) operation during solvent extraction operation. The dispersed phase generated in the annular region flows into the rotor region (separation zone) through rotating bowl inlet orifice due to negative pressure generated inside the rotating bowl. The dispersed phase settles inside the rotating bowl and a liquid-liquid interface is formed and a central air core is generated. The operating capacity of any ACE depends on the liquid-liquid interface position inside the rotating bowl, and it is a function of (i) dispersed phase height in the annular region, (ii) flow over the aqueous weir and (iii) flow over the organic weir. The above-complicated behavior of the flow adds several challenges in understanding the flow dynamics inside the rotating bowl in ACE. There is no clear picture of liquid pumping and in-depth knowledge of flow dynamics inside the rotor region from the available literature. Computational fluid dynamics (CFD) may be a pivotal tool to address or solve the above problems and also it can be used to evaluate the existing ACE to optimize the operating parameters and design a robust ACE. CFD can partly substitute for experiments and provides both qualitative and quantitative analyses of the flow within the contactor. It may reveal the detailed flow field and the concentration profile in the device, which significantly contributes to the in-depth study of flow and mass transfer mechanism.

CFD is one of the advanced subjects in fluid mechanics and it employs various numerical techniques and algorithms to solve the set of partial differential equations that represent the fluid flow in a complex environment. Advanced high performance computing facilities are used to perform millions of calculations required for CFD simulation in order to simulate the fluid flow and its interaction with surfaces defined by boundary conditions. CFD makes it possible to solve the flow and energy balances in complicated geometries numerically. The following steps [1] are followed in the CFD analyses.

(a) Equations governing fluid motion

A set of partial differential equations are written to describe the fluid flow, and it represents the conservation of mass, momentum (Navier-stokes equation), and energy. Each equation employs a different physical quantity and its dependent variables. It implies that there must be a balance among the various factors, which influence the variables.

(b) Discretization

The governing differential equations that relate to the dependent variables are discretized to produce a numerical analog for the equations. Then the entire domain is divided into small grids or elements. The systematic discretization of space and dependent variables makes it possible to replace the governing differential equations with simple algebraic equations, which can be solved with relative ease.

(c) Solver

Finally, the initial conditions and boundary conditions specific to the given problem are applied to solve these discretized equations. The solution method can be direct or iterative. Besides, specific control parameters are used to control the convergence, stability, and accuracy of the solution methods.

5.2 Literature survey

5.2.1 CFD simulation details in ACE at annular region

Deshmukh et al. [2, 3] studied single-phase CFD simulation in the ACE annular gap with simplified geometry without inlet and outlet boundary conditions. In the annular region, the inner cylinder is rotating and the outer cylinder is stationary. They simulated using standard k-epsilon and Reynolds Stress Model (RSM) over a wide range of Taylor numbers (Ta) and Reynolds numbers (Re). CFD simulation results were validated by comparing with experimental results and concluded that the RSM model is suitable for a wide range of Ta and Re values.

Wardle et al. [4] studied CFD simulation in simplified annular geometry with an inlet and outlet boundary conditions using Fluent software. They used the STD k-epsilon model and evaluated the effects of geometry (no. of bottom vanes) and rotating speed. Later, Wardle et al. [5] simulated two-phase (air/water) simulation in the annular region using a large eddy simulation (LES) model coupled with the Volume of Fluid (VOF). They incorporated non-iterative time advancement (NITA) algorithm to speed up the calculation time per time step. After NITA incorporation, a typical solution time of all simulations was about 100 h for 1 second of flow time. The frequency and magnitude of liquid height in the annular region are calculated from the simulation and compared with experimental results and concluded that the difference between measured and simulated value might be due to the coarse mesh used in the simulation. Further, they simulated [6] using the above models to understand the effect of liquid height in the annular zone with respect to different bottom vane designs.

Wang et al. [7] also simulated two-phase (air/water) steady-state simulation in simplified annular geometry using CFX software. They used the k-epsilon model coupled with the Eulerian-Eulerian model.

5.2.2 CFD simulation details in ACE at rotor region

N. T. Padial-Collins et al. [8] studied two-phase CFD simulation inside the rotor region in ACE using an in-house developed CartaBlanca computer simulation program. The main goal is to demonstrate the capability of the code in multiphase simulation. They studied the effect of inclination in rotor geometry and also the viscous model.

Wardle et al. [9] studied the two-phase simulation in commercially available CINC V-2 centrifugal extractor rotor region with air and water system. They used the laminar model coupled with the VOF model in a single reference rotating frame boundary condition. From the above simulation, they demonstrated a stable air column forming at the center of the rotating bowl. Further, zero point flow rate (It is defined as the flow rate where liquid starts to come out from the less-dense-phase exit) was simulated with and without venting in aqueous weir. An interesting flow phenomenon was observed in the region above the aqueous phase weir and helped explain the experimentally observed elevated and unstable aqueous phase throughput [10]. Based on the results, modifications in the aqueous weir region was suggested. Typical solution times for the above simulations are about 70 hrs for 1 second of flow time with 20 processors.

Gandhir et al. [11] continued the above simulation using open-source CFD software OpenFOAM. They considered the region from underflow to aqueous outlet situated above the aqueous weir. From the results, they proposed a vent above the aqueous weir cap to regulate pressure to ensure a smooth and predictable operation and modifications in the aqueous weir cap for smooth outlet flow.

Wardle [12] simulated two-phase CFD simulation using OpenFOAM software and was the first person to report the coupled-region model simulations for the combined annulus and rotor zones using multi moving reference frame. In the above simulation, the VOF model coupled with the LES model.

Patra et al. [13] simulated the single-phase CFD simulation in a simplified rotor to understand the flow pattern inside the rotating geometry using OpenFOAM software. They compared three different turbulent models (k-epsilon, RSM and SST-k-omega models) to calculate the pumping capacity and found that there was not much difference in the results. Further, they reported the pumping capacity of the rotating bowl for different diameters of rotating bowl and inlet orifice by using the k-epsilon model.

Li et al. [14] have done three-phase CFD simulation by coupling both the annular and rotor regions using commercial CFX software. They validated the simulation with experimental flooding results. In the above simulation, they used the Eulerian-Eulerian model coupled with RSM. Except Patra et al. [13] and Gandhir et al. [11], no one has done a detailed mesh independent test.

5.2.3 Flow visualization in inside rotor region of ACE

Xu et al. [15] measured the flow field inside the ACE rotor region using particle image velocimetry (PIV) technique. They developed transparent ACE using acrylic material and captured the velocity distribution and streamline at different heights inside the rotor region. Later, Eggert et al. [16] reported a non-invasive Computer Tomography (CT) measurement technique to visualize the intricate flow pattern inside the mixing and settling zone.

5.3 Objective

ACE is used in different process industries for solvent extraction operation and it acts as a mixer, settler and inter-stage pump during multistage operation. Still, its design procedure is empirical. In literature, there is no detailed systematic analysis of flow dynamics inside the rotor region. Flow dynamics inside the rotor region was studied using CFD simulation with different turbulent models. Results were compared with an experimental result to select the suitable turbulent model for 3D ACE simulation.

5.4 CFD Simulation Work

5.4.1 Governing equation

Four turbulent models are compared in this work to understand their effect on the ACE simulation. The governing and closure equations of four turbulent models (i) STD k-epsilon, (ii) RNG k-epsilon, (iii) SST k-omega, and (iv) RSM are shown in Table 5.1.

VOF method [17] is coupled with the above models for two-phase simulation. The main advantage of the VOF method is solving only one set of equations for two immiscible fluids with different densities and viscosities. To identify the phase volume fraction, function f(i,j,k,t) is incorporated in the Navier Strokes Equations. Function f(i,j,k,t) is defined as unity at any point occupied by the fluid and zero elsewhere. If f is between 0 to 1, then it is partially filled.

The governing equation for f, referred to the volume fraction is written as

$$\frac{\partial f}{\partial t}+\frac{\partial (fu)}{\partial x}+\frac{\partial (fv)}{\partial y}=0 \tag{5.1}$$

The physical properties of density and viscosity are averaged, and it is shown in equation 5.2 and 5.3, respectively.

$$\rho_{ij}=\rho_{liq}f_{ij}+\rho_{org}(1-f_{ij}) \tag{5.2}$$

$$\mu_{ij}=\mu_{liq}f_{ij}+\mu_{org}(1-f_{ij}) \tag{5.3}$$

The Continuum Surface Force model [18] is incorporated in VOF model simulation and the surface tension is reformulated as a volume force F_{sv} within free surfaces, i.e. at cells where 0 < f < l. The volume force is given by

$$\overline{F}_{sv}=\sigma\kappa\nabla f \tag{5.4}$$

Table 5.1: Model equations for turbulence

Transport property	Equations	
Continuity equation	$\nabla \cdot \left(\rho\langle u_k\rangle\right) = 0$	(5.4)
Momentum equation	$\nabla\left(\rho\langle u_k\rangle\langle u_k\rangle\right) = -\nabla\langle p\rangle + \nabla\cdot\bar{\tau}_k + \rho\vec{g} + \vec{F}$	(5.5)
	$\bar{\tau}_k = \mu\left(\nabla\langle u_k\rangle + \left(\nabla\langle u_k\rangle\right)^T - \frac{2}{3}\nabla.\langle u_k\rangle I\right)$	
k-ε model [19]		
k equation	$\left\{\rho\frac{\partial k}{\partial t}\right\} + \left\{\rho\langle u_k\rangle\frac{\partial k}{\partial x_k}\right\} = \left\{\tau_{ij}\frac{\partial\langle u_i\rangle}{\partial x_j}\right\} + \left\{\frac{\partial}{\partial x_k}\left(\frac{\mu_t}{\sigma_k}\frac{\partial k}{\partial x_k}\right)\right\} + \left\{\frac{\partial}{\partial x_k}\left(\mu\frac{\partial k}{\partial x_k}\right)\right\} + \left\{-\rho\varepsilon\right\}$	(5.6)
ε equation	$\left\{\rho\frac{\partial\varepsilon}{\partial t}\right\} + \left\{\rho\langle u_j\rangle\frac{\partial\varepsilon}{\partial x_j}\right\} = \left\{C_{\varepsilon 1}\frac{\varepsilon}{k}\tau_{ij}\frac{\partial\langle u_i\rangle}{\partial x_j}\right\} + \left\{\frac{\partial}{\partial x_j}\left(\frac{\mu_t}{\sigma_\varepsilon}\frac{\partial\varepsilon}{\partial x_j}\right)\right\} + \left\{\frac{\partial}{\partial x_j}\left(\mu\frac{\partial\varepsilon}{\partial x_j}\right)\right\} + \left\{-C_{\varepsilon 2}\rho\frac{\varepsilon^2}{k}\right\}$	(5.7)
RNG k-ε model [20]		
	In RNG model k and ε equations are same except constant $C_{\varepsilon 2}$ is replaced with $C^*_{\varepsilon 2}$	
	$C^*_{\varepsilon 2} = C_{\varepsilon 2} + \frac{C_\mu\eta^3\left(1-\eta/\eta_0\right)}{1+\beta\eta^3}$ & $\eta = Sk/\varepsilon$	(5.8)

SST k-ω model [21]

k equation

$$\left\{\rho\frac{\partial k}{\partial t}\right\}+\left\{\rho\langle u_k\rangle\frac{\partial k}{\partial x_k}\right\}=\left\{\tau_{ij}\langle u_k\rangle\frac{\partial\langle u_i\rangle}{\partial x_j}\right\}+\left\{\frac{\partial}{\partial x_k}\left(\frac{\mu_t}{\sigma_k}\frac{\partial k}{\partial x_k}\right)\right\}+\left\{\frac{\partial}{\partial x_k}\left(\mu\frac{\partial k}{\partial x_k}\right)\right\}+\left\{-\rho\varepsilon\right\} \tag{5.9}$$

ω equation

$$\left\{\rho\frac{\partial\omega}{\partial t}\right\}+\left\{\rho\langle u_j\rangle\frac{\partial\omega}{\partial x_j}\right\}=\left\{\alpha\frac{\omega}{k}\tau_{ij}\frac{\partial\langle u_i\rangle}{\partial x_j}\right\}+\left\{\frac{\partial}{\partial x_j}\left(\frac{\mu_t}{\sigma_\omega}\frac{\partial\omega}{\partial x_j}\right)\right\}+\left\{\frac{\partial}{\partial x_j}\left(\mu\frac{\partial\omega}{\partial x_j}\right)\right\}+\left\{-\beta\rho\omega^2\right\} \tag{5.10}$$

Reynolds Stress Model [22-24]

Reynolds stress equation

$$\begin{aligned}&\left\{\rho\frac{\partial\tau_{ij}}{\partial t}\right\}+\left\{\rho\langle u_k\rangle\frac{\partial\tau_{ij}}{\partial x_k}\right\}\\&=\left\{\rho\left(\tau_{ik}\frac{\partial\langle u_j\rangle}{\partial x_k}+\tau_{jk}\frac{\partial\langle u_i\rangle}{\partial x_k}\right)\right\}+\left\{\frac{\partial}{\partial x_k}\left(\frac{\mu_t}{\sigma_k}\frac{\partial\tau_{ij}}{\partial x_k}\right)\right\}+\left\{\frac{\partial}{\partial x_k}\left(\mu\frac{\partial\tau_{ij}}{\partial x_k}\right)\right\}+\left\{-\frac{2}{3}\varepsilon\delta_{ij}\right\}+\left\{\prod_{ij}\right\}\end{aligned} \tag{5.11}$$

ω equation

$$\left\{\rho\frac{\partial\omega}{\partial t}\right\}+\left\{\rho\langle u_j\rangle\frac{\partial\omega}{\partial x_j}\right\}=\left\{\alpha\frac{\omega}{k}\tau_{ij}\frac{\partial\langle u_i\rangle}{\partial x_j}\right\}+\left\{\frac{\partial}{\partial x_j}\left(\frac{\mu_t}{\sigma_\omega}\frac{\partial\omega}{\partial x_j}\right)\right\}+\left\{\frac{\partial}{\partial x_j}\left(\mu\frac{\partial\omega}{\partial x_j}\right)\right\}+\left\{-\beta\rho\omega^2\right\} \tag{5.12}$$

5.4.2 Single phase three dimensional simulation in ACE

In this work, the standard k-epsilon model was selected based on Patra et al. [13] results to understand the effect of internals in the centrifugal extractor's pumping capacity. CE 30 mm rotating bowl (Dimensions are shown in table 5.1 and figure 5.1) is selected for the steady-state 3D simulation. In single-phase CFD simulation, geometry up to aqueous weir was selected without any organic hardware.

Table 5.2: ACE 30mm bowl dimension

S. No	Bowl internals	
1.	Rotating bowl Inner diameter (mm)	30
2.	Organic weir diameter (mm)	15
3.	Aqueous weir diameter (mm)	17.4
4.	Settler region height (mm)	69.5
5.	Underflow width (mm)	3
6.	No of vertical baffles	4
7.	Inlet diameter (mm)	8

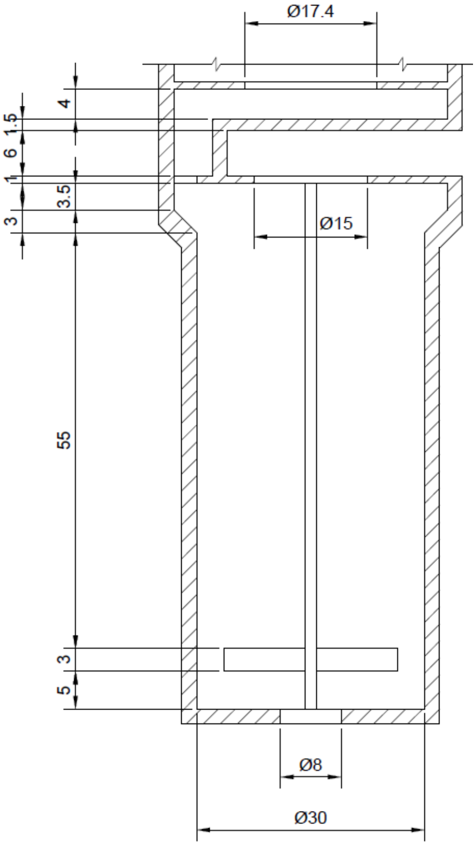

Figure 5.1: ACE 30 mm bowl drawing with dimensions

Four different unstructured meshes were generated using Gambit 6 software to complete the mesh independent test and they are (i) 388284 (with average wall distance of 1.35 mm), (ii) 894226 (with average wall distance of 0.742 mm), (iii) 1286601 (with average wall distance of 0.591 mm) and (iv) 1631308 (with average wall distance of 0.566 mm).

Boundary conditions used in this simulation are

1. Inlet = pressure inlet (0 Pa)

2. Outlet = pressure outlet (0 Pa)

3. Wall = moving wall (3000 rpm) and no slip

4. Convergence criteria = 10^{-3}

5. Operating fluid/liquid = Water

The standard wall function is used with y+ greater than 30 for all the cases. A SIMPLE algorithm was employed where turbulent kinetic energy and dissipation rate are assumed as 1 for both inlet and outlet boundary conditions. CE 30 mm bowl geometry with mesh size 1631308 up to the aqueous weir without organic hardware is shown in Fig. 5.2. Ansys Fluent Software version 13 was used in these simulations.

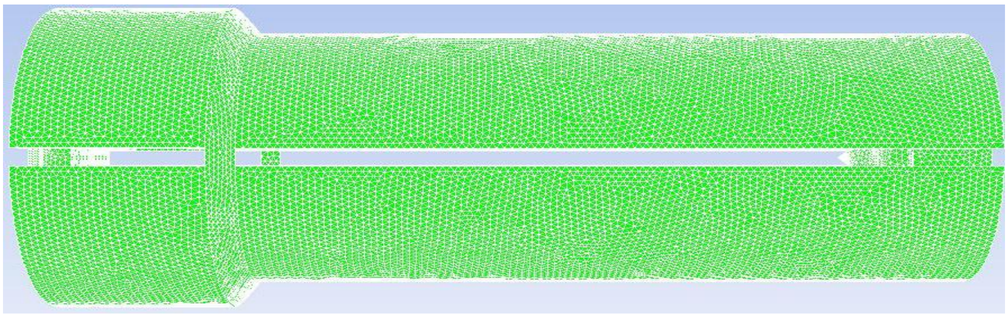

(a) side view

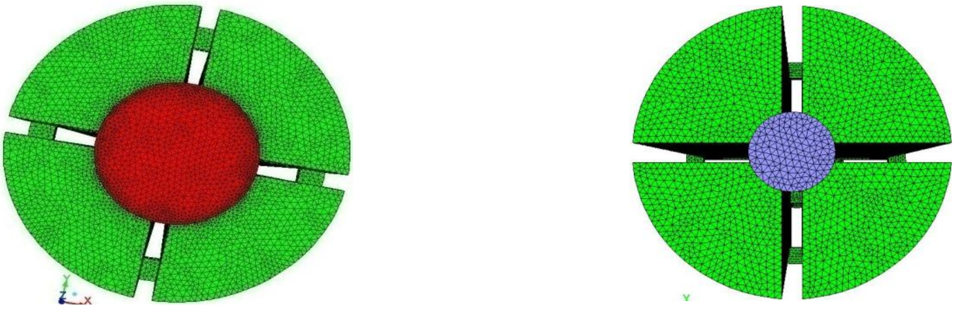

(b) Top view (aqueous outlet)

(c) Bottom view (inlet)

Figure 5.2: ACE 30 mm bowl geometry up to aqueous weir without organic hardware (Mesh size = 1631308)

5.4.3 Two phase 2D CFD simulation

5.4.3.1 Mesh independent test

Wardle et al. [9] reported that a typical solution time for 3D CFD simulation was about 70 hrs for 1 second of flow time with 20 processors with a laminar model coupled with VOF. After a thorough literature survey, it is decided to go for 2D, two-phases (water and air) with axisymmetric swirl and unsteady-state simulation for mesh independent test. CE 30 mm bowl geometry including, organic outlet portion is generated using Ansys Design Modular software version 14 and it is shown in figure 5.3. In this work, the standard k-epsilon model coupled with VOF is used for mesh independent tests. Ansys meshing software of version 14 was used to generate five different mesh sizes and they are i) 12376, (ii) 27711, (iii) 49082, (iv) 66336 and (v) 110476.

Figure 5.3: 2D geometry with aqueous and organic outlet

Following boundary conditions are used in the mesh independent test simulation.

Boundary conditions are

1. Inlet = velocity inlet (0.015 m/s, air = 0)

2. Aq outlet = pressure outlet (0 Pa, back flow for air =1)

3. Org outlet = pressure outlet (0 Pa, back flow for air =1)

4. Wall = stationary wall and no slip condition

5. Internal surface = Moving reference frame (rotating speed = 3000 rpm)

6. Convergence criteria = 10^{-3}

7. Operating fluid/liquid = Water (phase 1) and air (phase 2)
8. Two phase model = VOF model
9. Time step = 0.0001

PISO algorithm was employed and turbulent intensity and turbulent viscosity ratio is assumed as 5% and 10, respectively. VOF model is coupled with sharp interface modeling with the explicit formulation. Continuum surface force is enabled with surface tension coefficient value of 0.072 N/m.

5.4.3.2 Zero point flow simulation with different turbulent model.

Mesh size of 66336 is selected for zero point flow simulation based on mesh independent results. In literature, different turbulent models were reported for ACE simulation inside the rotating bowl geometry. In this work, four turbulent models (i) k-epsilon with STD wall function, (ii) k-epsilon RNG, (iii) SST k-omega, and (iv) RSM Models are selected to understand its effect in ACE simulation. Zero-point flow simulated with above turbulent models for different velocity inlet conditions and other boundary conditions is same as discussed in the mesh independent chapter.

5.5 Experimental work

5.5.1 Description of the setup

Schematic drawing for zero point flow [10] experimental setup is shown in Fig. 5.4. The setup consists single-stage ACE connected with an aqueous (heavy phase) pump (ISMATEC MFP Process drives + Q3 Pump heads) and an associated aqueous phase feed tank.

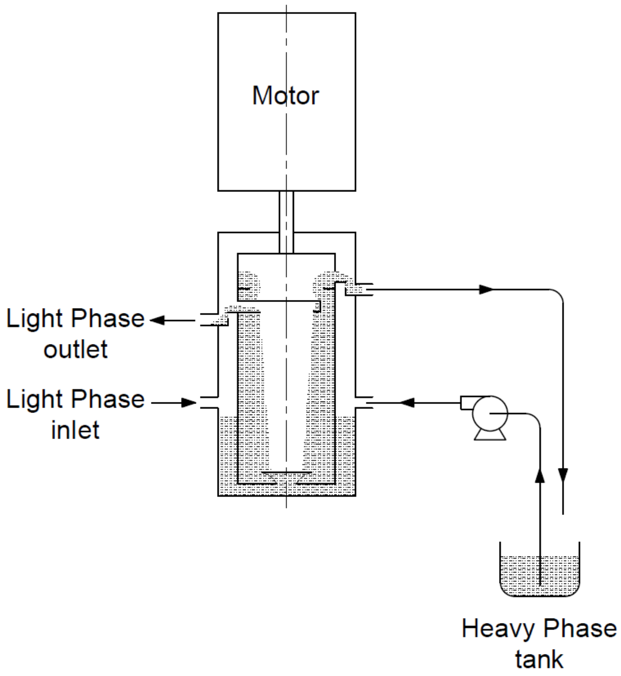

Figure 5.4: Schematic view of zero point flow experimental setup

5.5.2 Zero point flow experiment

During single-phase operation in ACE, the flow rate at which aqueous starts to come out from organic weir is called zero-point flow rate. In the zero point flow experiment, CE 30 mm bowl was operated at 3000 rpm, and water was feed into ACE through the heave phase pump from a heavy phase feed tank. Water comes out from heave phase weir and is collected into the heavy phase feed tank. Step by step water flow rate is increased until it comes out from the light phase outlet. In this experiment effect of internals in the zero point flow is evaluated by using CE 30 mm bowl with and without internals (vertical baffle plates and horizontal deflection plate) inside the settling region. Schematic drawings of a rotating bowl with and without internals are shown in Fig. 5.5 and 5.6, respectively.

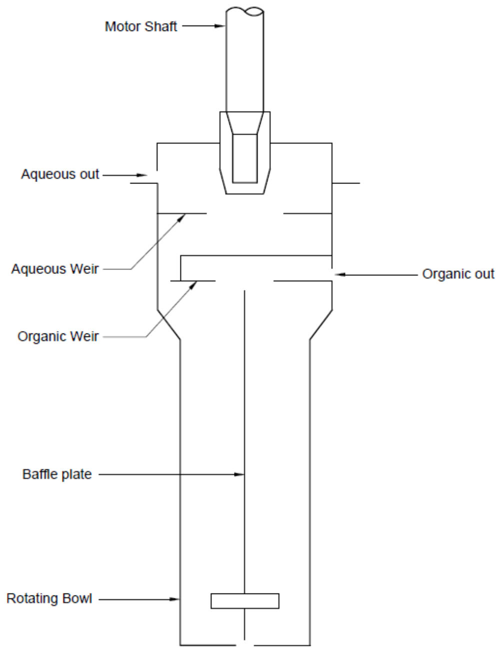

Figure 5.5: Schematic view of ACE 30 mm rotating bowl with vertical baffle plates and horizontal deflection plate

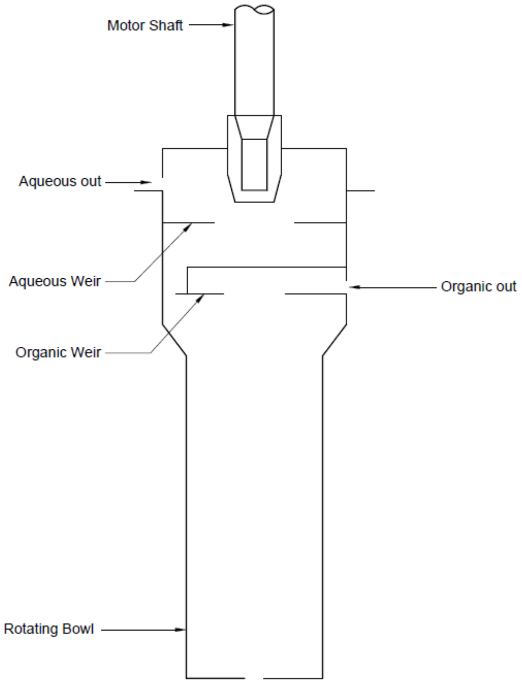

Figure 5.6: Schematic view of ACE 30 mm rotating bowl without vertical baffle plates and horizontal deflection plate

5.6 Results and Discussion

5.6.1 Single phase three dimensional simulation in ACE

Pumping capacity for CE 30 mm bowl calculated from single-phase 3D simulation for different mesh sizes is shown in Table 5.3. Velocity and pressure contour plot with respect to different mesh sizes are shown in Fig. 5.7 and 5.8, respectively.

Table 5.3: Pumping capacity with respect to different mesh size

Sr. No	Mesh size	Pumping capacity (L/h)
1.	388284	6.29
2.	894226	-4.56
3.	1286601	-11.30
4.	1631308	-11.78

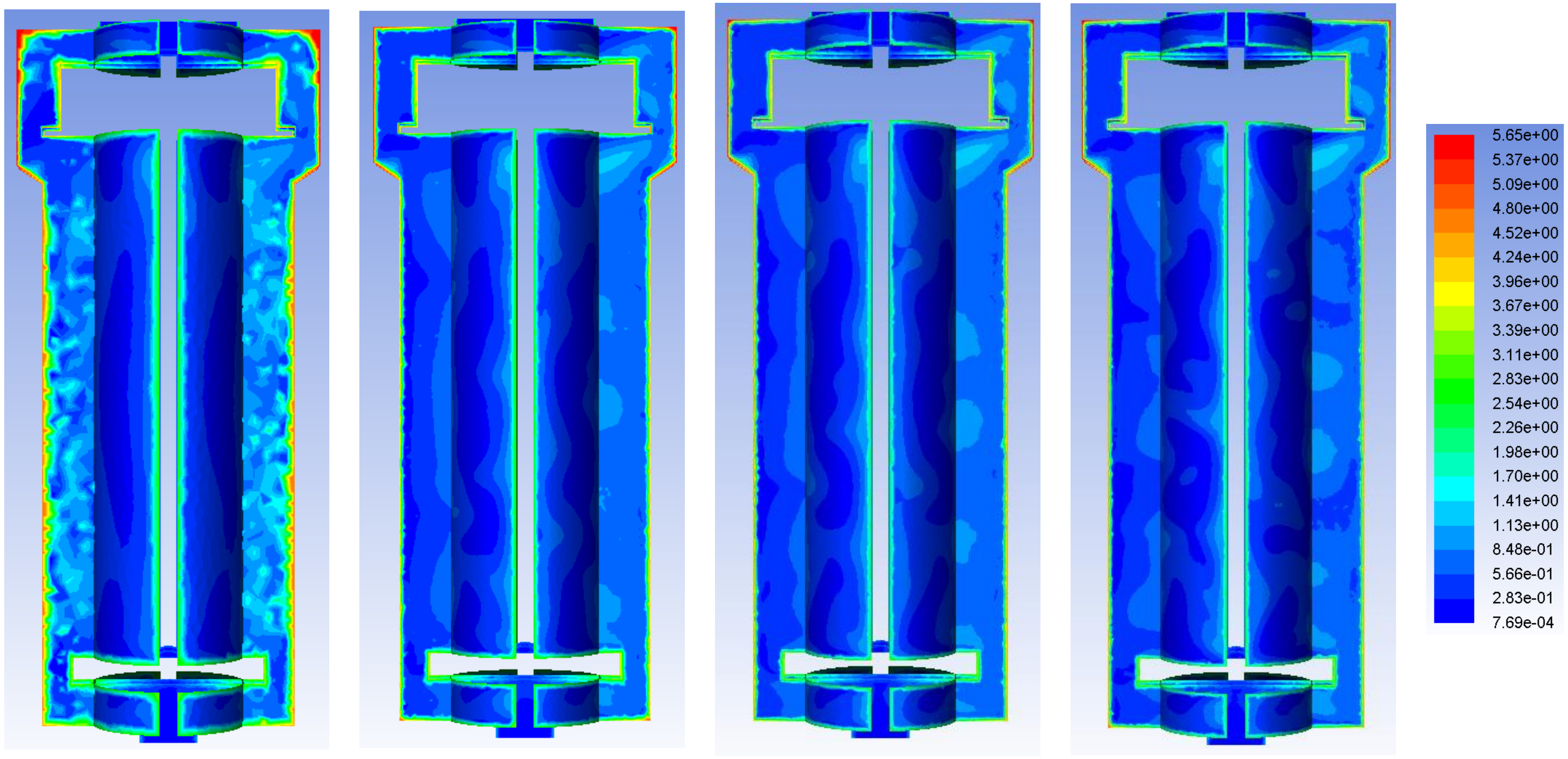

(a) (b) (c) (d)

Figure 5.7: Velocity magnitude contour plot at radial coordinate of 9 mm and y coordinate of 2 mm

(a) Mesh size = 388284, (b) Mesh size = 894226, (c) Mesh size = 1286601 and (d) Mesh size = 1631308

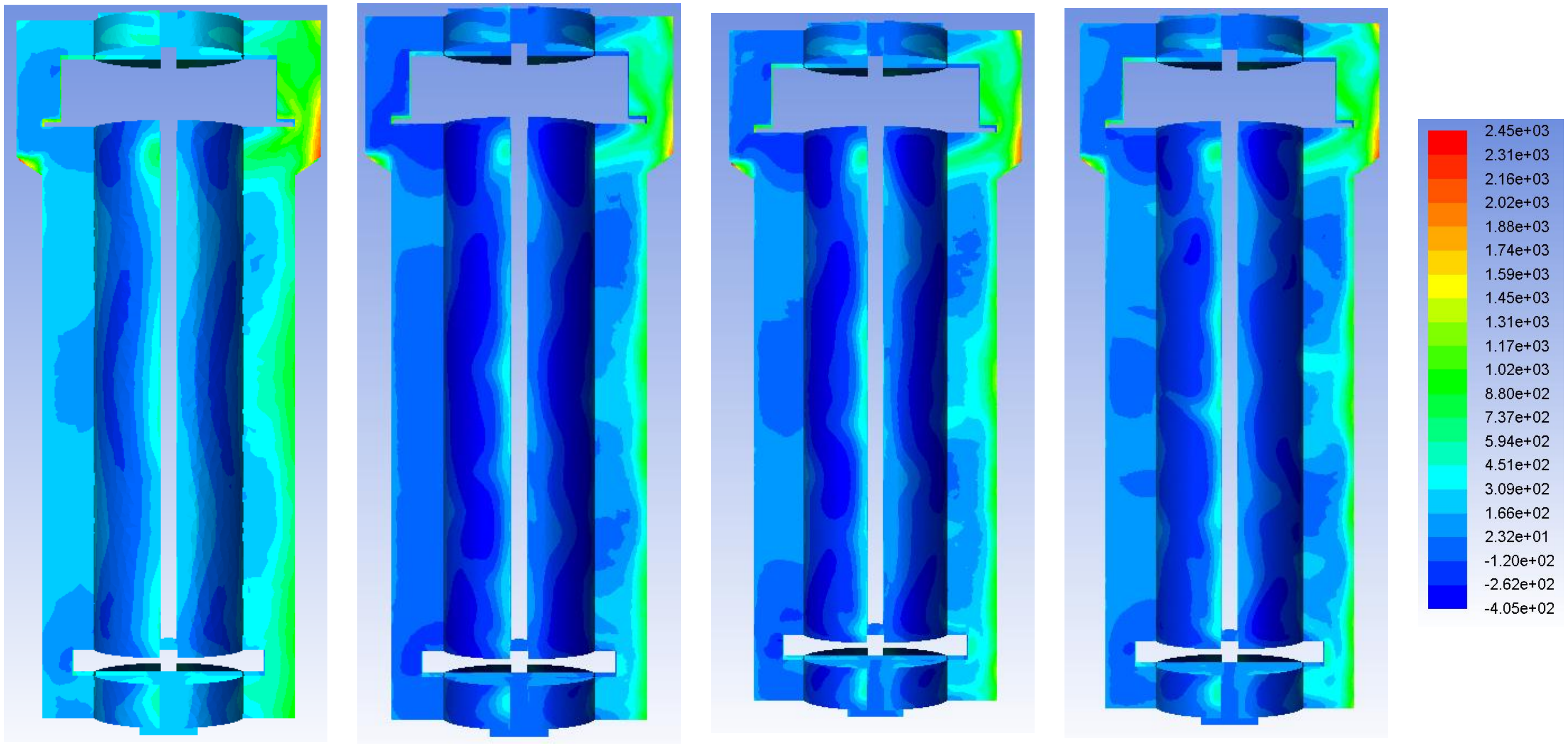

(a) (b) (c) (d)

Figure 5.8: Total pressure contour plot at radial coordinate of 9 mm and y coordinate of 2 mm

(a) Mesh size = 388284, (b) Mesh size = 894226, (c) Mesh size = 1286601 and (d) Mesh size = 1631308

3D mesh independent simulation results (Table 5.3) show that reverse flow was observed from aqueous outlet to inlet with an increase in the mesh size. In real condition, air-core forms at the center of the centrifugal extractor, and it reaches up to the horizontal deflection plate. The length of air-core depends upon the flow rate and bowl rotating speed. In single-phase simulation, liquid flows from top to bottom due to reverse flow at aqueous outlet similar to air core formation. From the above results, it is concluded that single-phase CFD simulations may not be suitable for ACE rotating bowl simulation.

5.6.2 Two phase 2D CFD simulation

5.6.2.1 Mesh independent test

The simulation with an inlet velocity of 0.015 m/s (throughput of 2.71 Kg/hr) was completed with different mesh sizes, and its results are shown in Table 5.4.

Table 5.4: Average mass flow rate of water for 0.1 sec with respect to different mesh size

S. No	Mesh	Inlet mass flow rate (Kg/hr)	Mass flow rate at Aq. Outlet (Kg/hr)	Mass flow rate at Org. Outlet (Kg/hr)	% mass imbalance
1.	12376	2.71	-1.39	-1.31	0.00
2.	27711	2.71	-1.95	-0.76	0.23
3.	49082	2.71	-2.18	-0.53	0.04
4.	66336	2.71	-2.51	-0.21	0.04
5.	110476	2.71	-2.51	-0.20	0.04

Contour plot for water volume fraction with respect to different mesh sizes is shown in below Fig. 5.9.

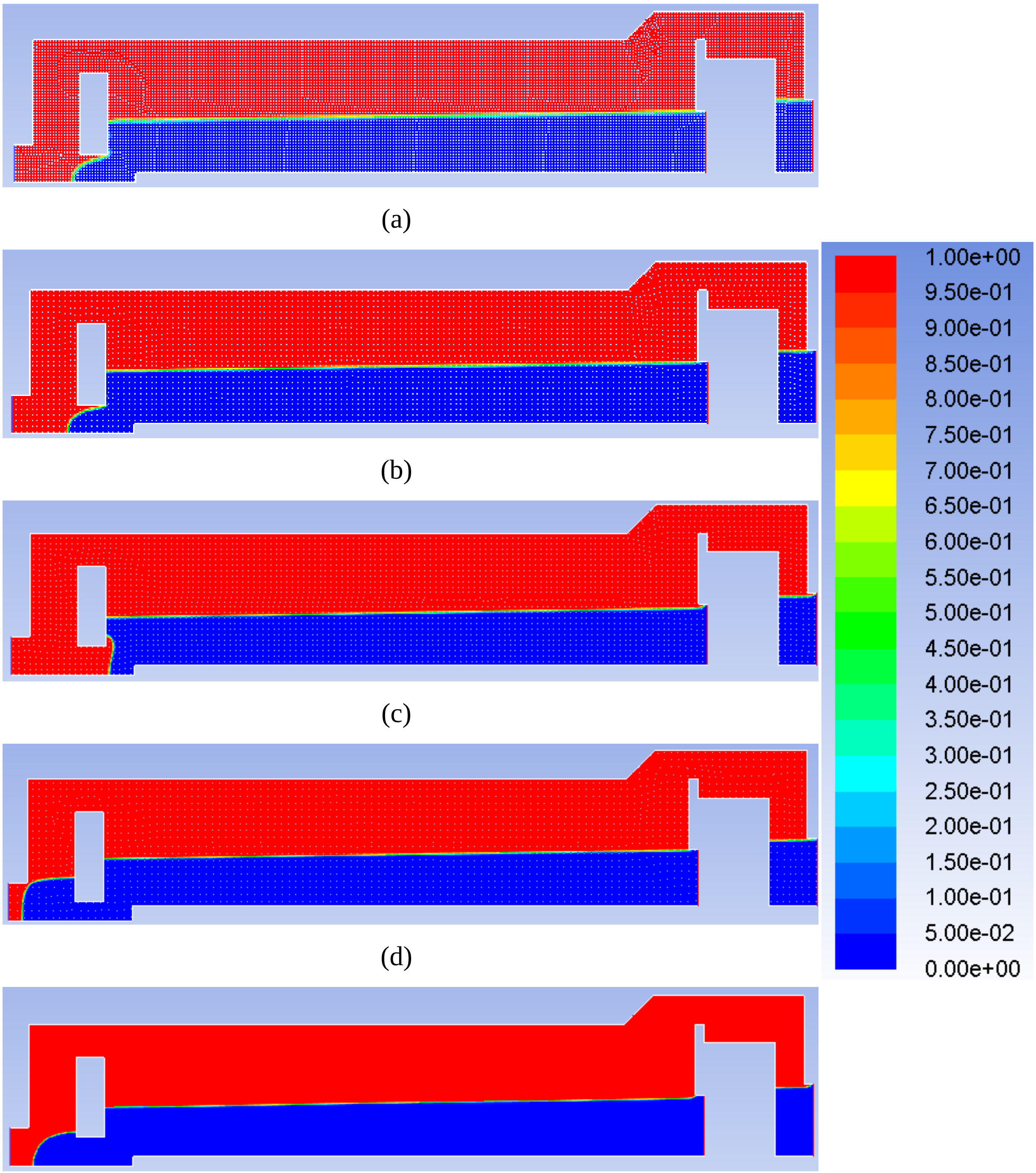

(a)

(b)

(c)

(d)

(e)

Figure 5.9: Water volume fraction contour plot from 2D, 2 phase CFD simulation for different mesh size

(a) 12376, (b) 27711, (c) 49082, (d) 66336 and (e) 110476

Mesh independent result shows that the mass flow rate at the organic outlet decreases with an increase in the mesh size, and in the aqueous outlet, it increases with mesh size. For mesh size 66336 and above, there was no change in the mass flow rate in aqueous and organic outlets. Based on the above simulation results, the mesh size 66336 is selected for zero point flow simulation.

5.6.2.2 Zero point flow simulation with different turbulent model.

Zero-point flow simulations, coupled with the VOF model, was completed with different turbulent models. During the simulation, inlet velocity is varied between 0.011 to 0.2 m/s, and the average water mass flow rate for 0.1 sec is calculated after 30 sec (enough time to reach the steady-state flow condition), and its results are shown in Table 5.5 to 5.9.

Table 5.5: Zero point flow CFD simulation results for k-ε model

S. No	Model	Inlet velocity of water (m/s)	Inlet mass flow rate (Kg/hr)	Mass flow rate at Aq. Outlet (Kg/hr)	Mass flow rate at Org. Outlet (Kg/hr)	% mass imbalance
1.	k-ε STD model	0.012	2.17	-2.17	0	0.26
2.		0.013	2.35	-2.35	0	0.06
3.		0.014	2.53	-2.45	-0.08	0.00
4.		0.015	2.71	-2.51	-0.21	0.04
5.		0.016	2.89	-2.56	-0.33	0.09
6.		0.018	3.25	-2.67	-0.58	0.10
7.		0.019	3.43	-2.75	-0.68	0.00
8.		0.02	3.61	-2.75	-0.86	0.00

Table 5.6: Zero point flow CFD simulation results for k-ε RNG model

S. No	Model	Inlet velocity of water (m/s)	Inlet mass flow rate (Kg/hr)	Mass flow rate at Aq. Outlet (Kg/hr)	Mass flow rate at Org. Outlet (Kg/hr)	% mass imbalance
1.	k-ε RNG model	0.005	0.90	-0.94	0	3.97
2.		0.011	1.99	-2.00	0	0.52
3.		0.013	2.35	-2.35	0	0.04
4.		0.014	2.53	-2.42	-0.10	0.00
5.		0.015	2.70	-2.45	-0.22	0.38
6.		0.018	3.25	-2.65	-0.60	0.00
7.		0.019	3.43	-2.65	0.78	0.00
8.		0.020	3.61	-2.65	-0.96	0.00

Table 5.7: Zero point flow CFD simulation results for SST K-ω model

S. No	Model	Inlet velocity of water (m/s)	Inlet mass flow rate (Kg/hr)	Mass flow rate at Aq. Outlet (Kg/hr)	Mass flow rate at Org. Outlet (Kg/hr)	% mass imbalance
1.	SST K-ω model	0.011	1.99	-2.00	0	0.23
2.		0.012	2.16	-2.14	-0.02	0.17
3.		0.013	2.35	-2.20	-0.15	0.04
4.		0.014	2.53	-2.26	-0.27	0.08
5.		0.015	2.71	-2.31	-0.39	0.28
6.		0.016	2.89	-2.43	-0.46	0.01
7.		0.018	3.25	-2.43	-0.82	0.00
8.		0.019	3.43	-2.43	-1.00	0.11
9.		0.020	3.61	-2.40	-1.21	0.06

Table 5.8: Zero point flow CFD simulation results for Reynolds Stress model

S. No	Model	Inlet velocity of water (m/s)	Inlet mass flow rate (Kg/hr)	Mass flow rate at Aq. Outlet (Kg/hr)	Mass flow rate at Org. Outlet (Kg/hr)	% mass imbalance
1.	Reynolds Stress model	0.012	2.17	-2.18	0.00	0.42
2.		0.013	2.35	-2.25	-0.09	0.08
3.		0.014	2.53	-2.33	0.20	0.06
4.		0.015	2.70	-2.41	0.29	0.10
5.		0.017	3.07	-2.42	-0.65	0.00
6.		0.018	3.25	-2.42	-0.83	0.10
7.		0.019	3.43	-2.40	-1.02	0.03
8.		0.020	3.61	-2.39	-1.23	0.16

Zero-point flow calculated from STD k-epsilon and k-epsilon RNG are the same, and it is around 2.35 kg/hr. The zero-point flow calculated from SST k-omega and RSM model is 1.99 and 2.17 kg/hr, respectively. In order to understand the flow behavior, contour plots for different turbulent models for an inlet velocity of 0.014 m/s are shown in Fig. 5.10.

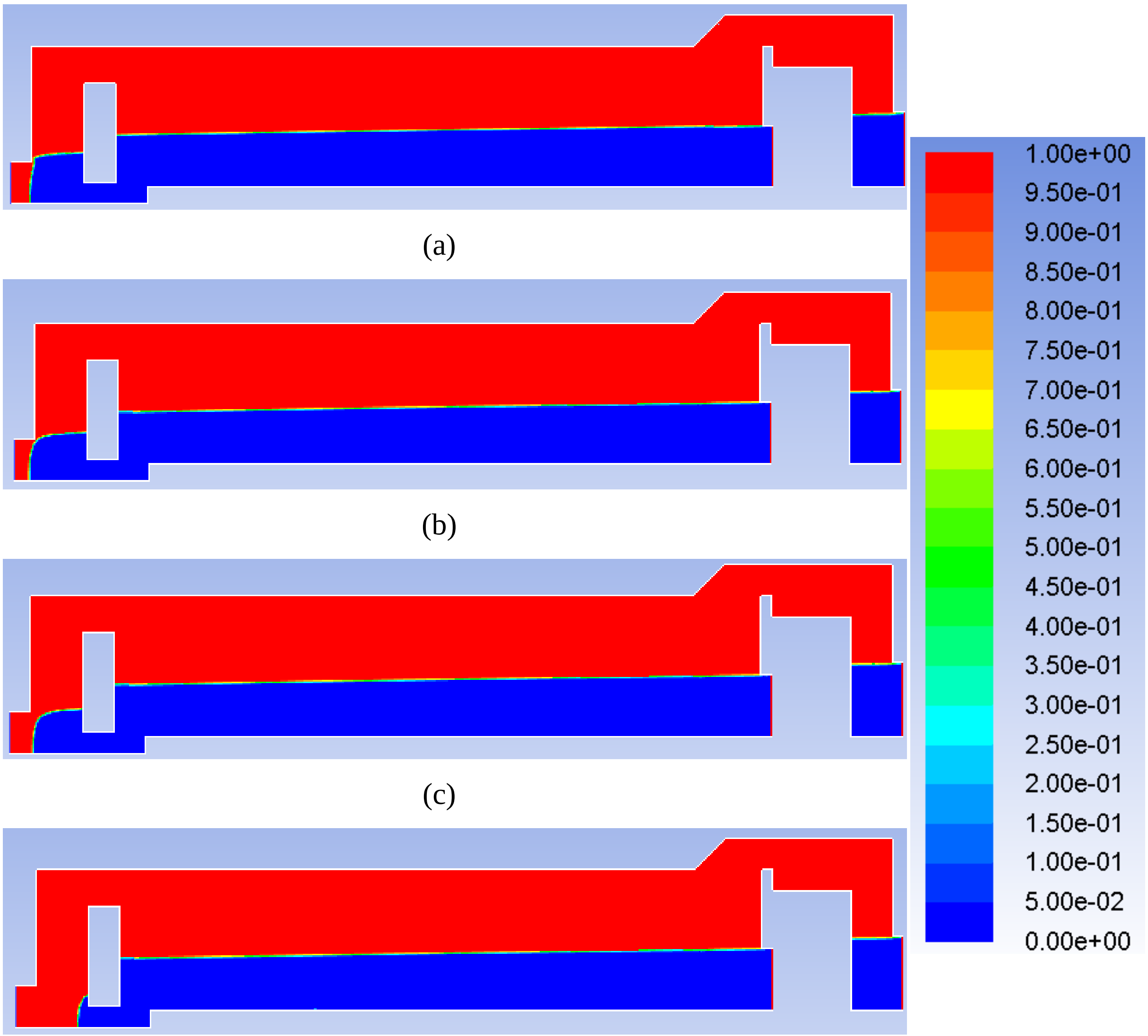

(a)

(b)

(c)

(d)

Figure 5.10: Water volume fraction contour plot from 2D, 2 phase CFD simulation for different turbulent model at velocity inlet of 0.014 m/s

(a) k-ε STD model, (b) k-ε RNG model, (c) SST K-ω model and (d) RSM

5.6.3 Zero point flow experiment

Zero-point flow experimental results for CE 30 mm bowl are shown in Table 5.9.

Table 5.9: Zero point flow in ACE 30 mm bowl

S. No	Bowl details	Zero point flow (Kg/hr)
1.	CE 30 mm bowl without vertical baffles and deflection plate	1.55
2.	CE 30 mm bowl with vertical baffles and deflection plate	25.5

From the above results it is understood that vertical baffle and diversion disk plays major role in hydrodynamic performance of ACE. Zero point flow for CE 30 mm bowl with vertical baffle plates and horizontal deflection plate is 16 times higher than that of the CE 30 mm bowl without any internals. Bernstein et. al. [25] explained the function of horizontal deflection plate and vertical baffles. The horizontal deflection plate diverts the dispersion phase near to rotor wall, where acceleration due to centrifugal force is very high and dispersed phase get separated easily. The vertical plate quickly accelerates the dispersed phase equal to the rotor speed and act as a chamber to arrest the vortex formation inside the rotor.

5.6.4 Comparison of experimental result with CFD simulation

Vertical baffle plate cannot be included in the 2D simulation. To validate CFD results, zero point flow in CE 30 mm bowl without internals is compared with simulation results. Zero point flow experiment result is compared to the other turbulent models and it is shown in below Table 5.10.

Table 5.10: Zero point flow with respect to different turbulent models

S. No	Details	Zero point flow (Kg/hr)
1.	Experiment	1.55
2.	k-ε STD model	2.35
3.	k-ε RNG model	2.35
4.	SST k-ω model	1.99
5.	Reynolds Stress model	2.17

From the above table, it is observed that zero point flow calculated from the SST k-omega model is near to experimental results when compared to the other models. Based on the above simulation results, the SST k-omega model is suitable for ACE simulations.

5.7 Conclusions

a) For the first time, the effect of the vertical baffle and deflection plate in the hydrodynamic performance of ACE is reported.

b) From the 3D single-phase simulation, it is concluded that the single-phase CFD simulation is not suitable for rotating bowl ACE.

c) Mesh independent in the ACE rotating bowl with respect to 2D simulation is completed, and from zero point flow simulation, it is concluded that SST k-omega model result is near to experimental result compared to the other turbulent models. Hence, the SST k-omega model is suggested for future simulations.

5.8 References

1. S. V. Patankar, “Numerical heat transfer and fluid flow”, *Boca Raton, CRC press,* **1980,** *1st Edition.*

2. S. S. Deshmukh, S. Vedantam, J. B. Joshi, “Computational Flow Modeling and Visualization in the Annular Region of Annular Centrifugal Extractor”, *Ind. Eng. Chem. Res.,* **2007,** *46(25),* 8343-8354.

3. S. S. Deshmukh, J. B. Joshi, “Flow visualization and Three-Dimensional CFD Simulation of the Annular Region of an Annular Centrifugal Extractor”, *Ind. Eng. Chem. Res.,* **2008,** *47(10),* 3677-3686.

4. K. E. Wardle, T. R. Allen, “Computational Fluid Dynamics (CFD) Study of the Flow in an Annular Centrifugal Contactor”, *Sep. Sci. Technol.,* **2006,** *41(10),* 2225-2244.

5. K. E. Wardle, T. R. Allen, M. H. Anderson, R. E. Swaney, “Free Surface Flow in the Mixing Zone of an Annular Centrifugal Contactor”, *AIChE Journal,* **2008,** *54(1),* 74-85.

6. K. E. Wardle, T. R. Allen, M. H. Anderson, R. E. Swaney, “Analysis of the Effect of Mixing Vane Geometry on the Flow in an Annular Centrifugal Contactor”, *AIChE Journal,* **2009,** *55(9),* 2244-2259.

7. C. Wang, S. Li, W. Duan, S. Cao, “CFD simulations of the air/water two-phase Flow in an Annular Centrifugal Contactor”, *Energy Procedia,* **2013,** 39, 467-473.

8. N. T. Padial-Collins, D. Z. Zhang, Q. Zou, X. Mia, W. B. VanderHeydan, “Centrifugal Contactors: Separation of an Aqueous and an Organic Stream in the Rotor Zone (LA-UR-05-7800), *Sep. Sci. and Tech.,* **2006,** *41(6),* 1001-1023.

9. K. E. Wardle, T. R. Allen, M. H. Anderson, R. E. Swaney, “CFD Simulation of the Separation Zone of an Annular Centrifugal Contactor”, *Sep. Sci. and Tech.,* **2009,** *44(3),* 517-542.

10. R. Leonard, M. S. Ragalbuto, S. Aase, H. Arafat, J. Falkenberg, “Hydraulic performance of a 5-cm contactor for caustic-side solvent extraction”, *Tech. Rep. ANL-02/18,* **2002,** Argonne National Laboratory.

11. A. Gandhir, K. E. Wardle, “CFD Analysis of Fluid Flow Above the Upper Weir of an Annular Centrifugal Contactor”, *Sep. Sci. and Tech.,* **2012,** *47(1),* 1-10.

12. K. E. Wardle, “Open-Source CFD Simulations of Liquid-Liquid Flow in the Annular Centrifugal Contactor”, *Sep. Sci. and Tech.,* **2011,** *46(15),* 2409-2417.

13. J. Patra, N. K. Pandey, U. K. Mudali, R. Natarajan, J. B. Joshi, “Hydrodynamic Study of Flow in the Rotor Region of Annular Centrifugal Contactors using CFD simulation”, *Chem. Eng. Comm.,* **2013,** *200(4),* 471-493.

14. S. Li, W. Duan, J Chen, J Wang, “CFD Simulation of Gas-Liquid-Liquid Three-Phase Flow in an Annular Centrifugal Contactor”, *Ind. Eng. Chem. Res.,* **2012,** *51(34),* 11245-11253.
15. Y. Xu, J. G. Wang, S. L. Zhao, Z. S. Bai, “PIV experimental study on the flow field in the rotor zone of an annular centrifugal contactor”, *Chem. Eng. Res. Des.,* **2015,** *94,* 691-701.
16. A. Eggert, T. Kogl, W. Arlt, A. Jupke, “Computer tomographic detection of the liquid-liquid mixing and separation within the Annular Centrifugal Contactor/Extractor”, *Chem. Eng. Res. Des.,* **2019,** *142,* 143-153.
17. C. W. Hirt, B. D. Nichols, “Volume of fluid (VOF) method for the dynamics of free boundaries,” *Journal of Computational Physics,* **1981,** *39(1),* 201-235.
18. J. U. Brackbill, D. B. Kote, C. Zemach, “A continuum method for modelling surface tension,” *Journal of Computational Physics,* **1992,** *100(2),* 335-354.
19. B. E. Launder, B. I. Sharma, "Application of the Energy Dissipation Model of Turbulence to the Calculation of Flow Near a Spinning Disc", *Letters in Heat and Mass Transfer,* **1974,** *1(2),* 131-138.
20. V. Yakhot, S. A. Orszag, S. Thangam, T. B. Gatski, C. G. Speziale, “Development of turbulence models for shear flows by a double expansion technique”, *Physics of Fluids A,* **1992,** *4(7),* 1510-1520.
21. F. R. Menter, “Zonal Two Equation k-ω Turbulence Models for Aerodynamic Flows”, *AIAA Paper,* **1993,** 1993-2906.
22. P. Chou, “On velocity correlations and the solutions of the equations of turbulent fluctuation”, *Quarterly of Applied Mathematics,* **1945,** *3(1),* 38-54.
23. J. Rotta, “Statistische theorie nichthomogener turbulenz”, *Zeitschrift für Physik A,* **1951,** *129(6),* 547-572.
24. B. E. Launder, G. J. Reece, W. Rodi, “Progress in the Development of a Reynolds-Stress Turbulent Closure”, *J. Fluid Mech.,* **1975,** *68(3),* 537-566.
25. G. J. Bernstein, D. E. Grodsvenor, J. F. Lene, N. M. Levitz, “A high capacity annular centrifugal extractor”, *Nucl. Technol.,* **1973,** *20(3),* 200-202.

CHAPTER 6

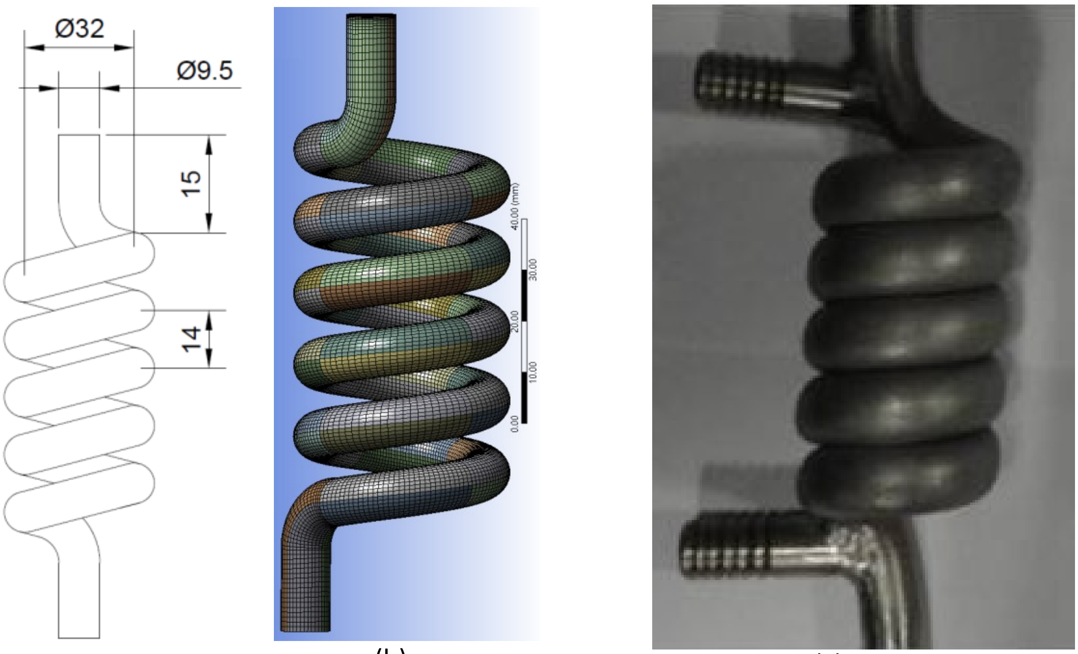

(a) (b) (c)

(a) Schematic drawing of helical coil with dimensions (No of turns = 5), (b) Geometry created in the ANSYS software and (c) actual experimental setup

DESIGN AND DEVELOPMENT OF HELICAL COIL BASED FLUIDIC DIODE PUMP

6 DESIGN AND DEVELOPMENT OF HELICAL COIL BASED FLUIDIC DIODE PUMP

6.1 Introduction

The pump used in the nuclear reprocessing plant should be highly reliable, with minimum moving parts and zero leak rates. Generally, four methods of liquid transfer systems without moving parts are used to handle radioactive liquids and they are (i) steam jets, (ii) airlift, (iii) vacuum and (iv) blow cases, etc [1]. Later, several fluidic devices based pumps were developed and successfully operated in the nuclear reprocessing facilities. They are Reverse flow diverter (RFD), Pulse Jet Mixer (PJM), Double Diode Pump (Vortex Diode), Vacuum Operated Slug Lift (VOSL), etc [2]. Each system has its advantage and disadvantages. For metering flow, especially for solvent extraction operations, the airlift or VOSL is generally selected because of its simple design and reliability. The performance of an airlift pump is dependent upon the submergence ratio, as well as the liquid operating temperature. Advantages are (i) Nil maintenance, (ii) no process liquid dilution or heating and (iii) excellent liquid metering. Its main disadvantages are (i) spreading of radioactive elements inside the reprocessing cell (aerosol generation), (ii) requirement of the disentrainment vessel and (iii) Lift height limited by liquid/air slippage, etc. Other types of fluidic pumps are the vortex diode and reverse flow diverter and generally used for liquid transfers. However, both these pumps are not suitable for metering purposes. The main disadvantage of both VD and the RFD pumps is the possible ingress of air into the feed tank, meaning the feed tank system may get pressurized.

Centrifugal extractor is widely used in solvent extraction operation, especially in fast reactor reprocessing application. Flow fluctuation in the centrifugal extractor system drastically affects the steady-state operation and reduces its mass transfer performance [3]. In a fast reactor reprocessing flow sheet, throughputs for aqueous and organic phases vary from few mL/min to L/min. The airlift and other fluidic pumping system are not suitable for low throughput metering operations. A new helical coil-based fluidic pump is developed for low throughput operation.

6.2 Literature survey

Helical coils are widely used for a variety of industrial applications and it comes under three basic configurations and they are (i) single, (ii) nested and (iii) tapered spiral coil. It is widely used in heat transfer applications [4] because of the high surface area to volume ratio. It is also used for mixing and mass transfer operations [4]. Compared to the straight tube, the flow inside the helical coil is not parallel to the wall due to curvature. Due to flow diversion inside the helical coil, centrifugal forces are developed and secondary flows (Dean Vortex) are developed [5, 6]. Secondary flow creates uniform mixing, uniform concentration and uniform temperature profile along transverse direction inside the helical coil.

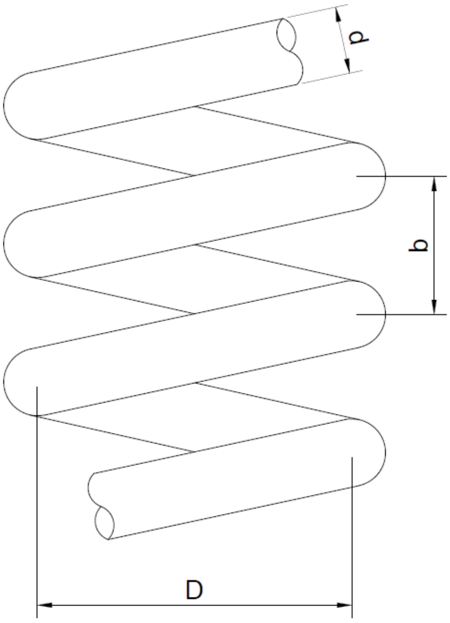

Figure 6.1: Basic geometry of helical coil

The helical coil geometry is shown in above Fig. 6.1. The friction factor for curved pipes can be calculated by using fanning friction factor by replacing straight pipe friction factor (f_s) with coiled friction factor (f_c).

$$\Delta P = 2 f_c L \rho v^2 / d \qquad (6.1)$$

$$L = \sqrt{(\pi D N)^2 + (bN)^2} \qquad (6.2)$$

Where (i) L = Helical coil length, (ii) D = Helical coil diameter, (iii) N = No of helical coils and (iv) b = Helical coil pitch

In helical coil, Reynolds number for the transition from laminar to the turbulent region is much higher than the straight tube (critical Reynolds number > 2100). In the published literature, a large number of empirical correlations have been proposed for the estimation of critical Reynolds number for curved pipes and some of these correlations are listed in Table 6.1.

Table 6.1: Correlation for critical Reynolds number calculation for helical pipe

Investigator	Correlation	Condition
Ito [7]	$N_{Re\,cr} = 20000\left(\frac{d}{D}\right)^{0.32}$	$15 < \left(\frac{D}{d}\right) < 860$
Kubair and Varrier [8]	$N_{Re\,cr} = 12730\left(\frac{d}{D}\right)^{0.32}$	$10 < \left(\frac{D}{d}\right) < 2000$
Schmidt [9]	$N_{Re\,cr} = 2300\,(1 + 8.6\left(\frac{d}{D}\right)^{0.45})$	$\left(\frac{D}{d}\right) < 200$
Srinivasan et al. [10]	$N_{Re\,cr} = 2100\,(1 + 12\left(\frac{d}{D}\right)^{0.25})$	$\left(\frac{D}{d}\right) < 200$
Mishra and Gupta [11]	$N_{Re\,cr} = 20000\left[\left(\frac{d}{D}/\left(1 + \left(\frac{b}{2\pi D}\right)^2\right)\right)^{0.32}\right]$	Incorporated finite pitch in the correlation
Cioncolini and Santini [12, 13]	$N_{Re\,cr} = 30000\left(\frac{d}{D}\right)^{0.47}$	$\left(\frac{D}{d}\right) \leq 24$
	$N_{Re\,cr} = 12500\left(\frac{d}{D}\right)^{0.31}$	$30 \leq \left(\frac{D}{d}\right) \leq 110$
	$N_{Re\,cr} = 120000\left(\frac{d}{D}\right)^{0.57}$	$30 \leq \left(\frac{D}{d}\right) \leq 110$
	$N_{Re\,cr} = 2300\,(1 + 210\left(\frac{d}{D}\right)^{1.12})$	$\left(\frac{D}{d}\right) \geq 150$

The following dimensionless numbers describe the flow inside any given helical coil. They are

Dean Number, $N_{De} = N_{Re}\left(\frac{d}{D}\right)^{0.5}$ (6.3)

Diameter of curvature, $D_c = D\left[1 + \left(\frac{b}{2\pi D}\right)^2\right]$ (6.4)

Helical coil number, $N_{He} = N_{Re}\left(\frac{d}{D}\right)^{0.5} = N_{De}\left[1 + \left(\frac{b}{2\pi D}\right)^2\right]^{-0.5}$ (6.5)

Germano Number, $N_{Gn} = N_{Re}\left[\frac{\pi^2(D/d)}{[\pi(D/d)]^2 + (b/d)^2}\right]$ (6.6)

Different correlations based on the above dimensionless numbers are available in the literature to calculate the friction factor f_c for the helical coil and it is valid only in certain conditions. Unlike a straight tube, there is no universal correlation for helical coil friction factor f_c. From literature, few correlations for helical coil friction factor for the laminar region are shown in Table 6.2 and similarly, for turbulent flow region are shown in Table 6.3.

Table 6.2: Correlation for friction factor calculation for helical coil in laminar region

Investigator	Correlation	Condition	Method
Dean [5]	$\frac{f_c}{f_s} = 1.03058\left(\frac{{N_{De}}^2}{288}\right)^2 + 0.1195\left(\frac{{N_{De}}^2}{288}\right)^4$	Small d/D, $N_{De} < 20$	Analytical
Ito [7]	$f_c\sqrt{\frac{d}{D}} = 0.079\left[N_{De}\left(\frac{d}{D}\right)^2\right]^{-0.2}$	$N_{Re}(d/D)^2 > 6$	Empirical
Kubair and Varrier [8]	$f_c = 0.7716\, exp(3.553\left(\frac{d}{D}\right)) * {N_{Re}}^{-0.5}$	$2000<N_{Re}<9000$ $0.037<d/D<0.097$	Empirical
Srinivasan et al. [10]	$f_c = 32/N_{Re}$ $f_c = 5.52\left(N_{Re}\sqrt{D/d}\right)^{-0.6}$ $f_c = 1.8\left(N_{Re}\sqrt{D/d}\right)^{-0.5}$ $f_c = 1.084\left(N_{Re}\sqrt{D/d}\right)^{-0.2}$	$0.0097<d/D<0.135$ $30<N_{De}<300$ $30<N_{De}<300$ $30<N_{De}<N_{Recr}(d/D)^{0.5}$ $N_{Re}<N_{Recr}$	Empirical
Mishra and Gupta[11]	$\frac{f_c}{f_s} = 1 + 0.033(\text{Log}_{10}N_{He})^4$	$1<N_{He}<3000$	Empirical
White[14]	$\frac{f_c}{f_s} = 1 - \left[1 - \left(\frac{11.6}{N_{De}}\right)^{0.45}\right]^{1/0.45}$	D/d = 5.15, 50, 2050	Empirical
Hart[15]	$f_c = 0.07725(\text{Log}_{10}(N_{He}/7))^2\left(1 + \left[\frac{0.090{N_{De}}^{1.5}}{70 + N_{De}}\right]\right)$	---	Correlation

Manlapaz and Churchill [16]	$f_c/f_s = [(1 - 0.018/(1 + (35/N_{He})^2)^{0.5})^m + (1 + d/3D)^2(N_{He}/88.33)]$	where m = 2 for N_{De} <20, m = 1 for 20< N_{De}<40, m = 1 for N_{De} >40	Numerical

Table 6.3: Correlation for friction factor calculation for helical coil in turbulent region

Investigator	Correlation	Condition	Method
Ito [7]	$f_c\left(\frac{D}{d}\right)^{0.5} = 0.029 + 0.304\left(Re\left(\frac{d}{D}\right)^2\right)^{-0.25}$	0.034< $N_{Re}\left(\frac{d}{D}\right)^2$ < 300	Theoretical
Ito [7]	$f_c\left(\frac{D}{d}\right)^{0.5} = 0.079[N_{Re}(d/D)^2]^{-0.2}$	$N_{Re}\left(\frac{d}{D}\right)^2 > 6$	Empirical
Kubair and Varrier [8]	$f_c = 0.003538{N_{Re}}^{0.09}exp(1.887d/D)$	9000<N_{Re}< 25000 10<D/d<27	Empirical
Mishra and Gupta [11]	$f_c = 0.0791{N_{He}}^{-0.25} + 0.0075\sqrt{d/D}$	4500<N_{Re}<10^5 6.7<D/d<346 0<b/D<25.4	Empirical
White [17]	$f_c/f_s = 0.08\,Re^{-0.25} + 0.012\left(\frac{d}{D}\right)^{0.5}$	15000<N_{Re}< $1*10^5$	Empirical

6.3 Objective

Design and demonstration of a helical coil based fluidic pump to replace the existing pumps to ensure a centrifugal extractor's smooth operation for low throughput operating conditions. CFD simulation is carried on a given helical to validate and understand the effect of various design parameters on the pressure drop across the helical coil.

6.4 Design basics

The working principle of the helical coil based fluidic pump is similar to the reciprocating pump. In a reciprocating pump, the piston pushes the liquid to and fro in a closed compartment. The outlet valve opens during the pumping cycle, and the inlet valve opens during the refill/suction cycle. Similarly, in a helical coil-based fluidic pump, the liquid is pulsed in the pulsing leg and helical coil connected to the inlet line. It acts as a leaky check valve during pumping and open valve during the refill cycle. Main advantages of the helical coil based fluidic pump are (i) mixing of air with process liquid during regular operation is nil, (ii) pumping capacity is independent of liquid operating temperature, (iii) easily scalable, (iv) it can be used as a metering pump and (v) air never enters inside the feed tank.

6.4.1 Description of helical coil based fluidic diode pump

The schematic diagram of a helical coil-based fluidic pump is shown in Fig. 6.2, and the photographic view of helical coil is shown in Fig. 6.3. During the filling cycle, fluid flows from the feed tank (1) to pulsing limb (3) through inlet line (9) and helical coil (2) by gravity and vacuum (12). During the pumping cycle, the liquid inside the pulsing limb (3) is pressurized by compressed air (11 and 4) and flows from pulsing limb to discharge tank (6) through the discharge line (10). Furthermore, part of the liquid flows into a feed tank (1) through helical coil (2) and inlet feed line (9) during the pumping cycle. The pressure drop across a given helical coil (2) during the pumping cycle is much higher than the pressure drop (due to elevation) in the discharge line (10) because of flow in the turbulent region. The compressed airline (11) has connected with a pulsing limb (3) through the pulsing unit, which consists of a timer (Make: SELEC XT5042 with an accuracy of 50ms) (5) and a three-way solenoid valve (4). Similarly, the vent/vacuum line (12) is connected with a pulsing unit through air ejector to control the pressure inside the pulsing limb during the pumping and refill cycle.

During the pumping experiment, the liquid level inside the feed tank (1) is maintained constant by pumping the liquid from the bottom tank (7) through a pump (8).

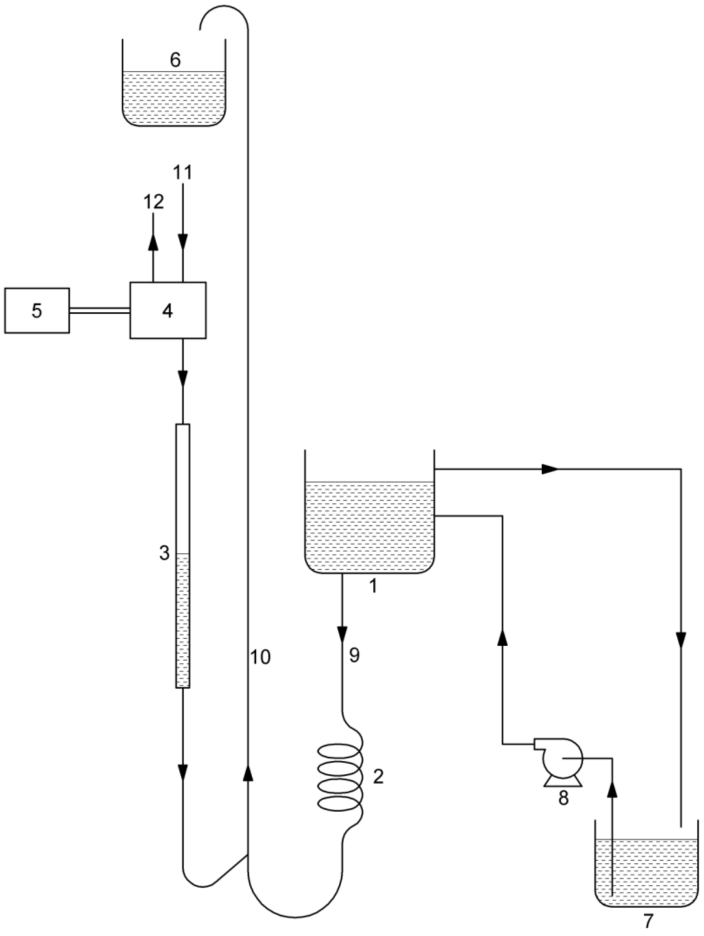

Figure 6.2: Schematic diagram of the helical coil based fluidic diode pump.

(1) feed tank, (2) helical coil, (3) pulsing limb, (4) three way solenoid valve, (5) timer, (6) discharge tank, (7) bottom tank, (8) pump, (9) liquid inlet line to helical coil from feed tank, (10) fluid discharge line to discharge tank, (11) compressed air inlet line to solenoid valve and (12) vacuum line connected to air ejector through solenoid valve.

Figure 6.3: Photographic view of helical coil.

6.4.2 Details of helical coil

Helical coil is made up of SS 304 seamless pipe (schedule 40).

1. No of turns = 5

2. Pipe inner diameter = 9.5 mm

3. Axial pitch = 14 mm

4. Helical diameter = 32 mm

6.4.3 Details of helical coil fluidic pump

1. Inlet liquid height from feed tank = 1650 to 1780 mm

2. Liquid discharge height = 3580 mm

3. Submergence ratio = 2.0

3. Discharge tube inner diameter = 9.5 mm

4. Pulsing limb inner diameter = 25.4 mm

6.5 Experimental procedure

6.5.1 Pressure drop experiment

Pressure drop experiments have been conducted at room temperature to calculate the friction factor across a given helical coil. In general, the critical Reynolds number (transition from laminar to turbulent flow regime) for the helical coil is much higher than the straight pipe. The critical Reynolds number for a given helical coil is back-calculated to understand the flow transition from friction factor calculation. By weighing technique [18], the water flow rate has been measured by using Scout-Pro portable 6 kg weigh balance with an accuracy of +/1 gm. Each experiment has been repeated for a minimum three times, and results were found to be within 1% of the relative standard deviation. The flow rate has been adjusted by adjusting the inlet valve opening.

Mercury manometer (with +/- 133 Pa accuracy) was connected across the helical coil to measure pressure drop at different flow rate conditions. The photographic view of pressure drop experimental setup is shown in Fig. 6.4. Prior to the experiment, the water density was measured at room temperature by the relative density (RD) method.

Figure 6.4: Photographic view of pressure drop experimental setup.

6.5.2 Pumping experiments

The pumping height and capacity for any given helical coil-based fluidic pumps depend upon various parameters and broadly classified as (1) equipment design parameters and (2) operating parameters

6.5.2.1 Equipment design parameters

(a) Feed line pipe diameter

(b) Helical coil diameter

(c) Helical coil pitch

(d) Number of helical coils

(e) Ratio of pulsing limb diameter vs discharge pipe diameter

(f) Height of pulsing limb below the feed tank height

6.5.2.2 Operating parameters

(a) Compressed air inlet pressure (pumping cycle)

(b) Vacuum (refill cycle)

(c) Pumping cycle time

(d) Refill cycle time

(e) Density of operating liquid

The effect of following operating parameters has been studied during pumping experiments, and they are (i) pumping cycle time, (ii) refill cycle time, (iii) compressed air inlet pressure, and (iv) compressed air inlet pressure to vacuum ejector (refill cycle vacuum).

During experiment, water was collected into measuring cylinder from pump discharge line (Make: Borosil, (i) capacity 100 cm^3 with an accuracy of $\pm$ 1 cm^3 at 27^oC and (ii) capacity 250 cm^3 with an accuracy of $\pm$ 2 cm^3 at 27^oC) and total throughput has been back calculated by using below Eq. 6.7. The average value of ten reading is taken as a volumetric throughput for a given experiment condition and results were found to be within 2.5% of relative standard deviation.

$$\text{Volume pumped} = \frac{\text{Volume of fluid collected per pumping cycle } (\text{cm}^3)}{\text{Pumping cycle time (s)} + \text{Refill cycle time (s)}} \qquad (6.7)$$

The efficiency of the helical fluidic pump is defined as the ratio of volume of liquid pumped to the volume of liquid pulsed inside the pulsing limb.

$$\text{Volumetric efficiency} = \eta_V = \frac{\text{Volume of fluid pumped}}{\text{Volume of fluid pulsed inside the pulsing limb}} \qquad (6.8)$$

6.6 Results and Discussion

6.6.1 Pressure drop

From pressure drop experiments, friction factor for a given helical coil was back calculated by using Eq. 6.1 and its results are shown in Table 6.4 and Fig. 6.5.

Table 6.4: Friction factor and Reynolds number from pressure drop experiment

S. No	Avg. volumetric flow rate (cm^3/s)	Pressure drop across helical coil (Pa)	Velocity (cm/s)	Friction factor f_c	Reynolds number (N_{Re})
1.	99	618	39	0.0382	3705
2.	160	1236	63	0.0296	5985
3.	235	2226	92	0.0246	8740
4.	272	2720	107	0.0225	10165
5.	318	3586	125	0.0217	11875
6.	368	4575	144	0.0207	13680
7.	397	5317	156	0.0206	14820
8.	447	6491	175	0.0198	16625
9.	511	8284	200	0.0194	19000
10.	648	12735	256	0.0186	24320
11.	681	13972	267	0.0184	25365
12.	750	16815	294	0.0183	27930
13.	779	17928	304	0.0181	28880
14.	853	21390	334	0.0180	31730

15.	873	22503	342	0.0180	32490

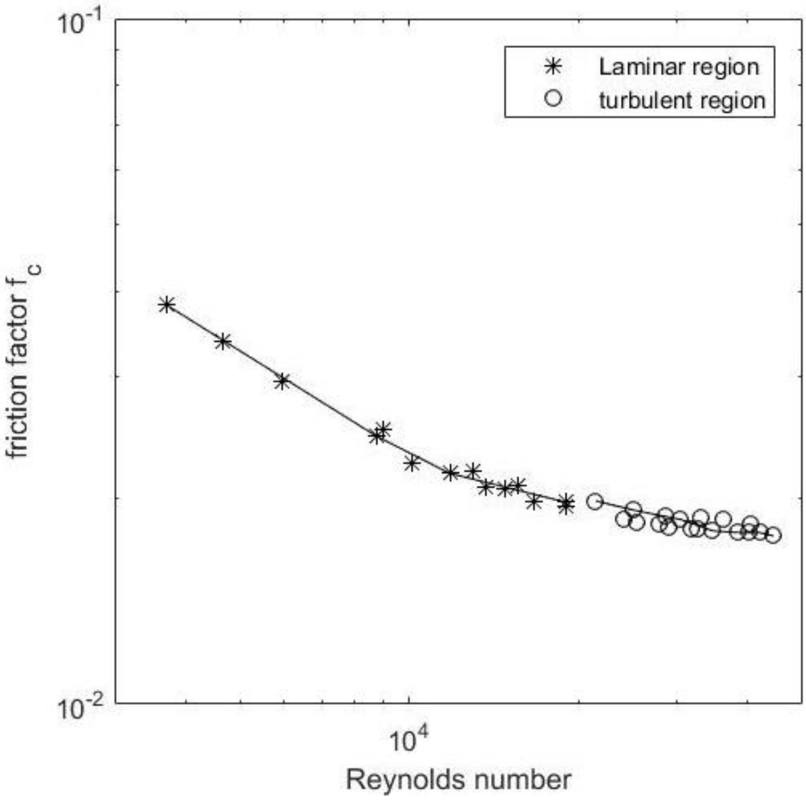

Figure 6.5: Friction factor fc vs Reynolds number for given helical coil

Experimentally the value of critical Reynolds number for a given helical coil was found to be in the range of 19000 to 21000, which is in agreement with the correlation of Srinivasan et al. [10].

6.6.2 Helical coil pumping capacity

6.6.2.1 Pumping capacity with respect to pumping on time and refill time

The pumping capacity for a given helical coil based pump had been measured at different operating conditions. They are (i) different pulsing on time (pumping cycle time), (ii) different refill time (pulsing off time), (iii) different inlet air pressure to the pulsing leg during pumping cycle time and (iv) different inlet air pressure to air ejector to create the vacuum during refill cycle. The pumping capacity for the above different operating condition is shown in Appendix Table A.3. During experiments, it was observed that less than 5 seconds of refill time leads to entering of air inside the discharge pipe. It is mainly due to the time required to refill the liquid in pulsing limb was found to be much lower than the discharge throughput. Similarly, pumping time less than 1.3 seconds leads to no pumping.

The diameter ratio of the liquid discharge pipe to the pulsing limb is 0.374. From the pumping experiment results, the volumetric efficiency of a given setup is back calculated by using Eq. 6.7 and its results are shown in Appendix Table A.3.

The 3D plots (Fig. 6.6 - 6.11) had drawn from pumping experiment results for different On and Off pulsing time with respect to different inlet air pressure to the pulsing leg and different air inlet pressure to ejector during refill time.

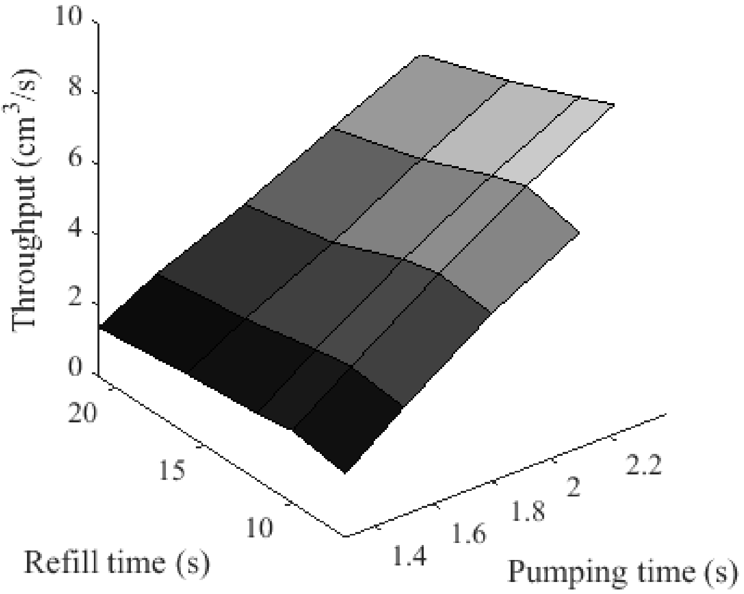

Figure 6.6: Pumping capacity of given helical coil pump at different on and off pulsing frequency (inlet pressure 49 kPa during pulsing on time and inlet pressure to ejector is 0 kPa (open to atmosphere) during pulsing off time)

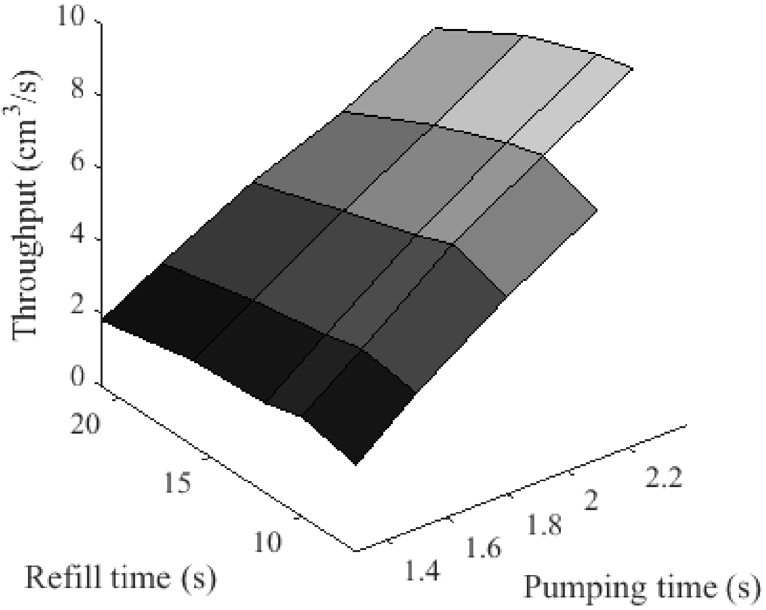

Figure 6.7: Pumping capacity of given helical coil pump at different on and off pulsing frequency (inlet pressure 49 kPa during pulsing on time and inlet pressure to ejector is 49 kPa during pulsing off time)

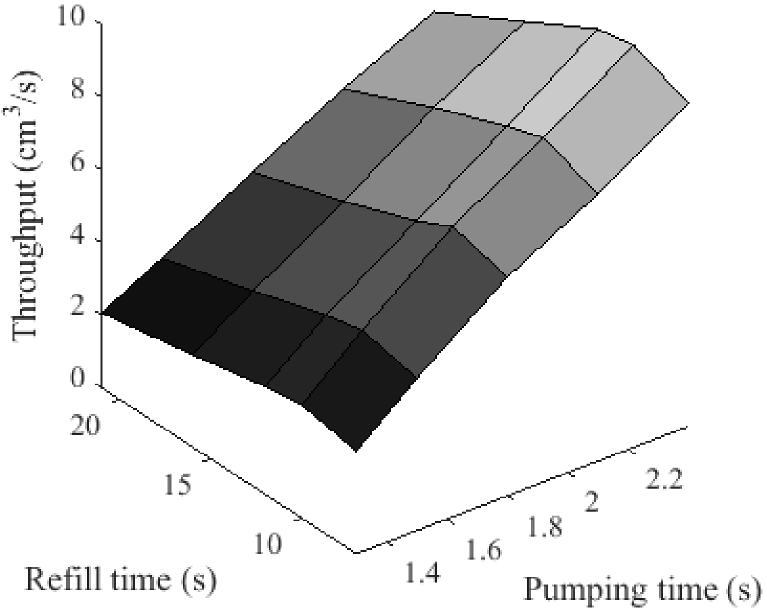

Figure 6.8: Pumping capacity of given helical coil pump at different on and off pulsing frequency (inlet pressure 49 kPa during pulsing on time and inlet pressure to ejector is 98 kPa during pulsing off time)

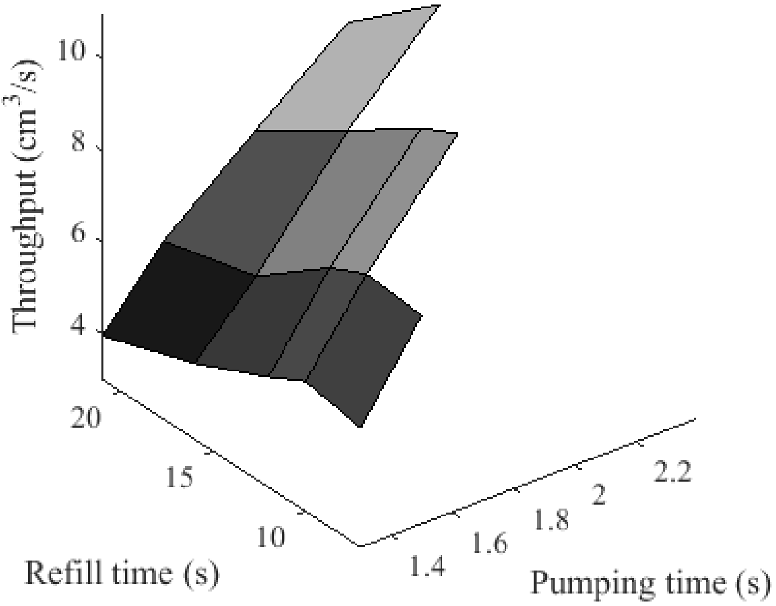

Figure 6.9: Pumping capacity of given helical coil pump at different on and off pulsing frequency (inlet pressure 98 kPa during pulsing on time and inlet pressure to ejector is 0 kPa (open to atmosphere) during pulsing off time)

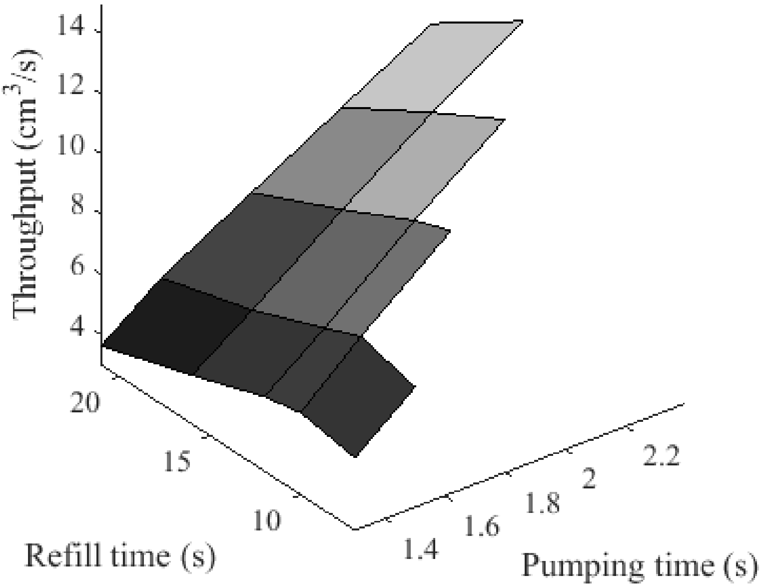

Figure 6.10: Pumping capacity of given helical coil pump at different on and off pulsing frequency (inlet pressure 98 kPa during pulsing on time and inlet pressure to ejector is 49 kPa during pulsing off time)

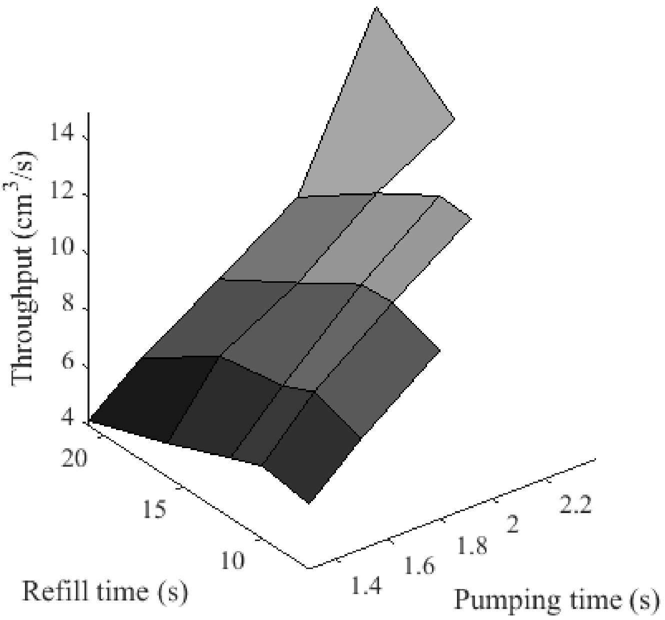

Figure 6.11: Pumping capacity of given helical coil pump at different on and off pulsing frequency (inlet pressure 98 kPa during pulsing on time and inlet pressure to ejector is 98 kPa during pulsing off time)

6.7 CFD simulation in helical coil

As already discussed, flow inside the helical coil is not parallel due to the curved axis of the bend, and it leads to the presence of a secondary motion caused by secondary flow. When flow enters at curvature/curved bed, centrifugal force acts outwards from the centre of curvature on fluid elements. Because of a no-slip condition at the wall, the velocity at centre is much faster than that wall. Due to the centrifugal force and pressure gradient, slower-moving fluid elements move toward the inner wall of the curved tube, leading to the onset of secondary flow. Due to secondary flow pressure drop inside the helical coil is much higher than the straight tube.

Pressure drop inside the helical coil decides the pumping capacity and height. It is function of (i) feed line pipe diameter/helical tube diameter, (ii) helical coil diameter, (iii) helical coil pitch, (iv) no of helical coils and (v) flow rate (Diameter ratio between a pulsing limb and discharge pipe for helical coil-based fluidic diode pump). As discussed in Chapter 6.2, there is no universal correlation for helical coil friction factor f_c.

Pressure drop experimental results (Chapter 6.6.1) for a given helical coil agree with the correlation of Srinivasan et.al.[10] in the laminar region (Fig. 6.12). It may be noted that Srinivasan et.al.[10] developed their correlation only for the laminar region. For the turbulent region, three correlations were tested against the experimental data. The results are shown in Fig. 6.13. It can be seen that the measurements are very close to the correlation of Mishra et.al.[11].

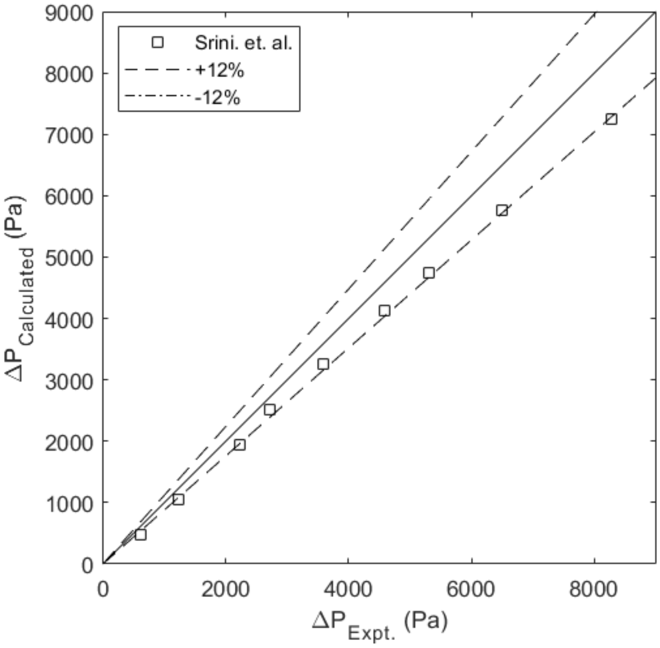

Figure 6.12: Parity plot for pressure drop (laminar region) between experimental measurements and correlation by Srinivasan et al. [10]

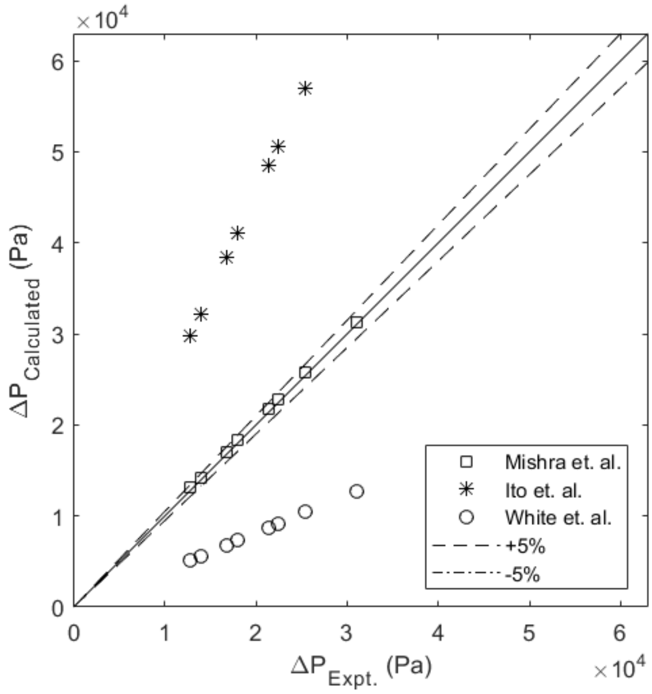

Figure 6.13: Parity plot for pressure drop (turbulent region) between experimental measurements and correlation by Mishra et al. [11], Ito et al. [7] and White et al. [17]

The foregoing discussion makes a comparison with the empirical correlations. Since the limitations of empiricism are known, it was thought important to undertake CFD simulations.

6.7.1 Previous work

Yang et al. [19] applied the standard k-epsilon model to study heat transfer and fully turbulent flow in a helical coil pipe and Lin et al. [20] also used the same model. Later, Kumar et al. [21] used a laminar model for heat transfer calculation and compared it with empirical correlation within the laminar flow region. Piazza et al. [22] compared the three different CFD turbulent models and its effect in helical coil numerical simulation. They are (i) k-epsilon (k-ε) with wall treatment, (ii) Shear stress transport k-omega (SST k-ω) and (iii) Reynolds stress omega model (RSM-ω). From results, they concluded the pressure drop predicted by SST k-ω and RSM-ω was in excellent agreement with literature data. Colombo et. al. [23] compared the three different k-epsilon models (standard, RNG and realizable) to understand its effect in helical coil simulation. Results show that the deviation between the above models, experimental data and Ito [7] correlation is less than 10%.

Lin et al. [24] compared three different turbulent models in helical coil simulation and they are (i) realizable k-epsilon, (ii) low-Reynolds k-epsilon and (iii) Reynolds stress model (RSM). They concluded there were no significant differences in the friction factor calculated by above models. They were predicted Nusselt number (Nu) from simulation and compared with experimental data. Predicated Nu numbers agree well with experimental data, although using different turbulence models leads to different predicted values. The Reynolds stress model yielded the highest Nu compared with the other two turbulence models. Bandyopadhyay et al. [25] have done the CFD simulation in helical coil for flow analysis. They used the laminar and k-epsilon model for laminar and turbulent regions respectively.

After the literature analysis, it has decided to compare the standard k-epsilon [26] model and SST k-omega [27] model to understand the pressure drop across the given helical coil. Based on pressure drop experimental results, the SST k-omega [27] model is selected to study the effect of various design parameters in helical design by using Ansys software version 17.

6.7.2 Governing equation

In this work, the SST k-omega model has adopted to carryout steady state 3D CFD simulation. In addition, simulations have also been performed using the STD k-epsilon model. The governing equations and the closure equations of the above two models are shown below.

Continuity equation

$$\nabla \cdot \left(\rho \langle u_k \rangle\right) = 0 \qquad (6.9)$$

Momentum equation

$$\nabla\left(\rho\langle u_k\rangle\langle u_k\rangle\right) = -\nabla\langle p\rangle + \nabla\cdot\bar{\tau}_k + \rho\vec{g} + \vec{F} \qquad (6.10)$$

$$\bar{\tau}_k = \mu\left(\nabla\langle u_k\rangle + \left(\nabla\langle u_k\rangle\right)^T - \frac{2}{3}\nabla.\langle u_k\rangle I\right)$$

k-ε model [26]

k equation

$$\left\{\rho\frac{\partial k}{\partial t}\right\} + \left\{\rho\langle u_k\rangle\frac{\partial k}{\partial x_k}\right\} = \left\{\tau_{ij}\frac{\partial\langle u_i\rangle}{\partial x_j}\right\} + \left\{\frac{\partial}{\partial x_k}\left(\frac{\mu_t}{\sigma_k}\frac{\partial k}{\partial x_k}\right)\right\} + \left\{\frac{\partial}{\partial x_k}\left(\mu\frac{\partial k}{\partial x_k}\right)\right\} + \left\{-\rho\varepsilon\right\} \qquad (6.11)$$

ε equation

$$\left\{\rho\frac{\partial \varepsilon}{\partial t}\right\} + \left\{\rho\langle u_j\rangle\frac{\partial \varepsilon}{\partial x_j}\right\} = \left\{C_{\varepsilon 1}\frac{\varepsilon}{k}\tau_{ij}\frac{\partial\langle u_i\rangle}{\partial x_j}\right\} + \left\{\frac{\partial}{\partial x_j}\left(\frac{\mu_t}{\sigma_\varepsilon}\frac{\partial \varepsilon}{\partial x_j}\right)\right\} + \left\{\frac{\partial}{\partial x_j}\left(\mu\frac{\partial \varepsilon}{\partial x_j}\right)\right\} + \left\{-C_{\varepsilon 2}\rho\frac{\varepsilon^2}{k}\right\} \qquad (6.12)$$

SST k-ω model [27]

k equation

$$\left\{\rho\frac{\partial k}{\partial t}\right\} + \left\{\rho\langle u_k\rangle\frac{\partial k}{\partial x_k}\right\} = \left\{\tau_{ij}\langle u_k\rangle\frac{\partial\langle u_i\rangle}{\partial x_j}\right\} + \left\{\frac{\partial}{\partial x_k}\left(\frac{\mu_t}{\sigma_k}\frac{\partial k}{\partial x_k}\right)\right\} + \left\{\frac{\partial}{\partial x_k}\left(\mu\frac{\partial k}{\partial x_k}\right)\right\} + \left\{-\rho\varepsilon\right\} \qquad (6.13)$$

ω equation

$$\left\{\rho\frac{\partial \omega}{\partial t}\right\} + \left\{\rho\langle u_j\rangle\frac{\partial \omega}{\partial x_j}\right\} = \left\{\alpha\frac{\omega}{k}\tau_{ij}\frac{\partial\langle u_i\rangle}{\partial x_j}\right\} + \left\{\frac{\partial}{\partial x_j}\left(\frac{\mu_t}{\sigma_\omega}\frac{\partial \omega}{\partial x_j}\right)\right\} + \left\{\frac{\partial}{\partial x_j}\left(\mu\frac{\partial \omega}{\partial x_j}\right)\right\} + \left\{-\beta\rho\omega^2\right\} \qquad (6.14)$$

6.7.3 Numerical framework, mesh details and boundary conditions

Mesh independent test has been performed in a 32 mm diameter helical coil and it is shown in Fig. 6.14. The other dimensions of the above helical coil (pitch, pipe diameter and number of turns, etc.) are fixed as per helical coil based fluidic diode pump (Please refer chapter 6.4.2).

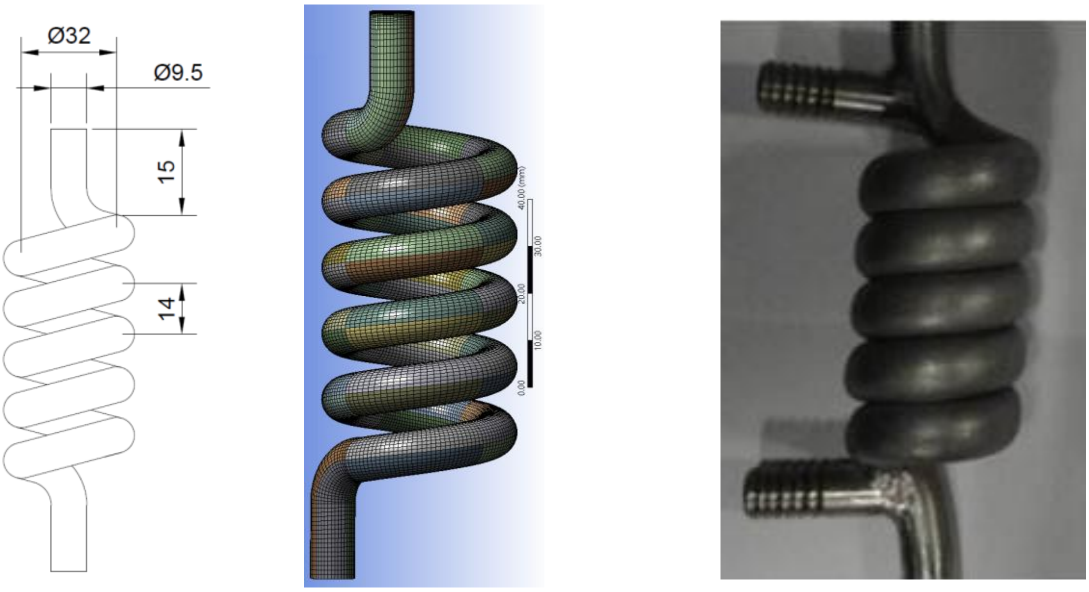

(a) (b) (c)

Figure 6.14*:* (a) Schematic drawing of helical coil with dimensions (No of turns = 5), (b) Geometry created in the ANSYS software and (c) actual experimental setup.

The structured grid (hexahedral mesh) has been chosen and five different mesh sizes are generated for each turbulence model by controlling the element size inside the geometry. Boundary layer thickness is maintained constant based for the turbulence model, irrespective of its mesh size.

Water was selected as a working fluid and velocity inlet boundary condition is applied for the fluid inlet zone. Since the upstream flow is assumed to be undisturbed, the turbulent intensity is specified as 5% for the inlet condition. The stationary wall with no-slip boundary condition is applied at the wall zone. Pressure outlet boundary condition is provided at outlet boundary with 5% backflow turbulent intensity and atmospheric pressure is considered as ambient pressure condition.

6.8 Results and Discussion

6.8.1 Mesh independent result

Grid independence simulation was done for both k-epsilon and SST k-omega model at an inlet velocity of 0.39m/s (laminar flow region) and 2.56m/s (turbulent flow region) and its results are shown in Table 6.5. Pressure and velocity contour plot at inlet velocity boundary condition of 2.56m/s for mesh size of 403990 for STD k-epsilon and mesh size of 379500 for SST k-omega model are shown in Fig. 6.15 & 6.16 respectively.

Table 6.5: Grid independent results

S. No	Pressure drop across the helical geometry (Pa)					
	STD k-epsilon model			SST k-omega model		
	Mesh size	V = 0.39 m/s	V = 2.56 m/s	Mesh size	V = 0.39 m/s	V = 2.56 m/s
1.	139725	787	16005	148770	513	12131
2.	166290	786	15972	233289	510	12171
3.	403990	774	15474	379500	507	12204
4.	642610	772	15427	574145	506	12218
5.	1102723	770	15382	759585	505	12218

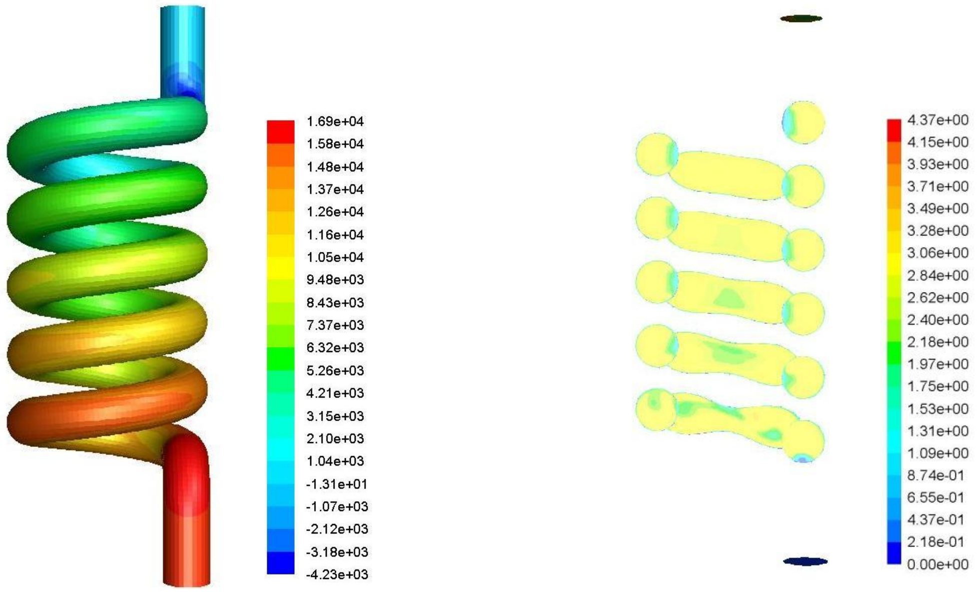

(a) Pressure contour plot (b) Velocity contour plot

Figure 6.15*:* Contour plot from STD k-epsilon model for mesh size of 403990 at inlet velocity of 2.52 m/s (a) Pressure contour plot (b) Velocity contour plot

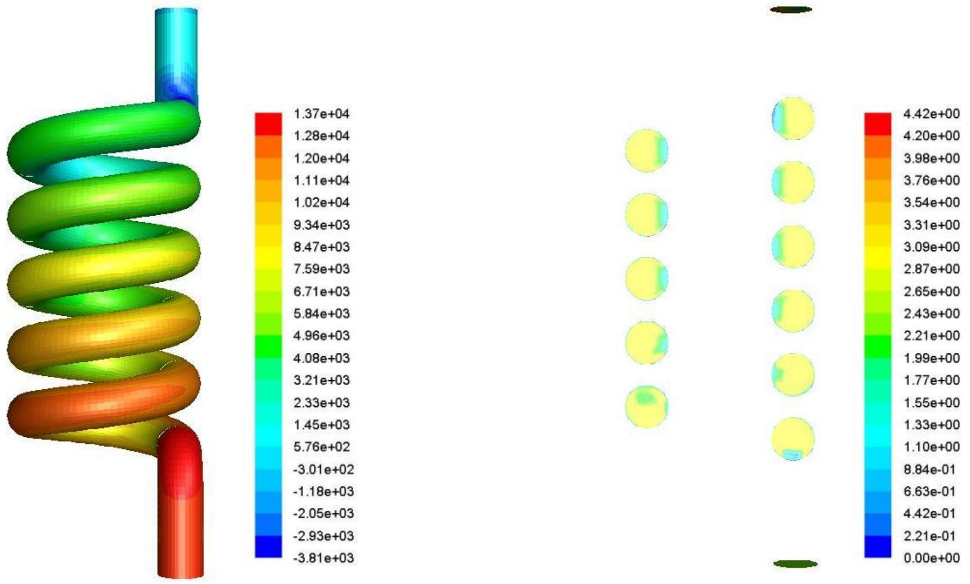

(a) Pressure contour plot (b) Velocity contour plot

Figure 6.16*:* Contour plot from SST k-omega model for mesh size of 379500 at inlet velocity of 2.52 m/s (a) Pressure contour plot (b) Velocity contour plot

6.8.2 Model validation

Based on mesh independent simulation results, 403990 and 379500 grid sizes are selected for k-epsilon and SST k-omega model respectively. The pressure drop with respect to different inlet velocity from 0.39m/s to 3.04m/s is calculated for a given helical coil. The simulation results are compared with pressure drop experiment results and it is shown in Table 6.6.

Table 6.6: Comparison between experiment and simulation results at different inlet velocity condition

S. No	Velocity (m/s)	Reynolds Number N_{Re}	Total Pressure drop (Pa)		
			k-epsilon model	SST-k-omega model	Experimental Result
1.	0.39	3705	774	507	618
2.	0.63	5985	1694	1092	1236
3.	0.92	8740	3121	2079	2226
4.	1.07	10165	3974	2698	2720
5.	1.25	11875	5088	3546	3586
6.	1.44	13680	6360	4564	4575
7.	1.56	14820	7211	5258	5317
8.	1.75	16625	8626	6427	6491
9.	2	19000	10607	8079	8284
10.	2.56	24320	15474	12204	12735
11.	2.67	25365	16493	13083	13972
12.	2.94	27930	19074	15336	16815
13.	3.04	28880	20156	16292	17928

The pressure drop calculated by the STD k-epsilon model is higher than the experimental results and over predicts by 25 percent (Fig. 6.17). Similarly, the pressure drop calculated by SST k-omega model performance is much better with rms error of 10 percent (Fig. 6.18). A similar result was also obtained by Piazza et al. [28]. However, this investigator have covered limited range of Reynolds number (< 48000) and helical coil geometries. Therefore in the present work, SST k-omega simulations have been performed for the given helical coil up to Reynolds number of 100000 and it is shown in Fig. 6.19.

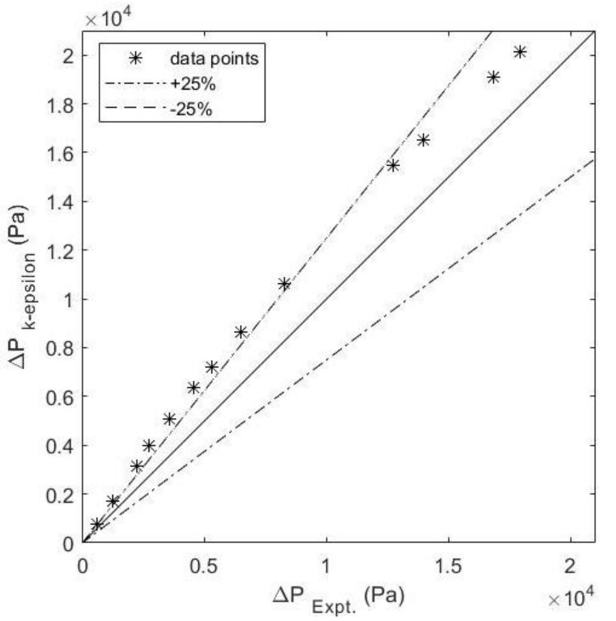

Figure 6.17*:* Pressure drop parity plot between the experiment and CFD simulation (STD k-epsilon model)

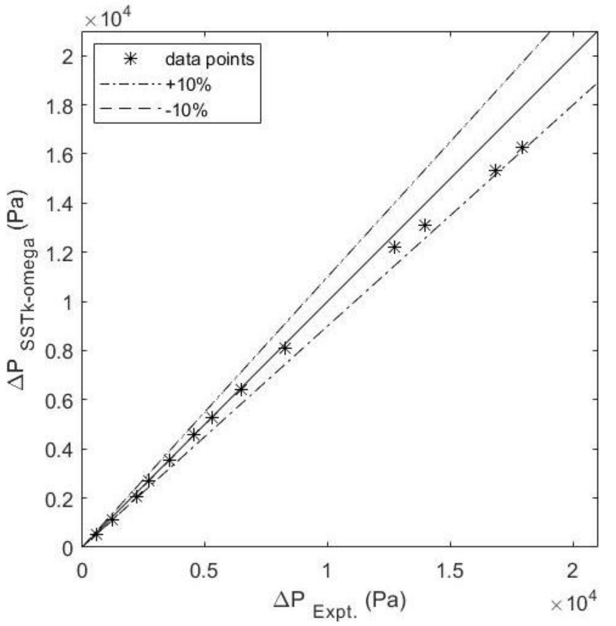

Figure 6.18*:* Pressure drop parity plot between the experiment and CFD simulation (SST k-omega model)

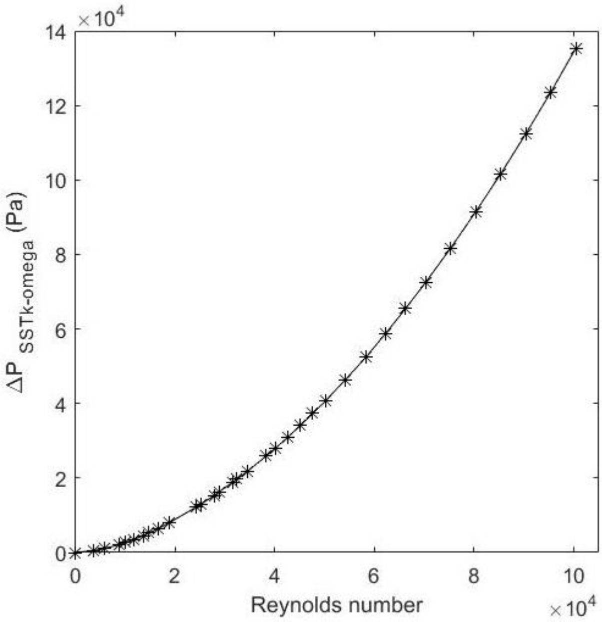

Figure 6.19*:* Pressure drop calculated by CFD simulation (SST k-omega model) across given helical coil up to 100000 Reynolds number

6.8.3 Effect of design parameter on pressure drop inside helical coil

Based on pressure drop simulation results, SST k-omega model has been used to understand the pressure drop across the helical coil with different geometrical parameters, and they are

1. Helical coil diameter
2. Helical coil pipe diameter
3. Helical coil pitch
4. Number of helical coils

6.8.3.1 Pressure drop with respect to different coil diameter

In this simulation, the pressure drop with respect to different coil diameter was simulated and its results are shown in Table 6.7 and Fig. 6.20 to 6.22.

Simulation details:-

(a) Geometry details:

Helical coil tube diameter : 9.5 mm

Helical coil pitch : 14 mm

No of turns : 5 nos

Working fluid : Water

(b) boundary conditions:

Inlet velocity : 2.56 m/sec (643 L/h)

Outlet condition : 0 Pa (open to atmosphere)

Table 6.7: Pressure drop with respect to different coil diameter

S. No	Coil Diameter (mm)	Pressure drop (Pa)
1.	16	11690
2.	24	11127
3.	32	12204
4.	40	13488

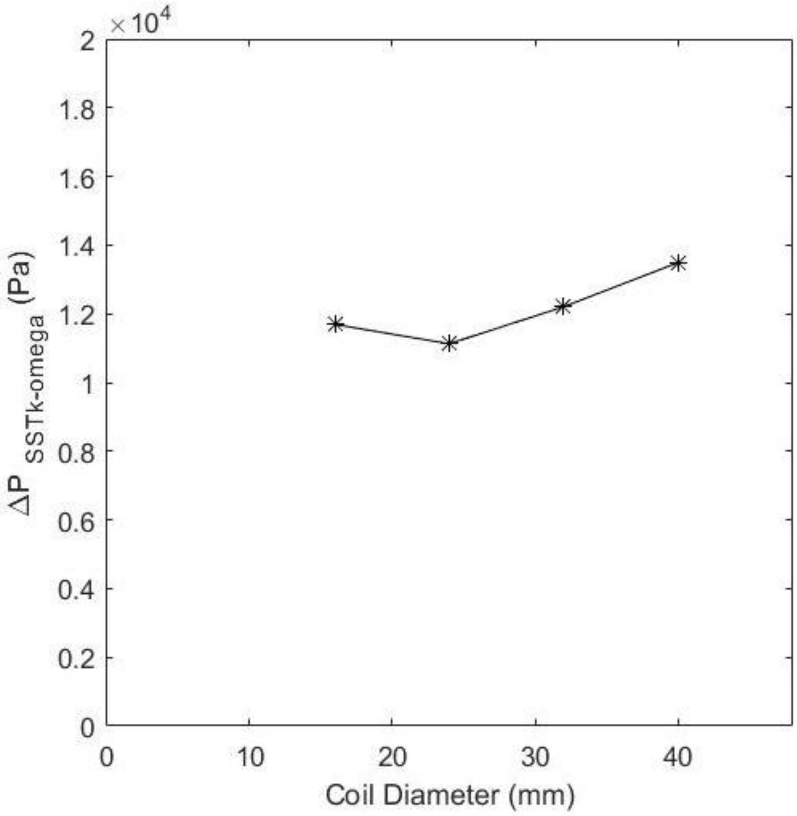

Figure 6.20: Pressure drop w.r.t to different coil diameter

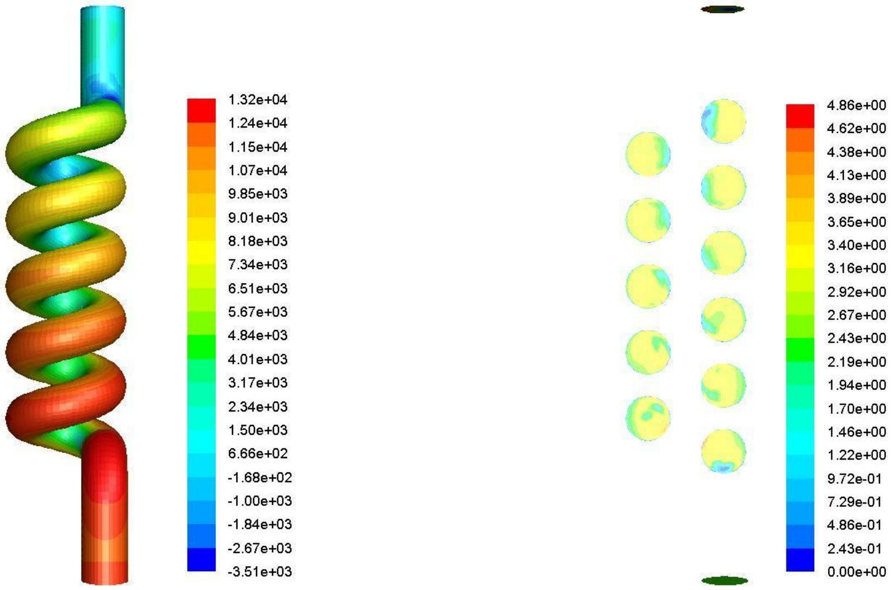

(a) Pressure contour plot (b) Velocity contour plot

Figure 6.21: Contour plot for 16 mm helical coil diameter (a) Pressure contour plot (b) Velocity Contour plot

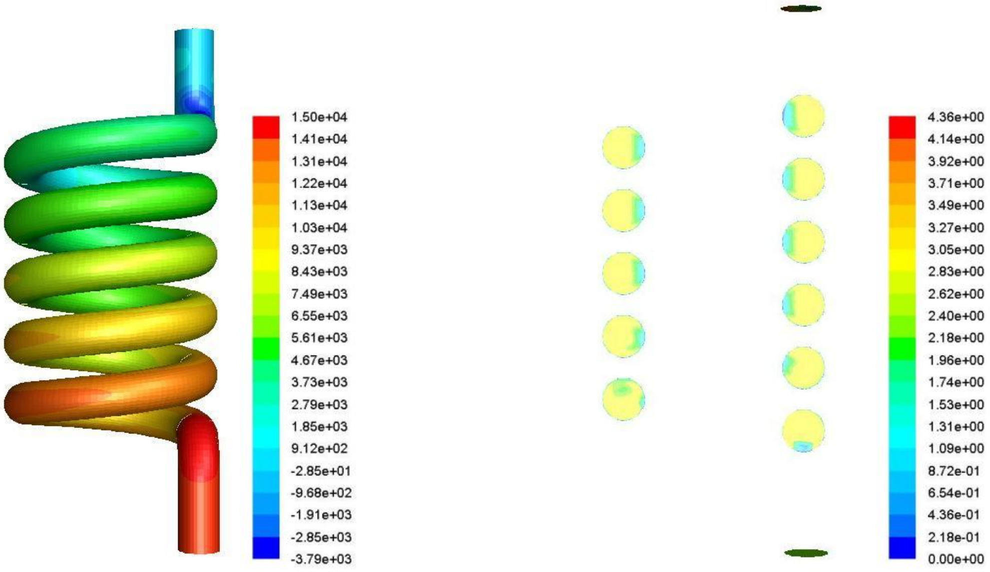

(a) Pressure contour plot (b) Velocity contour plot

Figure 6.22: Contour plot for 40 mm helical coil diameter (a) Pressure contour plot (b) Velocity Contour plot

6.8.3.2 Pressure drop with respect to different axial pitch

In this simulation, the pressure drop with respect to different axial pitch for a given helical coil was simulated and its results are shown in Table 6.8 and Fig. 6.23 to 6.25.

Simulation details:-

(a) Geometry details:

Helical coil tube diameter : 9.5 mm

Helical coil diameter : 32 mm

No of turns : 5 nos

Working fluid : Water

(b) boundary conditions:

Inlet velocity : 2.56 m/sec (643 L/h)

Outlet condition : 0 Pa (open to atmosphere)

Table 6.8: Pressure drop with respect to different helical coil pitch

S. No	Helical coil pitch (mm)	Pressure drop (Pa)
1.	10	12108
2.	14	12204
3.	18	12328
4.	20	12399

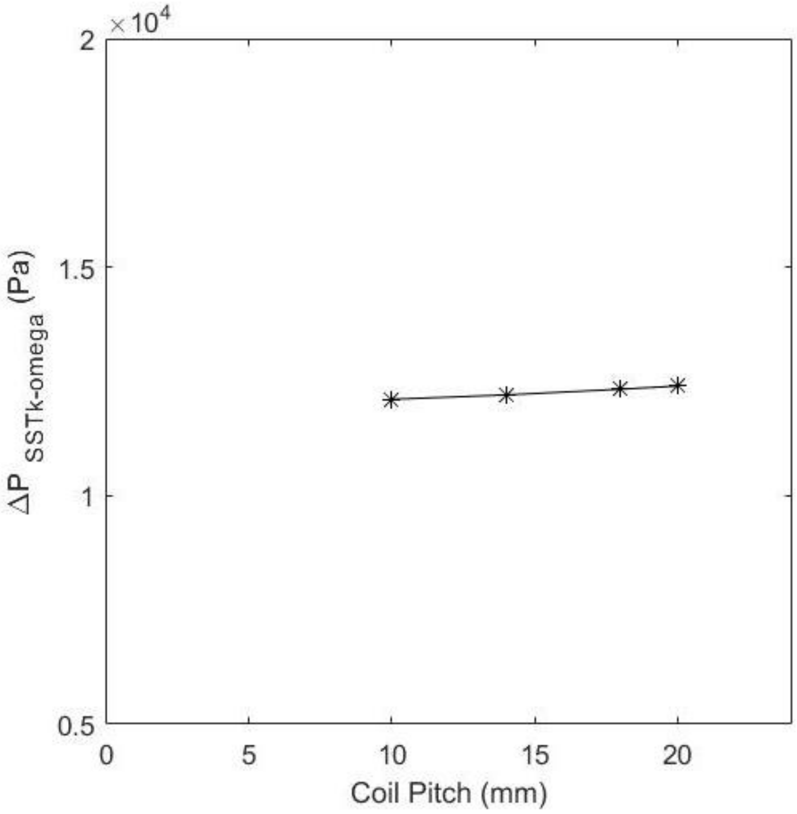

Figure 6.23: Pressure drop w.r.t to different helical coil pitch

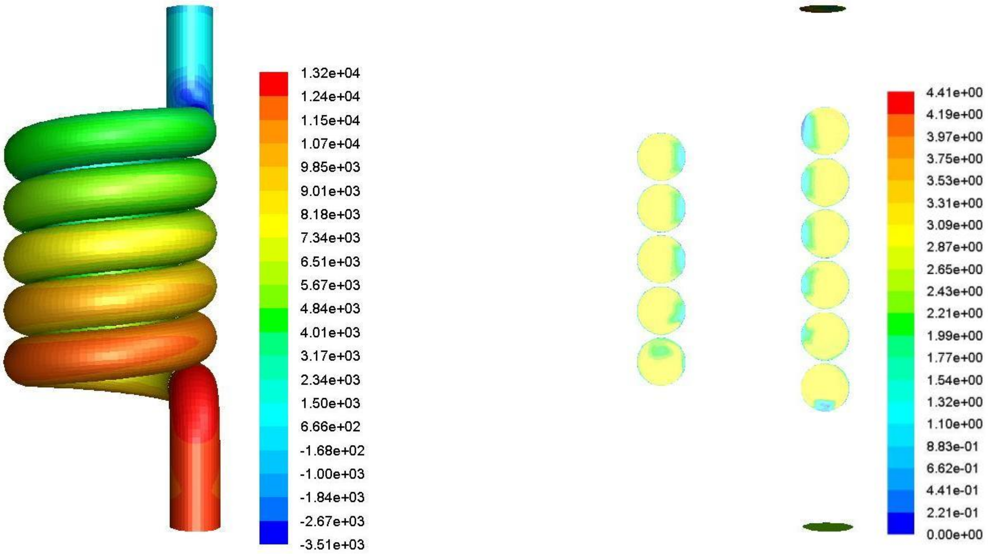

(a) Pressure contour plot

(b) Velocity contour plot

Figure 6.24: Contour plot for 10 mm helical coil pitch (a) Pressure contour plot (b) Velocity Contour plot

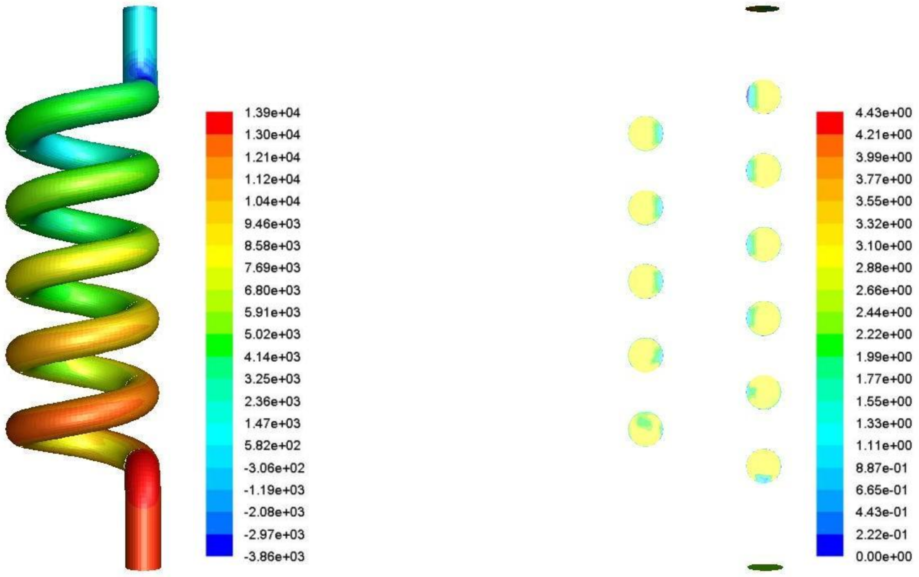

(a) Pressure contour plot (b) Velocity contour plot

Figure 6.25: Contour plot for 20 mm helical coil pitch (a) Pressure contour plot (b) Velocity Contour plot

6.8.3.3 Pressure drop with respect to Number of helical coils

In this simulation, the pressure drop with respect to the different number of helical coil turns was simulated and its results are shown in Table 6.9 and Fig. 6.26 to 6.28.

Simulation details:-

(a) Geometry details:

Helical coil tube diameter : 9.5 mm
Helical coil diameter : 32 mm
Helical coil pitch : 14 mm
Working fluid : Water

(b) boundary conditions:

Inlet velocity : 2.52 m/sec (643 L/h)
Outlet condition : 0 Pa (open to atmosphere)

Table 6.9: Pressure drop with respect to different number of helical coil turns

S. No	Number of helical coil turns	Pressure drop (Pa)
1.	2	6799
2.	4	10437
3.	5	12204
4.	6	13944
5.	8	17485
6.	10	21002

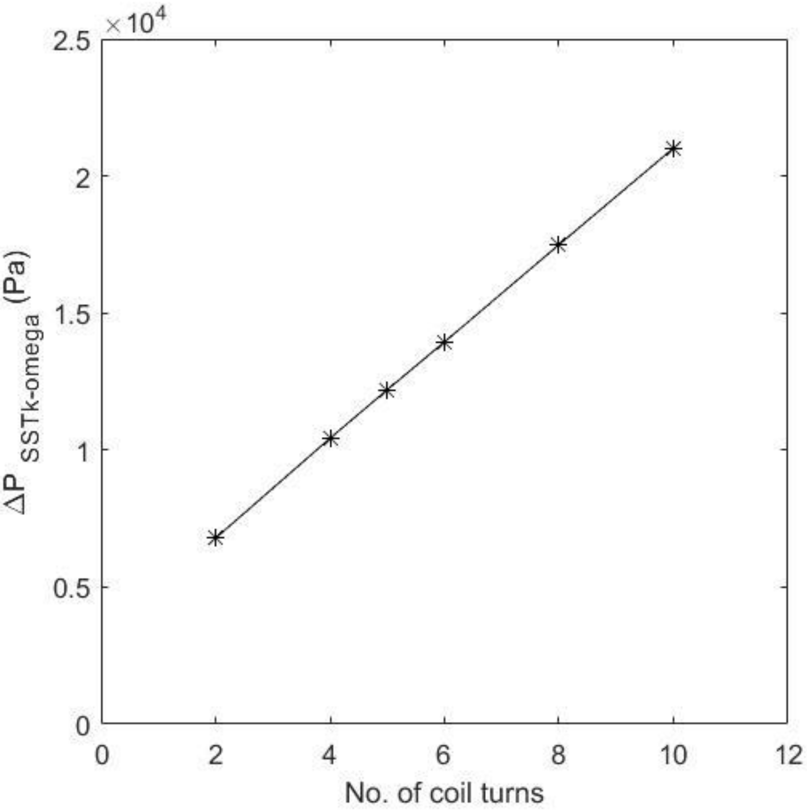

Figure 6.26: Pressure drop w.r.t to different helical coil turns

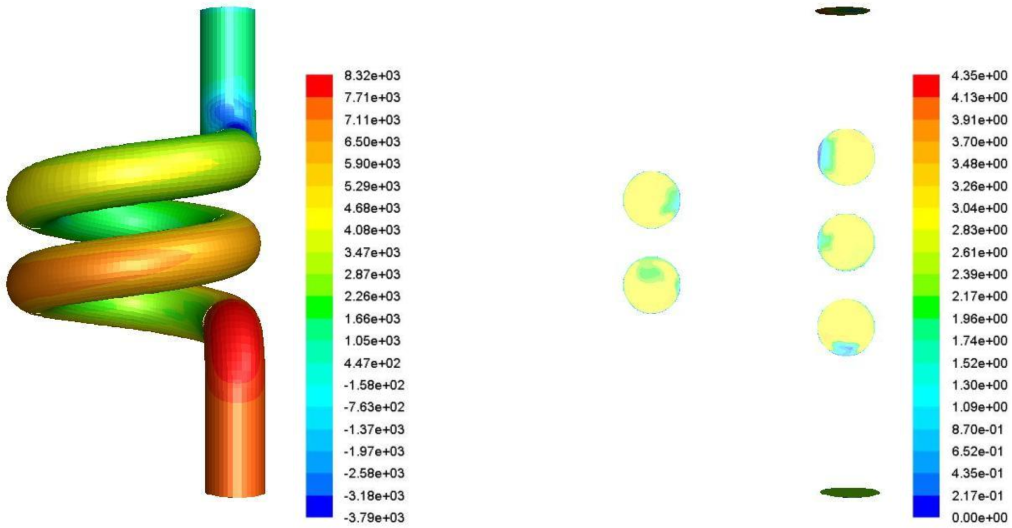

(a) Pressure contour plot (b) Velocity contour plot

Figure 6.27: Contour plot for helical coil with two turns (a) Pressure contour plot (b) Velocity Contour plot

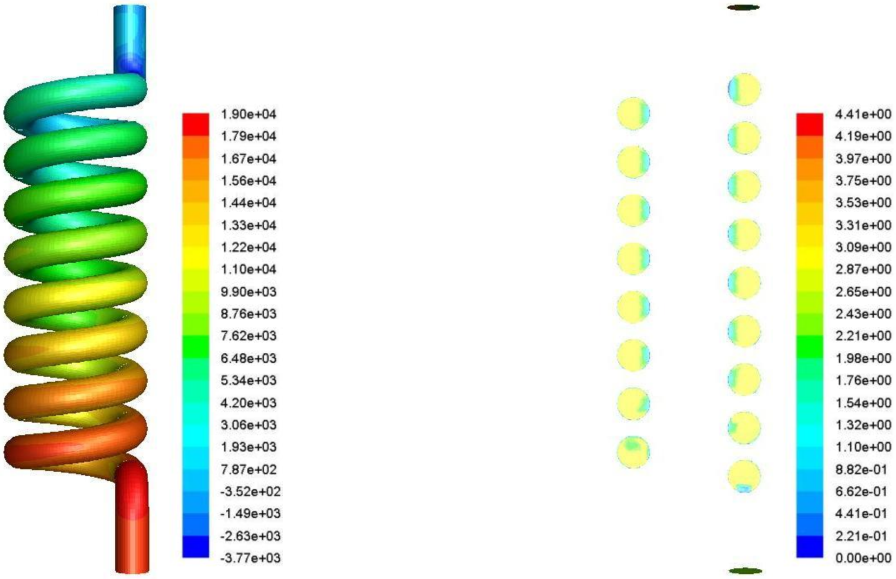

(a) Pressure contour plot (b) Velocity contour plot

Figure 6.28: Contour plot for helical coil with eight turns (a) Pressure contour plot (b) Velocity Contour plot

6.8.3.4 Pressure drop with respect to different pipe diameter

In this simulation, the pressure drop with respect to the different helical coil pipe diameters was simulated and its results are shown in Table 6.10 and Fig. 6.29 to 6.31.

Simulation details:-

(a) Geometry details:

Helical coil diameter	: 32 mm
Helical coil pitch	: 14 mm
No of turns	: 5 nos
Working fluid	: Water

(b) boundary conditions:

Inlet velocity	: 2.52 m/sec (643 L/h)
Outlet condition	: 0 Pa (open to atmosphere)

Table 6.10: Pressure drop with respect to different helical coil pipe diameter

S. No	helical coil pipe diameter (mm)	Pressure drop (Pa)
1.	4	24763
2.	6	16619
3.	8	13128
4.	9.5	12204

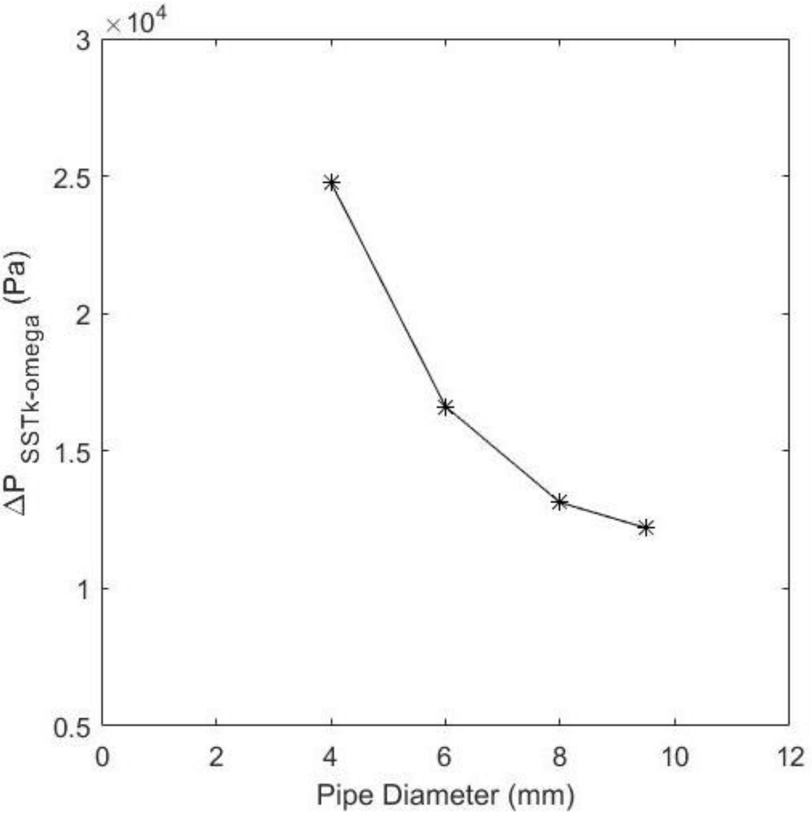

Figure 6.29: Pressure drop w.r.t to different helical coil pipe diameter

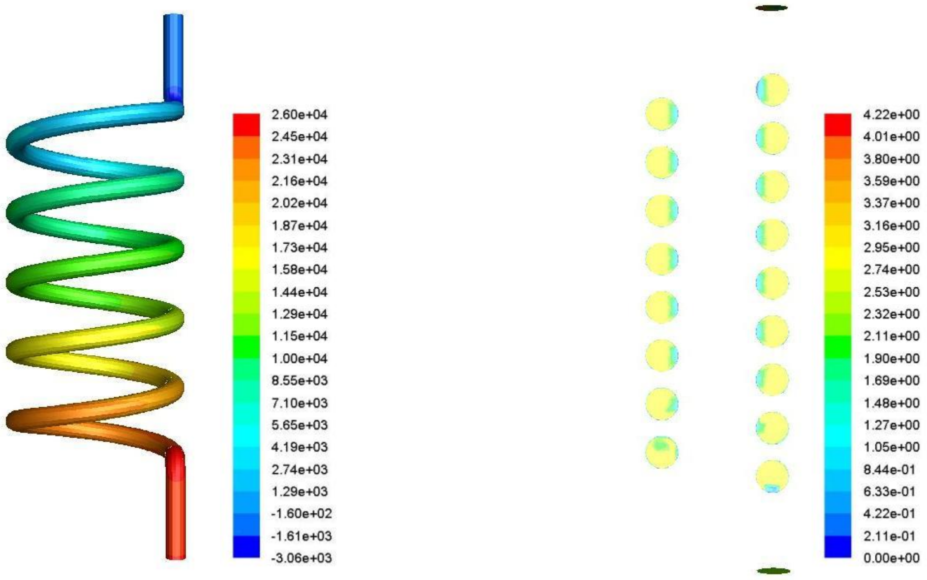

(a) Pressure contour plot (b) Velocity contour plot

Figure 6.30: Contour plot for 4 mm pipe diameter helical coil (a) Pressure contour plot (b) Velocity Contour plot

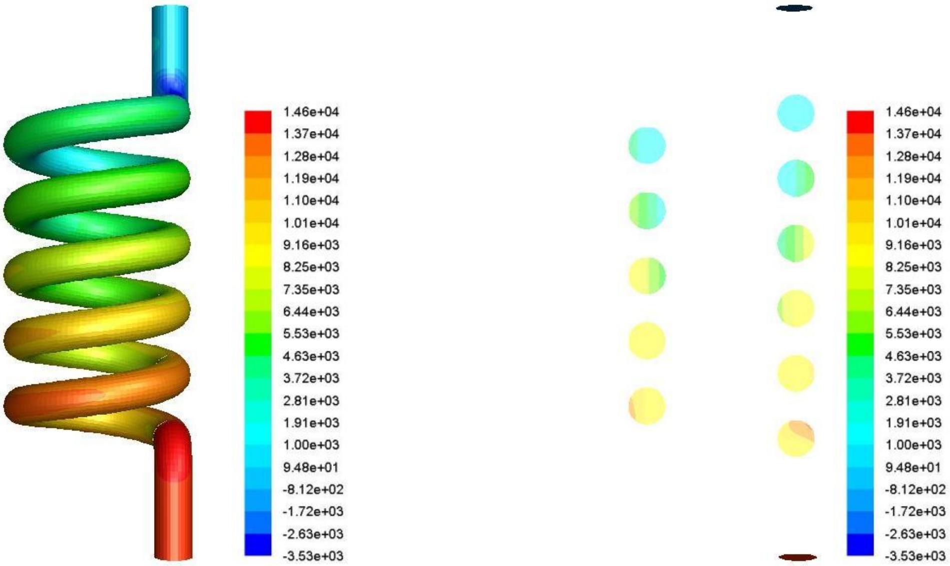

(a) Pressure contour plot (b) Velocity contour plot

Figure 6.31*:* Contour plot for 8 mm pipe diameter helical coil (a) Pressure contour plot (b) Velocity Contour plot

Results show,

(i) Pressure drop increases with an increase in helical coil diameter

(ii) Pressure drop increases linearly with respect to an increase in the number of helical coil turns

(iii) Pressure drop is constant and it is not varying with respect to increase in helical coil pitch

(iv) Finally, pressure drop decreased with an increase in pipe diameter.

6.9 Conclusions

The novel helical coil based fluidic pump was demonstrated as a pump. It may be used in nuclear reprocessing applications and other process industries to handle hazardous liquids. The pumping capacity of the given prototype pump increases with increasing pumping cycle pressure and also increases with increasing refill cycle vacuum pressure. Similarly, volumetric efficiency increases with increasing pumping throughput. From the pressure drop experiment, the critical Reynolds number for the given helical coil was calculated and in the range of 19 000 to 21 000.

The experimental pressure drop data was found to be closer to those estimated by the correlation of Srinivasan et al.[10] in the laminar region. However, for turbulent flow the correlation of Mishra et al.[11] was found to give superior estimates.

As regards to CFD simulation, SST k-omega model was found to perform superior as compared with the standard k-epsilon model. Since in the published literature, SST k-omega based CFD simulations have been performed over a limited range of Reynolds number (< 48000) and helical coil geometries, a wider range has been covered in the present work. From CFD simulation, the pressure drop with respect to various geometry parameter was studied and the effect of the axial pitch in pressure drop is negligible compared to other geometry parameters.

6.10 References

1. J. T. Long, "Engineering for Nuclear Fuel Reprocessing", *Office of Technical Information, U.S. Department of Energy,* **1978,** *2nd Edition.*
2. C. Philips, J.E. Richardson, P. Fallows, "Maintenance free Fluidic Transfer and Mixing Devices for Highly Radioactive Applications - Design, Development, Deployment and Operational Experience", *WM'06 Conference,* **2006,** *Feb. 26- March 2,* Tucoson, AZ
3. R. A. Leonard, D. B. Chamberlain, C. Coneer, "Centrifugal Contactors for Laboratory-Scale Solvent Extraction Tests", *Sep. Sci. Technol.,* **1997,** *32(1-4),* 193-210.
4. S. Vashisth, V. Kumar, K. D. P. Nigam, “A Review on the Potential Applications of Curved Geometries in Process Industry”, *Ind. Eng. Chem. Res.,* **2008,** *47,* 3291-3337.
5. W. R. Dean M. A., “XVI. Note on the motion of fluid in a curved pipe”, *The London, Edinburgh, and Dublin Philosophical Magazine and Journal of Science: Series 7,* **1927,** *4(20),* 208-223.

6. W. R. Dean M. A., "LXXII. The stream-line motion of fluid in a curved pipe (Second paper)" , *The London, Edinburgh, and Dublin Philosophical Magazine and Journal of Science: Series 7*, **1928,** 5*(30),* 673-695.
7. H. Ito, "Friction factors for turbulent flow in curved pipes", *ASME. J. Basic Eng.* **1959,** *81(2),* 123-132.
8. V. Kubair, C. B. S. Varrier, "Pressure drop for liquid flow in helical coils", *Trans. Indian Inst. Chem. Eng.,* **1961/62**, *14,* 93-97.
9. D. F. Schmidt, "Warmeubargang and Druckverlust in Rohrshlangen", *Chem. Eng. Tech.*, **1967,** *13,* 781-789.
10. P. S. Srinivasan, S.S. Nandapurkar, F.A. Holland, "Pressure drop and heat transfer in coils", *Chem. Eng.,* **1968,** 113-119.
11. P. Mishra, S. N. Gupta, "Momentum transfer in curved pipes 1. Newtonian fluids; 2. Non-Newtonian Fluids", *Ind. Eng. Chem. Process Des. Dev.*, **1979,** *18(1),* 130-137.
12. A. Cioncolini, Santini L., An Experimental investigation regarding the laminar to turbulent flow transition in helically coiled pipes. Exp. Therm. Fluid Sci. 2006, 30(4), 367.
13. Cioncolini A., L. Santini, "On the laminar to turbulent flow transition in diabatic helically coiled pipe flow", *Exp. Therm. Fluid Sci.*, **2006,** 30(7), 653-661.
14. C.M. White, "Fluid friction and its relation to heat transfer", *Trans. Inst. Chem. Eng. (London),* **1932,** *10,* 66-86.
15. J. Hart; J. Ellenberger, P. J. Hamersma, "Single and two-phase flow through helically coiled tubes", *Chem. Eng. Sci.,* **1988,** *43(4),* 775-783.
16. R.L. Manlapaz, S.W. Churchill, "Fully developed laminar flow in helically coiled of finite pitch", *Chem. Eng. Commun.,* **1980,** *7(1-3),* 57-78.
17. C.M. White, "Streamline flow through curved pipes", *Proc. R. Soc. London, Ser. A*, **1929,** *123(792),* 645-663.
18. ISO Standard 4185, "Measurement of liquid flow in closed conduits - Weighing method", *International Organization for Standardization,* **1980**.

19. G. Yang, M. A. Ebadian, “Turbulent Forced Convection in a Helicoidal Pipe with Substantial Pitch”, *Int. J. Heat and Mass Transfer,* **1996,** *39(10),* 2015-2022.

20. C. X. Lin, M. A. Ebadian, “Developing Turbulent Convective Heat Transfer in Helical Pipes”, *Int. J. Heat and Mass Transfer,* **1997,** *40(16),* 3861-3873.

21. V. Kumar, K. D. P. Nigam, “Numerical simulation of steady flow fields in coiled flow inverter”, *Int. J. Heat and Mass Transfer,* **2005,** 48, 4811–4828

22. I. D. Piazza, M. Ciofalo, “Numerical prediction of turbulent flow and heat transfer in helically coiled pipes”, *Int. J. Therm. Sci.,* **2010,** *49(4),* 653-663.

23. M. Colombo, A. Cammi, M. E. Ricotti, “Assessment of different turbulence models in helically coiled pipes through comparison with experimental data”, *International Conference on Nuclear Engineering, Proceedings, ICONE,* **2012,** *5,* 273-283.

24. W. C. Lin, Y. M. Ferng, C. C. Chieng, “Numerical computations on flow and heat transfer characteristics of a helically coiled heat exchanger using different turbulence models”, *Nucl. Eng. Des.,* **2013,** *263,* 77-86.

25. T. K. Bandyopadhyay, S. K. Das, “CFD Analysis for Flow of Liquids in Coils”, *J. Inst. Eng. India Ser. E,* **2015,** *97(1),* 9-18.

26. B. E. Launder, D. B. Spalding, “The numerical computation of turbulent flows”, *Comput. Methods Appl. Mech. Eng.,* **1974,** *3(2),* 269-289.

27. F. R. Menter, “Zonal Two Equation k-ω Turbulence Models for Aerodynamic Flows”, *AIAA Paper,* **1993,** 1993-2906.

28. I. D. Piazza, M. Ciofalo, “Numerical prediction of turbulent flow and heat transfer in helically coiled pipes”, *Int. J. Therm. Sci.,* **2010,** *49,* 653-663.

APPENDIX

Table A.1: Batch experiment dispersion number data with its variables

Sr. No	**N_D x 10^4**	**C/D ratio**	**σ (mN/m)**	**ρ_c (Kg/m^3)**	**ρ_d (Kg/m^3)**	**μ_c (mKg/ms^2)**	**μ_d (mKg/ms^2)**	**gravity const. (m/s^2)**
1	14.10	10.0	35.5	1000	780	1.00	0.59	9.81
2	12.93	5.0	35.5	1000	780	1.00	0.59	9.81
3	10.60	2.0	35.5	1000	780	1.00	0.59	9.81
4	8.59	1.0	35.5	1000	780	1.00	0.59	9.81
5	18.89	2.0	35.5	780	1000	0.59	1.00	9.81
6	14.96	5.0	35.5	780	1000	0.59	1.00	9.81
7	12.27	10.0	35.5	780	1000	0.59	1.00	9.81
8	15.38	10.0	16.2	1000	880	1.00	0.69	9.81
9	13.75	5.0	16.2	1000	880	1.00	0.69	9.81
10	15.95	2.0	16.2	1000	880	1.00	0.69	9.81
11	10.93	10.0	16.2	880	1000	0.69	1.00	9.81
12	12.76	10.0	58.3	1000	660	1.00	0.29	9.81
13	14.85	5.0	58.3	1000	660	1.00	0.29	9.81
14	10.69	2.0	58.3	1000	660	1.00	0.29	9.81
15	9.61	1.0	58.3	1000	660	1.00	0.29	9.81
16	10.29	2.0	58.3	660	1000	0.29	1.00	9.81
17	11.41	5.0	58.3	660	1000	0.29	1.00	9.81
18	8.92	5.0	48.5	1000	780	1.00	1.60	9.81
19	12.76	2.0	48.5	1000	780	1.00	1.60	9.81
20	11.79	1.0	48.5	1000	780	1.00	1.60	9.81
21	13.80	2.0	48.5	780	1000	1.60	1.00	9.81
22	15.50	5.0	48.5	780	1000	1.60	1.00	9.81
23	9.05	10.0	45.0	1200	1000	0.65	1.00	9.81

Sr. No	**N_D x 10^4**	**C/D ratio**	**σ (mN/m)**	**ρ_c (Kg/m^3)**	**ρ_d (Kg/m^3)**	**μ_c (mKg/ms^2)**	**μ_d (mKg/ms^2)**	**gravity const. (m/s^2)**
24	9.78	5.0	45.0	1200	1000	0.65	1.00	9.81
25	9.40	2.0	45.0	1200	1000	0.65	1.00	9.81
26	8.51	1.0	45.0	1200	1000	0.65	1.00	9.81
27	9.40	2.0	45.0	1000	1200	1.00	0.65	9.81
28	10.16	5.0	45.0	1000	1200	1.00	0.65	9.81
29	15.38	5.0	42.0	1300	1000	0.71	1.00	9.81
30	14.85	2.0	42.0	1300	1000	0.71	1.00	9.81
31	12.12	1.0	42.0	1300	1000	0.71	1.00	9.81
32	12.67	2.0	42.0	1000	1300	1.00	0.71	9.81
33	11.28	5.0	42.0	1000	1300	1.00	0.71	9.81
34	15.08	5.0	55.0	1000	850	1.00	0.41	9.81
35	13.75	2.0	55.0	1000	850	1.00	0.41	9.81
36	12.12	1.0	55.0	1000	850	1.00	0.41	9.81
37	10.99	2.0	55.0	850	1000	0.41	1.00	9.81
38	11.21	5.0	55.0	850	1000	0.41	1.00	9.81
39	5.45	1.5	17.9	1312	848	4.47	5.05	9.81
40	5.56	2.0	17.9	1312	848	4.47	5.05	9.81
41	5.90	2.3	17.9	1312	848	4.47	5.05	9.81
42	6.67	3.0	17.9	1312	848	4.47	5.05	9.81
43	8.11	4.0	17.9	1312	848	4.47	5.05	9.81
44	9.46	9.0	17.9	1312	848	4.47	5.05	9.81
45	5.88	1.0	17.9	848	1312	5.05	4.47	9.81
46	5.73	2.0	17.9	848	1312	5.05	4.47	9.81
47	6.29	3.0	17.9	848	1312	5.05	4.47	9.81
48	8.98	4.0	17.9	848	1312	5.05	4.47	9.81
49	7.68	9.0	17.9	848	1312	5.05	4.47	9.81
50	3.31	2.0	18.2	1420	848	8.65	5.05	9.81

Sr. No	N_D x 10^4	C/D ratio	σ (mN/m)	ρ_c (Kg/m^3)	ρ_d (Kg/m^3)	μ_c (mKg/ms^2)	μ_d (mKg/ms^2)	gravity const. (m/s^2)
51	3.97	1.0	18.2	848	1420	5.05	8.65	9.81
52	3.96	2.0	18.2	848	1420	5.05	8.65	9.81
53	5.51	4.0	18.2	848	1420	5.05	8.65	9.81
54	5.06	9.0	18.2	848	1420	5.05	8.65	9.81
55	3.32	2.0	16.7	1473	848	12.24	5.05	9.81
56	3.66	2.3	16.7	1473	848	12.24	5.05	9.81
57	3.86	3.0	16.7	1473	848	12.24	5.05	9.81
58	4.02	4.0	16.7	1473	848	12.24	5.05	9.81
59	7.72	1.0	16.7	848	1473	5.05	12.24	9.81
60	7.51	1.5	16.7	848	1473	5.05	12.24	9.81
61	7.93	1.5	16.7	848	1473	5.05	12.24	9.81
62	8.25	2.0	16.7	848	1473	5.05	12.24	9.81
63	10.06	4.0	16.7	848	1473	5.05	12.24	9.81
64	4.65	2.0	8.3	1312	862	4.47	7.57	9.81
65	5.08	3.0	8.3	1312	862	4.47	7.57	9.81
66	2.60	3.0	8.3	862	1312	7.57	4.47	9.81
67	2.42	2.0	9.4	1420	862	8.65	7.57	9.81
68	2.19	3.0	9.4	862	1420	7.57	8.65	9.81
69	2.34	2.0	9.9	1473	862	12.24	7.57	9.81
70	2.99	1.0	9.9	862	1473	7.57	12.24	9.81
71	2.81	2.0	9.9	862	1473	7.57	12.24	9.81
72	14.72	1.0	10.0	826	997	2.00	0.90	9.81
73	15.35	2.0	10.0	826	997	2.00	0.90	9.81
74	19.25	5.0	10.0	1016	826	1.00	2.00	9.81
75	8.51	1.0	10.0	826	1016	2.00	1.00	9.81
76	8.43	5.0	10.0	826	1016	2.00	1.00	9.81
77	22.29	10.0	10.0	1016	826	1.00	2.00	9.81

Sr. No	**N_D x 10^4**	**C/D ratio**	**σ (mN/m)**	**ρ_c (Kg/m^3)**	**ρ_d (Kg/m^3)**	**μ_c (mKg/ms^2)**	**μ_d (mKg/ms^2)**	**gravity const. (m/s^2)**
78	5.70	2.0	10.0	826	1016	2.00	1.00	9.81
79	5.78	2.0	10.0	826	1016	2.00	1.00	9.81
80	7.19	10.0	10.0	826	1016	2.00	1.00	9.81

Table A.2: Centrifugal extractor dispersion number data with its variables

Sr. No	**Di (m)**	**Q_C x 10^6 (m^3/s)**	**Q_D x 10^6 (m^3/s)**	**c (m)**	**d (m)**	**N (rps)**	**N_D x 10^4**	**C/D ratio**	**σ (mN/m)**	**ρ_C (Kg/m^3)**	**ρ_D (Kg/m^3)**	**μ_C (mKg/ms^2)**	**μ_D (mKg/ms^2)**	**a (m/s^2)**	**Ta x 10^8**	**N_{Re} x 10^3**
1	0.03	5.78	0.83	0.0075	0.002	23.30	9.83	6.96	58.3	660	1000	0.29	1.00	250	0.2510	36.22
2	0.03	5.08	1.39	0.0075	0.002	23.30	9.62	3.65	58.3	660	1000	0.29	1.00	250	0.2195	36.22
3	0.03	4.42	1.94	0.0075	0.002	23.30	9.45	2.28	58.3	660	1000	0.29	1.00	250	0.1911	36.22
4	0.03	3.77	2.50	0.0075	0.002	23.30	9.32	1.51	58.3	660	1000	0.29	1.00	250	0.1649	36.22
5	0.03	3.06	3.12	0.0075	0.002	23.30	9.19	0.98	58.3	1000	660	1.00	0.29	250	0.1411	15.94
6	0.03	3.61	2.48	0.0075	0.002	23.30	9.05	1.46	58.3	1000	660	1.00	0.29	250	0.1202	15.94
7	0.03	4.17	1.86	0.0075	0.002	23.30	8.96	2.24	58.3	1000	660	1.00	0.29	250	0.1019	15.94
8	0.03	5.82	0.83	0.0075	0.002	30.00	7.68	7.01	58.3	660	1000	0.29	1.00	414	0.5425	46.81
9	0.03	5.12	1.39	0.0075	0.002	30.00	7.52	3.68	58.3	660	1000	0.29	1.00	414	0.4749	46.81
10	0.03	4.47	1.94	0.0075	0.002	30.00	7.40	2.30	58.3	660	1000	0.29	1.00	414	0.4140	46.81
11	0.03	3.81	2.50	0.0075	0.002	30.00	7.28	1.52	58.3	660	1000	0.29	1.00	414	0.3573	46.81
12	0.03	3.06	3.14	0.0075	0.002	30.00	7.16	0.97	58.3	1000	660	1.00	0.29	414	0.3055	20.60
13	0.03	3.61	2.53	0.0075	0.002	30.00	7.09	1.43	58.3	1000	660	1.00	0.29	414	0.2616	20.60
14	0.03	4.17	1.93	0.0075	0.002	30.00	7.04	2.16	58.3	1000	660	1.00	0.29	414	0.2229	20.60
15	0.03	5.83	0.83	0.0075	0.002	36.70	6.29	7.02	58.3	660	1000	0.29	1.00	620	1.0006	57.44
16	0.03	5.15	1.39	0.0075	0.002	36.70	6.17	3.71	58.3	660	1000	0.29	1.00	620	0.8770	57.44
17	0.03	4.50	1.94	0.0075	0.002	36.70	6.08	2.32	58.3	660	1000	0.29	1.00	620	0.7651	57.44
18	0.03	3.86	2.50	0.0075	0.002	36.70	6.00	1.54	58.3	660	1000	0.29	1.00	620	0.6621	57.44
19	0.03	3.06	3.22	0.0075	0.002	36.70	5.93	0.95	58.3	1000	660	1.00	0.29	620	0.5690	25.28
20	0.03	3.61	2.60	0.0075	0.002	36.70	5.86	1.39	58.3	1000	660	1.00	0.29	620	0.4877	25.28
21	0.03	4.17	1.99	0.0075	0.002	36.70	5.81	2.10	58.3	1000	660	1.00	0.29	620	0.4157	25.28
22	0.03	5.50	1.11	0.0075	0.002	43.30	5.29	4.95	58.3	660	1000	0.29	1.00	863	1.5481	67.93
23	0.03	5.17	1.39	0.0075	0.002	43.30	5.25	3.72	58.3	660	1000	0.29	1.00	863	1.4487	67.93
24	0.03	4.52	1.94	0.0075	0.002	43.30	5.17	2.33	58.3	660	1000	0.29	1.00	863	1.2645	67.93
25	0.03	3.88	2.50	0.0075	0.002	43.30	5.10	1.55	58.3	660	1000	0.29	1.00	863	1.0948	67.93
26	0.03	3.06	3.27	0.0075	0.002	43.30	5.06	0.94	58.3	1000	660	1.00	0.29	863	0.9450	29.90
27	0.03	3.61	2.67	0.0075	0.002	43.30	5.02	1.35	58.3	1000	660	1.00	0.29	863	0.8135	29.90
28	0.03	5.13	0.83	0.0075	0.002	23.30	8.86	6.18	56.5	750	1000	0.36	1.00	250	0.2178	33.96

Sr. No	**Di (m)**	**$Q_C \times 10^6$ (m^3/s)**	**$Q_D \times 10^6$ (m^3/s)**	**c (m)**	**d (m)**	**N (rps)**	**$N_D \times 10^4$**	**C/D ratio**	**σ (mN/m)**	**ρ_C (Kg/m^3)**	**ρ_D (Kg/m^3)**	**μ_C (mKg/ms^2)**	**μ_D (mKg/ms^2)**	**a (m/s^2)**	**Ta $\times 10^8$**	**$N_{Re} \times 10^3$**
29	0.03	4.62	1.39	0.0075	0.002	23.30	8.93	3.32	56.5	750	1000	0.36	1.00	250	0.1908	33.96
30	0.03	4.12	1.94	0.0075	0.002	23.30	9.01	2.12	56.5	750	1000	0.36	1.00	250	0.1677	33.96
31	0.03	3.55	2.50	0.0075	0.002	23.30	8.99	1.42	56.5	750	1000	0.36	1.00	250	0.1462	33.96
32	0.03	3.06	3.00	0.0075	0.002	23.30	9.01	1.02	56.5	1000	750	1.00	0.36	250	0.1276	15.94
33	0.03	3.61	2.40	0.0075	0.002	23.30	8.93	1.50	56.5	1000	750	1.00	0.36	250	0.1105	15.94
34	0.03	5.18	0.83	0.0075	0.002	30.00	6.94	6.24	56.5	750	1000	0.36	1.00	414	0.4710	43.89
35	0.03	4.65	1.39	0.0075	0.002	30.00	6.97	3.35	56.5	750	1000	0.36	1.00	414	0.4126	43.89
36	0.03	4.17	1.94	0.0075	0.002	30.00	7.05	2.15	56.5	750	1000	0.36	1.00	414	0.3634	43.89
37	0.03	3.63	2.50	0.0075	0.002	30.00	7.08	1.45	56.5	750	1000	0.36	1.00	414	0.3182	43.89
38	0.03	3.06	3.03	0.0075	0.002	30.00	7.03	1.01	56.5	1000	750	1.00	0.36	414	0.2764	20.60
39	0.03	3.61	2.45	0.0075	0.002	30.00	7.00	1.47	56.5	1000	750	1.00	0.36	414	0.2403	20.60
40	0.03	5.34	0.83	0.0075	0.002	36.70	5.82	6.43	56.5	750	1000	0.36	1.00	620	0.8729	53.85
41	0.03	4.70	1.39	0.0075	0.002	36.70	5.75	3.38	56.5	750	1000	0.36	1.00	620	0.7629	53.85
42	0.03	4.22	1.94	0.0075	0.002	36.70	5.81	2.18	56.5	750	1000	0.36	1.00	620	0.6726	53.85
43	0.03	3.66	2.50	0.0075	0.002	36.70	5.81	1.46	56.5	750	1000	0.36	1.00	620	0.5884	53.85
44	0.03	3.06	3.07	0.0075	0.002	36.70	5.78	1.00	56.5	1000	750	1.00	0.36	620	0.5122	25.28
45	0.03	3.61	2.48	0.0075	0.002	36.70	5.75	1.46	56.5	1000	750	1.00	0.36	620	0.4450	25.28
46	0.03	4.45	1.39	0.0075	0.002	43.30	4.67	3.20	56.5	750	1000	0.36	1.00	863	1.2414	63.69
47	0.03	3.70	1.94	0.0075	0.002	43.30	4.51	1.91	56.5	750	1000	0.36	1.00	863	1.0637	63.69
48	0.03	2.50	3.00	0.0075	0.002	43.30	4.40	0.83	56.5	1000	750	1.00	0.36	863	0.9034	29.90
49	0.03	3.06	2.45	0.0075	0.002	43.30	4.41	1.25	56.5	1000	750	1.00	0.36	863	0.7770	29.90
50	0.03	4.73	0.83	0.0075	0.002	23.30	8.26	5.70	54.5	850	1000	0.41	1.00	250	0.2039	33.08
51	0.03	4.35	1.39	0.0075	0.002	23.30	8.53	3.13	54.5	850	1000	0.41	1.00	250	0.1787	33.08
52	0.03	3.98	1.94	0.0075	0.002	23.30	8.80	2.05	54.5	850	1000	0.41	1.00	250	0.1581	33.08
53	0.03	3.40	2.50	0.0075	0.002	23.30	8.77	1.36	54.5	850	1000	0.41	1.00	250	0.1378	33.08
54	0.03	3.06	2.98	0.0075	0.002	23.30	8.98	1.03	54.5	1000	850	1.00	0.41	250	0.1223	15.94
55	0.03	4.67	1.17	0.0075	0.002	30.00	6.74	3.99	54.5	850	1000	0.41	1.00	414	0.4094	42.75
56	0.03	4.48	1.39	0.0075	0.002	30.00	6.78	3.22	54.5	850	1000	0.41	1.00	415	0.3887	42.75
57	0.03	4.05	1.94	0.0075	0.002	30.00	6.92	2.09	54.5	850	1000	0.41	1.00	415	0.3433	42.75

Sr. No	Di (m)	Q_C x 10^6 (m^3/s)	Q_D x 10^6 (m^3/s)	c (m)	d (m)	N (rps)	N_D x 10^4	C/D ratio	σ (mN/m)	ρ_C (Kg/m^3)	ρ_D (Kg/m^3)	μ_C (mKg/ms^2)	μ_D (mKg/ms^2)	a (m/s^2)	Ta x 10^8	N_{Re} x 10^3
58	0.03	3.44	2.50	0.0075	0.002	30.00	6.86	1.38	54.5	850	1000	0.41	1.00	415	0.2987	42.75
59	0.03	3.06	3.02	0.0075	0.002	30.00	7.02	1.01	54.5	1000	850	1.00	0.41	415	0.2654	20.60
60	0.03	4.33	1.75	0.0075	0.002	36.70	5.74	2.47	54.5	850	1000	0.41	1.00	620	0.6664	52.46
61	0.03	3.76	2.26	0.0075	0.002	36.70	5.68	1.66	54.5	850	1000	0.41	1.00	620	0.5879	52.46
62	0.03	2.78	3.31	0.0075	0.002	36.70	5.75	0.84	54.5	1000	850	1.00	0.41	620	0.5234	25.28
63	0.03	3.06	3.05	0.0075	0.002	36.70	5.77	1.00	54.5	1000	850	1.00	0.41	620	0.4910	25.28
64	0.03	2.22	2.44	0.0075	0.002	43.30	3.73	0.91	54.5	1000	850	1.00	0.41	864	0.8393	29.90
65	0.03	2.50	2.22	0.0075	0.002	43.30	3.78	1.13	54.5	1000	850	1.00	0.41	864	0.7774	29.90
66	0.03	2.78	2.05	0.0075	0.002	43.30	3.86	1.36	54.5	1000	850	1.00	0.41	864	0.7276	29.90
67	0.03	3.06	1.67	0.0075	0.002	43.30	3.78	1.83	54.5	1000	850	1.00	0.41	864	0.6563	29.90
68	0.03	3.33	1.72	0.0075	0.002	23.30	7.51	1.94	53.0	1000	900	1.00	1.20	250	0.0492	15.94
69	0.03	3.61	1.60	0.0075	0.002	23.30	7.74	2.26	53.0	1000	900	1.00	1.20	250	0.0502	15.94
70	0.03	3.89	1.45	0.0075	0.002	23.30	7.94	2.68	53.0	1000	900	1.00	1.20	250	0.0512	15.94
71	0.03	3.50	1.69	0.0075	0.002	30.00	5.99	2.07	53.0	1000	900	1.00	1.20	415	0.1072	20.60
72	0.03	3.89	1.50	0.0075	0.002	30.00	6.22	2.59	53.0	1000	900	1.00	1.20	415	0.1102	20.60
73	0.03	4.17	1.42	0.0075	0.002	30.00	6.45	2.94	53.0	1000	900	1.00	1.20	415	0.1117	20.60
74	0.03	3.58	1.68	0.0075	0.002	36.70	4.96	2.13	53.0	1000	900	1.00	1.20	620	0.1984	25.28
75	0.03	3.89	1.58	0.0075	0.002	36.70	5.16	2.46	53.0	1000	900	1.00	1.20	620	0.2019	25.28
76	0.03	4.17	1.53	0.0075	0.002	36.70	5.38	2.73	53.0	1000	900	1.00	1.20	620	0.2043	25.28
77	0.03	3.97	0.83	0.0075	0.002	23.30	7.13	4.78	49.0	900	1100	1.00	0.65	250	0.0607	14.32
78	0.03	3.60	1.39	0.0075	0.002	23.30	7.42	2.59	49.0	900	1100	1.00	0.65	250	0.0697	14.32
79	0.03	3.06	1.94	0.0075	0.002	23.30	7.43	1.58	49.0	900	1100	1.00	0.65	250	0.0803	14.32
80	0.03	2.50	2.61	0.0075	0.002	23.30	7.60	0.96	49.0	1100	900	0.65	1.00	250	0.0914	27.40
81	0.03	3.06	2.32	0.0075	0.002	23.30	8.00	1.32	49.0	1100	900	0.65	1.00	250	0.1011	27.40
82	0.03	3.61	1.95	0.0075	0.002	23.30	8.26	1.85	49.0	1100	900	0.65	1.00	250	0.1120	27.40
83	0.03	4.15	0.83	0.0075	0.002	30.00	5.75	5.00	49.0	900	1100	1.00	0.65	415	0.1301	18.51
84	0.03	3.72	1.39	0.0075	0.002	30.00	5.90	2.68	49.0	900	1100	1.00	0.65	415	0.1492	18.51
85	0.03	3.17	1.94	0.0075	0.002	30.00	5.90	1.63	49.0	900	1100	1.00	0.65	415	0.1714	18.51
86	0.03	2.50	2.69	0.0075	0.002	30.00	5.99	0.93	46.0	1200	1000	0.65	1.00	415	0.2366	38.68

Sr. No	Di (m)	Q_C x 10^6 (m^3/s)	Q_D x 10^6 (m^3/s)	c (m)	d (m)	N (rps)	N_D x 10^4	C/D ratio	σ (mN/m)	ρ_C (Kg/m^3)	ρ_D (Kg/m^3)	μ_C (mKg/ms^2)	μ_D (mKg/ms^2)	a (m/s^2)	Ta x 10^8	N_{Re} x 10^3
87	0.03	3.06	2.41	0.0075	0.002	30.00	6.31	1.27	46.0	1200	1000	0.65	1.00	415	0.2605	38.68
88	0.03	3.61	2.12	0.0075	0.002	30.00	6.62	1.70	46.0	1200	1000	0.65	1.00	415	0.2842	38.68
89	0.03	4.27	0.83	0.0075	0.002	36.70	4.81	5.14	46.0	1000	1200	1.00	0.65	620	0.2925	25.28
90	0.03	3.74	1.39	0.0075	0.002	36.70	4.84	2.69	46.0	1000	1200	1.00	0.65	620	0.3353	25.28
91	0.03	3.26	1.94	0.0075	0.002	36.70	4.91	1.68	46.0	1000	1200	1.00	0.65	620	0.3810	25.28
92	0.03	2.50	2.86	0.0075	0.002	36.70	5.06	0.87	46.0	1200	1000	0.65	1.00	620	0.4280	47.47
93	0.03	3.06	2.53	0.0075	0.002	36.70	5.28	1.21	46.0	1200	1000	0.65	1.00	620	0.4732	47.47
94	0.03	3.61	2.20	0.0075	0.002	36.70	5.48	1.64	46.0	1200	1000	0.65	1.00	620	0.5185	47.47
95	0.03	4.33	0.83	0.0075	0.002	43.30	4.13	5.22	46.0	1000	1200	1.00	0.65	864	0.4816	29.90
96	0.03	3.79	1.39	0.0075	0.002	43.30	4.14	2.73	46.0	1000	1200	1.00	0.65	864	0.5515	29.90
97	0.03	3.41	1.94	0.0075	0.002	43.30	4.28	1.76	46.0	1000	1200	1.00	0.65	864	0.6206	29.90
98	0.03	2.50	3.01	0.0075	0.002	43.30	4.41	0.83	46.0	1200	1000	0.65	1.00	864	0.6953	56.14
99	0.03	3.06	2.65	0.0075	0.002	43.30	4.57	1.15	46.0	1200	1000	0.65	1.00	864	0.7699	56.14
100	0.03	3.61	2.23	0.0075	0.002	43.30	4.67	1.62	46.0	1200	1000	0.65	1.00	864	0.8523	56.14
101	0.03	4.13	0.83	0.0075	0.002	23.30	7.37	4.98	46.0	900	1200	1.00	0.71	250	0.0605	14.32
102	0.03	3.65	1.39	0.0075	0.002	23.30	7.49	2.63	46.0	900	1200	1.00	0.71	250	0.0696	14.32
103	0.03	3.21	1.94	0.0075	0.002	23.30	7.66	1.65	46.0	900	1200	1.00	0.71	250	0.0792	14.32
104	0.03	2.50	2.81	0.0075	0.002	23.30	7.89	0.89	46.0	1200	900	0.71	1.00	250	0.0892	27.07
105	0.03	3.06	2.42	0.0075	0.002	23.30	8.15	1.26	46.0	1200	900	0.71	1.00	250	0.0995	27.07
106	0.03	3.61	2.13	0.0075	0.002	23.30	8.53	1.69	46.0	1200	900	0.71	1.00	250	0.1086	27.07
107	0.03	4.30	0.83	0.0075	0.002	30.00	5.92	5.18	46.0	900	1200	1.00	0.71	415	0.1296	18.51
108	0.03	3.80	1.39	0.0075	0.002	30.00	5.99	2.73	46.0	900	1200	1.00	0.71	415	0.1487	18.51
109	0.03	3.33	1.94	0.0075	0.002	30.00	6.08	1.72	46.0	900	1200	1.00	0.71	415	0.1691	18.51
110	0.03	2.50	2.91	0.0075	0.002	30.00	6.25	0.86	43.0	1300	1000	0.71	1.00	415	0.2289	37.95
111	0.03	3.06	2.53	0.0075	0.002	30.00	6.45	1.21	43.0	1300	1000	0.71	1.00	415	0.2536	37.95
112	0.03	3.61	2.28	0.0075	0.002	30.00	6.80	1.58	43.0	1300	1000	0.71	1.00	415	0.2742	37.95
113	0.03	4.40	0.83	0.0075	0.002	36.70	4.94	5.30	43.0	1000	1300	1.00	0.71	620	0.2908	25.28
114	0.03	3.92	1.39	0.0075	0.002	36.70	5.01	2.82	43.0	1000	1300	1.00	0.71	620	0.3305	25.28
115	0.03	3.47	1.94	0.0075	0.002	36.70	5.11	1.79	43.0	1000	1300	1.00	0.71	620	0.3723	25.28

Sr. No	Di (m)	$Q_C \times 10^6$ (m^3/s)	$Q_D \times 10^6$ (m^3/s)	c (m)	d (m)	N (rps)	$N_D \times 10^4$	C/D ratio	σ (mN/m)	ρ_C (Kg/m^3)	ρ_D (Kg/m^3)	μ_C (mKg/ms^2)	μ_D (mKg/ms^2)	a (m/s^2)	Ta x 10^8	$N_{Re} \times 10^3$
116	0.03	2.50	3.06	0.0075	0.002	36.70	5.25	0.82	43.0	1300	1000	0.71	1.00	620	0.4158	46.57
117	0.03	3.06	2.67	0.0075	0.002	36.70	5.41	1.15	43.0	1300	1000	0.71	1.00	620	0.4602	46.57
118	0.03	3.61	2.38	0.0075	0.002	36.70	5.65	1.52	43.0	1300	1000	0.71	1.00	620	0.4995	46.57
119	0.03	4.45	0.83	0.0075	0.002	43.30	4.22	5.36	43.0	1000	1300	1.00	0.71	864	0.4790	29.90
120	0.03	3.97	1.39	0.0075	0.002	43.30	4.29	2.86	43.0	1000	1300	1.00	0.71	864	0.5439	29.90
121	0.03	3.50	1.94	0.0075	0.002	43.30	4.35	1.80	43.0	1000	1300	1.00	0.71	864	0.6129	29.90
122	0.03	2.50	3.10	0.0075	0.002	43.30	4.48	0.81	43.0	1300	1000	0.71	1.00	864	0.6836	55.08
123	0.03	3.06	2.70	0.0075	0.002	43.30	4.61	1.13	43.0	1300	1000	0.71	1.00	864	0.7570	55.08
124	0.03	3.61	2.43	0.0075	0.002	43.30	4.83	1.49	43.0	1300	1000	0.71	1.00	864	0.8194	55.08
125	0.03	2.78	1.00	0.0075	0.002	23.30	5.62	2.78	43.0	1300	1200	0.58	1.00	250	0.2160	36.16
126	0.03	3.33	0.85	0.0075	0.002	23.30	6.21	3.92	43.0	1300	1200	0.58	1.00	250	0.2331	36.16
127	0.03	3.89	0.78	0.0075	0.002	23.30	6.94	4.99	43.0	1300	1200	0.58	1.00	250	0.2439	36.16
128	0.03	2.78	1.03	0.0075	0.002	25.00	5.28	2.70	43.0	1300	1200	0.58	1.00	288	0.2658	38.84
129	0.03	3.33	0.88	0.0075	0.002	25.00	5.83	3.78	43.0	1300	1200	0.58	1.00	288	0.2869	38.84
130	0.03	3.89	0.80	0.0075	0.002	25.00	6.50	4.86	43.0	1300	1200	0.58	1.00	288	0.3010	38.84
131	0.03	2.78	1.05	0.0075	0.002	26.70	4.97	2.65	43.0	1300	1200	0.58	1.00	328	0.3232	41.52
132	0.03	3.33	0.89	0.0075	0.002	26.70	5.47	3.74	43.0	1300	1200	0.58	1.00	328	0.3497	41.52
133	0.03	3.89	0.82	0.0075	0.002	26.70	6.11	4.74	43.0	1300	1200	0.58	1.00	328	0.3661	41.52
134	0.03	7.65	0.83	0.0075	0.006	23.30	12.60	9.22	58.3	660	1000	0.29	1.00	250	6.5723	110.45
135	0.03	6.73	1.39	0.0075	0.006	23.30	12.07	4.84	58.3	660	1000	0.29	1.00	250	5.8945	110.45
136	0.03	5.85	1.94	0.0075	0.006	23.30	11.58	3.02	58.3	660	1000	0.29	1.00	250	5.2373	110.45
137	0.03	4.99	2.50	0.0075	0.006	23.30	11.13	2.00	58.3	660	1000	0.29	1.00	250	4.5917	110.45
138	0.03	4.13	3.06	0.0075	0.006	23.30	10.69	1.35	58.3	660	1000	0.29	1.00	250	3.9693	110.45
139	0.03	3.61	3.28	0.0075	0.006	23.30	10.24	1.10	58.3	1000	660	1.00	0.29	250	3.3845	48.61
140	0.03	4.17	2.46	0.0075	0.006	23.30	9.85	1.70	58.3	1000	660	1.00	0.29	250	2.8449	48.61
141	0.03	7.70	0.83	0.0075	0.006	30.00	9.85	9.28	58.3	660	1000	0.29	1.00	415	14.2424	142.74
142	0.03	6.68	1.39	0.0075	0.006	30.00	9.32	4.81	58.3	660	1000	0.29	1.00	415	12.7426	142.74
143	0.03	5.92	1.94	0.0075	0.006	30.00	9.07	3.05	58.3	660	1000	0.29	1.00	415	11.3784	142.74
144	0.03	5.04	2.50	0.0075	0.006	30.00	8.70	2.02	58.3	660	1000	0.29	1.00	415	9.9765	142.74

Sr. No	Di (m)	Q_C x 10^6 (m^3/s)	Q_D x 10^6 (m^3/s)	c (m)	d (m)	N (rps)	N_D x 10^4	C/D ratio	σ (mN/m)	ρ_C (Kg/m^3)	ρ_D (Kg/m^3)	μ_C (mKg/ms^2)	μ_D (mKg/ms^2)	a (m/s^2)	Ta x 10^8	N_{Re} x 10^3
145	0.03	4.16	3.06	0.0075	0.006	30.00	8.34	1.36	58.3	660	1000	0.29	1.00	415	8.6187	142.74
146	0.03	3.61	3.35	0.0075	0.006	30.00	8.04	1.08	58.3	1000	660	1.00	0.29	415	7.3916	62.83
147	0.03	4.17	2.55	0.0075	0.006	30.00	7.76	1.64	58.3	1000	660	1.00	0.29	415	6.2470	62.83
148	0.03	7.72	0.83	0.0075	0.006	36.70	8.07	9.30	58.3	660	1000	0.29	1.00	620	26.3181	175.14
149	0.03	6.82	1.39	0.0075	0.006	36.70	7.75	4.91	58.3	660	1000	0.29	1.00	620	23.6429	175.14
150	0.03	6.02	1.94	0.0075	0.006	36.70	7.51	3.10	58.3	660	1000	0.29	1.00	620	21.1191	175.14
151	0.03	5.11	2.50	0.0075	0.006	36.70	7.18	2.04	58.3	660	1000	0.29	1.00	620	18.5175	175.14
152	0.03	4.26	3.06	0.0075	0.006	36.70	6.91	1.39	58.3	660	1000	0.29	1.00	620	16.0693	175.14
153	0.03	3.61	3.47	0.0075	0.006	36.70	6.68	1.04	58.3	1000	660	1.00	0.29	620	13.8517	77.09
154	0.03	4.17	2.63	0.0075	0.006	36.70	6.42	1.59	58.3	1000	660	1.00	0.29	620	11.6812	77.09
155	0.03	7.28	1.11	0.0075	0.006	43.30	6.71	6.56	58.3	660	1000	0.29	1.00	864	41.2844	207.14
156	0.03	6.84	1.39	0.0075	0.006	43.30	6.58	4.92	58.3	660	1000	0.29	1.00	864	39.0905	207.14
157	0.03	5.98	1.94	0.0075	0.006	43.30	6.33	3.08	58.3	660	1000	0.29	1.00	864	34.8303	207.14
158	0.03	5.14	2.50	0.0075	0.006	43.30	6.11	2.06	58.3	660	1000	0.29	1.00	864	30.6594	207.14
159	0.03	4.33	3.06	0.0075	0.006	43.30	5.91	1.42	58.3	660	1000	0.29	1.00	864	26.7209	207.14
160	0.03	3.61	3.33	0.0075	0.006	43.30	5.55	1.08	58.3	1000	660	1.00	0.29	864	22.5065	91.18
161	0.03	6.79	0.83	0.0075	0.006	23.30	11.33	8.18	56.5	750	1000	0.36	1.00	250	5.7168	103.55
162	0.03	6.12	1.39	0.0075	0.006	23.30	11.16	4.40	56.5	750	1000	0.36	1.00	250	5.1269	103.55
163	0.03	5.45	1.94	0.0075	0.006	23.30	10.98	2.81	56.5	750	1000	0.36	1.00	250	4.5841	103.55
164	0.03	4.70	2.50	0.0075	0.006	23.30	10.70	1.88	56.5	750	1000	0.36	1.00	250	4.0507	103.55
165	0.03	3.97	3.06	0.0075	0.006	23.30	10.45	1.30	56.5	750	1000	0.36	1.00	250	3.5570	103.55
166	0.03	3.61	3.18	0.0075	0.006	23.30	10.09	1.14	56.5	1000	750	1.00	0.36	250	3.0807	48.61
167	0.03	6.86	0.83	0.0075	0.006	30.00	8.88	8.27	56.5	750	1000	0.36	1.00	415	12.3956	133.83
168	0.03	6.16	1.39	0.0075	0.006	30.00	8.72	4.43	56.5	750	1000	0.36	1.00	415	11.1164	133.83
169	0.03	5.52	1.94	0.0075	0.006	30.00	8.61	2.85	56.5	750	1000	0.36	1.00	415	9.9611	133.83
170	0.03	4.81	2.50	0.0075	0.006	30.00	8.44	1.92	56.5	750	1000	0.36	1.00	415	8.8380	133.83
171	0.03	4.01	3.06	0.0075	0.006	30.00	8.16	1.31	56.5	750	1000	0.36	1.00	415	7.7299	133.83
172	0.03	3.61	3.24	0.0075	0.006	30.00	7.91	1.11	56.5	1000	750	1.00	0.36	415	6.7171	62.83
173	0.03	7.07	0.83	0.0075	0.006	36.70	7.46	8.52	56.5	750	1000	0.36	1.00	620	22.9914	164.21

Sr. No	Di (m)	Q_C x 10^6 (m^3/s)	Q_D x 10^6 (m^3/s)	c (m)	d (m)	N (rps)	N_D x 10^4	C/D ratio	σ (mN/m)	ρ_C (Kg/m^3)	ρ_D (Kg/m^3)	μ_C (mKg/ms^2)	μ_D (mKg/ms^2)	a (m/s^2)	Ta x 10^8	N_{Re} x 10^3
174	0.03	6.22	1.39	0.0075	0.006	36.70	7.18	4.47	56.5	750	1000	0.36	1.00	620	20.5777	164.21
175	0.03	5.58	1.94	0.0075	0.006	36.70	7.10	2.88	56.5	750	1000	0.36	1.00	620	18.4562	164.21
176	0.03	4.84	2.50	0.0075	0.006	36.70	6.93	1.94	56.5	750	1000	0.36	1.00	620	16.3597	164.21
177	0.03	4.06	3.06	0.0075	0.006	36.70	6.72	1.33	56.5	750	1000	0.36	1.00	620	14.3436	164.21
178	0.03	3.61	3.28	0.0075	0.006	36.70	6.50	1.10	56.5	1000	750	1.00	0.36	620	12.4653	77.09
179	0.03	5.89	1.39	0.0075	0.006	43.30	5.82	4.24	56.5	750	1000	0.36	1.00	864	33.5992	194.21
180	0.03	4.90	1.94	0.0075	0.006	43.30	5.47	2.53	56.5	750	1000	0.36	1.00	864	29.3797	194.21
181	0.03	3.97	2.50	0.0075	0.006	43.30	5.18	1.59	56.5	750	1000	0.36	1.00	864	25.2707	194.21
182	0.03	3.06	3.24	0.0075	0.006	43.30	5.04	0.94	56.5	1000	750	1.00	0.36	864	21.8087	91.18
183	0.03	6.26	0.83	0.0075	0.006	23.30	10.54	7.54	55.0	850	1000	0.42	1.00	250	5.2929	100.10
184	0.03	5.76	1.39	0.0075	0.006	23.30	10.63	4.14	55.0	850	1000	0.42	1.00	250	4.7479	100.10
185	0.03	5.27	1.94	0.0075	0.006	23.30	10.72	2.72	55.0	850	1000	0.42	1.00	250	4.2737	100.10
186	0.03	4.50	2.50	0.0075	0.006	23.30	10.40	1.80	55.0	850	1000	0.42	1.00	250	3.7733	100.10
187	0.03	3.94	3.06	0.0075	0.006	23.30	10.40	1.29	55.0	850	1000	0.42	1.00	250	3.3685	100.10
188	0.03	6.18	1.17	0.0075	0.006	30.00	8.49	5.28	55.0	850	1000	0.42	1.00	415	10.8022	129.36
189	0.03	5.93	1.39	0.0075	0.006	30.00	8.45	4.27	55.0	850	1000	0.42	1.00	415	10.3458	129.36
190	0.03	5.36	1.94	0.0075	0.006	30.00	8.43	2.76	55.0	850	1000	0.42	1.00	415	9.2969	129.36
191	0.03	4.55	2.50	0.0075	0.006	30.00	8.14	1.82	55.0	850	1000	0.42	1.00	415	8.1994	129.36
192	0.03	3.99	3.06	0.0075	0.006	30.00	8.14	1.30	55.0	850	1000	0.42	1.00	415	7.3257	129.36
193	0.03	5.73	1.75	0.0075	0.006	36.70	7.06	3.27	55.0	850	1000	0.42	1.00	620	17.9614	158.72
194	0.03	4.98	2.26	0.0075	0.006	36.70	6.83	2.20	55.0	850	1000	0.42	1.00	620	16.0842	158.72
195	0.03	4.38	2.78	0.0075	0.006	36.70	6.76	1.58	55.0	850	1000	0.42	1.00	620	14.4409	158.72
196	0.03	4.04	3.06	0.0075	0.006	36.70	6.70	1.32	55.0	850	1000	0.42	1.00	620	13.5914	158.72
197	0.03	3.23	2.22	0.0075	0.006	43.30	4.36	1.45	55.0	850	1000	0.42	1.00	864	23.2245	187.72
198	0.03	2.50	2.94	0.0075	0.006	43.30	4.35	0.85	55.0	1000	850	1.00	0.42	864	21.5641	91.18
199	0.03	2.78	2.71	0.0075	0.006	43.30	4.39	1.03	55.0	1000	850	1.00	0.42	864	20.1742	91.18
200	0.03	3.06	2.21	0.0075	0.006	43.30	4.22	1.38	55.0	1000	850	1.00	0.42	864	18.1464	91.18
201	0.03	3.33	2.28	0.0075	0.006	23.30	8.34	1.46	53.0	1000	900	1.00	0.60	250	2.0939	48.61
202	0.03	3.61	2.12	0.0075	0.006	23.30	8.52	1.70	53.0	1000	900	1.00	0.60	250	2.0328	48.61

Sr. No	Di (m)	Q_C x 10^6 (m^3/s)	Q_D x 10^6 (m^3/s)	c (m)	d (m)	N (rps)	N_D x 10^4	C/D ratio	σ (mN/m)	ρ_C (Kg/m^3)	ρ_D (Kg/m^3)	μ_C (mKg/ms^2)	μ_D (mKg/ms^2)	a (m/s^2)	Ta x 10^8	N_{Re} x 10^3
203	0.03	3.89	1.92	0.0075	0.006	23.30	8.64	2.03	53.0	1000	900	1.00	0.60	250	1.9684	48.61
204	0.03	3.50	2.24	0.0075	0.006	30.00	6.63	1.56	53.0	1000	900	1.00	0.60	415	4.4745	62.83
205	0.03	3.89	1.98	0.0075	0.006	30.00	6.78	1.96	53.0	1000	900	1.00	0.60	415	4.2858	62.83
206	0.03	4.17	1.88	0.0075	0.006	30.00	6.98	2.22	53.0	1000	900	1.00	0.60	415	4.1940	62.83
207	0.03	3.58	2.22	0.0075	0.006	36.70	5.47	1.61	53.0	1000	900	1.00	0.60	620	8.2154	77.09
208	0.03	3.89	2.09	0.0075	0.006	36.70	5.64	1.86	53.0	1000	900	1.00	0.60	620	7.9959	77.09
209	0.03	4.17	2.02	0.0075	0.006	36.70	5.84	2.06	53.0	1000	900	1.00	0.60	620	7.8464	77.09
210	0.03	2.78	1.89	0.0075	0.016	23.30	6.94	1.47	49.0	1100	1000	0.58	1.00	250	51.4608	251.82
211	0.03	3.33	1.61	0.0075	0.016	23.30	7.34	2.07	49.0	1100	1000	0.58	1.00	250	56.9111	251.82
212	0.03	3.89	1.48	0.0075	0.016	23.30	7.98	2.63	49.0	1100	1000	0.58	1.00	250	60.6852	251.82
213	0.03	2.78	1.95	0.0075	0.016	25.00	6.55	1.43	49.0	1100	1000	0.58	1.00	288	63.4136	270.47
214	0.03	3.33	1.67	0.0075	0.016	25.00	6.93	1.99	49.0	1100	1000	0.58	1.00	288	70.0823	270.47
215	0.03	3.89	1.52	0.0075	0.016	25.00	7.49	2.56	49.0	1100	1000	0.58	1.00	288	74.9915	270.47
216	0.03	2.78	1.99	0.0075	0.016	26.70	6.19	1.40	49.0	1100	1000	0.58	1.00	328	77.2478	289.14
217	0.03	3.33	1.69	0.0075	0.016	26.70	6.51	1.97	49.0	1100	1000	0.58	1.00	328	85.6203	289.14
218	0.03	3.89	1.55	0.0075	0.016	26.70	7.06	2.51	49.0	1100	1000	0.58	1.00	328	91.4649	289.14
219	0.03	7.53	0.83	0.0075	0.016	23.30	12.43	9.07	45.0	1000	1200	1.00	0.65	250	27.1948	131.53
220	0.03	6.83	1.39	0.0075	0.016	23.30	12.22	4.91	45.0	1000	1200	1.00	0.65	250	29.7092	131.53
221	0.03	5.80	1.94	0.0075	0.016	23.30	11.50	2.99	45.0	1000	1200	1.00	0.65	250	32.9265	131.53
222	0.03	4.95	2.50	0.0075	0.016	23.30	11.07	1.98	45.0	1000	1200	1.00	0.65	250	36.6292	131.53
223	0.03	4.40	3.06	0.0075	0.016	23.30	11.09	1.44	45.0	1000	1200	1.00	0.65	250	40.2079	131.53
224	0.03	3.61	3.70	0.0075	0.016	23.30	10.87	0.98	45.0	1200	1000	0.65	1.00	250	44.6172	246.96
225	0.03	7.87	0.83	0.0075	0.016	30.00	10.04	9.48	45.0	1000	1200	1.00	0.65	415	59.1411	169.99
226	0.03	7.06	1.39	0.0075	0.016	30.00	9.76	5.08	45.0	1000	1200	1.00	0.65	415	64.5513	169.99
227	0.03	6.01	1.94	0.0075	0.016	30.00	9.18	3.10	45.0	1000	1200	1.00	0.65	415	71.3624	169.99
228	0.03	5.10	2.50	0.0075	0.016	30.00	8.77	2.04	45.0	1000	1200	1.00	0.65	415	79.3904	169.99
229	0.03	4.57	3.06	0.0075	0.016	30.00	8.81	1.49	45.0	1000	1200	1.00	0.65	415	86.8767	169.99
230	0.03	3.61	4.02	0.0075	0.016	30.00	8.81	0.90	45.0	1200	1000	0.65	1.00	415	95.0330	319.15
231	0.03	8.10	0.83	0.0075	0.016	36.70	8.43	9.76	45.0	1000	1200	1.00	0.65	620	109.5343	208.57

Sr. No	Di (m)	$Q_C \times 10^6$ (m^3/s)	$Q_D \times 10^6$ (m^3/s)	c (m)	d (m)	N (rps)	$N_D \times 10^4$	C/D ratio	σ (mN/m)	ρ_C (Kg/m^3)	ρ_D (Kg/m^3)	μ_C (mKg/ms^2)	μ_D (mKg/ms^2)	a (m/s^2)	Ta $\times 10^8$	$N_{Re} \times 10^3$
232	0.03	7.10	1.39	0.0075	0.016	36.70	8.01	5.11	45.0	1000	1200	1.00	0.65	620	119.8107	208.57
233	0.03	6.18	1.94	0.0075	0.016	36.70	7.66	3.19	45.0	1000	1200	1.00	0.65	620	131.7324	208.57
234	0.03	5.42	2.50	0.0075	0.016	36.70	7.47	2.17	45.0	1000	1200	1.00	0.65	620	145.0616	208.57
235	0.03	4.80	3.06	0.0075	0.016	36.70	7.42	1.57	45.0	1000	1200	1.00	0.65	620	159.0596	208.57
236	0.03	3.61	4.17	0.0075	0.016	36.70	7.34	0.87	45.0	1200	1000	0.65	1.00	620	174.5689	391.58
237	0.03	8.21	0.83	0.0075	0.016	43.30	7.23	9.89	45.0	1000	1200	1.00	0.65	864	181.4238	246.68
238	0.03	7.19	1.39	0.0075	0.016	43.30	6.86	5.17	45.0	1000	1200	1.00	0.65	864	198.2988	246.68
239	0.03	6.47	1.94	0.0075	0.016	43.30	6.73	3.34	45.0	1000	1200	1.00	0.65	864	216.2497	246.68
240	0.03	5.71	2.50	0.0075	0.016	43.30	6.57	2.28	45.0	1000	1200	1.00	0.65	864	237.2737	246.68
241	0.03	5.03	3.06	0.0075	0.016	43.30	6.47	1.64	45.0	1000	1200	1.00	0.65	864	260.2112	246.68
242	0.03	3.61	4.23	0.0075	0.016	43.30	6.27	0.85	45.0	1200	1000	0.65	1.00	864	288.2817	463.11
243	0.03	7.83	0.83	0.0075	0.016	23.30	12.87	9.43	42.0	1000	1300	1.00	0.71	250	27.0703	131.53
244	0.03	6.92	1.39	0.0075	0.016	23.30	12.35	4.98	42.0	1000	1300	1.00	0.71	250	29.6123	131.53
245	0.03	6.09	1.94	0.0075	0.016	23.30	11.94	3.14	42.0	1000	1300	1.00	0.71	250	32.4826	131.53
246	0.03	5.33	2.50	0.0075	0.016	23.30	11.64	2.13	42.0	1000	1300	1.00	0.71	250	35.7476	131.53
247	0.03	4.59	3.06	0.0075	0.016	23.30	11.37	1.50	42.0	1000	1300	1.00	0.71	250	39.4499	131.53
248	0.03	3.61	4.04	0.0075	0.016	23.30	11.37	0.89	42.0	1300	1000	0.71	1.00	250	43.0354	242.30
249	0.03	8.16	0.83	0.0075	0.016	30.00	10.38	9.83	42.0	1000	1300	1.00	0.71	415	58.8987	169.99
250	0.03	7.21	1.39	0.0075	0.016	30.00	9.93	5.19	42.0	1000	1300	1.00	0.71	415	64.2613	169.99
251	0.03	6.32	1.94	0.0075	0.016	30.00	9.54	3.26	42.0	1000	1300	1.00	0.71	415	70.3998	169.99
252	0.03	5.52	2.50	0.0075	0.016	30.00	9.26	2.21	42.0	1000	1300	1.00	0.71	415	77.4027	169.99
253	0.03	4.80	3.06	0.0075	0.016	30.00	9.07	1.57	42.0	1000	1300	1.00	0.71	415	85.1029	169.99
254	0.03	3.61	4.32	0.0075	0.016	30.00	9.15	0.84	42.0	1300	1000	0.71	1.00	415	92.1807	313.13
255	0.03	8.35	0.83	0.0075	0.016	36.70	8.66	10.06	42.0	1000	1300	1.00	0.71	620	109.1624	208.57
256	0.03	7.44	1.39	0.0075	0.016	36.70	8.33	5.35	42.0	1000	1300	1.00	0.71	620	118.7616	208.57
257	0.03	6.58	1.94	0.0075	0.016	36.70	8.04	3.39	42.0	1000	1300	1.00	0.71	620	129.6362	208.57
258	0.03	5.80	2.50	0.0075	0.016	36.70	7.83	2.32	42.0	1000	1300	1.00	0.71	620	141.9579	208.57
259	0.03	5.06	3.06	0.0075	0.016	36.70	7.66	1.65	42.0	1000	1300	1.00	0.71	620	155.7288	208.57
260	0.03	3.61	4.51	0.0075	0.016	36.70	7.66	0.80	42.0	1300	1000	0.71	1.00	620	169.0703	384.19

Sr. No	Di (m)	Q_C x 10^6 (m^3/s)	Q_D x 10^6 (m^3/s)	c (m)	d (m)	N (rps)	N_D x 10^4	C/D ratio	σ (mN/m)	ρ_C (Kg/m^3)	ρ_D (Kg/m^3)	μ_C (mKg/ms^2)	μ_D (mKg/ms^2)	a (m/s^2)	Ta x 10^8	N_{Re} x 10^3
261	0.03	8.44	0.83	0.0075	0.016	43.30	7.41	10.17	42.0	1000	1300	1.00	0.71	864	180.8668	246.68
262	0.03	7.53	1.39	0.0075	0.016	43.30	7.13	5.42	42.0	1000	1300	1.00	0.71	864	196.5983	246.68
263	0.03	6.64	1.94	0.0075	0.016	43.30	6.86	3.42	42.0	1000	1300	1.00	0.71	864	214.6029	246.68
264	0.03	5.88	2.50	0.0075	0.016	43.30	6.70	2.35	42.0	1000	1300	1.00	0.71	864	234.6343	246.68
265	0.03	5.12	3.06	0.0075	0.016	43.30	6.54	1.67	42.0	1000	1300	1.00	0.71	864	257.4386	246.68
266	0.03	4.61	3.61	0.0075	0.016	43.30	6.57	1.28	42.0	1000	1300	1.00	0.71	864	278.6088	246.68
267	0.03	4.06	0.83	0.0075	0.002	23.30	7.27	4.89	35.5	780	1000	0.59	1.00	250	0.0959	21.16
268	0.03	3.57	1.39	0.0075	0.002	23.30	7.37	2.57	35.5	780	1000	0.59	1.00	250	0.0905	21.16
269	0.03	3.11	1.94	0.0075	0.002	23.30	7.51	1.60	35.5	780	1000	0.59	1.00	250	0.0855	21.16
270	0.03	2.50	2.65	0.0075	0.002	23.30	7.66	0.94	35.5	1000	780	1.00	0.59	250	0.0809	15.94
271	0.03	3.06	2.19	0.0075	0.002	23.30	7.80	1.40	35.5	1000	780	1.00	0.59	250	0.0766	15.94
272	0.03	3.61	1.74	0.0075	0.002	23.30	7.95	2.07	35.5	1000	780	1.00	0.59	250	0.0726	15.94
273	0.03	4.17	1.31	0.0075	0.002	23.30	8.15	3.18	35.5	1000	780	1.00	0.59	250	0.0690	15.94
274	0.03	4.09	0.83	0.0075	0.002	30.00	5.68	4.93	35.5	780	1000	0.59	1.00	415	0.2071	27.35
275	0.03	3.60	1.39	0.0075	0.002	30.00	5.76	2.59	35.5	780	1000	0.59	1.00	415	0.1955	27.35
276	0.03	3.15	1.94	0.0075	0.002	30.00	5.88	1.62	35.5	780	1000	0.59	1.00	415	0.1850	27.35
277	0.03	2.50	2.68	0.0075	0.002	30.00	5.98	0.93	35.5	1000	780	1.00	0.59	415	0.1749	20.60
278	0.03	3.06	2.21	0.0075	0.002	30.00	6.08	1.38	35.5	1000	780	1.00	0.59	415	0.1655	20.60
279	0.03	3.61	1.78	0.0075	0.002	30.00	6.22	2.03	35.5	1000	780	1.00	0.59	415	0.1572	20.60
280	0.03	4.17	1.36	0.0075	0.002	30.00	6.38	3.07	35.5	1000	780	1.00	0.59	415	0.1496	20.60
281	0.03	4.10	0.83	0.0075	0.002	36.70	4.65	4.94	35.5	780	1000	0.59	1.00	620	0.3819	33.56
282	0.03	3.62	1.39	0.0075	0.002	36.70	4.73	2.60	35.5	780	1000	0.59	1.00	620	0.3607	33.56
283	0.03	3.16	1.94	0.0075	0.002	36.70	4.81	1.63	35.5	780	1000	0.59	1.00	620	0.3412	33.56
284	0.03	2.50	2.72	0.0075	0.002	36.70	4.93	0.92	35.5	1000	780	1.00	0.59	620	0.3231	25.28
285	0.03	3.06	2.26	0.0075	0.002	36.70	5.02	1.35	35.5	1000	780	1.00	0.59	620	0.3061	25.28
286	0.03	3.61	1.83	0.0075	0.002	36.70	5.13	1.97	35.5	1000	780	1.00	0.59	620	0.2909	25.28
287	0.03	4.17	1.40	0.0075	0.002	36.70	5.26	2.98	35.5	1000	780	1.00	0.59	620	0.2768	25.28
288	0.03	3.87	1.11	0.0075	0.002	43.30	3.98	3.49	35.5	780	1000	0.59	1.00	864	0.6126	39.69
289	0.03	3.64	1.39	0.0075	0.002	43.30	4.02	2.62	35.5	780	1000	0.59	1.00	864	0.5956	39.69

Sr. No	Di (m)	$Q_C \times 10^6$ (m^3/s)	$Q_D \times 10^6$ (m^3/s)	c (m)	d (m)	N (rps)	$N_D \times 10^4$	C/D ratio	σ (mN/m)	ρ_C (Kg/m^3)	ρ_D (Kg/m^3)	μ_C (mKg/ms^2)	μ_D (mKg/ms^2)	a (m/s^2)	$Ta \times 10^8$	$N_{Re} \times 10^3$
290	0.03	3.18	1.94	0.0075	0.002	43.30	4.10	1.64	35.5	780	1000	0.59	1.00	864	0.5635	39.69
291	0.03	2.50	2.73	0.0075	0.002	43.30	4.18	0.92	35.5	1000	780	1.00	0.59	864	0.5335	29.90
292	0.03	3.06	2.30	0.0075	0.002	43.30	4.29	1.33	35.5	1000	780	1.00	0.59	864	0.5063	29.90
293	0.03	3.61	1.88	0.0075	0.002	43.30	4.39	1.92	35.5	1000	780	1.00	0.59	864	0.4817	29.90
294	0.03	2.30	0.83	0.0075	0.002	23.30	4.65	2.77	16.2	880	1000	2.00	1.00	250	0.0179	6.92
295	0.03	2.02	1.39	0.0075	0.002	23.30	5.07	1.45	16.2	880	1000	2.00	1.00	250	0.0227	6.92
296	0.03	1.94	1.75	0.0075	0.002	23.30	5.48	1.11	16.2	1000	880	1.00	2.00	250	0.0275	15.94
297	0.03	2.50	1.50	0.0075	0.002	23.30	5.95	1.67	16.2	1000	880	1.00	2.00	250	0.0324	15.94
298	0.03	3.06	1.24	0.0075	0.002	23.30	6.39	2.47	16.2	1000	880	1.00	2.00	250	0.0373	15.94
299	0.03	3.61	0.99	0.0075	0.002	23.30	6.84	3.65	16.2	1000	880	1.00	2.00	250	0.0421	15.94
300	0.03	4.17	0.74	0.0075	0.002	23.30	7.30	5.64	16.2	1000	880	1.00	2.00	250	0.0468	15.94
301	0.03	2.32	0.83	0.0075	0.002	30.00	3.64	2.80	16.2	880	1000	2.00	1.00	415	0.0386	8.95
302	0.03	2.03	1.39	0.0075	0.002	30.00	3.95	1.46	16.2	880	1000	2.00	1.00	415	0.0489	8.95
303	0.03	1.94	1.78	0.0075	0.002	30.00	4.29	1.09	16.2	1000	880	1.00	2.00	415	0.0590	20.60
304	0.03	2.50	1.52	0.0075	0.002	30.00	4.64	1.64	16.2	1000	880	1.00	2.00	415	0.0696	20.60
305	0.03	3.06	1.25	0.0075	0.002	30.00	4.98	2.45	16.2	1000	880	1.00	2.00	415	0.0804	20.60
306	0.03	3.61	1.00	0.0075	0.002	30.00	5.32	3.61	16.2	1000	880	1.00	2.00	415	0.0906	20.60
307	0.03	4.17	0.77	0.0075	0.002	30.00	5.70	5.42	16.2	1000	880	1.00	2.00	415	0.1001	20.60
308	0.03	2.32	0.83	0.0075	0.002	36.70	2.97	2.80	16.2	880	1000	2.00	1.00	620	0.0712	10.98
309	0.03	2.05	1.39	0.0075	0.002	36.70	3.25	1.47	16.2	880	1000	2.00	1.00	620	0.0898	10.98
310	0.03	1.94	1.79	0.0075	0.002	36.70	3.52	1.08	16.2	1000	880	1.00	2.00	620	0.1086	25.28
311	0.03	2.50	1.54	0.0075	0.002	36.70	3.81	1.62	16.2	1000	880	1.00	2.00	620	0.1277	25.28
312	0.03	3.06	1.28	0.0075	0.002	36.70	4.10	2.39	16.2	1000	880	1.00	2.00	620	0.1471	25.28
313	0.03	3.61	1.03	0.0075	0.002	36.70	4.38	3.50	16.2	1000	880	1.00	2.00	620	0.1657	25.28
314	0.03	4.17	0.79	0.0075	0.002	36.70	4.68	5.28	16.2	1000	880	1.00	2.00	620	0.1835	25.28
315	0.03	2.19	1.11	0.0075	0.002	43.30	2.64	1.97	16.2	880	1000	2.00	1.00	864	0.1325	12.99
316	0.03	2.06	1.39	0.0075	0.002	43.30	2.76	1.48	16.2	880	1000	2.00	1.00	864	0.1479	12.99
317	0.03	1.94	1.80	0.0075	0.002	43.30	2.99	1.08	16.2	1000	880	1.00	2.00	864	0.1788	29.90
318	0.03	2.50	1.54	0.0075	0.002	43.30	3.23	1.62	16.2	1000	880	1.00	2.00	864	0.2107	29.90

Sr. No	Di (m)	Q_C x 10^6 (m^3/s)	Q_D x 10^6 (m^3/s)	c (m)	d (m)	N (rps)	N_D x 10^4	C/D ratio	σ (mN/m)	ρ_C (Kg/m^3)	ρ_D (Kg/m^3)	μ_C (mKg/ms^2)	μ_D (mKg/ms^2)	a (m/s^2)	Ta x 10^8	N_{Re} x 10^3
319	0.03	3.06	1.30	0.0075	0.002	43.30	3.49	2.35	16.2	1000	880	1.00	2.00	864	0.2414	29.90
320	0.03	3.61	1.06	0.0075	0.002	43.30	3.74	3.41	16.2	1000	880	1.00	2.00	864	0.2712	29.90
321	0.03	4.21	0.83	0.0075	0.002	23.30	7.49	5.07	58.3	660	1000	0.29	1.00	250	0.2423	36.72
322	0.03	3.70	1.39	0.0075	0.002	23.30	7.57	2.66	58.3	660	1000	0.29	1.00	250	0.2048	36.72
323	0.03	3.22	1.94	0.0075	0.002	23.30	7.67	1.66	58.3	660	1000	0.29	1.00	250	0.1739	36.72
324	0.03	2.50	2.75	0.0075	0.002	23.30	7.80	0.91	58.3	1000	660	1.00	0.29	250	0.1477	15.94
325	0.03	3.06	2.27	0.0075	0.002	23.30	7.92	1.35	58.3	1000	660	1.00	0.29	250	0.1254	15.94
326	0.03	3.61	1.80	0.0075	0.002	23.30	8.04	2.01	58.3	1000	660	1.00	0.29	250	0.1071	15.94
327	0.03	4.17	1.35	0.0075	0.002	23.30	8.21	3.09	58.3	1000	660	1.00	0.29	250	0.0920	15.94
328	0.03	4.24	0.83	0.0075	0.002	30.00	5.85	5.11	58.3	660	1000	0.29	1.00	415	0.5239	47.46
329	0.03	3.73	1.39	0.0075	0.002	30.00	5.91	2.68	58.3	660	1000	0.29	1.00	415	0.4433	47.46
330	0.03	3.26	1.94	0.0075	0.002	30.00	6.00	1.68	58.3	660	1000	0.29	1.00	415	0.3771	47.46
331	0.03	2.50	2.77	0.0075	0.002	30.00	6.08	0.90	58.3	1000	660	1.00	0.29	415	0.3197	20.60
332	0.03	3.06	2.29	0.0075	0.002	30.00	6.18	1.34	58.3	1000	660	1.00	0.29	415	0.2718	20.60
333	0.03	3.61	1.84	0.0075	0.002	30.00	6.29	1.96	58.3	1000	660	1.00	0.29	415	0.2332	20.60
334	0.03	4.17	1.40	0.0075	0.002	30.00	6.43	2.98	58.3	1000	660	1.00	0.29	415	0.2010	20.60
335	0.03	4.25	0.83	0.0075	0.002	36.70	4.79	5.12	58.3	660	1000	0.29	1.00	620	0.9664	58.24
336	0.03	3.75	1.39	0.0075	0.002	36.70	4.85	2.70	58.3	660	1000	0.29	1.00	620	0.8187	58.24
337	0.03	3.31	1.94	0.0075	0.002	36.70	4.95	1.71	58.3	660	1000	0.29	1.00	620	0.6993	58.24
338	0.03	2.50	2.83	0.0075	0.002	36.70	5.03	0.88	58.3	1000	660	1.00	0.29	620	0.5947	25.28
339	0.03	3.06	2.35	0.0075	0.002	36.70	5.11	1.30	58.3	1000	660	1.00	0.29	620	0.5065	25.28
340	0.03	3.61	1.89	0.0075	0.002	36.70	5.19	1.91	58.3	1000	660	1.00	0.29	620	0.4344	25.28
341	0.03	4.17	1.45	0.0075	0.002	36.70	5.30	2.88	58.3	1000	660	1.00	0.29	620	0.3750	25.28
342	0.03	4.01	1.11	0.0075	0.002	43.30	4.10	3.61	58.3	660	1000	0.29	1.00	864	1.4691	68.88
343	0.03	3.77	1.39	0.0075	0.002	43.30	4.13	2.71	58.3	660	1000	0.29	1.00	864	1.3534	68.88
344	0.03	3.29	1.94	0.0075	0.002	43.30	4.18	1.70	58.3	660	1000	0.29	1.00	864	1.1514	68.88
345	0.03	2.50	2.83	0.0075	0.002	43.30	4.26	0.88	58.3	1000	660	1.00	0.29	864	0.9814	29.90
346	0.03	3.06	2.38	0.0075	0.002	43.30	4.35	1.29	58.3	1000	660	1.00	0.29	864	0.8403	29.90
347	0.03	3.61	1.94	0.0075	0.002	43.30	4.44	1.86	58.3	1000	660	1.00	0.29	864	0.7242	29.90

Sr. No	Di (m)	Q_C x 10^6 (m^3/s)	Q_D x 10^6 (m^3/s)	c (m)	d (m)	N (rps)	N_D x 10^4	C/D ratio	σ (mN/m)	ρ_C (Kg/m^3)	ρ_D (Kg/m^3)	μ_C (mKg/ms^2)	μ_D (mKg/ms^2)	a (m/s^2)	Ta x 10^8	N_{Re} x 10^3
348	0.03	3.38	0.83	0.0075	0.002	23.30	6.26	4.07	58.3	660	1000	0.29	1.00	250	0.2305	36.72
349	0.03	2.96	1.39	0.0075	0.002	23.30	6.47	2.13	58.3	660	1000	0.29	1.00	250	0.1903	36.72
350	0.03	2.58	1.94	0.0075	0.002	23.30	6.72	1.33	58.3	660	1000	0.29	1.00	250	0.1595	36.72
351	0.03	2.50	2.20	0.0075	0.002	23.30	6.99	1.14	58.3	1000	660	1.00	0.29	250	0.1346	15.94
352	0.03	3.06	1.82	0.0075	0.002	23.30	7.25	1.68	58.3	1000	660	1.00	0.29	250	0.1147	15.94
353	0.03	3.61	1.44	0.0075	0.002	23.30	7.51	2.51	58.3	1000	660	1.00	0.29	250	0.0987	15.94
354	0.03	4.17	1.08	0.0075	0.002	23.30	7.80	3.86	58.3	1000	660	1.00	0.29	250	0.0860	15.94
355	0.03	3.40	0.83	0.0075	0.002	30.00	4.88	4.10	58.3	660	1000	0.29	1.00	415	0.4984	47.46
356	0.03	2.99	1.39	0.0075	0.002	30.00	5.06	2.15	58.3	660	1000	0.29	1.00	415	0.4123	47.46
357	0.03	2.61	1.94	0.0075	0.002	30.00	5.25	1.35	58.3	660	1000	0.29	1.00	415	0.3459	47.46
358	0.03	2.50	2.22	0.0075	0.002	30.00	5.45	1.13	58.3	1000	660	1.00	0.29	415	0.2917	20.60
359	0.03	3.06	1.83	0.0075	0.002	30.00	5.65	1.67	58.3	1000	660	1.00	0.29	415	0.2482	20.60
360	0.03	3.61	1.47	0.0075	0.002	30.00	5.86	2.46	58.3	1000	660	1.00	0.29	415	0.2147	20.60
361	0.03	4.17	1.12	0.0075	0.002	30.00	6.11	3.72	58.3	1000	660	1.00	0.29	415	0.1877	20.60
362	0.03	3.40	0.83	0.0075	0.002	36.70	3.99	4.10	58.3	660	1000	0.29	1.00	620	0.9190	58.24
363	0.03	3.00	1.39	0.0075	0.002	36.70	4.14	2.16	58.3	660	1000	0.29	1.00	620	0.7611	58.24
364	0.03	2.62	1.94	0.0075	0.002	36.70	4.30	1.35	58.3	660	1000	0.29	1.00	620	0.6387	58.24
365	0.03	2.50	2.25	0.0075	0.002	36.70	4.48	1.11	58.3	1000	660	1.00	0.29	620	0.5409	25.28
366	0.03	3.06	1.88	0.0075	0.002	36.70	4.66	1.63	58.3	1000	660	1.00	0.29	620	0.4626	25.28
367	0.03	3.61	1.52	0.0075	0.002	36.70	4.84	2.38	58.3	1000	660	1.00	0.29	620	0.4006	25.28
368	0.03	4.17	1.16	0.0075	0.002	36.70	5.03	3.59	58.3	1000	660	1.00	0.29	620	0.3496	25.28
369	0.03	3.21	1.11	0.0075	0.002	43.30	3.46	2.89	58.3	660	1000	0.29	1.00	864	1.3800	68.88
370	0.03	3.02	1.39	0.0075	0.002	43.30	3.53	2.17	58.3	660	1000	0.29	1.00	864	1.2589	68.88
371	0.03	2.64	1.94	0.0075	0.002	43.30	3.66	1.36	58.3	660	1000	0.29	1.00	864	1.0573	68.88
372	0.03	2.50	2.26	0.0075	0.002	43.30	3.81	1.11	58.3	1000	660	1.00	0.29	864	0.8943	29.90
373	0.03	3.06	1.91	0.0075	0.002	43.30	3.98	1.60	58.3	1000	660	1.00	0.29	864	0.7682	29.90
374	0.03	3.61	1.56	0.0075	0.002	43.30	4.14	2.31	58.3	1000	660	1.00	0.29	864	0.6673	29.90
375	0.242	500.00	444.44	0.022	0.025	19.00	5.72	1.13	48.5	1000	780	1.00	3.00	1239	133.0800	1252.39
376	0.242	527.78	416.67	0.022	0.025	19.00	5.72	1.27	48.5	780	1000	3.00	1.00	1239	104.9297	319.35

Sr. No	Di (m)	Q_C x 10^6 (m^3/s)	Q_D x 10^6 (m^3/s)	c (m)	d (m)	N (rps)	N_D x 10^4	C/D ratio	σ (mN/m)	ρ_C (Kg/m^3)	ρ_D (Kg/m^3)	μ_C (mKg/ms^2)	μ_D (mKg/ms^2)	a (m/s^2)	Ta x 10^8	N_{Re} x 10^3
377	0.242	750.00	166.67	0.022	0.025	19.00	5.55	4.50	48.5	780	1000	3.00	1.00	1239	51.8777	319.35
378	0.242	583.33	500.00	0.022	0.025	23.80	5.24	1.17	48.5	1000	780	1.00	3.00	1944	271.6977	1573.84
379	0.242	500.00	583.33	0.022	0.025	23.80	5.24	0.86	48.5	1000	780	1.00	3.00	1944	220.8867	1573.84
380	0.242	666.67	416.67	0.022	0.025	23.80	5.24	1.60	48.5	780	1000	3.00	1.00	1944	179.4440	401.34
381	0.242	805.56	277.78	0.022	0.025	23.80	5.24	2.90	48.5	780	1000	3.00	1.00	1944	126.7018	401.34
382	0.242	638.89	583.33	0.022	0.025	26.80	5.25	1.10	48.5	1000	780	1.00	3.00	2465	374.1145	1775.23
383	0.242	583.33	638.89	0.022	0.025	26.80	5.25	0.91	48.5	1000	780	1.00	3.00	2465	331.0290	1775.23
384	0.242	722.22	500.00	0.022	0.025	26.80	5.25	1.44	48.5	780	1000	3.00	1.00	2465	275.3969	452.71
385	0.242	805.56	416.67	0.022	0.025	26.80	5.25	1.93	48.5	780	1000	3.00	1.00	2465	228.9763	452.71
386	0.242	888.89	333.33	0.022	0.025	26.80	5.25	2.67	48.5	780	1000	3.00	1.00	2465	190.2618	452.71
387	0.242	944.44	277.78	0.022	0.025	26.80	5.25	3.40	48.5	780	1000	3.00	1.00	2465	168.1047	452.71
388	0.242	722.22	638.89	0.022	0.025	30.90	5.07	1.13	48.5	1000	780	1.00	3.00	3277	589.3958	2050.96
389	0.242	611.11	750.00	0.022	0.025	30.90	5.07	0.81	48.5	1000	780	1.00	3.00	3277	473.0843	2050.96
390	0.242	833.33	527.78	0.022	0.025	30.90	5.07	1.58	48.5	780	1000	3.00	1.00	3277	400.9608	523.04
391	0.242	972.22	388.89	0.022	0.025	30.90	5.07	2.50	48.5	780	1000	3.00	1.00	3277	304.0168	523.04
392	0.242	1027.78	333.33	0.022	0.025	30.90	5.07	3.08	48.5	780	1000	3.00	1.00	3277	272.0456	523.04
393	0.242	1111.11	250.00	0.022	0.025	30.90	5.07	4.44	48.5	780	1000	3.00	1.00	3277	230.1849	523.04
394	0.242	611.11	416.67	0.022	0.025	19.00	6.22	1.47	48.5	1000	780	1.00	3.00	1239	158.5228	1252.39
395	0.242	527.78	472.22	0.022	0.025	19.00	6.05	1.12	48.5	1000	780	1.00	3.00	1239	132.4967	1252.39
396	0.242	472.22	527.78	0.022	0.025	19.00	6.05	0.89	48.5	1000	780	1.00	3.00	1239	114.0927	1252.39
397	0.242	583.33	416.67	0.022	0.025	19.00	6.05	1.40	48.5	780	1000	3.00	1.00	1239	98.2102	319.35
398	0.242	638.89	333.33	0.022	0.025	19.00	5.89	1.92	48.5	780	1000	3.00	1.00	1239	80.4237	319.35
399	0.242	694.44	277.78	0.022	0.025	19.00	5.89	2.50	48.5	780	1000	3.00	1.00	1239	68.8657	319.35
400	0.242	833.33	416.67	0.022	0.025	28.50	5.05	2.00	48.5	1000	780	1.00	3.00	2788	663.6094	1889.49
401	0.242	722.22	472.22	0.022	0.025	28.50	4.82	1.53	48.5	1000	780	1.00	3.00	2788	562.1534	1889.49
402	0.242	611.11	527.78	0.022	0.025	28.50	4.60	1.16	48.5	1000	780	1.00	3.00	2788	468.3144	1889.49
403	0.242	500.00	583.33	0.022	0.025	28.50	4.37	0.86	48.5	1000	780	1.00	3.00	2788	382.6579	1889.49
404	0.242	638.89	388.89	0.022	0.025	28.50	4.15	1.64	48.5	780	1000	3.00	1.00	2788	305.6598	481.85
405	0.242	694.44	277.78	0.022	0.025	28.50	3.92	2.50	48.5	780	1000	3.00	1.00	2788	237.7163	481.85

Sr. No	**Di (m)**	**Q_C x 10^6 (m^3/s)**	**Q_D x 10^6 (m^3/s)**	**c (m)**	**d (m)**	**N (rps)**	**N_D x 10^4**	**C/D ratio**	**σ (mN/m)**	**ρ_C (Kg/m^3)**	**ρ_D (Kg/m^3)**	**μ_C (mKg/ms^2)**	**μ_D (mKg/ms^2)**	**a (m/s^2)**	**Ta x 10^8**	**N_{Re} x 10^3**
406	0.242	833.33	472.22	0.022	0.025	33.30	4.51	1.76	48.5	1000	780	1.00	3.00	3806	987.5365	2212.60
407	0.242	694.44	527.78	0.022	0.025	33.30	4.22	1.32	48.5	1000	780	1.00	3.00	3806	818.3933	2212.60
408	0.242	555.56	583.33	0.022	0.025	33.30	3.93	0.95	48.5	1000	780	1.00	3.00	3806	659.3720	2212.60
409	0.242	638.89	416.67	0.022	0.025	33.30	3.65	1.53	48.5	780	1000	3.00	1.00	3806	512.9099	564.28
410	0.242	694.44	277.78	0.022	0.025	33.30	3.36	2.50	48.5	780	1000	3.00	1.00	3806	381.6250	564.28
411	0.242	833.33	416.67	0.022	0.025	38.00	3.78	2.00	48.5	1000	780	1.00	3.00	4956	1590.5177	2529.62
412	0.242	750.00	611.11	0.022	0.025	38.00	4.12	1.23	48.5	1000	780	1.00	3.00	4956	1166.8269	2529.62
413	0.242	611.11	666.67	0.022	0.025	38.00	3.87	0.92	48.5	1000	780	1.00	3.00	4956	959.4174	2529.62
414	0.242	722.22	472.22	0.022	0.025	38.00	3.62	1.53	48.5	780	1000	3.00	1.00	4956	767.0187	645.15
415	0.242	777.78	333.33	0.022	0.025	38.00	3.36	2.33	48.5	780	1000	3.00	1.00	4956	592.3019	645.15
416	0.242	833.33	194.44	0.022	0.025	38.00	3.11	4.29	48.5	780	1000	3.00	1.00	4956	437.9308	645.15
417	0.125	175.14	175.14	0.0115	0.015	33.33	5.37	1.00	17.9	847.76	1311.71	5.05	4.47	1969	14.9144	112.11
418	0.125	227.59	113.80	0.0115	0.015	33.33	5.24	2.00	17.9	1311.71	847.76	4.47	5.05	1969	17.8420	197.74
419	0.125	281.33	92.84	0.0115	0.015	33.33	5.74	3.03	17.9	1311.71	847.76	4.47	5.05	1969	19.4854	197.74
420	0.125	427.33	106.83	0.0115	0.015	33.33	8.20	4.00	17.9	1311.71	847.76	4.47	5.05	1969	20.4594	197.74
421	0.125	411.66	45.28	0.0115	0.015	33.33	7.01	9.09	17.9	1311.71	847.76	4.47	5.05	1969	22.6138	197.74
422	0.125	117.92	117.92	0.0115	0.015	33.33	3.62	1.00	18.2	847.76	1420.07	5.05	8.65	1969	8.4971	112.11
423	0.125	157.04	78.52	0.0115	0.015	33.33	3.61	2.00	18.2	1420.07	847.76	8.65	5.05	1969	8.3483	109.65
424	0.125	264.89	66.22	0.0115	0.015	33.33	5.08	4.00	18.2	1420.07	847.76	8.65	5.05	1969	8.1585	109.65
425	0.125	272.27	29.95	0.0115	0.015	33.33	4.64	9.09	18.2	1420.07	847.76	8.65	5.05	1969	7.9811	109.65
426	0.125	229.58	229.58	0.0115	0.015	33.33	7.04	1.00	16.7	847.76	1473.02	5.05	12.24	1969	6.2873	112.11
427	0.125	268.67	179.11	0.0115	0.015	33.33	6.87	1.50	16.7	847.76	1473.02	5.05	12.24	1969	6.7179	112.11
428	0.125	283.10	189.68	0.0115	0.015	33.33	7.25	1.49	16.7	1473.02	847.76	12.24	5.05	1969	5.8553	79.99
429	0.125	327.41	163.70	0.0115	0.015	33.33	7.53	2.00	16.7	1473.02	847.76	12.24	5.05	1969	5.5591	79.99
430	0.125	480.67	120.17	0.0115	0.015	33.33	9.22	4.00	16.7	1473.02	847.76	12.24	5.05	1969	4.9881	79.99
431	0.125	89.03	89.03	0.0115	0.015	33.33	2.73	1.00	9.9	861.51	1473.03	7.57	12.24	1969	4.2418	75.52
432	0.125	111.48	55.74	0.0115	0.015	33.33	2.57	2.00	9.9	1473.03	861.51	12.24	7.57	1969	4.2733	79.99
433	0.125	116.54	38.46	0.0115	0.015	33.33	2.38	3.03	8.3	1311.72	861.51	4.47	7.57	1969	16.0256	197.74
434	0.125	98.16	32.39	0.0115	0.015	33.33	2.00	3.03	9.4	1420.07	861.51	8.65	7.57	1969	6.7694	109.65

Sr. No	Di (m)	Q_C x 10^6 (m^3/s)	Q_D x 10^6 (m^3/s)	c (m)	d (m)	N (rps)	N_D x 10^4	C/D ratio	σ (mN/m)	ρ_C (Kg/m^3)	ρ_D (Kg/m^3)	μ_C (mKg/ms^2)	μ_D (mKg/ms^2)	a (m/s^2)	Ta x 10^8	N_{Re} x 10^3
435	0.125	132.04	66.02	0.0115	0.015	33.33	3.04	2.00	16.7	1473.02	847.76	12.24	5.05	1969	5.5595	79.99
436	0.125	152.57	65.48	0.0115	0.015	33.33	3.35	2.33	16.7	1473.02	847.76	12.24	5.05	1969	5.4163	79.99
437	0.125	172.71	57.57	0.0115	0.015	33.33	3.53	3.00	16.7	1473.02	847.76	12.24	5.05	1969	5.2002	79.99
438	0.125	192.00	48.00	0.0115	0.015	33.33	3.68	4.00	16.7	1473.02	847.76	12.24	5.05	1969	4.9882	79.99
439	0.125	184.63	92.31	0.0115	0.015	33.33	4.25	2.00	8.3	1311.71	861.5	4.47	7.57	1969	13.7242	197.74
440	0.125	227.08	75.69	0.0115	0.015	33.33	4.65	3.00	8.3	1311.71	861.5	4.47	7.57	1969	15.9711	197.74
441	0.125	92.78	46.39	0.0115	0.015	33.33	2.14	2.00	9.9	1473.02	861.5	12.24	7.57	1969	4.2737	79.99
442	0.125	96.30	48.15	0.0115	0.015	33.33	2.22	2.00	9.4	1420.07	861.51	8.65	7.57	1969	6.4182	109.65
443	0.125	131.11	65.56	0.0115	0.015	33.33	3.02	2.00	18.2	1420.07	847.76	8.65	5.05	1969	8.3483	109.65
444	0.125	194.83	129.89	0.0115	0.015	33.33	4.98	1.50	17.9	1311.71	847.76	4.47	5.05	1969	16.6264	197.74
445	0.125	220.56	110.28	0.0115	0.015	33.33	5.08	2.00	17.9	1311.71	847.76	4.47	5.05	1969	17.8417	197.74
446	0.125	246.06	105.61	0.0115	0.015	33.33	5.40	2.33	17.9	1311.71	847.76	4.47	5.05	1969	18.4670	197.74
447	0.125	298.54	99.51	0.0115	0.015	33.33	6.11	3.00	17.9	1311.71	847.76	4.47	5.05	1969	19.4481	197.74
448	0.125	386.89	96.72	0.0115	0.015	33.33	7.42	4.00	17.9	1311.71	847.76	4.47	5.05	1969	20.4592	197.74
449	0.125	505.00	56.11	0.0115	0.015	33.33	8.61	9.00	17.9	1311.71	847.76	4.47	5.05	1969	22.5940	197.74
450	0.104					33.26	14.00	3.03	10.0	1016	826	1.00	2.00	830		
451	0.104					33.26	10.00	0.50	10.0	826	1016	2.00	1.00	830		
452	0.104					33.26	11.00	1.00	10.0	826	1016	2.00	1.00	830		
453	0.104					33.26	11.00	2.50	10.0	826	1016	2.00	1.00	830		
454	0.104					49.97	14.00	3.03	10.0	1016	826	1.00	2.00	1873		
455	0.104					49.97	11.00	0.50	10.0	826	1016	2.00	1.00	1873		
456	0.104					49.97	12.00	1.00	10.0	826	1016	2.00	1.00	1873		
457	0.104					49.97	14.00	2.50	10.0	826	1016	2.00	1.00	1873		
458	0.262					29.10	17.00	5.00	10.0	1021	846	1.00	2.00	635		
459	0.262					29.10	12.00	0.50	10.0	846	1021	2.00	1.00	635		
460	0.262					29.10	14.00	1.00	10.0	846	1021	2.00	1.00	635		
461	0.262					29.10	18.00	2.00	10.0	846	1021	2.00	1.00	635		
462	0.262					29.10	19.00	4.00	10.0	846	1021	2.00	1.00	635		

Table A.3: The pumping capacity of a given helical coil based fluidic pump at different operating condition

S. No	Pulsing height (cm)	Volume pumped (cm^3/s)	Pulsing time		Air pressure (kPa)		Volumetric efficiency η_V
			Pumping time (s)	Refill time (s)	Inlet pressure to pulsing leg	Inlet pressure to air ejector	
1	52	1.8	1.3	7	49	0	6
2	58	3.1	1.5	7	49	0	9
3	66	4.8	1.8	7	49	0	13
4	73	6.1	2.1	7	49	0	15
5	54	2.1	1.3	10	49	0	9
6	61	3.2	1.5	10	49	0	12
7	70	4.9	1.8	10	49	0	16
8	79	6.4	2.1	10	49	0	19
9	88	7.8	2.4	10	49	0	22
10	54	1.9	1.3	12	49	0	9
11	61	3.1	1.5	12	49	0	13
12	72	4.7	1.8	12	49	0	18
13	82	6.1	2.1	12	49	0	21
14	91	7.4	2.4	12	49	0	23
15	55	1.7	1.3	16	49	0	11
16	63	2.6	1.5	16	49	0	15
17	73	3.8	1.8	16	49	0	18
18	84	5.2	2.1	16	49	0	22
19	95	6.5	2.4	16	49	0	25
20	55	1.4	1.3	21	49	0	11
21	63	2.3	1.5	21	49	0	16
22	74	3.3	1.8	21	49	0	20
23	85	4.5	2.1	21	49	0	24
24	97	5.6	2.4	21	49	0	27
25	55	2.4	1.3	7	49	49	7
26	60	3.8	1.5	7	49	49	10

S. No	Pulsing height (cm)	Volume pumped (cm^3/s)	Pulsing time		Air pressure (kPa)		Volumetric efficiency η_V
			Pumping time (s)	Refill time (s)	Inlet pressure to pulsing leg	Inlet pressure to air ejector	
27	70	5.5	1.8	7	49	49	14
28	77	6.9	2.1	7	49	49	16
29	57	2.8	1.3	10	49	49	11
30	65	4.0	1.5	10	49	49	14
31	75	5.9	1.8	10	49	49	19
32	84	7.4	2.1	10	49	49	21
33	93	8.9	2.4	10	49	49	23
34	57	2.5	1.3	12	49	49	11
35	65	3.7	1.5	12	49	49	15
36	76	5.5	1.8	12	49	49	20
37	87	7.1	2.1	12	49	49	23
38	96	8.6	2.4	12	49	49	25
39	59	2.4	1.3	16	49	49	14
40	67	3.4	1.5	16	49	49	17
41	79	4.9	1.8	16	49	49	22
42	91	6.3	2.1	16	49	49	25
43	102	7.8	2.4	16	49	49	28
44	59	1.8	1.3	21	49	49	13
45	67	2.8	1.5	21	49	49	18
46	78	4.0	1.8	21	49	49	23
47	91	5.0	2.1	21	49	49	25
48	103	6.4	2.4	21	49	49	29
49	57	2.8	1.3	7	49	98	8
50	63	4.2	1.5	7	49	98	11
51	72	6.0	1.8	7	49	98	15
52	79	7.4	2.1	7	49	98	17
53	86	8.9	2.1	7	49	98	18
54	60	3.1	1.3	10	49	98	12

S. No	Pulsing height (cm)	Volume pumped (cm^3/s)	Pulsing time		Air pressure (kPa)		Volumetric efficiency η_V
			Pumping time (s)	Refill time (s)	Inlet pressure to pulsing leg	Inlet pressure to air ejector	
55	68	4.5	1.5	10	49	98	15
56	78	6.4	1.8	10	49	98	19
57	89	7.9	2.1	10	49	98	21
58	97	9.5	2.4	10	49	98	24
59	60	3.0	1.3	12	49	98	13
60	67	4.3	1.5	12	49	98	17
61	80	5.9	1.8	12	49	98	20
62	91	7.6	2.1	12	49	98	23
63	101	9.3	2.4	12	49	98	26
64	61	2.5	1.3	16	49	98	14
65	69	3.7	1.5	16	49	98	18
66	82	5.2	1.8	16	49	98	22
67	94	6.8	2.1	16	49	98	26
68	105	8.2	2.4	16	49	98	29
69	61	2.1	1.3	21	49	98	15
70	70	2.9	1.5	21	49	98	19
71	81	4.3	1.8	21	49	98	24
72	95	5.7	2.1	21	49	98	27
73	107	6.8	2.4	21	49	98	30
74	65	5.6	1.3	7	98	0	14
75	79	10.4	1.5	7	98	0	22
76	71	5.8	1.3	10	98	0	18
77	79	7.7	1.5	10	98	0	22
78	92	10.0	1.8	10	98	0	25
79	73	5.4	1.3	12	98	0	20
80	82	7.3	1.5	12	98	0	24
81	95	9.6	1.8	12	98	0	27
82	74	4.7	1.3	16	98	0	22

S. No	Pulsing height (cm)	Volume pumped (cm^3/s)	Pulsing time		Air pressure (kPa)		Volumetric efficiency η_V
			Pumping time (s)	Refill time (s)	Inlet pressure to pulsing leg	Inlet pressure to air ejector	
83	84	6.0	1.5	16	98	0	25
84	100	8.5	1.8	16	98	0	30
85	114	10.4	2.1	16	98	0	33
86	75	3.9	1.3	21	98	0	23
87	86	5.5	1.5	21	98	0	29
88	102	7.2	1.8	21	98	0	32
89	117	8.7	2.1	21	98	0	34
90	66	5.4	1.3	7	98	49	13
91	73	7.0	1.5	7	98	49	16
92	71	5.7	1.3	10	98	49	18
93	81	7.5	1.5	10	98	49	21
94	92	9.8	1.8	10	98	49	25
95	73	5.5	1.3	12	98	49	20
96	79	7.0	1.5	12	98	49	24
97	97	9.4	1.8	12	98	49	27
98	109	11.6	2.1	12	98	49	30
99	74	4.6	1.3	16	98	49	21
100	85	6.0	1.5	16	98	49	24
101	101	8.2	1.8	16	98	49	29
102	115	10.3	2.1	16	98	49	32
103	129	12.2	2.4	16	98	49	34
104	75	3.6	1.3	21	98	49	21
105	86	5.1	1.5	21	98	49	26
106	102	6.8	1.8	21	98	49	30
107	119	8.5	2.1	21	98	49	33
108	133	10.1	2.4	21	98	49	35
109	70	6.3	1.3	7	98	98	15
110	77	7.9	1.5	7	98	98	17

S. No	Pulsing height (cm)	Volume pumped (cm^3/s)	Pulsing time		Air pressure (kPa)		Volumetric efficiency η_V
			Pumping time (s)	Refill time (s)	Inlet pressure to pulsing leg	Inlet pressure to air ejector	
111	86	9.9	1.8	7	98	98	20
112	75	6.5	1.3	10	98	98	19
113	85	8.4	1.5	10	98	98	23
114	97	10.5	1.8	10	98	98	25
115	81	12.4	2.1	10	98	98	36
116	76	6.1	1.3	12	98	98	21
117	87	7.9	1.5	12	98	98	24
118	101	10.4	1.8	12	98	98	28
119	113	12.5	2.1	12	98	98	31
120	78	5.2	1.3	16	98	98	23
121	95	7.5	1.5	16	98	98	27
122	105	9.0	1.8	16	98	98	30
123	120	11.1	2.1	16	98	98	33
124	134	12.7	2.4	16	98	98	34
125	79	4.2	1.3	21	98	98	23
126	90	5.6	1.5	21	98	98	28
127	108	7.4	1.8	21	98	98	31
128	123	9.2	2.1	21	98	98	34
129	139	14.8	2.4	21	98	98	49

Thesis Highlight

Name of the Student : M. Balamurugan
Name of CI : Indira Gandhi Centre for Atomic Research **Enrolment No.:** ENGG02201204014
Thesis Title : Hydrodynamic characteristics of annular centrifugal extractor and helical coil based fluidic diode pump
Discipline : Engineering Sciences **Sub-Area of Discipline:** Chemical Engineering
Date of viva voce : 04/06/2021

Annular Centrifugal Extractor (ACE) is a robust solvent extraction equipment and candid candidate for fast breeder nuclear reprocessing applications. ACE design is based on various thumb rules. However, the reliable design and scale-up of ACE are yet to be developed. Flow inside the ACE is highly turbulent, unsteady due to liquid level fluctuation in the annular region, air ingression and three-phase (air, heavy and light phase) operation during solvent extraction operation.

The dispersion number (N_D) is a primary design input and decides the size and operating speed of annular centrifugal extractor (ACE) for any given process throughput. N_D value depends upon the system's physical properties, such as density, viscosity and interfacial tension. The measurement of N_D is impossible for hazards (radioactive, corrosive, etc.) systems. In this work, the N_D is measured by gravity/centrifugal separation for different aqueous and organic systems to cover wide range of physical properties. Based on experimental and literature results, a novel data driven correlation containing physical properties and separation forces has been developed using the Random Forest technique for dispersion number.

During multistage operation, failure of motor/bearing in any single stage leads to the stoppage of an entire ACE cascade. In nuclear reprocessing applications, the stoppage of cascade leads to solvent degradation and defeats the advantage of ACE. A simple and innovative modification of inclined overflow line has been developed, demonstrated and validated by flooding and mass transfer experiments in motor/bearing failed condition.

The understanding of flow inside the rotating bowl is one of the grey areas in the ACE design. Computational fluid dynamics (CFD) may be a key tool to address or solve the above problem and also it can be used to evaluate the existing ACE to optimize the operating parameters. The 2D CFD simulations have been performed for the prediction of zero-point flow rate with different turbulent models. The predictions of the SST k-omega model are closer to the experimental measurements.

Airlift pumps are widely used for metering applications in reprocessing plants. However, airlift and fluidic pumps are not suitable for low throughput metering operations. A suitable alternate pumping system of a helical coil-based pulsating pump has been developed and demonstrated by pumping experiments with different operating conditions. The CFD simulations have been performed for the prediction of the pressure drop across the given helical coil. The simulation is extended to understand the pressure drop across the helical coil for various design parameters.

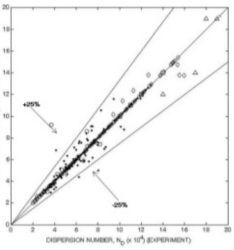

Fig. 1: Parity plot for the comparison of N_D measured experimentally against Random Forest based correlation.

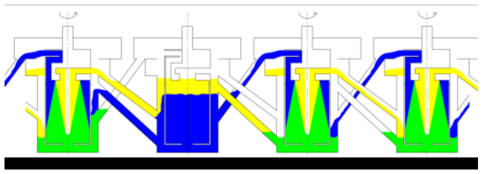

Fig. 2: Schematic view of aqueous and organic flow with inclined overflow (3rd stage motor failure condition) (blue colour - heavy phase, green colour - mixture, yellow colour - light phase)

Table 1: Zero-point flow w.r.t different turbulent models

S. No	*Details*	*Zero-point flow (Kg/hr)*
1.	*Experimental*	*1.5*
2.	*k-epsilon STD model*	*2.35*
3.	*k-epsilon RNG model*	*2.35*
4.	*SST K-omega model*	*1.99*
5.	*Reynolds Stress model*	*2.17*

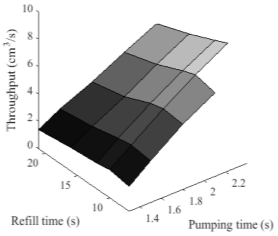

Fig. 3: Pumping capacity of given helical coil pump at different on and off pulsing frequency time